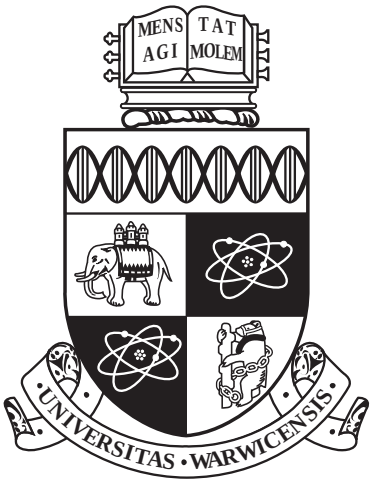

Development of Approaches for Screening Antimalarial Compounds Based on Their Modes of Action

by

Arturas Grauslys

Thesis

Submitted to the University of Warwick

for the degree of

Doctor of Philosophy

Systems Biology DTC

February 2016

THE UNIVERSITY OF
WARWICK

Contents

List of Tables

List of Figures

Acknowledgments

It would be hard to count all the people that have played a part in the successful completion of my PhD project. I am sure I will forget some, but I'm sincerely thankful to everyone nonetheless. First I would like to thank my PhD advisors: prof. David Wild and prof. Steve Ward. Besides their invaluable advice they always trusted my judgement and allowed me freedom I could not have expected. They did not just help me develop the skills for science but also independence and initiative. My supervisors were instrumental in the success of my work, however it is hard to overestimate the help of all the people around me that shared their knowledge and advice day-to-day. Dr. Felicity Curie was a great teacher to me at the very beginning. She was always first to offer ideas and stress scientific rigor above everything else. I am grateful for numerous inspiring discussions we had that left me thinking and that were the most rewading. I'm thankful to Dr. Marie Phelan, who persevered through my countless trials and errors. Who was always there with her advice, encouragement and optimism. I would like to express my love and gratitude to my parents Laimute and Algis, who have always supported me with love and patience, who were always on my side even when they did not agree with my decisions, and always had the words I needed to hear. To my younger siter Lina I want to say many thanks for her encouragement, inspirationa and her sense of humour regardless of the situation. But most importantly my greatest love and earnest gratitude to Eva - my wonderful partner in life and science. For her support and encouragement, advice and lessons, honest criticism, and for countless hours spent helping me I am forever in her debt. This work would truly be impossible without her.

Declarations

Research presented in this thesis is completely original and my own, with exception of where acknowledged below. I confirm that this thesis has not been submitted for another degree at any other University. NMR spectroscopy parameter set up used for experiments presented in Chapter 6 were selected by Dr. Marie Phelan, Shared Research Facility Manager of the NMR Centre at the University of Liverpool. Cellular extractions performed in experiments presented in Chapter 6 were collected with the assistance of Eva Caamano-Gutierrez. Drug exposure assays and high content imaging analyses presented in Chapter 7 were performed with the assistance of Dr. Paul Bedingfield.

Abstract

Malaria is an infectious tropical disease responsible for hundreds of thousands of deaths every year. It is caused by a parasite from genus *Plasmodium* of which *falciparum* is the most deadly and the focus of this study. The limited number of currently available drugs are further threatened by the rising frequency of resistance. This has greatly emphasised the need for new drugs with novel modes of action. The current drug development pipelines rely on large scale compound library screens for antimalarial effect. Computational chemometric methods are then used for selecting promising hits for further investigation. Such analyses however rely on indirect characterisation of compound effects. In this project we investigated three approaches aimed at developing compound screening assays based on compound effects on live cells. The first two approaches relied on metabolomics techniques. Based on the assumption that the drug induced metabolic changes in the malaria parasite could be uniquely assigned to the drug mode of action we hypothesised that if such metabolic states could be measured they could be used to cluster the compunds into groups based on their modes of action. By comparison to well established antimalarials the clusters of novel compounds could then be characterised and novel compound clusters identified. The third method relied on the phenotypic information for drug exposed malaria parasites derived from the analysis of fluorescent microscopy images. This assay aimed at characterising the modes of action of the compounds as well as the speed of kill. The first method investigated was based on metabolic fingerprinting using Fourier transform infrared spectroscopy. The sample preparation and data acquisition protocols were developed and tested. The results suggested that the sensitivity of the technique was

insufficient for the detection of drug induced effects in *P. falciparum*. Next a nuclear magnetic resonance (NMR) spectroscopy-based method was developed. While the method was promising in terms of high throughput capabilities, consistency and the breadth of information posed a series of issues, mainly associated with sensitivity. In the absence of a suitable automated data processing solution a custom software "ProcNMR" was developed and used to process the data collected in the experiments. A full experimental procedure was developed and tested, however the NMR sensitivity issues, exacerbated by the complex intraerythrocytic nature of *P. falciparum* resulted in suboptimal outputs. Lastly a high content imaging-based technique was investigated. Data processing and predictive analysis methods were developed and implemented. A pilot experiment was used to demonstrate the potential of the technique to discriminate between fast and slow acting drugs. The compounds of the "Malaria Box" were screened using this technique and a gorup of fast acting compounds identified.

Abbreviations

1D	One-dimensional
2D	Two-dimensional
ACT	Artemisinin-based combination therapy
ADC	Analog-to-digital converter
AQ	Amodiaquine
AT	Artemisinin
ATO	Atovaquone
CE	Capillary electrophoresis
CM	Complete medium
COSY	Correlation spectroscopy
CPMG	Carr-Purcell-Meiboom-Gill
CQ	Chloroquine
DALY	Disability-adjusted life-years
DA-PC	Discriminant analysis of principal components
DHFR	Dihydrofolate reductase
DMPK	Drug metabolism and pharmakokinetics
FA	Fusidic acid
FID	Free induction decay
FIR	Far infrared
FT-IR	Fourier-transform infrared spectroscopy
GC	Gas cromatography
GSK	GlaxoSmithKline
HC	Hierarchical clustering

HCI	High content imaging
HSQC	Heteronuclear single quantum correlation
IC_{50}	Half maximal inhibitory concentration
IR	Infrared
iRBC	Infected red blood cell
KO	Knock-out
LC	Liquid chromatography
LDA	Linear discriminant analysis
MIR	Mid-wavelength infrared
MMV	Medicines for Malaria Venture
MS	Mass spectrometry
NCBI	National Centre for Biotechnology Information
NIR	Near infrared
NMR	Nuclear magnetic resonance
NOESY	Nuclear Overhauser effect spectroscopy
P	*Plasmodium*
PC	Principal component
PCA	Principal component analysis
PG	Proguanil
PLS	Partial least squares
PLS-DA	Partial least squares discriminant analysis
QCDs	Quinoline containing drugs
RBC	Red blood cell
ROS	Reactive oxygen species
RPMI	Roswell Park Memorial Institute medium
SEM	Standard error of the mean
STOCSY	Statistical total correlation spectroscopy
TCA	Trycarboxylic acid cycle
TMS	Tetramethylsilane
TOCSY	Total correlation spectroscopy

TSP	3-(Trimethylsilyl) propionic acid
vs	Versus
WHO	World Health Organisation
WT	Wild-type

Chapter 1

Introduction

1.1 Malaria

Malaria is an infectious tropical disease caused by parasites of the genus *Plasmodium*. There are five species that cause disease in man: *Plasmodium falciparum*, *malariae*, *vivax*, *ovale* and *knowlesi*. Parasites are transmitted to humans through the bite of a female mosquito of genus *Anopheles*. There are up to 800 million cases of malaria every year in tropical and subtropical regions including sub-Saharan Africa, Southeast Asia, Oceania and some regions of Central America. Of those about 500,000 cases end in death from severe complications, especially among children and pregnant women [WHO, 2014]. The global burden of malaria in disability-adjusted life-years (DALY) as quoted by Hotez et al. [2014] is 83 million, where DALY is a number of years lost due to disability or early death caused by a disease. While the most prevalent strain of *Plasmodium* is *P. vivax* the most of the deaths from malaria are in cases of infection with *P. falciparum* [WHO, 2014]. It is distinguished from other strains by its ability to infect erythrocytes of any age allowing parasitemia of up to 80% as well as the production of proteins that facilitate red blood cell (RBC) binding to endothelial cells on capillaries - sequestration - especially in the brain, causing a range of severe complications including bleeding, seizures and coma [Rowe et al., 2009].

1.1.1 The Deadliest Strain

There are around 120 *Plasmodium* species that infect mammals and birds of which five are known to infect humans. Almost all malaria deaths in humans are caused by *P. falciparum*. Understanding of its life-cycle has helped greatly in the search for measures to fight the spread of infection and look for treatments. *P. falciparum*

has a 42-53 hour life-cycle depending on the growth conditions (Fig. 1.1).

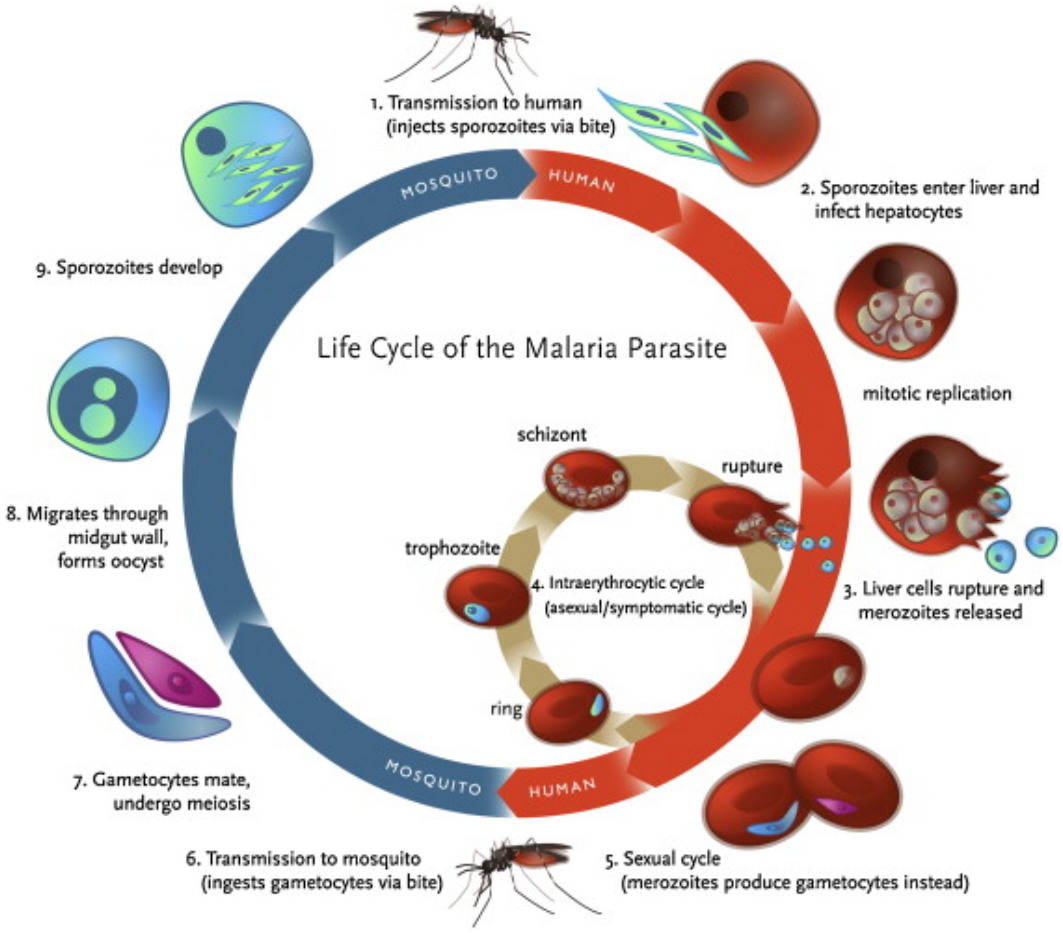

Figure 1.1: A schematic illustration of the lifer-cycle of *P. falciparum* (source: Klein [2013])

When an infected female *Anopheles* mosquito takes a bloodmeal it releases *Plasmodium* sporozoites into the bloodstream of the host where they are taken to the liver and infect hepatocytes. In the hepatocytes the parasites undergo the first asexual replication that ends in the production of the first generation of merozoites that are then released into the bloodstream and invade red blood cells (RBCs). When the merozoite invades the RBC it develops within a vacuole formed from the host cell material until it reaches maturity. The parasite starts the life cycle at the ring stage and over around 18 hours develops into a trophozoite stage. In the process it consumes hemoglobin as a source of amino acids. Heme - the toxic side product of hemoglobin digestion - is stored in an exclusion body in a crystalline form known as hemozoin. When the parasite reaches the trophozoite stage it starts to produce

protein adhesins on the erythrocyte membrane that allow the red blood cells to bind to the endothelial cells in the host microcirculation. The process is called sequestration and protects the infected RBCs from removal from the bloodstream by the spleen. The parasites spend the last 24-34 hours of their development in this state. During this time they develop into schizonts and produce on average 16 merozoites each. Once the parasites are fully mature the RBC is ruptured, the merozoites enter the bloodstream and infect new RBCs. The cycle continues subsequently raising the the level of parasitemia up to 20 times every 48 hours. Some of the parasites do not go through the asexual replication cycle and instead develop into sexual stages - gametocytes. The gametocytes, when ingested by a mosquito during a bloodmeal, undergo gametogenesis that result in formation of micro- and macrogametes. Microgametes fertilize macrogametes that result in formation of zygotes and subsequently oocysts. Through asexual replication oocysts produce sporozoites thus completing the life-cycle of *Plasmodium*. Almost any part of this life cycle can be targeted by treatment and prevention measures. The exclusive focus of this thesis will be the asexual intra-erythrocytic part of the *P. falciparum* life-cycle, the life cycle stage associated with the clinical manifestations of malaria.

1.1.2 Prevention and Treatment

The fight against malaria has been ongoing since the formal discovery of the disease at the end of the nineteenth century [Cox, 2010]. The efforts towards eradication of malaria have been divided between vaccine development, vector control and treatment of infection.

Due to extensive antigenic variation and the complex immune evasion response of *Plasmodia* the attempts to develop vaccines have proven difficult. RTS,S - a fusion of the hepatitis B surface antigen and a recombinant antigen protein derived from sporozoite coating - was for a while considered the most promising vaccine candidate. After successful human trials [Agnandji et al., 2012, 2014] the vaccine was approved for commercial use by European regulators in July, 2015. It is the first vaccine registered for use against malaria and the first registered vaccine against any human parasite. Malaria vector control is another major contributor to the fight against malaria. Insecticide-treated bednets and repellents have been effective in considerably reducing infection rates [Muller et al., 2006; Giardina et al., 2014]. Despite the success of these prevention measures the treatment of malaria patients remains the largest part of the fight against malaria. The main objectives of treatment of malaria are to kill parasites (treatment) or prevent infection from becoming established (prophylaxis) thereby avoiding the severe complications

that can often lead to morbidity and death. Currently available antimalarial drugs can be classified into four main categories: quinoline-like compounds; artemisinins; mitochondrial inhibitors, of which atovaquone is the only one available; and antifolates. Some antibacterial compounds, including sulfones, macrolides, tetracyclins, lincosamides and chloramphenicol have antimalarial activity but are rarely used and only ever in combination with other more active compounds.

Quinoline-like compounds including quinine, chloroquine (CQ), amodiaquine, piperaquine, mefloquine and others act by inhibiting haem detoxification within the asexual parasite food vacuole e.g. chloroquine binds to heamoglobin degradation products, inhibits haem dimerisation and hemozoin formation. The heam toxicity is therefore the explanation of the mode of action of quinolines [Fitch, 2004].

Artemisinins are endoperoxides derived from a natural product found in the *Artemisia annua* plant. They are fast acting compounds capable of affecting the broadest range of the parasite asexual life cycle. There are a range of artemisinins currently in use including artemether, dihydroartemisinin and artesunate. The exact mode of action of the artemisinins is still controversial, although it is thought that it could be linked to iron-dependent cleavage of the unique endoperoxide bridge, triggering formation of carbon-based radicals and epoxides that then target essential parasite macromolecules generating drug adducts [Olliaro et al., 2001].

Atovaquone inhibits the parasite electron transport chain by targeting the cytochrome bc_1 complex. This results in the collapse of the mitochondrial membrane potential and inhibition of pyrimidine biosynthesis [Srivastava et al., 1997].

Antifolates including pyrimethamine, cycloguanil and trimethoprim interfere with pyrimidine synthesis in *P. falciparum* by inhibition of dihydrofolate reductase - thymidylate synthase (DHFR) [Muller and Hyde, 2010].

The range of currently used antimalarials is very limited and in all cases examples of resistance have been reported. Resistance to CQ was first reported in the 1960s [Harinasuta et al., 1965]. It is associated with increased loss of drug from parasite digestive vacuole [Martin et al., 2009] and is linked to point mutations in the CQ resistance transporter (PfCRT) gene [Fidock et al., 2000]. *P. falciparum* multidrug resistence genes PfMDR1h and PfMRP1 have also been linked to CQ resistance [Duraisingh and Cowman, 2005; Nkrumah et al., 2009] as well as other

quinolines - mefloquine and quinine [Price et al., 2004; Nkrumah et al., 2009]. The efficacy of antifolates is reduced up to 1000-fold by a mutations in DHFR (N51I, C59R, S108N) and DHPF (A437G,K540E) genes that reduce the binding affinity of the drug [Gregson and Plowe, 2005]. Resistance to atovaquone arises from point-mutations (N268N/S/C) in the cytochrome-b encoding gene [Srivastava et al., 1999]. Artemisinin resistance has emerged in recent years and is reported to be associated with mutations in the *P. falciparum* protein *kelch* encoded on chromosome 13 [Ariey et al., 2014; Takala-Harrison et al., 2015]. Artemisinin combination therapies are currently the preferred treatment for malaria worldwide. While artemisinin monotherapies are now not recommended and are being gradually phased out following the WHO recommendations [WHO, 2015] the emergence of artemisinin resistance threatens the efficacy of combination therapies as well.

1.1.3 Drug Discovery

Resistance to antimalarial drugs has been rising since the 1960s and now blights all available drug classes having a major impact on malaria control and treatment efforts worldwide. The only solution to this problem is the discovery of new drugs with unique mechanisms of action. Today new antimalarial drug discovery is a worldwide effort led mainly by a few private-public organisations including the Medicines for Malaria Venture (www.mmv.com) as well as the Drugs for Neglected Diseases initiative (www.dndi.org).

The development of new drugs is usually carried out either by modification of well established drugs, in order to circumvent the resistance or some other unwanted property, or by searching for completely new scaffolds with new mechanisms of action. The latter approach can include high throughput whole-cell assays as well as biochemical assays against a specific biochemical target within the parasite. The whole-cell assays comprise of high throughput screens of compounds in search for new molecules with *in vitro* activity against *Plasmodium*. Biochemical assays are designed to show activity against a specific target that is usually an enzyme involved in a pathway vital to the parasite [Flannery et al., 2013]. After the sequencing of the *P. falciparum* genome [Gardner et al., 2002] bioinformatic analysis was expected to yield a vast array of new targets, however the majority of newly identified targets have been intractable with the exception of dihydroorotate dehydrogenase. The discovery of this enzyme has helped to identify a new compound DSM265 [Coteron et al., 2011] which became the first compound to emerge from a rational genetic analysis pipeline. Compounds inferred from genetic and chemioinformatic analysis still have to be validated as they must adhere to the requirements

for efficacy in live cells, acceptable toxicity margins and good drug metabolism and pharmacokinetics (DMPK) including adequate oral bioavailability [Flannery et al., 2013]. For example, cysteine proteases such as falcipains are vital to *Plasmodium* life cycle [Rosenthal, 2011] and nonspecific inhibitors of cysteine proteases are effective against the parasite [Joachimiak et al., 2001], however none of the potential compounds that target this pathway have successfully reached the clinic due to problems with toxicity as well as poor pharmacokinetics. Development of high thoughput whole cell screens has allowed rapid identification of novel compounds in high numbers [Plouffe et al., 2008]. Such compounds have guaranteed activity against the parasites without any detailed understanding of their targets or modes of action. Millions of compounds have been screened in whole-cell assays in recent years. The effort was led by St. Jude Children Hospital who screened 300,000 compounds against *P. falciparum* [Guiguemde et al., 2010], GlaxoSmithKline (GSK) screening over 2,000,000 compounds [Gamo et al., 2010] and an academic/industry consortium led by Novartis that screened over 800,000 compounds [Rottmann et al., 2010; Plouffe et al., 2008]. These screens have resulted in the identification of thousands of compounds with activity against *Plasmodium* that have been collected in the ChEMBL repository for medicinal chemistry data directed at neglected tropical diseases (http://www.ebi.ac.uk/chemblntd). Due to obvious restrictions in financial and time cost the vast number of hits requires a further selection of compounds for more detailed study. Such an triaging effort was carried out by MMV in the generation of the "Malaria Box", a selected set of validated hits that are recommended for further investigation [Spangenberg et al., 2013]. The "Malaria Box" includes 400 compounds that have been selected in two categories: drug-like compounds and probe-like compounds. These compounds are publicly available on request from the MMV as is a newer screening compound set called the "Pathogen Box".

1.2 Aims of The Study

The potential chemical space which antimalarial compounds can come from is enormous and high throughput screening studies are producing thousands of hits that need to be investigated further. This represents a significant challenge in terms of costs and time. Further insight into the properties of the compounds found to have antimalarial activity would allow extensive triaging and clustering of the current hits into more manageable sets. Strategies that contribute to understanding the compound space in terms of their specific targets and modes of action would greatly increase our efficiency of turning hits into drugs. It would facilitate better under-

standing of currently used compounds as well allowing selection of compounds with novel mode of action. This thesis is focused on the study of strategies that can help classify antimalarial hits based on their mode of action.

In order to classify compounds by mechanism a metabolomic fingerprinting approach was chosen. This choice was made based on a series of assumptions. Firstly it was assumed that *P. falciparum* has a finite number of druggable targets. This assumption implies that if there are more effective compounds than potential targets there is redundancy in the compound set that should allow clustering based on mechanism. It was also assumed that drugs with different modes of action induce different metabolic perturbations in the parasite leading to arrest of development or death. If those metabolic states could be identified and uniquely assigned to the modes of action they could serve as a proxy for compound classification.

The metabolic fingerprinting approach was chosen for the measurement of the global metabolic state in the parasite after exposure to compounds. A series of currently used compounds will be first employed in order to develop and validate the method followed by experiments involving the "Malaria Box" compounds with unknown mechanism. The data collected from experiments using well-understood antimalarial drugs as probes will generate the framework against which the clustering structure of the unknown compounds can be evaluated, highlighting clusters with novel modes of action.

1.3 Metabolomics

Metabolomics is the field of study of small molecules, with molecular mass lower than 2kDa, as products of metabolism in cells and intracellular space as a whole called the "metabolome". In the literature the name metabolomics was first mentioned in the 1990s [Oliver et al., 1998] however the study of the metabolome is a couple of decades older. The first paper that could be considered a metabolomics study was published in 1971 and described analysis of urine vapour and breath by gas chromatography [Pauling et al., 1971]. In 1999 another similar term "metabonomics" was introduced by Nicholson *et* al. with the definition of the "quantitative measurement of the dynamic, multiparametric, metabolic response of living systems to pathophysiologic stimuli or genetic modification" [Nicholson et al., 1999]. Since then the terms have largely lost the differences meant by the authors and are used interchangeably to refer to the study of the metabolome. In this text we will follow this trend as well. Depending on the scope of the study the metabolome can include the metabolites in a cell, organ or the whole organism. It is a well established mem-

ber of the '-omics' family together with genomics, transcriptomics and proteomics. It is often seen as arguably being "closer to phenotype" subject of study. Significant changes at the metabolite level have been demonstrated to be possible even when changes in transcript or protein concentrations are relatively low [Kell and Mendes, 2000]. Metabolomics in the most general sense is a global discovery science. In many cases analysis starts without a hypothesis and aims at identifying "points of interest" around which hypotheses can be built. Depending on the aims of the study, the analysis can take one of a few configurations including (a) fingerprinting, (b) footprinting, (c) profiling, (d) flux analysis and (e) targeted analysis. Metabolic fingerprinting is a global investigation of all measurable metabolites in the system without identification or quantification. It is usually performed for comparison of system metabolic states under different conditions. Footprinting is fingerprinting of the metabolome outside of the targeted system or the environment of the system and is usually performed for investigation of metabolite exchange. Metabolome profiling includes identification of metabolites and relative quantification in order to establish an interpretable profile of the metabolome under specific conditions. Tracing isotope labelled molecules allows flux analysis of metabolites in the target system and between the system and its environment. Targeted metabolomics usually refers to identification and absolute quantification of pre-specified metabolites in order to quantitatively characterise the effects of treatments or experimental conditions at the metabolic pathway level. All of these methods of study of the metabolome are only possible because of the progress in analytic platforms as well as the associated data analysis techniques.

1.3.1 Analytic Techniques and Applications

In principle collection of metabolomics data is a complex task. Metabolites in a biological system include a wide range of organic compounds such as nucleotides, amino acids, vitamins, hormones and other signalling molecules. There is no single analytic technique that would be able to quantify or even detect all the metabolites in the system. A range of analytic techniques have been adopted including Fourier transform infrared spectroscopy (FT-IR) and Raman spectroscopy, nuclear magnetic resonance (NMR) spectroscopy and mass spectrometry (MS) in metabolomic studies in order to acquire data appropriate for the aims of the study.

FT-IR and Raman spectroscopy are two techniques often referred to as vibrational spectroscopy. FT-IR is based on the principle that when infrared light is emitted towards the sample, the functional groups in the molecules absorb part of the energy and convert it into rotational or vibrational energy. The infrared light

that is not absorbed is detected and the absorbance spectrum is obtained. The absorption pattern then can be correlated to the chemical species present in the sample [Stuart, 2006]. This forms a spectrum that can be unique to the sample like a "fingerprint". While FT-IR is not as sensitive as other spectroscopic techniques such as mass spectrometry, its high throughput and reproducibility are seen as valuable advantages in a wide range of applications such as biomarker discovery [Harrigan and Goodacre, 2003], food science [Ellis et al., 2002] and bacterial metabolism studies [Kaderbhai et al., 2003]. Raman spectroscopy is different from FT-IR with the exchange of energy from a source is measured usually in the visible part of the electromagnetic spectrum. The Raman shift in energy of the light is observed that is traceable to specific chemical species. The advantage of Raman spectroscopy over FT-IR is that the water signal is not present and therefore the samples can be in tissue, in solution or even *in vivo* [Hata et al., 2000; Buschman et al., 2000; Yu et al., 2006]. The main limitation of Raman spectroscopy is that the Raman effect is weak and therefore the sensitivity of the technique is low compared to FT-IR.

Nuclear magnetic resonance (NMR) spectroscopy is a technique based on the phenomenon of nuclear magnetic resonance and provides information on the electronic environment of atoms including ^{1}H , ^{13}C, ^{15}N and ^{31}P (for more detailed discussion see Section 1.5). It produces information rich data however interpretation of spectra and information extraction is challenging. One-dimensional (1D) NMR experiments are the most popular however in complex mixtures like biological samples peak overlap becomes a problem due to high number and complexity of different resonances. Traditional 1D NMR experiments include nuclear Overhauser effect spectroscopy (NOESY) and Carr Purcell-Meiboom-Gill (CPMG) experiments. In order to address the problem of peak overlap in 1D spectra, two-dimensional (2D) spectra are used [Jeannerat and Furrer, 2012]. It gives additional information on signal connections in the spectra providing additional evidence for peak co-dependence. Common 2D NMR experiments include homonuclear correlation spectroscopy (COSY) [Xi et al., 2006] and total correlation spectroscopy (TOCSY) [Sandusky and Raftery, 2005], heteronuclear single-quantum correlation spectroscopy (HSQC) [Meier and Beeren, 2014] and J-resolved NMR spectroscopy [Huang et al., 2014]. Another limitation of NMR, especially in 2D experiments, is low sensitivity. This issue is partly remedied by improvements in technology such as increase in magnetic field strength [Gruetter et al., 1998], introduction of superconducting cryoprobes and low volume microprobes [Grimes and O'Connell, 2011]. While NMR spectroscopy has limitations it presents a variety of advantages over

other spectroscopic approaches. Firstly the relatively low sensitivity is compensated by very high reproducibility [Keun et al., 2002]. It requires small volume of sample and, in case of biofluids such as urine, blood plasma or cerebrospinal fluid, requires little sample preparation. It is also non-destructive and has relatively fast data acquisition. Due to non-destructive nature of the technique it allows other analyses to be performed on the same samples. No prior knowledge of the sample contents or separation steps (as in case of MS) is required. The samples can be analysed in an exploratory manner and sample contents inferred from the resulting data. For these reasons NMR is often used in untargeted metabolomics studies such as fingerprinting or footprinting where simple discrimination between samples from different treatments or experimental conditions is desired.

Mass spectrometry (MS) is a technique aimed at studying of molecular structure by measuring mass to charge ratios (m/z) of ionized molecules in a vacuum environment. The ionised molecules of the sample are produced in the ion source, accelerated and sorted by their m/z in the ion-analyzer and eventually measured by some form of detector. The relative abundance of each ion or ion fragment with unique m/z is then outputted as a peak in a spectrum. For accurate results each of the steps has to optimized and the system needs calibration as no single set of parameters is optimal for all types of analytes. The ion source [Bhardwaj and Hanley, 2014] and the ion analyzer [Forcisi et al., 2013] have to be carefully selected according to the type of study. MS suffers from the same problem as NMR when complex mixtures are analysed. Due to m/z overlap between ions the identification and quantification of molecules is difficult. This is partly solved by coupling MS with molecular separation techniques such as gas chromatography (GC) [Tsugawa et al., 2011], liquid chromatography (LC) [Becker et al., 2012] or capillary-electrophoresis (CE) [Volpi and Maccari, 2013]. These allow analytes to be eluted over time and therefore reduce the complexity of the mixture. MS is currently the most popular technique used in metabolomics. It is often used in metabolic profiling and targeted metabolomics studies where information on change in concentration of specific metabolites is required.

1.3.2 Metabolomics in Drug Discovery

A relatively new application of metabolomics is in the area of drug discovery and development. As a "close-to-phenotype" approach it provides tools to track and better understand drug action in cells and organisms [Kosmides et al., 2013]. Metabolomic techniques have been used in a variety of ways in the drug discovery and development process. These include investigation of drug modes of action [Creek

and Barrett, 2014], lead identification [Wu et al., 2012], quality control [Frederich et al., 2011; van der Kooy et al., 2009] as well as bioactivity assessment of natural sources of bioactive molecules such as medicinal plants [Yuliana et al., 2011]. Many metabolomic studies have focused on the search for diagnostic biomarkers especially in cancer [Patel and Ahmed, 2015]. Biomarker identification can be instrumental in drug development as well. Biomarkers can be used for disease progression and prognosis under treatment in order to assess drug efficacy and variability in patient response. Such approaches have already shown positive results in investigations of biomarkers for progression and prognosis of chronic kidney disease [Nkuipou-Kenfack et al., 2014], arthritis [Weljie et al., 2007] and lung cancer [Mathe et al., 2014] among other diseases. Another important application of metabolomics in drug development is assessment of drug toxicity through identification of toxicity biomarkers [Lindon et al., 2004; Vangala and Tonelli, 2007]. For example in Robertson et al. [2000] Wistar rats were exposed to hepatotoxic (CCI_4 and α-naphthylisothiocyanate) and nephrotoxic (4-aminophenol and 2-bromoethylamine) compounds. Urine samples from the rats analysed using 1D ^{1}H NMR showed differences between the rats experiencing toxicity and the healthy controls. In another study 1D ^{1}H NMR was used to show toxicity of candidate drugs by analysis of Wistar rat urine samples after administration of the drug [Dieterle et al., 2006b].

One of the most promising metabolomic approaches in drug discovery and development is metabolic fingerprinting. Due to the high throughput nature it can be used in high volume studies for lead selection or target validation. An example of target validation for specific compounds could be carried out as follows. A wild-type (WT) strain of a microorganism and a knock-out (KO) strain for the targeted enzyme could be used as controls. The drug exposure experiment would be carried out treating both strains with the compound generating a total of four conditions: WT, KO and both strains treated with the compound (WT+ and KO+). A fingerprinting approach e.g. NMR or MS could be used to collect the data and a chemometrics technique e.g. PCA or PLS-DA could be applied to investigate the sample clustering structure. In theory such a study could produce four different patterns in the results depending on the compound activity. If the compound was inactive, the data would show that the samples from each strain cluster together showing only difference induced by the knock-out. If the compound was active and specific to the target the WT+ would cluster with the KO and KO+ since the effects of target inactivation would be detected. In case of active but non-specific compound the treated samples would form a separate cluster as some secondary effects would be detected in both strains. The most ambiguous case would be if the

compound was active but specific to a different target. In such case no clusters would be formed as each sample group would show a different combination of metabolic effects. As the development of KO strains can be challenging it is important to note that the same aim could be achieved by using other well understood inhibitor of the target or monoclonal antibodies. A similar approach has been applied to show that 8-azaxanthine is a selective inhibitor of urate oxidase in *Aspergillus nidulans* Forgue et al. [2006]; D-Cycloserine (a tuberculosis drug) is a non-selective inhibitor and that alanine racemase is not its lethal target as previously thought [Halouska et al., 2007]. A similar study was performed with the aim to infer modes of action of unknown active compounds against tuberculosis [Halouska et al., 2012a]. Here instead of the KO strain a group of well known drugs were used as positive controls and the modes of action of unknown compounds were predicted from the clustering of metabolic readouts after exposure to known and unknown drugs.

1.4 Fourier Transform Infrared Spectroscopy

FT-IR is a spectroscopic technique based on the phenomenon that when molecules are irradiated with an infrared beam functional groups in the molecules will absorb part of the radiation and convert it into vibrations of chemical bonds. It has been used for decades in chemistry for compound characterisation and since the 1990's it has found its way into the biological sciences. As biological mixtures can be highly complex FT-IR has been used as a fingerprinting method for discrimination of samples collected under different conditions e.g. different microorganism strains, healthy and diseased tissues, biofluids from healthy and unhealthy individuals (see Section 1.3). FT-IR is a very rapid technique that can be performed on samples in a range of physical states including solutions, suspensions, viscous liquids, solids or powders [Colthup et al., 1990]. In principle there are no restrictions to the sample conditions employed including temperature, pH or pressure. This property is very convenient in biological and biomedical research where sample conditions are often desired to be altered as little as possible between the natural state and the measurement state. The rapid data acquisition and versatility in sample conditions makes FT-IR a potent tool for biological studies including high throughput screening.

1.4.1 Working Principles Behind FT-IR

Infrared (IR) radiation is a bandwidth between visible light and microwaves on the electromagnetic spectrum. The origin of IR radiation is usually thermal emission from a hot source. According to a convention IR is usually subdivided into three

regions, namely near infrared (NIR; 0.75 - 5 μm,), mid-wavelength infrared (MIR; 5-30 μm) and far infrared (FIR; 30-1000 μm), although some studies use different subdivisions. For most biological applications NIR or MIR is used. While the wavelength of electromagnetic radiation is usually measured in μm in IR studies it is often substituted for the wavenumber, which is the number of waves of the particular length that fit into a length unit, usually a centimetre, and measured in cm^{-1}. The IR spectrum consists of the measurements of IR radiation before (I_S) and after (I_R) passing through the sample. Data is usually presented in units of absorption $A = -log(I_S/I_R)$. The different bands in the spectra are the result of interaction between molecules in the sample and the IR light. The molecules in the sample absorb part of the energy at specific frequency and transform it into vibrational motions of the chemical bonds. The amount of energy at each frequency absorbed by the sample during the measurement forms the IR spectrum. FT-IR is different to traditional (dispersive) IR spectroscopy techniques in that a range of frequencies are emitted and measured at the same time. The data collected is called an interferogram and is mathematically processed into a spectrum. This approach provides much higher speed of measurement compared to dispersive IR. Emission of the range of frequencies is achieved through a Michelson interferometer that consists of two mirrors and a beam splitter that splits the IR beam into to equal parts (Fig. 1.2). One mirror is stationary and the other is movable.

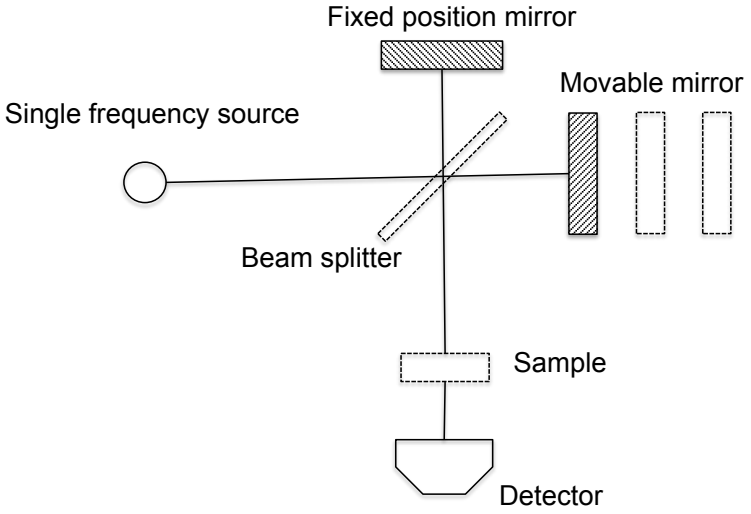

Figure 1.2: A schematic illustration of the FT-IR spectrometer.

The light originates at the source and is split by the beam splitter into two parts. One part is reflected to the stationary mirror and the other onto the

movable one. The beams reflected from the mirrors are combined and directed to the detector, where the difference of the intensities of the beams are measured as a function of the paths travelled by each beam. The measured signal is then amplified, digitized by the analog-to-digital converter and recorded. The result is a wave in time domain called an interferogram (Fig. 1.3).

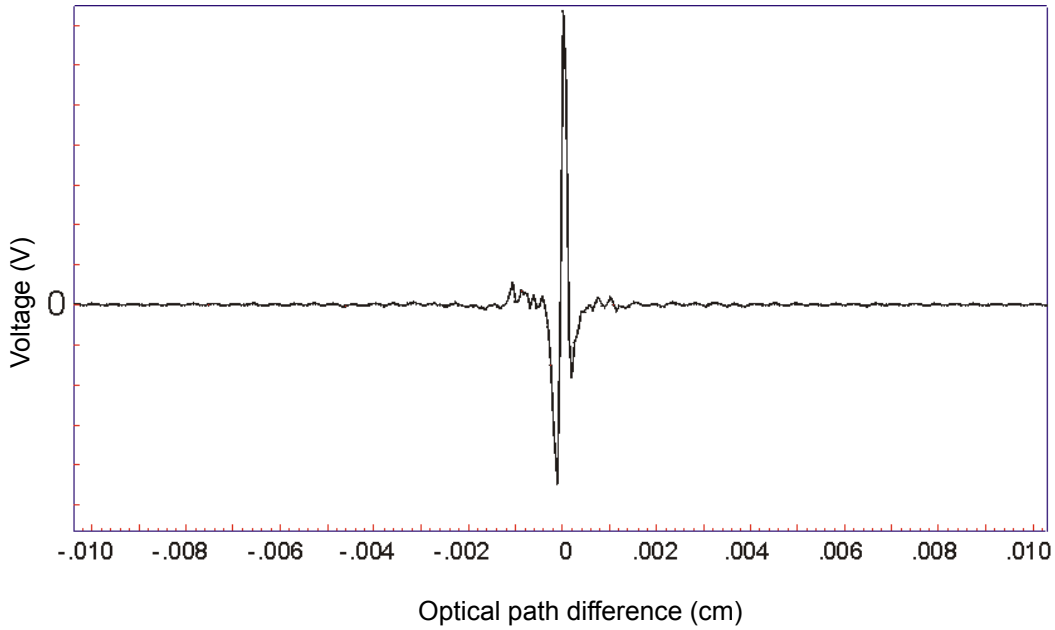

Figure 1.3: An example interferogram from an FT-IR reading.

The interferogram contains all frequencies of IR measured in the experiment superimposed into one signal. In order to convert the time domain interferogram into a frequency domain spectrum a Fourier transform is performed on the data (Fig. 1.3). After the transformation the data is ready to be processed and analysed.

1.4.2 Data Acquisition and Analysis

FT-IR readouts are usually taken of the sample positioned on a specially designed silicon plate. If the sample is in solvent a measurement of the background is taken in order to later be able to subtract the signal from traces of solvent molecules and gases dissolved in the solvent. In biological studies the data is acquired in the 4000-600 cm^{-1} range as it contains the molecule vibrational modes and in principle can be assigned to specific functional groups in the sample (Table 1.1). For metabolic fingerprinting applications the data is subject to multivariate analysis. Prior to the analysis the data is corrected for the CO_2 absorbances and parts of the spectra are often removed due to the non-relevant information contained in those parts. The

data is then scaled to unit variance to prevent variables with relatively greater values being weighted heigher in the results of the analysis. The data processing results in a data set where each sample is represented by a spectrum, and each spectrum consists of numeric values corresponding to absorbances at each wavenumber. In this format data can be subject to statistical analysis. The multivariate analysis techniques often used on FT-IR (and other spectroscopic techniques) data are discussed in Section 1.7.

Table 1.1: Tentative assignment of bands frequently found in biological FT-IR spectra.

Frequency (cm^{-1})	Assignment
3500	O-H str of hydroxyl groups
3200	N-H str (amide A) of proteins
2959	C-H str (asym) of -CH_3
2934	C-H str (asym) of $> CH_2$
2921	C-H str (asym) of $> CH_2$ in fatty acids
2898	C-H str of $\rightarrow$C-H methine
2872	C-H str (sym) of -CH_3
2852	C-H str (sym) of $> CH_2$ in fatty acids
1741-1715	$> C = O$ str of esters, carbonic acids, nucleic acids
1695	Amide I band components
1685	resulting from antiparallel β-pleated sheets
1675	β-turns of proteins
1655	Amide I of α-helical structures
1637	Amide I of β-pleated sheet structures
1548	Amide II
1515	"Tyrosine" band
1468	C-H def of $> CH_2$
1400	C=O str (sym) of COO^-
1310-1240	Amide III band components of proteins
1250-1220	P=O str (asym) of $> PO_2^-$ phosphodiesters
1200-900	C-O-C, C-O dominated by ring vibrations
	or carbohydrates, C-O-P, P-O-P
1085	P=O str (sym) of $> PO_2^-$
720	C-H rocking of $> CH_2$
900-600	"Fingerprint region"

Key: asym = asymmetric; sym = symmetric; str = stretching; def = deformation.

1.5 Nuclear Magnetic Resonance Spectroscopy

NMR spectroscopy is a powerful tool for metabolomics. It relies on elements that possess a magnetic spin number higher than zero and most of elements in organic compounds have an isotope with this property. The technique is operated in a magnetic field and uses electromagnetic radiation at radiofrequencies that allow for non-destructive data collection. It is also very robust and reproducible further adding to its value as a metabolomics tool. The one disadvantage of NMR spectroscopy is its low sensitivity compared to techniques like mass spectrometry. The most abundant nucleus observed by NMR is ^1H and therefore 1D ^1H NMR is the most popular among metabolomics researchers. We chose this type of NMR for this study and therefore all the following discussions of NMR spectroscopy will be describing 1D ^1H NMR experiments.

1.5.1 Working Principles Behind NMR

Nuclear magnetic resonance is a property of the nucleus of an atom that arises from its magnetic property called spin (I). Nuclei of atoms can have a range of values of I, the most useful for NMR are nuclei with $I = \frac{1}{2}$. This includes ^{1}H, ^{13}C, ^{15}N, ^{19}F, ^{31}P. A nuclear spin can be understood as an equivalent to a bar magnet. Placed in a magnetic field a particle with $I = \frac{1}{2}$ aligns itself either along or against the magnetic field entering one of two possible energy states. The nuclei in parallel with the magnetic field are in the lower energy state while the nuclei that oppose the direction of the external magnetic field are in the higher energy state. A pulse of radiofrequency can be absorbed by the nuclei in the lower energy state and be shifted to the higher energy state. This absorption or subsequent gradual release of the energy as the nuclei shift back to the lower energy state is recorded as the free induction decay (FID) and is the output of the spectrometer. In a sample each particle is affected by not just the external magnetic field but also the magnetic force exerted by the nearby particles. The effective magnetic field arising from combined magnetic influences to a nucleus determines the frequency of radiation it absorbs - its effective resonance frequency. Each observable nucleus in the sample contributes a signal to the spectrum at its resonance frequency with the area under the curve proportional to the abundance of that chemical group in the sample.

The Anatomy of an NMR Spectrometer

The NMR instrument consists of several major components:

- the magnet

- the probe
- radiofrequency sources
- the field frequency lock system
- the shim system
- signal amplifier
- analog/digital converter (ADC)
- computer

The magnet provides the external magnetic field B_0 to the sample. Nowadays it usually is a superconducting magnet, consisting of a coil submerged into liquid helium in order to reduce the electric resistance in the coil to zero. The probe is positioned inside the magnet within a shim tube. It contains the receiver/transmitter coil (in some cases two coils tuned to different frequencies) that detects the signal. The radiofrequency sources produce the sine/cosine shaped waves as well as modulated and shifted waves that are used to excite the nuclei during the experiment. The signal amplifiers are connected to the probe and are used to amplify the signal delivered from the probe before it reaches the ADC. The signal detected in the NMR spectrometer is analog and has to be digitised before it can be subject to Fourier transformation. The digitisation of the signal is performed by the ADC. Usually 16 - 18 bit digitizers are used which places a bound on the signal amplitude resolution at 2^{18} points. Due to this technical limitation the receiver gain of the spectrometer has to be adjusted so that the peak with the highest amplitude in the spectrum is as close to 2^{18} as possible to achieve the maximum amplitude resolution. The digitized signal is then sent to the computer where it is stored, processed and analysed.

The shim system is a system of small coils that act as adjustable magnets around the sample. Since the signal depends on the magnetic field strength a highly homogeneous magnetic field is required to collect high resolution data. Inhomogeneity of the magnetic field in the sample would result in broadening of the peaks in the spectrum due to slightly varying frequencies of resonance of the same functional groups in different parts of the sample volume. The shimming system is used to correct such inhomogeneities in the magnetic field provided by the main coil.

The deuterium lock system is used to ensure the stability of the magnetic field. The magnetic field in the spectrometer drifts over time. Due to the field drift the resonance frequencies of nuclei also drift resulting in peak broadening. The lock system measures the frequency of deuterium in the sample (every sample is prepared with deuterated solvent) and uses its peak position as the anchor-point to keep the magnetic field stable. As the magnetic field changes over time it is detected by the

lock system as a shift in the deuterium peak which prompts the system to adjust the magnetic field so the peak is shifted back to its original position consequently keeping the data signal stable.

Origin of the NMR Signal

As mentioned previously NMR spectroscopy relies on nuclear spin that gives rise to the effect of nuclear magnetic resonance. Spin is a fundamental property of elementary particles and can have values that are multiples of $\frac{1}{2}$. Proton has a spin of $\frac{1}{2}$ and is the most popular nucleus (we will refer to it as proton) in NMR studies. The spin can be understood through the analogy of a magnet bar that has south and north poles, or a needle of a compass and can be represented as a magnetic vector. When placed in a magnetic field B_0 the magnetic vector aligns to the direction of the field in a parallel or anti-parallel way that corresponds to two energy levels: lower α and higher β, respectively. A proton in α state can absorb a photon of a specific energy and shift to the β state. The energy of the photon is

$$E = h\gamma B \tag{1.1}$$

where γ is the gyromagnetic ration of the particle (for hydrogen, $\gamma = 42.58$ MHz/T), B is the magnetic field strength and h is Planck's constant ($h = 6.626 \times 10^{-34} Js$). This energy is equal to the energy difference between the α and β states. In the experimental conditions we always speak about a group of protons in the sample as opposed to each proton separately. All the protons align parallel or anti-parallel to the external magnetic field. The populations of protons in each spin state at room temperature are not equal. The number of protons in the lower energy level (N^+) is higher than the number of protons in the higher (N^-). From Boltzmann statistics

$$\frac{N^-}{N^+} = e^{-E/kT} \tag{1.2}$$

where E is the energy difference between the spin energy states, k is the Boltzman constant ($k = 1.3805 \times 10^{-23} J/K$) and T is the temperature in Kelvin. As the temperature increases the ratio approaches one. The signal in the NMR originates from the differences in energy absorbed and subsequently released by the spins as they transition between energy states. For this reason the signal is proportional to the difference between populations in each state.

The energy difference between spin states determines the energy of the photon needed to be absorbed for the particle to shift to the higher energy state. This

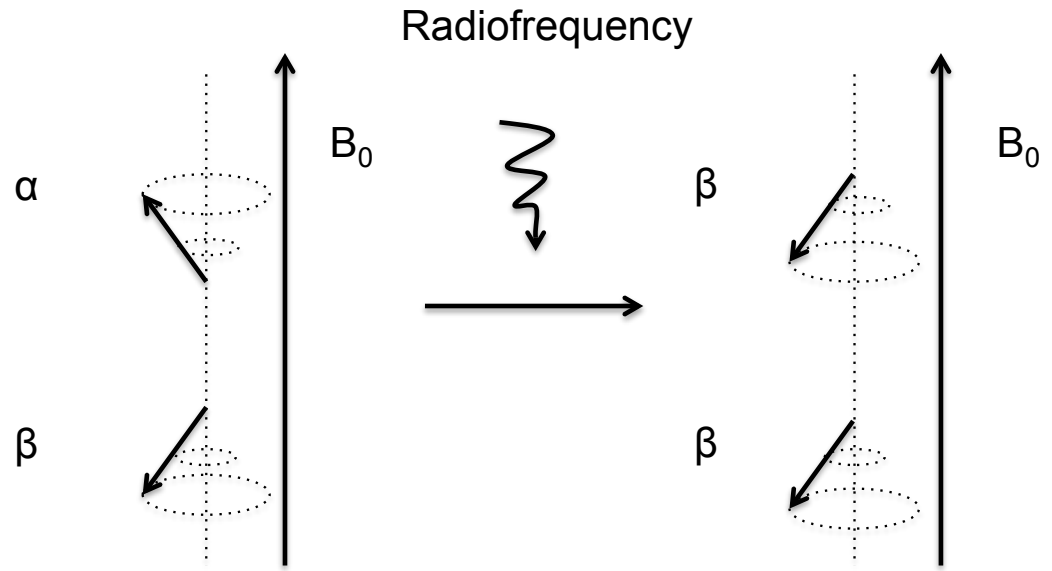

Figure 1.4: Schematic illustration of the flip of magnetisation vectors of nuclear spins through application of a radiofreaquency in the NMR probe. B_0 - external magnetic field, α, β - two energy states of the nuclei.

energy depends on the magnetic field strength the particle is in. In an NMR experiment the magnet provides the external field (B_0) however this field is not experienced equally by all protons. The magnetic field affecting each proton is altered by the magnetic fields created by the neighbouring nuclei. This alteration is often called the magnetic shielding and it determines the size of the effective magnetic field (B_{eff}) a particle is affected by. The energy required to excite a proton to the higher energy state therefore depends on B_{eff} rather than B_0. Subsequently in experimental conditions the population of protons consists of subpopulations that differ in the energy required to excite the protons in that subpopulation.

In an NMR experiment the energy is provided by the electromagnetic pulse that contains a range of frequencies. The energy can be related to frequency (ν) through

$$E = h\nu \tag{1.3}$$

and in an NMR experiment falls in the radiofrequency range. The differences in excitation energy (frequency) are recorded in the NMR spectrum as different peaks.

When the spins are in the magnetic field aligned to the magnetization vector of the external magnetic field, the alignment is not perfectly parallel or anti-parallel

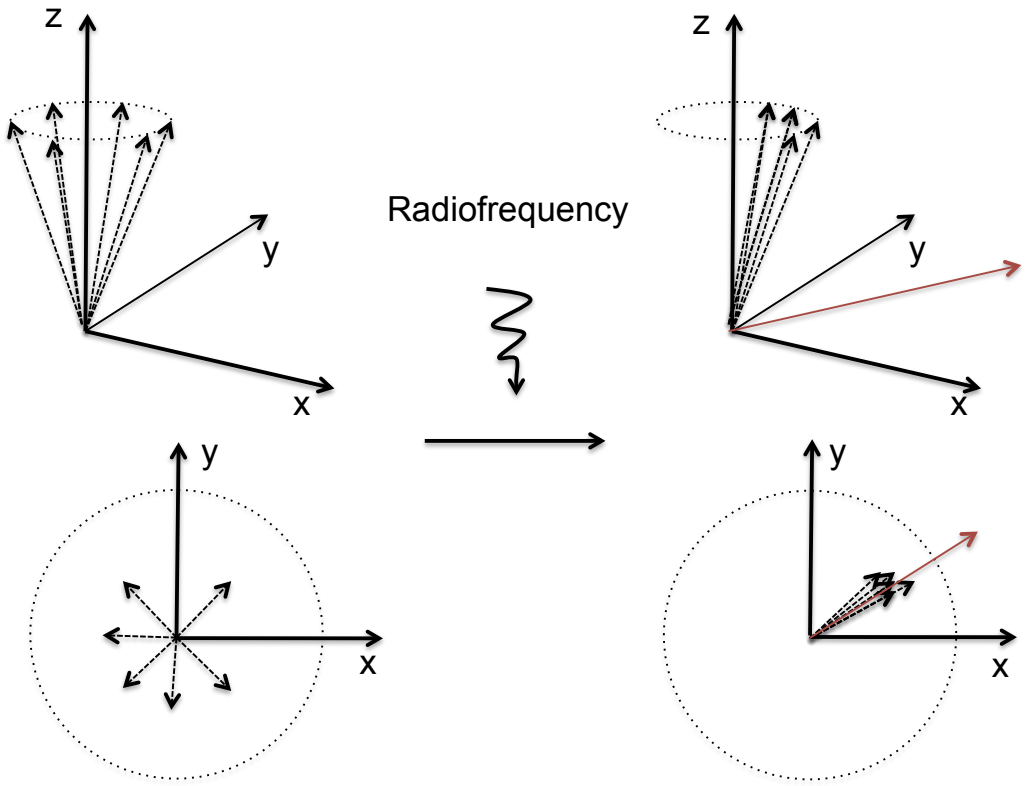

Figure 1.5: Schematic illustration of magnetisation vector synchronisation after the application of the radiofrequency pulse. Top - a view in 3 dimensions, bottom - projection onto the xy plane. The red arrows represent the projection of the net magnetisation vector in the xy-plane that is measured by the detector.

to the field. The spins form an angle with the vertical magnetization vector of the external field (as a convention in a 3-dimensional (xyz) representation of the system the external field magnetization vector is thought to be on the vertical (z) axis). Furthermore the magnetization vector of each particle is not stationary but precesses around the vertical axis. If we look at the projection of the vector in the xy plane it would appear as a vector rotating around the origin. Since the protons in a real system are not correlated in phase the sum magnetization vector on the xy plane is zero. A pulse of radiofrequency can be used to correlate the phase of the precession of magnetization vectors that makes the sum projection on the xy-plane greater than zero and therefore measurable by the detector. Since the detector only records the signal on one axis the signal oscillates like a sine function as the magnetization vector rotates around the z axis. Over time the system returns to the initial equilibrium state and the the magnetization on the xy plane reduces to zero. This is referred to as relaxation. The signal recorded by the detector is therefore a

decaying oscillation over time - the free induction decay.

1.5.2 An NMR Experiment

Data Acquisition

An NMR experiment consists of the following steps:

- preparation and insertion of the sample
- setting the temperature
- locking
- shimming
- acquisition parameter set-up
- tuning of the probe
- calibration of the 90° pulse
- data acquisition

The sample is prepared with a deuterated lock solution and a reference compound, typically tetramethylsilane (TMS) or trimethylsilyl propionic acid (TSP). The sample is transferred to a glass NMR tube (1.7mm, 3mm or 5mm diameter) and placed into a spinner. The spinner with the sample is then placed at the top of the magnet and lowered into the probehead via air-lift. Setting the correct temperature is important depending on the sample properties e.g. higher temperature is recommended for more viscous samples. Once the sample is placed in the probehead the lock is set. Locking to the deuterium signal is required in order to keep the magnetic field from drifting. Since each sample has slightly varying magnetic properties shimming is carried out. This consists of adjusting shimming coils in order to homogenize the magnetic field in the sample in order to avoid peak broadening. The probe has to be tuned to each sample as well due to the varying impedance of each sample. Sample properties such as ionic strength and pH can significantly influence the signal. The signal in the NMR spectrometer is detected when the magnetisation is flipped to the xy plane. The pulse that flips the magnetisation has to be adjusted for each sample by adjusting the pulse duration. This is usually achieved by repeated collection of spectra with increments of pulse duration until the maximum value of the signal is found which corresponds to the signal achieved with optimal 90° pulse. The data can then be collected according to the acquisition parameters set for the experiment.

Data Processing

The acquired data is in the form of a FID. It is a complex composite signal consisting of a series of oscillating signals (one for each group of nuclei with unique resonance frequency) that is detected by the receiver, amplified, digitized and recorded. In order to obtain an NMR spectrum ready for analysis from a FID there are a series of processing steps:

1. FID processing
   (a) apodization
   (b) zero-filling
   (c) Fourier transform
2. spectrum processing
   (a) phase correction
   (b) baseline correction
   (c) warping
   (d) binning and integration
3. bin processing
   (a) normalization
   (b) scaling

Apodization is a transformation of the FID in order to manipulate spectral resolution and signal to noise ratio (S/N). The resolution of the spectrum depends on the speed of decay of the FID therefore the amount of signal remaining will determine the resolution (more signal at the end of the FID means more resolution). The S/N on the other hand depends on the amount of the signal at the beginning of the FID. Therefore by manipulating the FID it is possible to trade between S/N and resolution. e.g. multiplying the FID by an exponential function (exponential apodization)

$$W(t) = e^{-\pi lbt} \tag{1.4}$$

where lb is the value of line broadening to apply, will result in improved S/N at the cost of resolution, while multiplication by a Lorentz-to-Gaussian

$$W(t) = e^{\pi lbt} \times e^{-gbt^2} \tag{1.5}$$

where lb is the line broadening factor and gb is the centre of the Gaussian emphasizes the middle and tail parts of the FID and will increase the resolution at the cost of S/N.

Zero filling is a procedure used to maximise the resolution of the spectrum obtained from the Fourier transform. It consists of adding a series of zeros after the FID equal to the number of points in the FID. After the zero-fill the Fourier transform is performed in order to transform the time domain FID into the frequency domain spectrum. The Fourier theorem states that every periodic function can be decomposed into a series of sine and cosine functions with different frequencies and is defined as

$$f(\omega) = \int_{-\infty}^{\infty} f(t)e^{-i\omega t}dt = \int_{-\infty}^{\infty} f(t)[cos(\omega t) - isin(\omega t)]dt \tag{1.6}$$

where ω is the frequency and t is time. In practice the FID is discrete and the Fourier transformation is performed using the Cooley-Tukey fast Fourier transform (FFT) algorithm [Cooley and Tukey, 1965] which converts a discrete time-series x_k of length N into a spectrum with N points:

$$f[n] = \frac{1}{\sqrt{N}} \sum_{k=0}^{N-1} x_k e^{-2\pi kn/N} \tag{1.7}$$

It has a constraint that the number of points in the FID has to be a power of 2. Therefore the number of points collected in a FID is usually 16384, 32764, 65536, etc.

The phase of the NMR signals in the spectrum depends on the phase at the begining of the FID which is determined by the phase of the magnetization vector in relation to the receiver coil. If it starts as a sine wave the spectrum is going to be purely dispersive (asymmetric peaks) while if FID starts as a cosine wave it is purely absorptive (symmetric peaks). The purely absorptive signal makes the analysis easier as the narrower base peak differentiation makes it more convenient. In order to achieve the pure absorptive signal the measurement would have to start at exact moment after the pulse. However due to cable delay as well as the delay for protection of the probe against overload the signal detection and digitization delayed. For this reason in order to obtain a purely absorptive spectrum post-acquisition phasing has to be performed. It is usually done by hand by adjusting the phasing angle until a fully positive-valued spectrum is achieved, however algorithms for automatic phasing have been proposed [Cieslar et al., 1988; Chen et al., 2002; Bao et al., 2013]. For effective NMR data analysis it is desirable that the baseline of the spectrum is

as flat as possible. This is not always achieved by default and baseline correction is required in the processing phase. A variety of methods for baseline correction of NMR spectra have been proposed [Bartels et al., 1995; Brown, 1995; Golotvin and Williams, 2000; Xi and Rocke, 2008]. The methods are based on fitting functions to the baseline and subtracting the fitted values from the spectrum to flatten the baseline. Another frequent problem in preparation of NMR data for analysis especially in metabolomics studies is peak shifts due to pH and ionic strength variation between samples. This makes data comparison, especially using automated methods, harder. There have been a series of algorithms proposed for automatic alignment (warping) of NMR spectra [Forshed et al., 2003; Lee and Woodruff, 2004; Veselkov et al., 2009]. The algorithms are usually based on dividing the spectra into segments and using an optimization algorithm to shift the segments until the optimal alignment is achieved.

In metabolomic studies, after the spectrum is processed it is reduced in dimensionality through binning and integration under the curve. Since the spectra acquired in the NMR experiments often contain more than 30,000 data points it is not efficient to perform statistical analysis on such a high-dimensional dataset. Therefore the spectra are divided into segments and for each segment the area under the curve is computed. The most popular methods of binning are "uniform", when binning is performed in intervals of a constant preset length (e.g. 0.05 ppm), and "adaptive", when the intervals are of variable length and each spans a peak or a group of peaks. The latter can be performed manually by creating a bin table that is used for the whole experiment or through the use of an automated algorithm [Keun et al., 2003; Davis et al., 2007; Worley and Powers, 2015].

A binned dataset is then subject to normalization and scaling. Normalization is a process of transformation of data to account for differences between samples (e.g. dilution factors) making them comparable to each other. In such a case the spectra can be normalized either by the area of a peak that is invariant between samples, the reference peak or the total integral of the spectrum [Craig et al., 2006]. Data scaling on the other hand is performed on each variable (in this case each bin) across the dataset. It makes the variables more comparable and avoids unwanted weighting of the data without biological content contributing to the results and suggesting errorneus conclusions [van den Berg et al., 2006].

Correct data processing is a key step to obtaining high quality data that will yield high quality information and correct interpretation of the results. In the NMR experiments many of the processing steps have a range of alternative methods to choose from and often there is no "gold standard". It is often trial and error that

yields the best results for each specific case.

1.6 High Content Imaging

High content imaging (HCI) technique, often more generally called high content screening (HCS), can be defined as imaging based approaches for understanding cell processes, morphological structures, viability and drug interactions. Its most popular applications are cell assays in biological and biomedical research and especially drug discovery. Automated cell imaging techniques have been used in drug discovery research for at least two decades. They have been used in identification of a variety of compounds, including monastrol - a mitotic inhibitor [Mayer et al., 1999] and *src* family kinase inhibitor SU6656 [Blake et al., 2000]. It has also been applied in quantitative studies such as the characterisation of NF-κB translocation to the nucleus [Ding et al., 1998]. With the development of high content imaging (HCI) technology, combining automated bright-field and fluorescent imaging with powerful image analysis methods, the imaging-based studies have gained scalability and their applications have broadened to include high throughput studies such as cell-screening assays [Rausch, 2006]. Besides the rapid data collection the high content imaging platforms have the ability to collect a diverse set of parameters that are rich in information for analysis. HCI is used in, among others, cell viability assays [Gilbert et al., 2011], tracking the effects of gene knockdown [Winograd-Katz et al., 2009; Zhang and Boutros, 2013] and gene function analysis through temporal cell phenotyping [Neumann et al., 2010; Failmezger et al., 2013]. Due to its high throughput capabilities HCI has been rapidly adopted in the field of drug discovery. It has been applied for drug target identification for cancer [Adams et al., 2014] and obesity [Kim et al., 2014], drug toxicity assays [Persson et al., 2013; Peyre et al., 2015], lead identification assays for diabetic cardiopathy [Drawnel et al., 2014], Hutchinson-Gilford Progeria Syndrome (HGPS) [Kubben et al., 2015] and infectious tropical diseases such as trypanosomiasis [Sykes and Avery, 2015], leishmaniasis [Siqueira-Neto et al., 2012; Aulner et al., 2013] as well as onchocerciasis and lymphatic filariasis [Clare et al., 2015]. HCI has been applied to a variety of aspects of malaria biology including drug efficacy assays [Biagini et al., 2012], target validation [McNamara et al., 2013] as well as life stage classification and viability quantification [Moon et al., 2013].

1.6.1 HCI Experiments and Data Collection

The three key components in an HCI experiment are cells bound with a fluorophore in order to visualize appropriate cellular components, an image collection platform and image analysis algorithms. The fluorophores can roughly be classified into three categories: autofluorescing proteins that are engineered into the cells [Talman et al., 2010], fluorescent dyes that enter the cells and concentrate in a particular compartment or bind intracellular components such as SYBR Green [Zipper et al., 2004] or Hoetch [Latt et al., 1975], and antibodies with affinity to the desired target that are directly tagged with a fluorescent molecule. The fluorescent tag helps to visualize the target component of the cell.

The image collection platform usually consists of a fluorescence microscope, a dynamic system for positioning the cell culture plate under the microscope, a high resolution camera system for capturing the images and a mechanism for data storage [Gough and Johnston, 2006]. The system is usually equipped with a set of excitation and emission filters to allow for selection of wavelengths during image capture. This allows multiple probes to be used in the same sample without much interference. Some systems (Opera, Perkin Elmer) come with multiple digital cameras that allow simultaneous multichannel image capture. Simultaneous image capture is quicker than the sequential method however it requires careful selection of fluorescent probes to avoid wavelength overlap [Lee and Howell, 2006].

Software plays a very important part in the high content imaging pipeline. The first part is the software that controls the imaging system. It is used to set the parameters for the experimental procedure. It collects the images and stores them in a database system, reports faults and performs quality control. The second part of the software in the pipeline is the data analysis software. The analysis software is used for data visualization and data processing which includes artefact detection, selection of the fluorescent signal fields and measurement of a variety of parameters including size, intensity, various shape and texture parameters, and behaviour over time. The user defines the analysis parameters and the images are automatically processed. Once the assay is tested and validated the system can run mostly automatically allowing for robust high throughput data collection [Berlage, 2005; Pepperkok and Ellenberg, 2006].

1.7 Statistical Data Analysis

Both metabolomics and high content screening studies produce multivariate data. Whether it is a raw spectrum, a set of spectral bins or a set of measurements of image

regions the data consists of multiple measurements per sample and often the number of variables (measurements) exceeds the number of samples. Such cases demand multivariate techniques for analysis - data explorations and hypothesis generation, pattern detection or hypothesis testing. Here we briefly introduce the statistical techniques used in this work. We discuss some mathematical definitions, the intuition behind the methods and result interpretation as well as suitable applications and their merits.

1.7.1 Principal Component Analysis

Principal component analysis (PCA) is a linear data transformation that yields a set of latent (unobserved) variables, usually referred to as principal components (PC). Principal components are linear combinations of raw variables such that the first principal component contains the most variation from the original data. The subsequent principal components are selected to be orthogonal to the first one and contain maximum variance unaccounted by preceding PCs. This procedure creates a new data set where each variable is substituted by a PC however only a small number of PCs is required to account for the majority of the variance in the original data. As only a small amount of variance is accounted for by a large set of PCs they can be ignored without losing much information, effectively reducing the data set to a smaller number of variables. PCA is often referred to as a dimensionality reduction technique as the reduction of number of variables can be seen as projecting the data to a lower-dimensional space. PCA is usually performed in order to reduce the dimensionality of the data for easier visualization or more robust modelling. Plotting the first two or three principal components as a scatterplot is often used as an exploratory method to get insight into the structure in the data. For example clustering of data points (each point represents a sample) might be observed suggesting similarities between treatment effects if points cluster together (and *vice versa*). PCA is often used to reduce the number of variables before applying a predictive modelling technique as the smaller number of variables often lead to simpler and subsequently more robust models.

PCA is usually performed in one of two ways: either through Eigen decomposition of the covariance matrix of the data or through singular value decomposition (SVD). The latter method is more numerically stable and therefore is preferred in most cases. SVD decomposes a mean-centered (each column has its mean subtracted from it) $m \times n$ matrix $\mathbf{X}$ into three parts:

$$\mathbf{X} = \mathbf{U}\mathbf{D}\mathbf{V}^T \tag{1.8}$$

where $\mathbf{U}$ is an $m \times m$ matrix containing the left singular vectors, $\mathbf{D}$ is an $a \times a$ diagonal matrix containing the singular values and $\mathbf{V}$ is a $n \times a$ matrix of right singular vectors. The product $\mathbf{UD}$ constitutes the so called PCA scores matrix. The scores matrix is the transformed data obtained from the PCA and used for visualization of further analysis. The $\mathbf{V}$ matrix is the loadings matrix whose columns contain the weights of the original variables in each PC. They can be investigated in order to determine variable contribution to each PC. The diagonal matrix $\mathbf{D}$ contains values whose squares are proportional to the variances accounted for by each corresponding PC

$$\lambda_i = d_i^2/(n-1) \tag{1.9}$$

where λ is the variance of the i-th component and the fraction of variance accounted for by each PC can be calculated from

$$F(i) = \lambda_i / \sum_{j=1}^{a} \lambda_j \tag{1.10}$$

The fraction of the variance accounted for by each PC can be used to assess the information provided by keeping each principal component. Often the first few principal components account for the majority of the variance and the structure in the data can be adequately visualized by plotting the PCs.

1.7.2 Linear Discriminant Analysis of Principal Components

Linear discriminant analysis (LDA) is a classification technique that transforms the data into a different space where the discrimination between groups in data is maximised while within group differences are minimised. It is similar to PCA in that the data is linearly transformed into a different space, however while PCA aims to find the directions of maximum variance in the data as a whole, LDA finds the directions of maximum separation between groups. LDA is therefore performed on data that has grouping labels (e.g. sample treatment groups) and is often used as a technique to show differences between treatments. The resulting model can also be used to assign new data samples to groups in the data that model was built on (this procedure is usually referred to as model training). Formally the LDA finds the linear combination of variables $\mathbf{a}$ that maximises the ratio of the sum of square differences between groups $\mathbf{B}$ and the sum of square differences within groups $\mathbf{W}$:

$$\mathbf{a}^T\mathbf{Ba}/\mathbf{a}^T\mathbf{Wa} \tag{1.11}$$

where $\mathbf{W}$ and $\mathbf{B}$ are calculated as

$$\mathbf{W} = \sum_{i=1}^{G} \tilde{\mathbf{X}}_i^T \tilde{\mathbf{X}}_i \tag{1.12}$$

$$\mathbf{B} = \sum_{i=1}^{G} n_i (\bar{\mathbf{x}}_\mathbf{i} - \bar{\mathbf{x}})(\bar{\mathbf{x}}_\mathbf{i} - \bar{\mathbf{x}})^T \tag{1.13}$$

where G is the number of groups, $\tilde{\mathbf{X}}_\mathbf{i}$ is the mean-centered data matrix only containing objects of group i, $\bar{\mathbf{x}}_\mathbf{i}$ is the mean vector for the group i and $\bar{\mathbf{x}}$ is the mean vector for the whole data. The $\mathbf{W}$ is the variation within each group (around group centre) and $\mathbf{B}$ is the variation of the group centres around the global mean. The solution a is found by maximising Equation 1.11.

As the number of variables in the data increases the LDA model becomes less robust and requires more data. In cases when the data is high-dimensional it is often beneficial to reduce the dimensionality of the data before performing LDA. PCA is a frequently used method for this purpose. The technique is then referred to as LDA-PC or DA-PC. In order to build a robust LDA-PC model and avoid fitting to the noise in the data (overfitting) the number of PCs to be used for LDA has to be determined. A popular way of model selection is cross-validation. It consists of splitting the data into subsets and training the model on the data leaving one subset out - so called N-fold cross-validation, where N is the number of partitions - and using that partition to test the model. A robust model will perform similarly on each of the partitions. Such a cross-validated scheme of model building can be then used on data consisting of increasing number of principal components and each time a model fit metric e.g. Q^2 can be used to assess the model. The best average metric value will determine the optimal number of PCs to use.

1.7.3 Partial Least Squares Discriminant Analysis

Partial least squares discriminant analysis (PLS-DA) is an application of partial least squares (PLS) regression method using a nominal response vector (or matrix in case of more than 2 group problem) in order to perform classification. PLS is similar to PCA in that it also computes a linear combination of data variables. However while PCA aims to produce a weights matrix that reflects the structure of the covariance between the data variables (predictors), PLS aims to find a weights matrix that reflects structure of the covariance between the predictor and the response variables. Given data matrix $\mathbf{X}$ and response matrix $\mathbf{Y}$ PLS computes a weight matrix $\mathbf{W}$ that is used to produce a score matrix $\mathbf{T}$

$$\mathbf{T} = \mathbf{XW} \tag{1.14}$$

such that covariance between $\mathbf{Y}$ and $\mathbf{T}$ is maximised. Ordinary least squares procedures are used to regress $\mathbf{Y}$ on $\mathbf{T}$ in order to compute a weights matrix $\mathbf{Q}$ such that

$$\mathbf{Y} = \mathbf{TQ} + \mathbf{E} \tag{1.15}$$

where $\mathbf{E}$ is an error matrix. The model is then defined as

$$\mathbf{Y} = \mathbf{XB} + \mathbf{E} \tag{1.16}$$

$$\mathbf{B} = \mathbf{WQ} \tag{1.17}$$

The model is usually computed using the NIPALS algorithm [Geladi and Kowalski, 1986]. While PLS regression is used to predict response variables PLS-DA is used to predict classes of the observations. It is done by using "dummy" variables to form a binary $n \times p$ matrix $\mathbf{Y}$ where n is the number of observations and p is the number of groups minus one such that $\mathbf{Y}_{ij} = 1$ if observation i belongs to class j and otherwise $\mathbf{Y}_{ij} = 0$. This matrix is then used in the PLS algorithm as the response matrix. In order to avoid model over-fitting an appropriate number of components to be used in the model has to be selected. For this purpose the same cross-validation procedure as in Section 1.7.2 can be used.

1.7.4 Permutation Test

A permutation test is a type of statistical randomization test when the null distribution of a test statistic is obtained by random permutations of the class labels on the observations. It is assumed under the null hypothesis that if there is no difference between groups (treatments, classes) of the observations, permutation of the class labels will not influence the statistic. However is the null hypothesis is false the test statistic will differ based on the label assignment. The null distribution derived from the random permutations of class labels is used to calculate the p-value of the test statistic of the real-labelled data. For example if a two-sample test of difference between the means ($\Delta\bar{x}$) had to be computed the null distribution for the $\Delta\bar{x}$ could be obtained by randomly permuting the group membership labels on the samples and calculating the difference between the means of the "new" data groups ($\Delta\bar{x}^*$). Repeating this a number of times (1000 is a good rule of thumb) forms a distribu-

tion of possible $\Delta\bar{x}$ values under the null hypothesis. The p-value would then be the proportion of the samples as or more extreme than the value obtained from the correctly labelled data.

The permutation test is a non-parametric test that is useful in cases where assumptions about the distribution of the test statistic are weak or the distribution is intractable.

1.7.5 Hierarchical Clustering

Hierarchical clustering (HC) is an algorithm designed to describe grouping structure in the data. Clustering algorithms are usually used for finding groups of observations where no information about the grouping of observations is present. The HC algorithm builds a clustering tree based on the similarity/dissimilarity of the observations. The similarity is usually defined as a distance function, most often the Euclidean distance between data points. The algorithm works in either agglomerative (most popular) or divisive fashion. In the first case the data points start as separate clusters and based on the similarity the two closest points are linked together and become a cluster. The cluster substitutes the points and the distance matrix is recalculated to include the cluster. The same procedure is repeated until there are no unlinked points left. In the divisive case the process is opposite : all points are linked, the least similar clusters are found in each iteration and separated until there are as many clusters as there are points. There is a variety of linkage methods that can be used to compare the points/clusters. Given two clusters of points (if there is only one point in the cluster its position is used) the single linkage measures the distance between the closest points in each cluster, the average linkage between the centres of the clusters, while the complete linkage takes into account the most distant points in each cluster. The result of HC is a tree-like structure of cluster memberships. The most popular way to visualize the result is a dendrogram - a tree diagram with the stem at the top and "leaves" that represent observations at the bottom. The vertical distances between the branches are proportional to the distances between the neighbouring groups. All the "leaves" are connected to the stem and the branching structure describes the similarity between the observations. The dendrogram does not perform clustering *per se* but assigns a hierarchical structure to similarities of the points. It has to be cut across the branches to separate the observations into groups. The usual way to cut the dendrogram is to find the longest vertical distance between branching points on the dendrogram and cut the it at that level. The cutting of the dendrogram assigns the cluster membership to each observation. Hierarchical clustering is a popular technique as the intuitive tree

structure of data representation is informative and easy to interpret. However it has a downside that there is no failsafe mechanism to prevent the algorithm from finding clusters in the data where there is no clustering structure. In such cases the tree can still be built and, when cut, will produce cluster assignments. The easiest way to avoid this is through data exploration or prior knowledge. Plotting original observations is often helpful in order to find general patterns in the data. If the data is known (or seen in the plots) to contain some clustering structure it can be expected to be present in the dendrogram and the clustering results. When applying hierarchical clustering it is advisable to be careful with data lacking known structure and exploratory analysis prior to clustering is often very useful.

1.7.6 Multiple Dataset Integration

Multiple dataset integration is a Bayesian correlated clustering method that performs clustering of observations between multiple datasets [Kirk et al., 2012]. The clustering is called correlated because the clustering structure within one dataset influences the clustering within the other datasets. This method was developed in order to detect similar clustering structure between datasets that contained similar information from different data sources, e.g. gene expression and protein-protein interaction data. Each dataset is modelled separately and the similarities between clustering structures in each dataset are learned. This provides the ability to use datasets of various data types (real-valued, categorical, time-series) together. The model produces cluster assignments for each measured entity (gene expression, metabolite concentration, etc.) in each dataset and thus provides information about the groups of measured entities that show similar behaviour. On the other hand MDI can also be used to compare datasets containing measurements of the same variables but under different conditions (drug treatments, growth conditions, etc.). Similar clustering structure would then suggest similarity between conditions and *vice versa*. The method is significantly more complex than other methods described above a and more detailed explanation is omitted here.

Chapter 2

Materials and Methods

In this chapter we describe methods of *P. falciparum* culture, experimental procedures, setups for FT-IR, NMR and high content imaging data acquisition and the data analysis techniques used in this study. The methods are described in detail to allow reproducibility of the experiments. Method development procedures that resulted in some of the experimental protocols provided below are discussed in the following chapter.

2.1 Parasite Cultures

The *P. falciparum* cultures were maintained in standard medium containing human erythrocytes at 2.5% haematocrit and below 10% parasitemia, incubated at $37°C$. All the manipulations were performed in an Envair class-II laminar flow cabinet in aseptic conditions. 70% Ethanol (Aldrich Chemical Co.) was used during work in the safety cabinets in order to minimize risk of contamination. All solutions were prepared with distilled water and filter-sterilized through a bottle top filter with a 0.22 μm membrane (Fisher Scientific) and stored at $4°C$. Parasites were cultured in 25 cm^2 and 75 cm^2 Nunc^{TM}tissue culture flasks (Fisher Scientific). *P. falciparum* strain 3D7 was used throughout this study.

2.1.1 Culture Medium

The culture medium was prepared by adding 12.5 mL of sterile 1M HEPES (4-(2-hydroxyethyl)-1-piperazine ethane sulphonic acid), 200 μL of 50 mg/mL gentamycin (Sigma, UK), 25 mL of 5% Albumax I (Gibco, UK) solution and 5 mL of 4 mM hypoxanthine solution to 500mL of RPMI-1640 (Sigma, UK) [Trager and Jensen, 1976; Radfar et al., 2009b]. Culture medium was filter sterilized before use unless

specified otherwise. It was prepared each week with unused medium discarded after one week.

HEPES - 1 M stock solution was prepared from powder (VWR International, UK) in distilled water and pH adjusted to 7.4 with NaOH. The stock HEPES solution was then filter sterilized and stored at $4°C$ for up to 6 months.

Albumax I - 5% stock solution was prepared from powder (Gibco, UK) in distilled water, filter sterilized and stored at $4°C$ for up to 6 months.

Hypoxanthine - 4 mM stock solution was prepared from powder (Sigma, UK) in 0.1 M solution of NaOH, filter sterilized and stored at $4°C$ for up to 3 months.

2.1.2 Uninfected Red Blood Cells

Uninfected red blood cells (RBCs) used in cultures were obtained from whole O+ human blood, donated by the North West Regional Transfusion Service, Liverpool, UK. The blood was supplied in citrate-phosphate-dextrose bags after being tested for HIV and HBV antibodies. The blood was stored at $4°C$ for up to 2 weeks and RBCs were separated only immediately before use. In order to separate RBCs from the other constituents of blood, RPMI-1640 and gentamycin solution (200 μM of 50 mg/mL gentamycin in 500 mL of RPMI-1640) was added to the whole blood aliquots, the suspension was centrifuged at 3000 rpm for 5 min and the supernatant together with the while buffy coat layer of cells was removed using a sterile glass aspiration pipette. The procedure was repeated 3 times in order to obtain a pellet of washed packed RBCs. The RBC suspension was then stored at $4°C$ for up to a week. In the experiments where uninfected RBC cultures were used as controls, the RBCs were cultivated in the same conditions as infected RBC cultures for 2 days prior to the experiment.

2.1.3 Gas Phase

It has been shown by Scheibel et al. [1979] that successful growth of *Plasmodium* for extended periods of time requires optimum atmosphere composition that is different from normal air, micro-anaerobic. The gas used for parasite incubation in this study was supplied by British Oxygen Special Gases. The composition of the gas was 4% CO_2, 3% O_2 and 93% N_2. The gas was administered to the culture flasks through a sterile cotton plugged pipette for 1 minute per 75 cm^2 flask and 30 seconds per 25 cm^2 flask.

2.1.4 Parasite Synchronisation

For all experiments highly synchronous parasite cultures were used. A standard procedure for parasite synchronisation with sorbitol described in Lambros and Vanderberg [1979] was used. The method is based on the fact that in later stages of the parasite life cycle the "new permeability pathway" allows sorbitol to enter through plasma membranes, followed by water causing the parasite to swell and eventually lyse and die. This procedure allows selection of young ring stage parasites and results in synchronised cultures. 5% Sorbitol (Sigma, UK) solution was used for the procedure. Cultures were transferred to sterile 50 mL tubes and centrifuged at 500 g for 5 minutes, the supernatant removed and discarded. Then ten volumes of sorbitol solution was added to the pellet and gently shaken. Cultures were then incubated at $37°C$ for 12 minutes gently shaking every 4 minutes. After incubation cultures were washed three times in full standard culture medium. The washing was carried out by adding 30 mL of full culture medium to each pellet, gently mixing and centrifuging at 500 g for 5 minutes. The supernatant was then removed and procedure repeated for a total of three washes. Washed pellets were then introduced into new flasks with fresh culture medium and incubated as usual for no less than 48 hours prior to any experiment.

2.1.5 Estimation of Parasitemia

Parasite cultures were maintained below 10% parasitemia for most efficient growth. The excess parasites were removed by dilution of cultures with fresh uninfected RBCs. The parasitemia was estimated by counting infected and non-infected RBCs on thin blood film slides. The slides were prepared by spreading a drop of RBCs from each culture onto a glass slide (Fisher Scientific, UK) forming a thin film of cells. The blood film was then fixed for 5 seconds in 100% methanol (Fisher Scientific, UK) and stained in 10% Giemsa solution (VWR International Ltd, UK) for 10 minutes, then washed under running tap water and dried. The prepared slides were then inspected through an oil immersion microscope (Zeiss, Germany) at x1000 magnification. The parasitemia was estimated by counting infected and uninfected RBCs, no fewer than 500 in total per per slide. The percentage of parasitemia was estimated as follows:

$$Parasitemia(\%) = \frac{\#\text{ of infected RBCs}}{\#\text{ of total counted RBCs}} \times 100\% \tag{2.1}$$

2.1.6 Haemocytometry

For FT-IR experiments an accurate cell count had to be established for determination of a standard uniform sample size. The cells were counted using a heamocytometer (Hawksley, UK). The red blood cell suspension was diluted in culture medium at ratio 1:99. The suspension was well mixed and 10 μL was transferred into the heamocytometer chamber. The cells were then counted under a microscope with 50x magnification in a central square of the chamber. The total cell count per millilitre was then calculated by multiplying the count by 50 000.

2.1.7 Magnetic Separation of Infected Erythrocytes

For FT-IR experiments the synchronous parasite cultures were purified to 90% parasitemia using magnetic column "VarioMACS" (Miltenyi Biotec, Germany). The purification was performed when parasites were at the trophozoite stage and at a 8-10% parasitemia.

Cytoprotective solution - consisted of 2% bovine serum albumin (BSA) and 20 mM glucose in 1x PBS solution.

For the purification cultures were transferred to sterile 50 mL tubes and centrifuged at 500 g for 5 minutes, the supernatant was removed and the pellets of infected RBCs were suspended in 10 volumes of cytoprotective solution. The magnetic column was assembled and placed into the magnet. The suspensions were poured through the column. Every three cultures the column was removed from the magnet and the cells trapped in the column eluted by pouring cytoprotective solution through the column. The elutant was collected in a sterile 50 mL tube. A Giemsa stain slide was prepared and inspected to confirm the success of the procedure after the last cultures were purified. The concentrated infected cells were then centrifuged at 500 g for 5 minutes, the supernatant was removed and cells were re-suspended in full culture medium.

2.1.8 Cryopreservation of Parasites

P. falciparum cultures were initiated by thawing frozen high parasitemia cultures. The cultures were cryopreserved according to a modified method presented by Rowe et al. [1968]; Wilson et al. [1977]. Cultures of over 5% parasitemia were transferred to sterile 50 mL tubes, centrifuged at 500 g for 5 minutes and the supernatant was removed. An equal volume of cryoprotectant solution was added to the pellet. The

suspension was left to rest for 5 minutes at room temperature, then mixed with the pipette and aliquoted into cryotubes (Nunc, UK) as 1 mL of suspensions. The tubes were then transferred to a liquid nitrogen tank (vapour phase) for storage.

Cryoprotectant solution - 1.9 g sodium chloride (Sigma Chemical Co, UK) was added to 200 mL of distilled water to obtain 0.95% physiological saline. Then 8.4 g of sorbitol (Sigma, UK) and 70 g of glycerol (Sigma Chemical Co, UK) was added to obtain the cryoprotectant solution. The resulting solution was filter sterilized and stored at $4°C$.

For thawing of the parasite cultures the tubes with frozen pellets were removed from liquid nitrogen storage and allowed to thaw at room temperature. An equal volume of 3.5% sodium chloride solution was then added to the thawed culture, mixed and the tubes centrifuged at 500 g for 5 minutes. The supernatant was removed and cell pellet was washed twice in an equal volume of full culture medium. The cell pellet was then introduced into a sterile 25 cm^2 culture flask with fresh medium, gassed and incubated at 37°C for 48 hours.

2.1.9 Determination of IC_{50} Concentrations of Drugs

Cultures for The IC_{50} concentration determination were prepared as usual (see Section 2.1.). The cultures were transferred to sterile 50 mL tubes and centrifuged at 500 g for 5 minutes. The supernatant was removed and the cell pellet used for the experiment.

The stock drug solutions of 2 mM were prepared in DMSO or methanol. Artemisinin was used as a positive control and fresh culture medium was used as negative control. 96-well plates were used for the experiments. The experimental set-up is shown in Figure 2.1.

Each drug to be tested (up to 2 per plate) was diluted as follows: 600 μL of 2 μM drug solution was added to a sterile 1.5 mL tube. For each drug seven more tubes containing 400 μL of fresh medium were prepared and a 1/3 serial dilution was performed by transferring 200 μL from the first tube to the next and repeating for each subsequent tube. This resulted in eight concentrations of each drug. Artemisinin was used at 2 μM concentration.

On the 96-well plate the wells on three of the edges of the plate were filled with 100 μL of fresh medium and not used due to different drying effects in those regions. The rest of the plate was filled with 50 μL of medium containing appropriate drug concentration or fresh medium for negative controls (Figure 2.1). Wells B-G

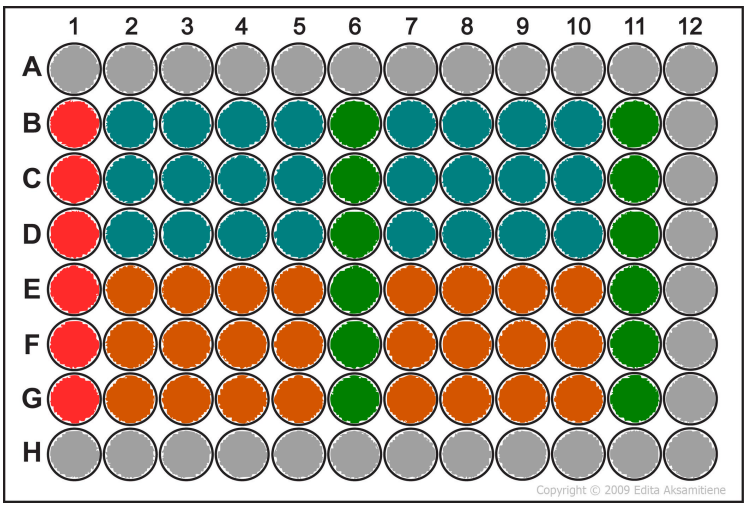

Figure 2.1: 96-well plate setup for determination of drug IC_{50} concentrations. Color code: grey - 100 μL of culture medium, not used in the experiment; red - Artemisinin; green - culture medium, positive control; teal - drug 1 serial dilutions, 3 replicates (1 row each); orange - drug 2 serial dilutions, 3 replicates (1 row each).

in column 1 were used for positive control and contained medium with Artemisinin. The same wells in the columns 6 and 11 were used for negative controls and contained fresh medium. The rest of the wells (columns 2-5 and 7-10) in order from left to right contained the serial dilutions of drugs in medium. Rows B, C and D were reserved for one drug and rows E, F and G for another 50 μL of parasite pellet was then added to each well of the 96-well plate. The plates were appropriately labelled and placed into a modular gas chamber. The chamber was gassed for 2 minutes with the standard gas mixture (Section 2.1.3) and incubated at $37°C$ for 48 hours. After incubation the plates were removed from the chamber and refrigerated to $-20°C$ for storage until fluorescence measurement. 1 Hour before reading the plates and the SYBR green solution were removed from the freezer and thawed in a laminar flow cabinet.

Lysis Buffer - The buffer is composed of EDTA 5 mM (Sigma Aldrich E5154), Triton x100 0.08% (BDH chemicals 30632), Tris 20 mM (Sigma Aldrich, T1503) and saponin 0.08% (Sigma Aldrich, S7900).

The lysis buffer was diluted 1:9 in distilled water and 0.2 μL of SYBR green (Sigma Aldrich, S9430) was added per 1 mL of the solution. 100 μL of the solution was added to each well used for the experiment and the plates were incubated for 1 hour at $37°C$. The fluorescence in the wells was measured using a "Varioskan" (Thermo Electron, US) spectrophotometer. The readings were performed at 100 ms

duration, three times per well and values were averaged. The excitation wavelength was 485 nm and emission - 518 nm. The three replicates were averaged, positive control was subtracted from the average and the result divided by the negative control value obtaining the percentage of inhibition by the drug with respect to positive control. A logistic curve was then fitted to these percentages to obtain the IC_{50} value and associated error.

2.2 Experimental Procedures for FT-IR Metabolomics Experiments

Prior to experiments FT-IR plates were washed with a 5% SDS solution then rinsed with distilled water, iso-propanol solution and dried in a $40°C$ oven for at least an hour. A randomized template for sample placement on the plate was created for each experiment in order to reduce effects of any systematic errors or machine drift.

2.2.1 Sample Preparation

Parasite cultures were prepared for the experiments as explained in Section 2.1. All cultures were randomized during culturing procedure in terms of treatment order and placement in the incubator. Parasite cultures were synchronized (Section 2.1.4) and purified (Section 2.1.7) to 90% parasitemia. The amount of cells in each suspension was estimated using haemocytometry (Section 2.1.6) and the volume containing the required number of cells (2×10^7) was calculated. For the time-series experiments 24-well flat bottom culture plates (Costar, USA) were used. Samples on the plates were randomized in the same way as on FT-IR plates.

2.2.2 Sampling at T=0 h and Time-Course Set-up

A standard volume of each suspension, containing 2×10^7 RBCs, was transferred to sterile 15 mL tubes on ice containing 5 mL of ice-cold PBS solution, mixed and put on ice. The tubes were centrifuged at 500 g in a centrifuge chilled to $4°C$, supernatant was carefully removed and the wash step was repeated. After the second wash step the cell pellets were transferred onto a prepared FT-IR plate using a 10 μL pipette according to the randomized template, followed by drying.

24-Well plates were prepared for time course experiments by adding 2 mL of full medium containing $3 \times IC_{90}$ concentration of drug or an equivalent amount of DMSO. A standard volume of each sample containing 2×10^7 RBCs was then added to an appropriate well on the plate. The plates were closed, appropriately labelled

and put into a modular gas chamber (Billups-Rothenberg, US). The chamber was then gassed for 2 minutes with the standard gas mixture (Section 2.1.3) and the chamber was placed into an incubator at 37°C.

2.2.3 Sampling at Later Time-points

At sampling time points the plates were removed from the chamber and placed on ice to quench the cell metabolism. Each sample was then transferred to a sterile 15 mL tube containing 5 mL of ice-cold PBS solution, mixed and put on ice. The tubes were then centrifuged at 500 g at $4°C$, supernatant was carefully removed and the wash step was repeated using 5 mL of ice-cold PBS. After the second wash the supernatant was carefully removed without disturbing the pellets and cells were transferred onto a prepared FT-IR plate using a 10 μL pipette according to a randomized placement template, followed by drying. The complete plates were transferred to a desiccator and kept until the FTIR reading within 24 hours.

2.2.4 FTIR Readings

FT-IR experiments were performed using a Bruker Equinox 55 FT-IR spectrometer using OPUS software v.4. Spectra were collected in the absorbance mode within the wavenumber range of 4000-600 cm^{-1} with 4 cm^{-1} resolution and sampling time of 64 scans. The raw values of the spectra were extracted from Bruker digital files using a specialized MATLAB (The MathWorks, UK) script and annotated in Excel (Microsoft, US). All the FT-IR data manipulations and analysis were performed using R statistical computing software.

2.3 Experimental Procedures for NMR Metabolomics Experiments

Each NMR metabolomics experiment was performed following the procedures described below. First the required number of parasite cultures were cultivated (Section 2.1) to 8-10% parasitemia at the early trophozoite stage. Each flask was prepared with 1 mL of infected RBCs. However to account for cell loss during culture and manipulation procedures it was assumed that each flask had 800 μL of infected RBCs per flask.

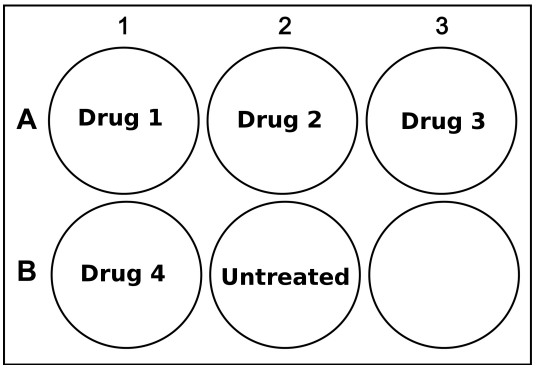

Figure 2.2: A standard 6-well plate set-up for a drug exposure experiment. 4 Drugs were used usually with one well left for negative control. If only 2 drugs were used, 2 replicates would be fit on one plate also adding another control sample.

2.3.1 Drug Exposure Time-Course Setup

Each parasite culture was transferred to a sterile 50 mL tube, centrifuged at 500 g for 5 minutes, and supernatant removed by aspiration. The resulting cell pellets were then pooled. Full culture medium aliquots containing calculated concentration of drugs were prepared and added to 6-well plates, 8 mL per well, arranged as shown in Figure 2.2. For the specific concentrations drugs and solvents used refer to Table 2.1. 250 μL of pooled parasite culture was added to each well. Each plate was treated as a replicate of the experiment.

The plates were appropriately labelled and placed into a modular gas chamber (Billups-Rothenberg, US). For improved gas access to each plate a custom made shelf was constructed to be placed inside a chamber in order to avoid directly stacking plates onto each other. The chamber was then closed and gassed for 2 minutes with the standard gas mixture (Section 2.1.3).

Table 2.1: Drugs used in NMR experiments. MW - molecular weight; * - in-house determined $IC_{90}(nM)$ concentrations.

Drug name	MW (g/mol)	$IC_{90}(nM)$*	Solvent
Chloroquine	319.87	50	Water
Amodiaquine	355.86	50	DMSO
CK-268	443.85	50	DMSO
5-Fluoroorotic acid	174.09	15	DMSO
Piperaquine	535.51	50	DMSO

For experiments including 1 mL cell samples and a 5 or 6 hour time-courses the plates were substituted with $25cm^2$ flasks containing 10 mL of culture medium.

For the 48 hour time-course experiment the $75cm^2$ flasks containing 40 mL of culture medium were used. The gas chamber was not used and the flasks were gassed individually 30 seconds per $25cm^2$ flask and 1 minute per $75cm^2$ flask.

2.3.2 Sampling

At time $T = 0$ h the samples were taken from the pooled parasite culture. 250-1100 μL (depending on the experiment) of culture was taken for each sample and transferred to sterile 15 mL tubes containing 5 mL of ice-cold PBS. The samples were gently shaken and centrifuged in a 4°C centrifuge at 500 g for 5 minutes. Supernatant was removed and the wash was repeated. After the second wash 200-1000 μL of each pellet was transferred to a 1.5 mL tube containing four volumes of extraction solution (2.3.3). In case of 1 mL sample the pellet was split between 3 tubes (333 μL each), each extraction was carried out separately and the extracted material pooled back together at the end of the procedure (Figure 2.3).

At later time-points the sampling was performed depending on the containers the cells were incubated in. When plates were used, the samples were transferred to sterile 15 mL tubes containing 5 mL of ice-cold PBS using a 12 mL cotton-plugged pipette and washed as described in case of T=0 h sampling. In cases when flasks were used for incubation the cells were re-suspended into the medium by gently shaking the flasks and transferred to sterile 15 mL tubes containing 5 mL of ice-cold PBS using a 12 mL cotton-plugged pipette and washed as described above. After the washes 200-1000 μL of each pellet was transferred to a 1.5 mL tube containing four volumes of extraction solution (2.3.3). The 1000 μL samples were split into three tubes each for extraction as explained above.

2.3.3 Metabolite Extraction

The metabolite extraction procedure was adapted from Beckonert et al. [2007b]. The changes made and the motivation is discussed in more detail in Chapter 3.

Extraction solution - was prepared by mixing experiment grade acetonitrile (VWR, UK), methanol (VWR, UK) and distilled water (VWR, UK) in proportions $2 : 2 : 1$. The solution was mixed thoroughly and stored at $4°C$.

Prepared extraction solution was added to appropriately labelled 1.5 mL tubes prior to the experiment, at volume 4x the planned sample volume. Each sample was then added to the designated tube with extraction solution, vortexed

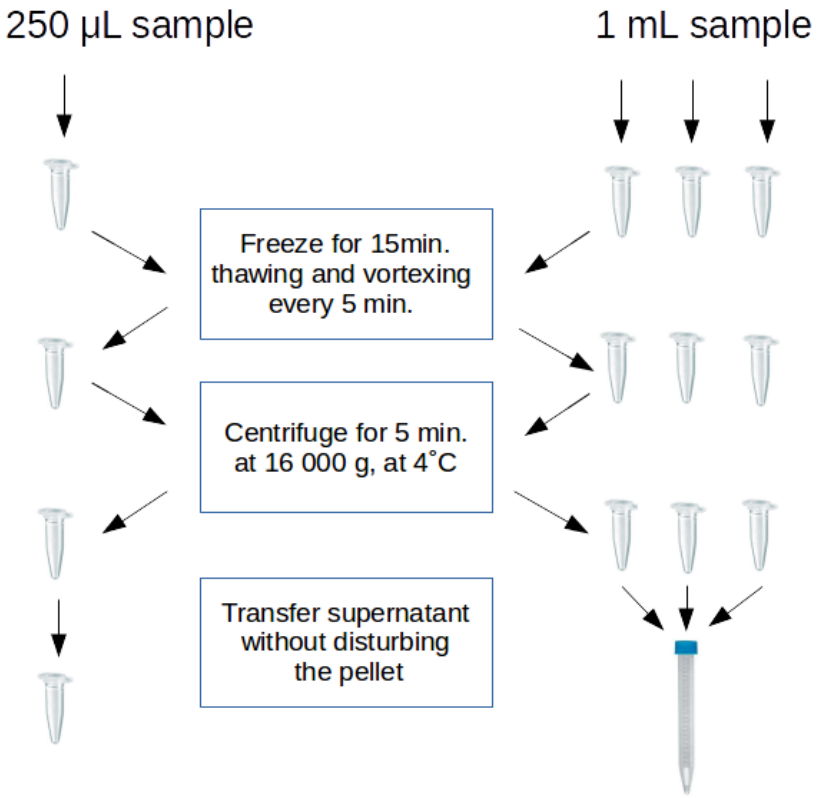

Figure 2.3: A schematic of metabolite extraction procedure for 250 μL and 1 mL cell samples. Each 1 mL sample was split into three 333 mL samples and extraction is performed separately on each part. The extracts were pooled at the end before drying.

for 5 seconds and frozen on dry ice. The samples were then kept on dry ice for 15 minutes, thawing and vortexing every 5 minutes. After the extraction procedure samples were centrifuged at 13000 g, supernatant was transferred to fresh tubes, frozen and stored at $-80°C$ until lyophilisation.

2.3.4 Lyophilisation

Before the NMR experiments were performed all the samples were freeze-dried to remove any solvent that would interfere with the readings. The lyophilisation procedure was carried out using a Heto PowerDry LL3000 freeze-dryer (Thermo Scientific) equipped with a RV5 (Thermo Scientific) vacuum pump. Each tube containing a frozen sample had a hole made in the cap and was placed into a plastic freeze-drying container and left overnight in the freeze-dryer loop. Dried samples were then stored

at $-80°C$ until the NMR readings could be performed.

2.3.5 Sample Preparation For NMR Readings

The lyophilised samples were re-suspended in 580 μL of NMR buffer (see below) and vortexed for 10 seconds. The samples were then centrifuged at 13000g and 550 μL of supernatant was each transferred to a clean 1.5 mL Eppendorf tube. Each sample was then transferred from the 1.5 mL tube to a 5 mm glass NMR tube (Fisher Scientific, UK) using a glass pipette (Fisher Scientific, UK). The outside of each tube was cleaned with a tissue to remove any fingerprints or dust. The samples were then placed into a 96-tube rack (Bruker, UK) and loaded into an automatic sample changer (SampleJet, Bruker). In cases when the 800 MHz spectrometer was used the samples were changed manually and a spinner was used instead of tube rack.

NMR buffer - 100 mM sodium phosphate buffer solution, pH 7.4 in deuterated water (^2H_2O) containing 0.3 mM TSP as chemical shift reference Beckonert et al. [2007b].

2.3.6 NMR Parameter Set-up

NMR experiments were performed using 600 MHz and 800 MHz Bruker Avance III spectrometers equipped with TCI gradient cryoprobes. The 600 MHz spectrometer was fitted with a SampleJet autosampler. The spectrometers were controlled using Bruker TopSpin 3.1 software (Bruker, UK) operating in Centos 5 Linux OS.

The NMR readings were collected using standard Bruker 1D NOESY and CPMG pulse sequences unless stated otherwise. 128 Scans were collected for each sample with 4 dummy scans (DS) and spectral width of 20 ppm at 298 K. For each experiment the temperature was calibrated using a standard deuterated methanol sample. A pre-saturation water suppression technique was used throughout the experiments.

2.4 Experimental procedures for High Content Imaging Study

Here we describe the procedures used in the high content imaging experiments. We first discuss the experimental set-up followed by the data acquisition and processing.

2.4.1 Experimental Set-up

High content imaging studies were carried out according to the following procedures. The parasites were cultured in a standard manner described in Section 2.1. The parasites were synchronised using the sorbitol method (Section 2.1.4) twice within 6 hours in order to obtain a narrow synchronization window. The cultures were then continued for additional an 48 hours until the next life-cycle, changing medium after 24 hours. At 48 hours the synchronous cultures were at ring stage (0.2% haematocrit and 5% parasitemia) and were exposed to the antimalarial compounds at $9 \times IC_{50}$ concentrations in a flat-bottomed 96-well plate (Fischer, UK) and incubated for 32 hours until the negative control cultures reached late trophozoite stage. The cells were then transferred to a 384-well imaging plate (Perkin Elmer, Cell-Carrier 384 TC) at final haematocrit of 0.02%. The cells were incubated with 1 μg/mL of Hoechst fluorescent stain for 3 minutes. After 3 minute incubation paraformaldehyde was added up to 1% concentration. The imaging experiments were performed using Operetta High Content Imaging Platform (PerkinElmer) at 60x high numeric aperture objective. The images were collected at 20 ms exposure time, 100% excitation using an excitation filter of 360 - 400 nm and emission filter of 410 - 480 nm. 42 fields were collected per well resulting in 500-1000 detected cells in each well.

2.4.2 Data Acquisition and Processing

Images collected in the study were first analysed using Harmony High Content Imaging and Analysis software (PerkinElmer). The measurements collected included a set of size, intensity and texture features (Table 2.2). The texture features were detected using the Laws convolution filters [Laws, 1980]. The filters when applied highlighted various texture elements (Fig. 2.4) in the images and highlighting their location. Subsequently the intensity values of the highlighted features were averaged and presented as texture parameter values for the analysis.

The data acquisition was constrained to exclude any obvious artefacts as given in the Table 2.3. After object selection the data was saved and further processing was performed using R statistical programming environment [R Core Team, 2013].

The data was further cleaned by removal of the most anomalous cases in terms of *Area* and *Intensity* values. This was accomplished by fitting a multivariate Gaussian distribution to *Area* and *Intensity* variables and calculating the probability of each measured case under the fitted distribution. The data points with probability

Table 2.2: The measurements of the cell nucleus selections in the Harmony software. Laws - the average intensity of the selection after application of a respective Laws [Laws, 1980] filter indicated by the parameter name.

Parameter	Description
Area	The area of the selection in μm
Intensity	The average intensity of the selection
Length-to-width ratio	The ratio of 2 perpendicular measurements of a selection
Roundness	The roundness of the selection
Spot	Laws filter
Hole	Laws filter
Edge	Laws filter
Ridge	Laws filter
Valley	Laws filter
Saddle	Laws filter

Table 2.3: The Image analysis constraints on the selected field inclusion in the dataset. * - intensity constraints varied between experiments due to varying focus of the objective and stain binding.

Variable	min	max
Intensity	100-400*	4000
Area (μm^2)	0.5	80
Width-to-length ratio	0.3	-

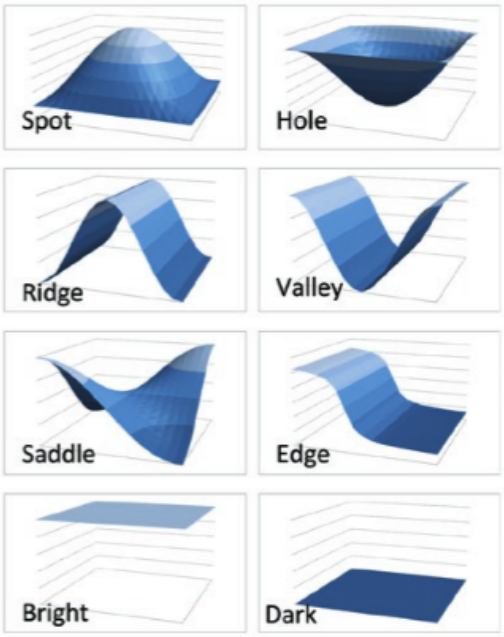

Figure 2.4: The shapes of texture features detected by the Laws filters in the Harmony softare.

of 0.1 or less were removed from further analysis. This allowed us to reduce the data to approximately 90% of the most "average" cases.

2.5 Data Analysis

In this section we present statistical methods used for analysis of the data collected in the experiments conducted. We present the methods in sections corresponding to various techniques used to collect the data. For more in-depth explanations of each technique refer to the data analysis part of the Chapter 1. All of the following analysis was performed using R statistical computing language unless specified differently.

2.5.1 FTIR Data Analysis

FT-IR data was imported and processed using the R statistical programming environment. As each well was measured three times the data was averaged by well and assembled to one data set for further analysis. Processed data was subject to PCA (Section 1.7.1) and LDA-PC (Section 1.7.2). The LDA-PC was performed using R package "adegenet" [Jombart and Ahmed, 2011].

2.5.2 NMR Data Analysis

NMR data was first subject to processing using our custom software ProcNMR (ref. to Chapter 4). The standard procedure of data processing included exponential line broadening by 0.3 Hz, Fourier transformation and automatic phasing and referencing to TSP signal. We also performed quality control by measurement of TSP mid-peak width in Hz. A measurement of over 1.5 Hz was taken as an indication of badly calibrated readings. The data was then binned either uniformly, selecting 0.05 ppm width bins or a custom binning pattern was used. The custom binning pattern was developed based on the data obtained in the experiments and included the peaks that did not vary in terms of chemical shift. The binned data was then subject to multivariate analysis. The raw data was also retained for visual inspection.

Principal Component Analysis was the most regularly employed technique for the NMR data analysis. Before the analysis the data was mean centred and each variable normalised by the standard deviation. Pareto scaling was also tried but did not significantly improve the results compared to scaling by the standard deviation. The first two principal components were plotted as a scatter plot. In some cases further principal components were plotted for better visualization of the data.

Hierarchical Cluster Analysis was another multivariate technique employed in the analysis of NMR data. Since the first 2-3 principal components in PCA did not always account for the majority of variance HCA was employed in order to investigate the data further. The technique was performed using Euclidean distance metric and complete linkage method. The results were plotted as a dendrogram.

Multiple Dataset Integration was used for modeling the data including the time-related information. The source code for the software was obtained from "http://github.com/smason/mdipp" and compiled for the Linux operating system. Simulations were run for 100,000 iterations and the clustering agreement matrices were plotted for inspection. The data was mean-centred prior to analysis. Analysis was performed on infected RBC data before and after the subtraction of control RBC data.

2.5.3 Image analysis

As noted above the image data was cleaned and presented as a standard data matrix with samples in the rows and variables in the columns. All data manipulation and

permutation testing programs were custom written for this work in the R statistical programming environment.

The data modelling was performed using PLS-DA (1.7.3) models using 10-fold cross validation for hyperparameter fitting and 20 model ensemble for testing and predictions (Fig. 2.5). The data set X was first randomly split into training set X_{tr} and test set X_{ts} keeping the ratio of samples in each group as close to the starting ratio as possible. In this case there was 5:4 ratio of "fast" drug samples to "slow". Both resulting data sets kept the ratio of samples close to 5:4. Next a 10-fold cross-validation procedure was applied in order to select the number of components $\hat{n}$ to be used in the final model. The training data set X_{tr} was randomly split into a training subset X'_{tr} and a validation subset X_v. A PLS-DA model was then fitted to the data X'_{tr} 10 times with a different value of $n = \{1..10\}$. The resulting models were tested on the data X_v and Q^2 metric calculated for each model. The procedure was repeated ten times and the resulting Q^2 values collected into a 10x10 matrix. The mean Q^2 value was then calculated for each value of n. The n with the highest mean Q^2 was then selected to be used in the final model. A PLS-DA model was then fitted to the dataset X_{tr} and tested on the dataset X_{ts}. Q^2 was calculated and stored with the model for further use. The whole procedure was repeated 20 times. It resulted in 20 models that had been fitted to various splits of data. The predictions were then performed using the whole ensemble of 20 models. The 20 predictions were combined by averaging the predicted probabilities of the sample being in the "fast" group.

After processing Image data was subjected to permutation testing by fitting PLS-DA models to the data with random permutations of labels as explained in Section 1.7.4. A total of 1000 permutations were run on each dataset with 10-fold cross-validation for selection of number of components for PLS-DA and 20 model ensemble used for prediction. An empirical distribution of model "goodness-of-prediction" metric Q^2 was constructed and a p-value for Q^2 of correctly labelled data was calculated. The models fitted to the real-labelled data were then used for classification of the MMV data. Each sample group membership was predicted by averaging the predictions of the 20 models.

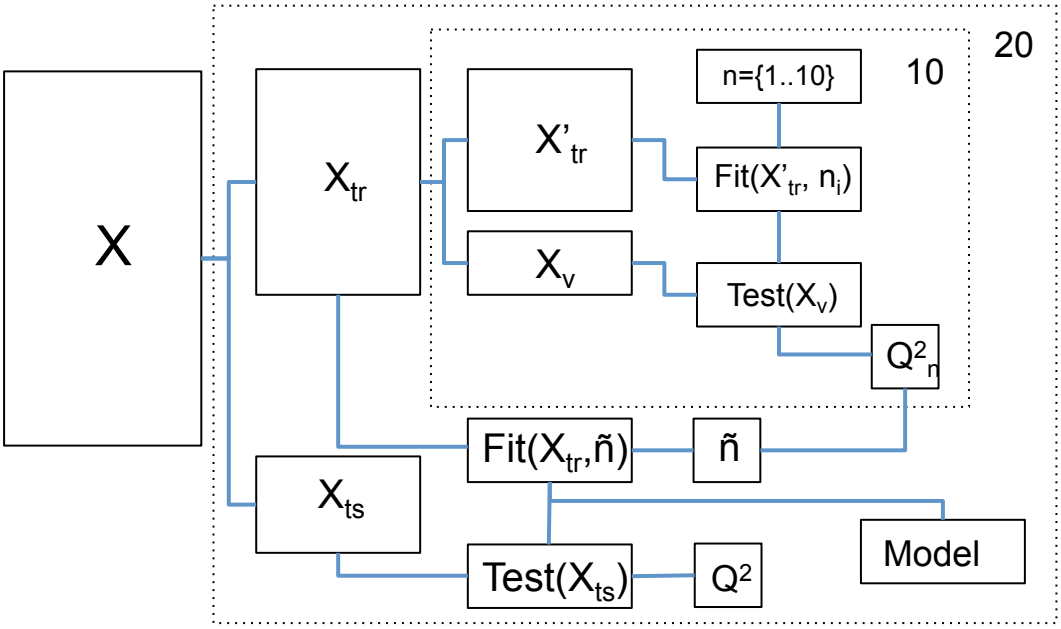

Figure 2.5: A schematic illustration of the model training, testing and validation approach employed for image analysis. Each block of operations contained in a dotted square is repeated a number of times given in the top right corner of the square.

Chapter 3

Method Development

3.1 Introduction

As an integral part of this thesis there has been the need to develop and optimize a series of methods and experimental protocols for which no well-established methods were present or where no consensus was reached from evaluation of the literature. The experimental procedure for the FT-IR did not require any special sample preparation; the sampled RBCs were washed and used intact. Since no FT-IR experiments involving *plasmodium* infected RBCs had been published previously we had to optimize the sample size before the experiments could be performed effectively. The experiment designed for RBC sample size optimization is described in Section 3.2. Sample preparation for NMR experiments was more complex. There had been a wide range of metabolomics studies performed using NMR to study a range of microorganisms, tissues and biofluids [Beckonert et al., 2007a; Brennan, 2014; Schripsema, 2010; Zhang et al., 2013]. The samples for NMR readings are usually in solution (solid-state NMR was not applicable to this study and is omitted from the discussion). In cases of biofluids the analytes are already dissolved and the sample preparation usually only focused on removal of undesired components in the sample before analysis [Vuckovic, 2013; Sheedy et al., 2010]. When dealing with tissues, cell membrane disruption and metabolite extraction is a key step in the sample preparation and a variety of methods have been proposed [Mushtaq et al., 2014]. Metabolite extraction methods are often adapted from studies on similar tissues or organisms; for example in Tiziani et al. [2009] a metabolite extraction method developed for fish liver extraction was adapted for leukemia cells and in Bolten et al. [2007] metabolites of various bacteria were extracted using a protocol developed for yeast. At the time of this study there were very few NMR metabolomics studies of *P.*

falciparum. Studies reported in the literature included Olszewski and Llinas [2013]; Teng et al. [2009, 2014] however none of the methods used had been developed with high throughput fingerprinting or profiling in mind. These studies focused primarily on metabolite identification and quantification. Our aim was to develop a procedure for collecting *p. falciparum* infected RBC samples at any stage of the parasite intra-erythrocytic life-cycle, performing metabolite extraction and preparing the extracts for NMR spectroscopy, preferably with high numbers of samples, in a robust, validated and reproducible manner. We have adapted and tested metabolite extraction methods used in NMR and LC-MS experiments on *P. falciparum* as well as other organisms [Olszewski and Llinas, 2013; Brennan, 2014]. Sample drying is another important step in sample preparation. While sample drying under a nitrogen flow is a standard procedure in drying of organic solvents some authors prefer freeze-drying due to the low temperatures deployed during the process [Tiziani et al., 2009]. We tested both methods of drying of metabolite extracts in order to select the optimal method for these studies. The optimisation of metabolite extraction and drying is described in Section 3.4. Acquisition of NMR spectra is dependant on a range of parameters and settings such as pulse sequence, temperature, sampling rate and number of scans. We started the study using a standard Bruker NOESY pulse sequence with presaturation (noesypr1d) for NMR data acquisition on a 600 MHz spectrometer. However as the experiments increased in complexity we introduced a CPMG pulse sequence, sample quality control as well as the use of an 800MHz NMR spectrometer for higher resolution data. The optimisation steps for NMR data acquisition are discussed in Section 3.5.

3.2 Determination of Optimal RBC Count for FT-IR Experiments

In this study RBC suspension was used as samples in FT-IR experiments. In order to keep the data comparable and optimize the signal the sample size had to be kept uniform. As the samples were not in solution the number of cells per sample was the most accurate measure of the sample size. Optimal signal intensity in FT-IR sepectroscopy experiments needs to be in the 0.4-1.4 AU range and the protocols were adapted to achieve this. In this range the signal is known to be linear and is most appropriate for statistical analysis. Therefore the optimal signal in an FT-IR experiment is as close as possible to but below 1.4 AU. A 2-fold serial dilution $(1 - 1/16)$ of RBC samples was prepared starting with a 1.7 million cell sample and FT-IR spectra were collected in order to determine the optimal cell count per

sample needed to obtain the desired signal intensity. The data was inspected (Fig. 3.1) by plotting an overlay of all the spectra. It was clear that the 1/2 dilution was the closest to the 1.4 AU target while still being under 1.4 AU. This dilution corresponded to 865,000 cells per sample. In all further FT-IR experiments the sample size was kept around 850,000 cells.

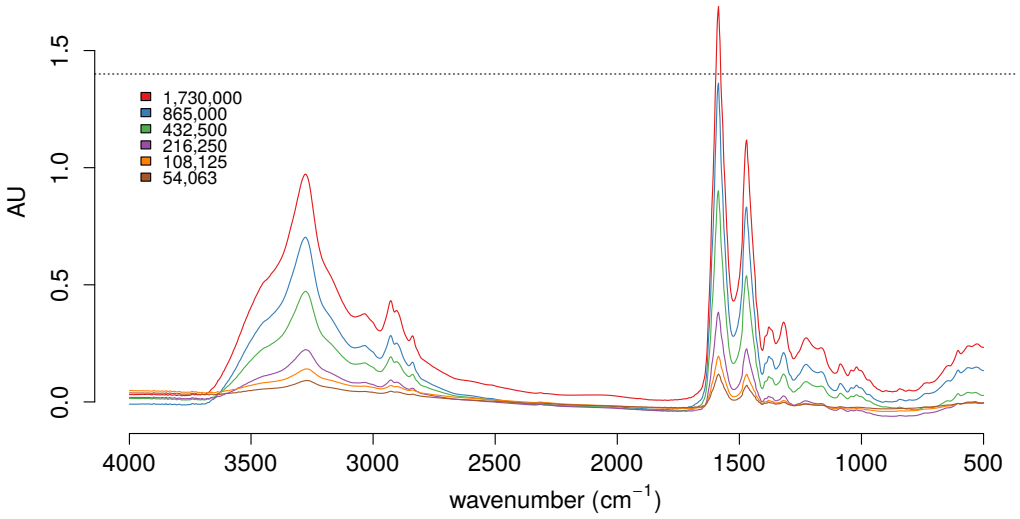

Figure 3.1: FT-IR spectra acquired from a 2-fold serial dilution of RBCs starting with 1.7 million cells as the initial count. The dotted line represents the 1.4 AU cut-off. For an optimal signal the spectrum under 1.4 AU is desired.

3.3 Signal Maximisation in NMR Experiments of *P. falciparum* Infected RBCs.

Before starting the discussion of the sample preparation for this study it is important to note that the intraerythrocytic nature of *P. falciparum* presents a unique challenge for metabolomic studies. The parasites are cultured in human red blood cells and the parasitemia in normal conditions does not reach much higher than 10-12%. If metabolite extraction would be performed on a sample of such a culture the metabolites from the red blood cells would account for a large portion of the total metabolome signal apparent in the extract. Consequently, in order to investigate the *P. falciparum* metabolism some concessions have to be made for which there are

a range of alternative approaches. The parasites can be removed from RBCs before metabolite extraction using for example saponin lysis [Bangham et al., 1962]. This allows subsequent metabolite extraction without RBC metabolome contamination. This procedure however is most effective in the later stages (late trophozoite) of the parasite life-cycle [Fernandez, 2008]. This was not an option in the curent studies where methods were required that could analyse any part of the parasite 48h life-cycle. This was essential in order to explore drug effects that could operate at any stage of cell cycle of the parasite. An alternative method is to obtain high parasitemia cultures thereby reducing the relative contribution of the RBC metabolome to the signal. There are multiple ways to achieve high parasitemia *P. falciparum* cultures including procedures using magnetic separation [Kim et al., 2010] of infected RBCs and maintaining low haematocrit cultures [Radfar et al., 2009a]. The magnetic separation is only possible in the trophozoite stage of the parasite due to the presence of paramagnetic heme in malaria pigment. It is then possible to control the number of RBCs added to the culture in order to obtain high parasitemia of ring-stage parasites in the next life cycle following separation with the magnet. We tested the magnetic separation (Section 2.1.7) and reinvasion strategy however the results were erratic and suboptimal. The parasitemia levels obtained were very variable between cultures, the rate of multiple cell invasion of merozoites was higher than desirable and the parasite growth after the procedure was atypical and slower than standard indicating that the viability of the separated parasites was compromised in some way. This made it impossible to plan and get timings of experiments optimised. The procedure was also time consuming and did not provide clear improvement in signal over lower (10-12%) starting parasitemia samples (results discussed in more detail further in the text). Therefore it was concluded that while magnetic separation is a viable strategy for achieving high parasitemia, the resultant stress to the cultures and the bottlenecks it introduced raised serious concerns about the impact this could have on the underlying metabolome. Another, indirect, way of separating the parasite signal from the RBC signal could be conducted after data acquisition. The infected RBC samples could be duplicated with non-infected RBCs under identical experimental conditions. The signal from the RBCs could then, at least in theory, be subtracted from the parasite plus RBC signal yielding the data specifically originating from the parasite metabolite pool. This method increases the size and complexity of each experiment and slows down throughput considerably. Lastly the experiments could be designed with the aim of maximising the overall signal. This would potentially provide enough contribution from the parasite metabolites over the signal from the RBCs. This alternative

poses less restrictions on the experimental design than any other and the culture conditions can be held as "natural" as possible.

We decided to rely on a mixture of the two last strategies: subtraction of the parasite-free RBC signal and maximisation of overall signal and number of replicates. This strategy was considered the the most likely to generate data that was reproducible and biologically relevant to parasite life in standard culture conditions.

3.4 Development of Sample Preparation Procedures for NMR Experiments

As mentioned previously there are a range of metabolite extraction methods for *P. falciparum* samples described in the literature [Teng et al., 2014, 2009; Olszewski and Llinas, 2013]. The most widely used extraction solutions included pure perchloric acid, pure methanol as well as mixtures of acetonitrile, methanol and water, methanol and water, and methanol and chloroform. The perchloric acid extraction strategy was suggested by Teng et al. [2009] to be superior to other methods due to the higher number of polyamines and adenine nucleotides detected in the sample extracts using this method. However, such measure of efficiency of sample extraction was inadequate for the aims of our studies. We based our choice on extraction reproducibility, robustness and suitability for high throughput experiments. We aimed for a simple metabolite extraction procedure that would limit the number of steps in order to reduce the experimental error. A simple extraction procedure also allowed us to maximise the number of samples processed per unit time, supporting the high throughput demands of our experimental approach. We rejected the perchloric acid and methanol:chloroform based extractions without testing. The decision against using a perchloric acid extraction protocol was made due to likely higher variance in sample pH after extraction as well as formation of perchlorate salts [Mushtaq et al., 2014] that can interfere with the subsequent analysis. Due to the nature of NMR spectroscopy pH variation between samples as well as salt content has a severe negative impact on data quality making it highly undesirable. This approach would have demanded manual adjustment of pH and removal of perchlorate salts making it more time consuming and opening up additional apportunities to introduce variability into the extraction process. The methanol and chloroform based extraction method was rejected due to its relative complexity without clear improvement in results [Teng et al., 2009]. Therefore, the remaining candidate methods included variations on the theme of acetonitrile, methanol and water mixtures.

3.4.1 Optimisation of Metabolite Extraction Protocol

First we tested two extraction solutions: equal amounts of methanol and water and a 2:2:1 mixture of acetonitrile, methanol and water. The latter had been used previously in NMR experiments [Olszewski and Llinas, 2013] as well as in mass spectrometry experiments in our in-house facility. We adapted the extraction method used by our group for mass spectrometry sample preparation using ice-cold extraction solutions as follows:

1. Spin the cultures at 500 g for 5 min. and remove the culture medium.
2. Add 10ml of ice-cold saline and mix.
3. Spin at 500 g for 5 min. and remove the supernatant.
4. Repeat steps 2-3.
5. Transfer 100 μl of cell pellet to a 1.5 ml tube containing 500 μl of ice-cold extraction solution and vortex.
6. Spin the sample at 500 g and transfer supernatant to a sterile 1.5 ml tube for drying.
7. Dry the samples under the flow of N_2 and store at $-20°C$.

Two *P. falciparum* samples were extracted according to this protocol using either methanol:water and acetonitrile:methnol:water extraction solutions. The samples were dried under the flow of nitrogen and stored at $-20°C$. Before NMR data acquisition each sample was resuspended in 580 μL of NMR buffer, containing 100 mM phosphate buffer, pH 7.4 in ^2H_2O and 0.3 mM trimethylsilyl propionate (TSP), following the method of Beckonert et al. [2007b]. TSP was used as chemical shift reference (δ = 0 ppm). We acquired 1D ^{1}H NMR spectra using a standard Bruker NOESY pulse sequence with presaturation (noesypr1d) collecting 64 scans per sample at 298K.

The resulting spectra (Fig. 3.2) contained a high number of broad peaks (compare to Figure 3.3) originating from larger molecules - likely proteins - and masking the majority of narrow peaks of small molecules that were of interest. The presence of protein in the samples is a frequent problem in metabolomics experiments and a range of solutions have been tried ranging from ultrafiltration [Daykin et al., 2002] to use of magnetic micro-particles [Konig et al., 2013], however such methods are expensive and require special equipment. Simpler solutions using organic acids and salts and centrifugation, including perchloric acid treatment have also been shown to be effective however we rejected these approaches for the reasons discussed

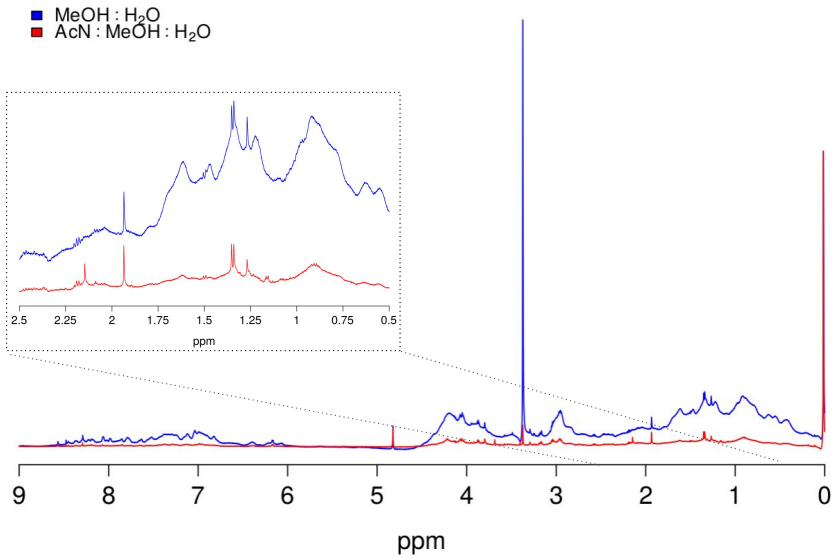

Figure 3.2: 1D ^{1}H NMR spectra of *P. falciparum* infected RBC samples, extracted using ice-cold 1:1 methanol and water and 2:2:1 acetonitrile, methanol and water. The spectra were referenced to tsp signal at 0 ppm. Both spectra contain broad peaks suggesting high abundance of protein in the samples.

previously. We decided to modify our protocol as suggested in Olszewski and Llinas [2013] and include freezing and sonication steps in the extraction protocol. It was argued that these steps help disrupt the cell membranes as well as facilitate protein precipitation. The metabolite extraction protocol was therefore modified as follows (steps 1-5 were kept the same):

1. Spin the cultures at 500 g for 5 min. and remove the culture medium.
2. Add 10ml of ice-cold saline and mix.
3. Spin at 500 g for 5 min. and remove the supernatant.
4. Repeat steps 2-3.
5. Transfer 100 μl of cell pellet to a 1.5 ml tube containing 500 μl of ice-cold extraction solution and vortex.
6. Freeze the samples on dry ice for 15 min. vortexing every 5 min.
7. Spin the sample at 13 000 g at 4°C and transfer supernatant to a sterile tube for drying.
8. Add 500 μl ice-cold extraction solution to the remaining pellet.
9. Sonicate for 15 min.

10. Spin the sample at 13 000 g at 4°C and transfer supernatant to the tube containing the first half of the extract.

11. Dry the samples under the flow of N_2 and store at $-20°c$.

The experiment was repeated following the modified protocol. The metabolite extraction this time was performed on dry ice at -78.2°C and included an additional step of sonication to improve cell membrane disruption [Olszewski and Llinas, 2013]. As can be seen in Figure 3.3 the protein signal in the resulting spectra was reduced and sharp small molecule peaks were much more prominent. Apparent differences between the two extraction solvents however were minimal. Lacking replicate samples, a definitive decision as to which method to select could not made.

Samples were also prepared using the same metabolite extraction protocol but omitting the sonication step in order to assess the improvement of the extraction by the additional sonication based cell disruption (Fig. 3.4). While the samples prepared using the protocol including sonication seemed to contain fewer braod peaks, the overall intensity of many peaks was smaller. The "one step" extraction method seemed to be at least as good, containing some higher intentsity peaks, especially in the aliphatic region. Due to this observation as well as the "one step" extraction being simpler and faster we chose to omit the sonication step in the extraction procedure.

3.4.2 Comparison of Metabolite Extraction Solutions

In order to further compare the extraction procedures and decide which extraction solution performed better the experiment was repeated with an increased number of replicates. As a measure of quality the variance each method added to a group of samples was compared. The procedure that introduced the least random variation into the data was preferable. The variance in the data was compared by inspection of PCA scores plots.

Two sets of conditions were compared. Infected and uninfected RBCs were extracted using methanol:water and acetonitrile:methanol:water and dried using either freeze-drying or enhanced N_2 evaporation. NMR spectra were collected using NOESY pulse sequence with presaturation, 64 scans per sample at 298K. The obtained spectra were uniformly binned into 0.05 ppm bins and PCA was performed. A scatterplot of the first two principal components was produced (Fig. 3.5).

The assessment was carried out as follows. Given two groups of data points that were separable in a PCA scatterplot (in this case infected and uninfected RBCs) and two methods of sample preparation (two different extraction solutions) the

difference in the spread of data points within each preparation group would suggest the randomness introduced by each method to be different, while similar spread would mean that neither method made a higher contribution to sample variation. The between-group spread of points (here separation of infected and uninfected RBCs) could be interpreted as information content. If the two groups of samples had significant biological differences the method with higher difference between groups in the plot would be superior as it would provide more information about the biological differences between the samples.

The plot (Fig. 3.5) clearly showed differences between the groups of points corresponding to the two extraction techniques suggesting different compositions of each extract. Furthermore, the samples extracted using acetonitrile, methanol and water showed less spread within groups of infected and uninfected RBC samples forming tight clusters of points while between group separation was clear. The data corresponding to samples extracted using methanol and water formed much more sparse clusters that were hardly separable between groups. These observations suggested that acetonitrile, methanol and water extraction was more robust and was preferable over the methanol and water extraction.

3.4.3 Comparison of Sample Drying Methods

An important step in sample preparation for NMR is sample drying. Up to this point we relied on N_2 flow drying. However freeze-drying or liophylisation has been shown to be a valuable alternative [Mushtaq et al., 2014]. We therefore compared the two sample drying methods in a similar manner to the comparison of extraction solutions (see previous section). We collected NMR spectra of samples of infected and uninfected RBCs dried with either method. The spectra were collected using NOESY pulse sequence with presaturation, 64 scans per sample at 298K, uniformly binned into 0.05 ppm bins, processed and PCA was performed on the resulting data.

We plotted the first two principal components and inspected the clustering of the data (Fig. 3.6). Since the difference between extraction methods was significant we inspected each group of points (RBC/i-RBC and both extraction methods) separately. Both drying methods performed similarly however in the group of samples extracted using methanol and water the spread of points corresponding to the samples dried under the flow of N_2 was larger. To make a decision we took into account the fact that a freeze-dryer is a closed system and no contamination is possible during the procedure, a situation that does not apply to drying under the flow of N_2. Freeze drying also has the advantage of low temperature preventing any unwanted enzymatic reactions taking place during sample preparation due to

protein enzyme contamination. The resultant data indicated that freeze drying was best drying technique for the further experiments.

3.4.4 Optimization of Sample Size

The effect of the sample volume on the quality of NMR results was investigated. Up to this point in each experiment we had been using 100 μL of cell pellet. We aimed to investigate how the information we could derive from the data changes in samples prepared from varying volumes of cell pellet. This was motivated by the need to optimise signal to noise ratio against a background concern over sensitivity and low biomass. We tested the chosen method of sample extraction using acetonitrile, methanol and water and freeze-drying. Samples of three volumes of cells, namely 50 μL, 100 μL and 200 μL from either parasite cultures at 10% parasitemia or concentrated 90% parasitemia samples obtained from magnetic separation were evaluated.

The ability to capture the differences between the various stages of life cycle of *P. falciparum* was chosen as the information measure. At each stage the parasite metabolic activity is different and we chose to investigate how sample volume affected our ability to discriminate between samples prepared from different parasite stages. The results of the experiment are shown in Figure 3.7. The samples were separated into groups. While the presence of replicates would have definitely improved the interpretation, it was clear that the samples in each group were displaced in different directions from the zero point indicating difference in the data. It is interesting to note that 50 μL samples were clearly separated from the higher volume samples (in relation to 0 point) and the 200μL samples were the furthest from 0. The high parasitemia samples were in between the ring and trophozoite stage parasites which was unexpected as the parasites selected by magnetic separation were predominantly trophozoite stage. We did not observe the expected large discrimination between the high parasitemia samples and the uninfected RBCs or low parasitemia samples. Since high parasitemia samples contain more parasite derived analyte content there was an expectation that this would be reflected in the information content of these samples compared to uninfected controls and samples from low parasitemia cultures.

The raw data was also inspected (Fig. 3.8). Overall the spectra collected from the 100 μL and 200 μL samples were very similar in peak area while there was a distinct difference between these samples and the 50 μL samples, especially in ring stage parasite samples. While this suggested that 100 μL pellet was not significantly different from 200 μL the PCA results indicated that the global pattern of the peaks

provided additional information for sample separation. These results, coupled with the bottleneck introduced by the need for magnetic separation, led to the conclusion that the most pragmatic approach to sample processing was to use a 200 μL cell pellet obtained from 10% parasitemia culture for all further investigations.

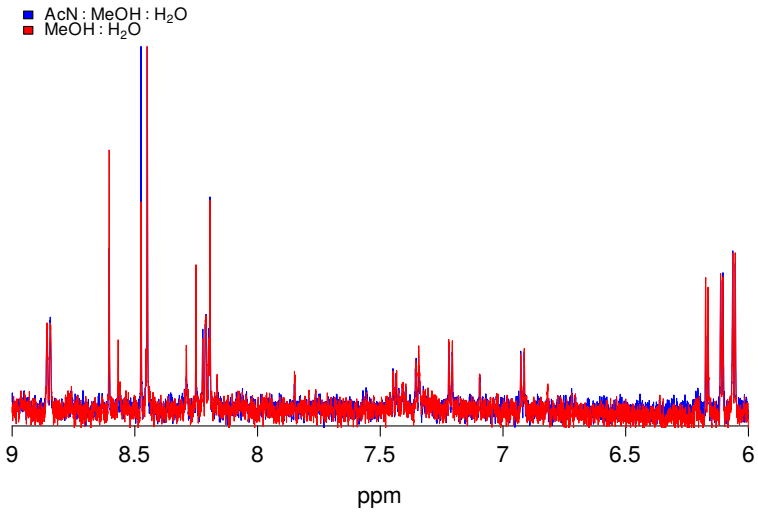

(a)

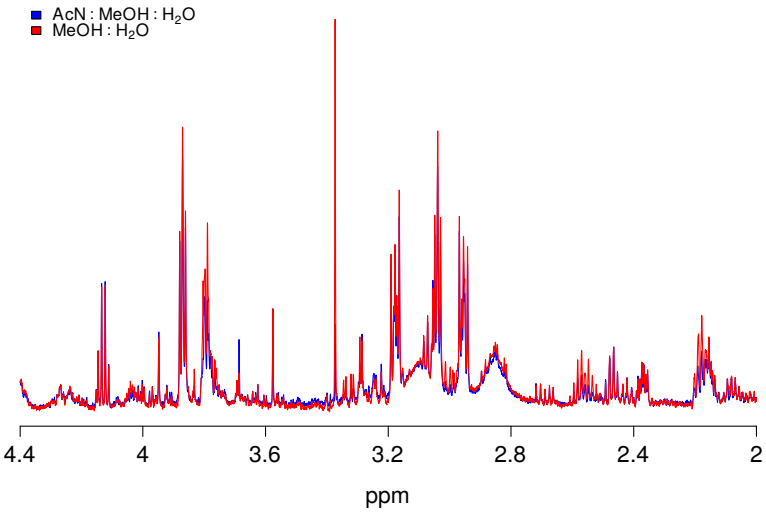

(b)

Figure 3.3: A comparison of two 1D ^{1}H NMR spectra of *P. falciparum* infected RBC samples, extracted using 1:1 methanol and water and 2:2:1 acetonitrile, methanol and water following the modified metabolite extraction protocol at dry-ice temperature $-70°$C. The aromatic region of the spectrum is shown in (a) while aliphatic region in (b).

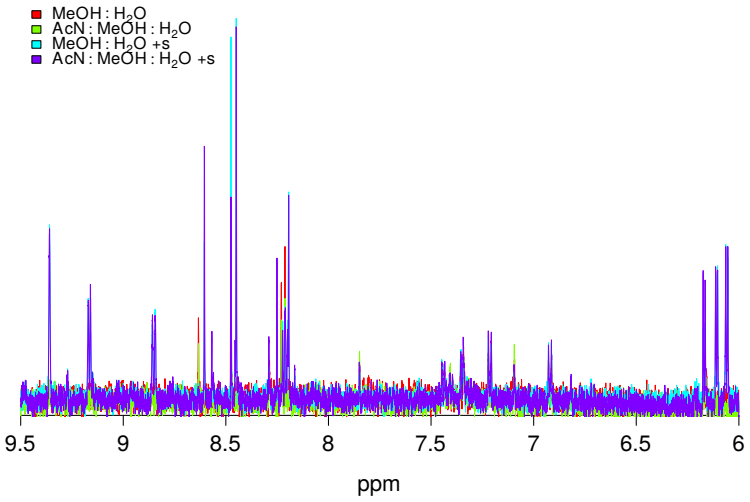

(a)

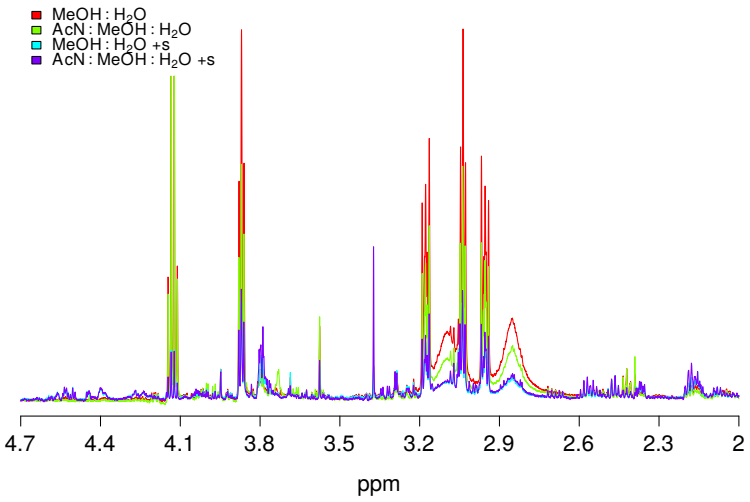

(b)

Figure 3.4: A comparison of two 1D ^{1}H NMR spectra of *P. falciparum* infected RBC samples, extracted using 1:1 methanol and water and 2:2:1 acetonitrile, methanol and water following the modified metabolite extraction protocol on dry-ice at -78.2°C. Two samples were extracted including a sonication step (+s). Two separate regions of the spectra overlay are shown. The spectra are similar in the aromatic region (a). The aliphatic region (b) has peaks of different height with sonicated samples (+s) showing lower signal intensity.

Figure 3.5: PCA scores plot of the NMR experiment carried out using two different metabolite extraction approaches and two different sample drying methods. The points are labelled by cells extracted: RBC - uninfected red blood cells, Inf - *P. falciparum* infected red blood cells at 10% parasitemia. The number in the brackets on the axes specifies the percentage of variance accounted for by the principal component.

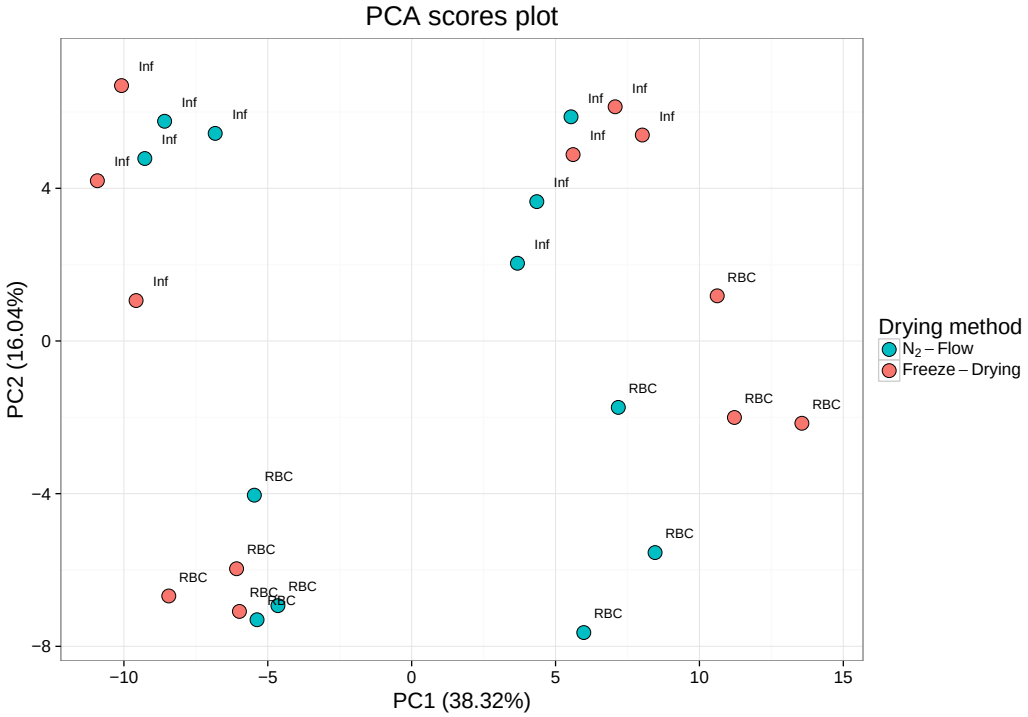

Figure 3.6: A PCA scores plot of the NMR experiment carried out using two different metabolite extraction approaches and two different sample drying methods. The point are labelled by cells extracted: RBC - uninfected red blood cells, Inf - *P. falciparum* infected red blood cells. The number in the brackets on the axes specifies the percentage of variance accounted for by the principal component.

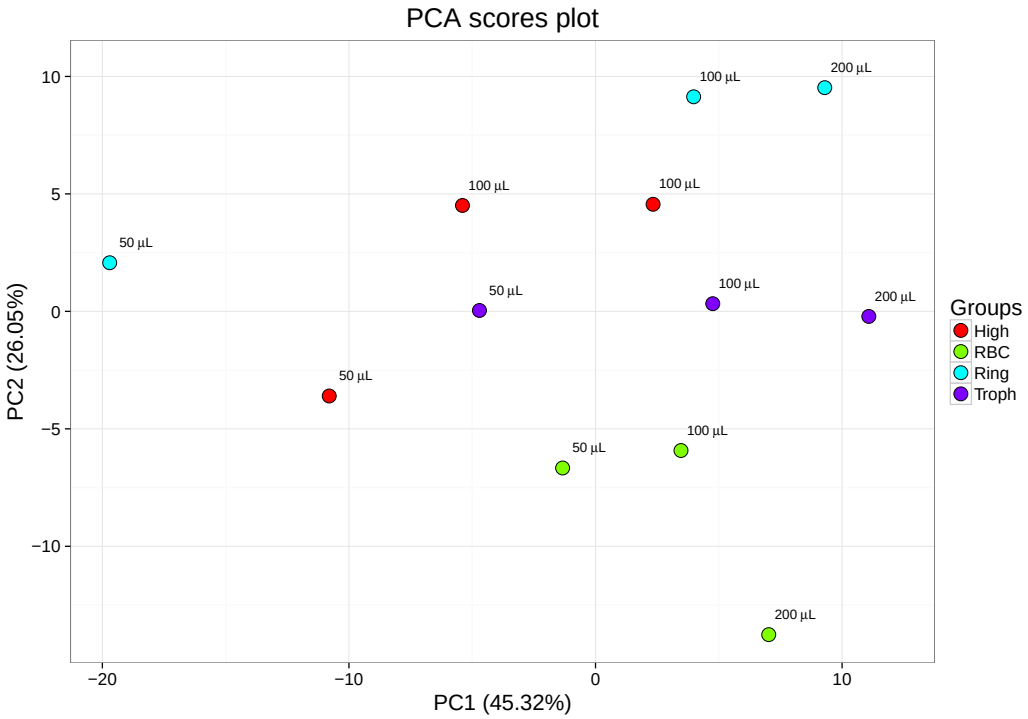

Figure 3.7: A PCA scores plot of the NMR spectra acquired from an experiment carried out on various stages of *P. falciparum* parasites life cycle and at different volumes of culture used per sample. High - 90% parasitemia samples, RBC - uninfected red blood cells, Ring - ring stage parasites, Troph - trophozoite stage parasites.

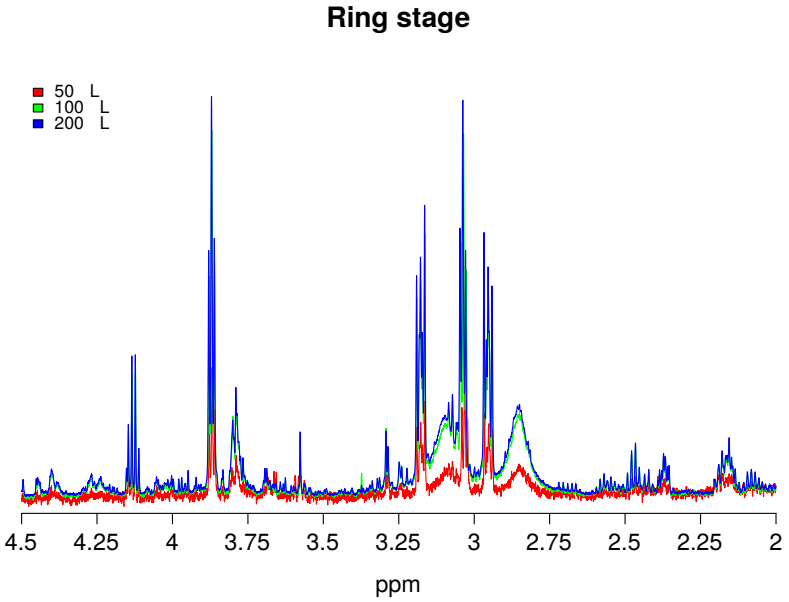

(a)

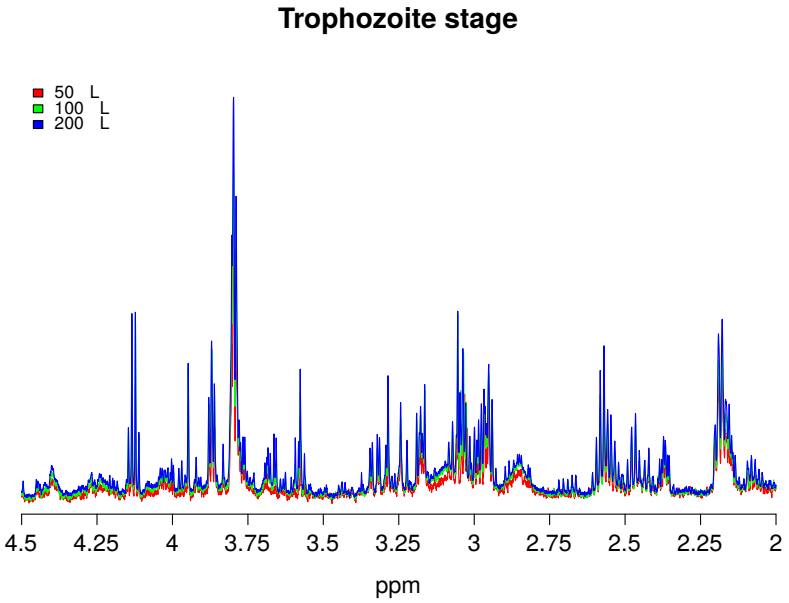

(b)

Figure 3.8: A comparison of three 1D ^{1}H NMR spectra acquired from *P. falciparum* infected RBC metabolite extracts, using varying volumes of cell pellet. The ring stage parasite extracts show larger differences between the $50\mu L$ sample and the $100 - 200\mu L$ samples. The differences between the $100\mu L$ and $200\mu L$ samples are minimal. Ring stage parasite extract data given in (a) and trophozoite in (b).

3.5 Determination of Optimal NMR Parameter Set

At the beginning of the study we adopted the NMR acquisition parameter set used in work performed in [**?**]. The ^{1}H NMR spectra were acquired using a nuclear Overhauser enhancement spectroscopy (NOESY) pulse sequence with pre-saturation (noesypr1d) with $t_1 = 4$ μs and t_m =100 ms. We collected spectra at 298K, collecting 128 free induction decays (FIDs) with 4 "dummy scans". The ppm range of spectra collected was -5 - 15 ppm, with 32,768 data points collected. The data was processed using 0.3 Hz line broadening by multiplication with an exponential function and the number of frequency domain points was doubled by a zero fill at the end of the FID before Fourier transform.

The spectra initially contained a significant protein contamination signal. The quality of the spectra was improved by alterations in sample preparation procedure (ref. to Section 3.4). While this manoeuvre resulted in higher spectral quality, further improvements and refinements were made once the experiments had been optimised and the experimental complexity had increased.

3.5.1 Introduction of CPMG Pulse Sequence

In order to further improve the quality of the data we tested a Carr-Purcell-Meiboom-Gill (CPMG) pulse sequence for NMR data acquisition. This pulse sequence is convinient when acquisition of small molecule data is desired [Meiboom and Gill, 1958] while ignoring the signal from large molecules such as proteins. As we increased the volume of cell pellet per sample to 1 mL we noticed an increase in protein signal in the resulting spectra. CPMG was a potential solution to the problem. We performed an experiment (the results are discussed in Section 6.3) involving a time course of *P. falciparum* infected RBCs exposed to antimalarial compounds and collected spectra using the standard NOESY with presaturation and CPMG pulse sequences. The spectra were compared visually in order to assess the baseline and the presence of broad peaks corresponding to residual protein signal (Fig. 3.9).

The spectra acquired using CPMG pulse sequence had a flatter baseline than spectra acquired using NOESY and did not have any noticeable protein signal. The NOESY results however were similar to our earlier collected spectra when testing the 1 mL cell pellet extracts. While the quality of the spectra was acceptable the baseline shifts and the broad peaks underneath the small molecule peaks were skewing the data and making the analysis inaccurate. Due to higher quality data we changed the standard NMR data acquisition procedure to include the CPMG pulse sequence.

3.5.2 Quality Control and Resolution Increase

Since we were developing a high throughput screening method a quality control procedure for NMR spectra was needed. Checking data would be time consuming and was undesired. Automated NMR spectra acquisition had calibration steps (such as shimming) that did not always finish successfully. We needed an automated and reliable way to identify spectra that were not collected optimally. A feature of bad calibration that we decided to exploit for quality control was peak width increase. The spectra that were collected after unsuccessful calibration had broader peaks. We implemented an automatic step in the data processing that measured the width at the mid-height of the TSP peak in Hz. A measure greater than 1.5 Hz was considered to indicate a badly calibrated data acquisition event and indicate the spectra to be of low quality. These data were discarded.

The experimental procedures and data acquisition parameters in this study were optimized using a Bruker Avance II 600 MHz spectrometer. However, in order to test the possible improvement of signal with increased resolution we also collected spectra using a Bruker Avance III 800 MHz spectrometer. This experiment was aimed at assessing the possibility of using the more powerful spectrometer for our routine data collection. We performed a drug exposure experiment (for more detailed discussion of the results refer to section 6.3) and collected the data on both spectrometers using CPMG pulse sequence with 128 scans per sample at 298K. We carried out the routine FID processing and inspected the raw data for comparison (Fig. 3.10). As expected, the spectra collected using the 800 MHz spectrometer were of significantly higher resolution. This resulted in new peaks being resolved that were unobserved in the spectra acquired using the less powerful machine. This prompted us to rely on the 800 MHz spectrometer for all further data collection. While only the 600 MHz spectrometer was equipped with automatic sample changer the difference in signal quality was a deciding factor. The data for the time course experiments (see Sections 6.3 - 6.4) were collected using the 800 MHz NMR spectrometer.

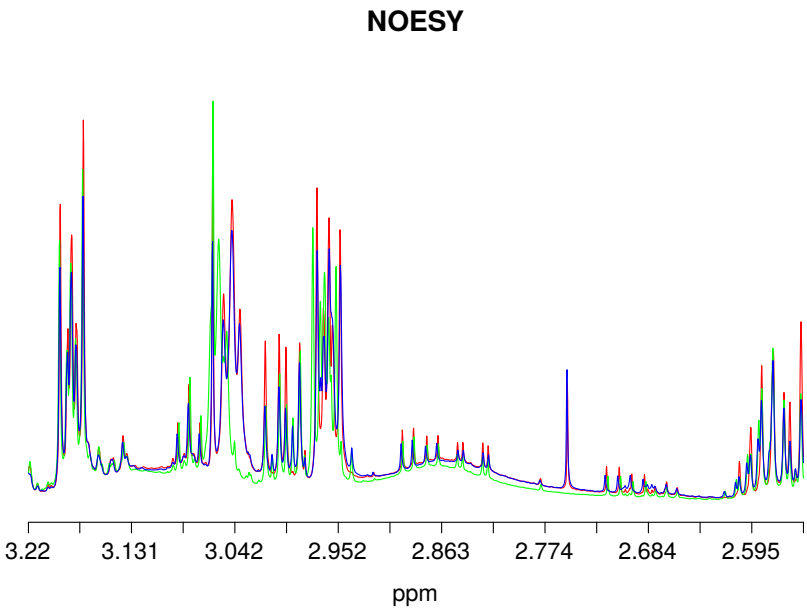

(a)

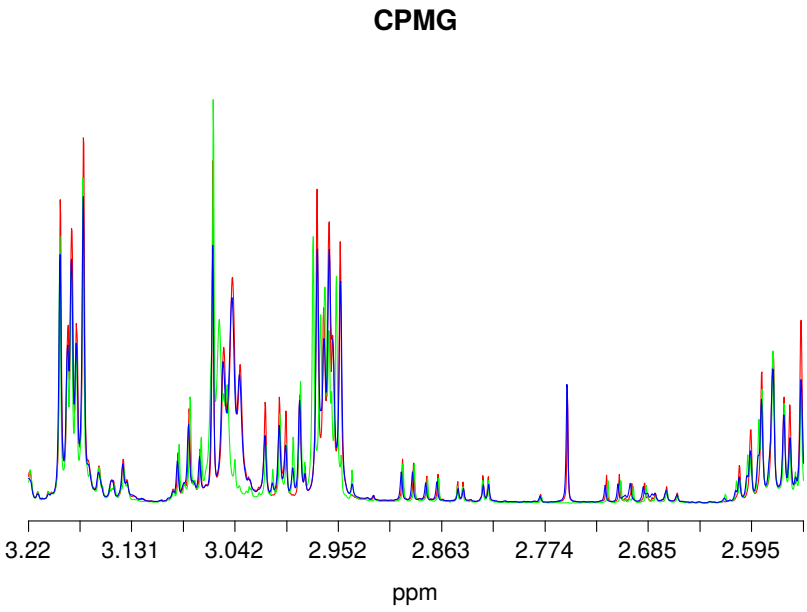

(b)

Figure 3.9: A comparison of 1D ^{1}H NMR spectra acquired from *P. falciparum* infected RBC metabolite extracts, using two different pulse sequences: nuclear Overhauser enhancement spectroscopy (NOESY) and Carr-Purcell-Meiboom-Gill (CPMG). The spectra acquired using CPMG pulse sequence have a flatter baseline and less broad peaks.

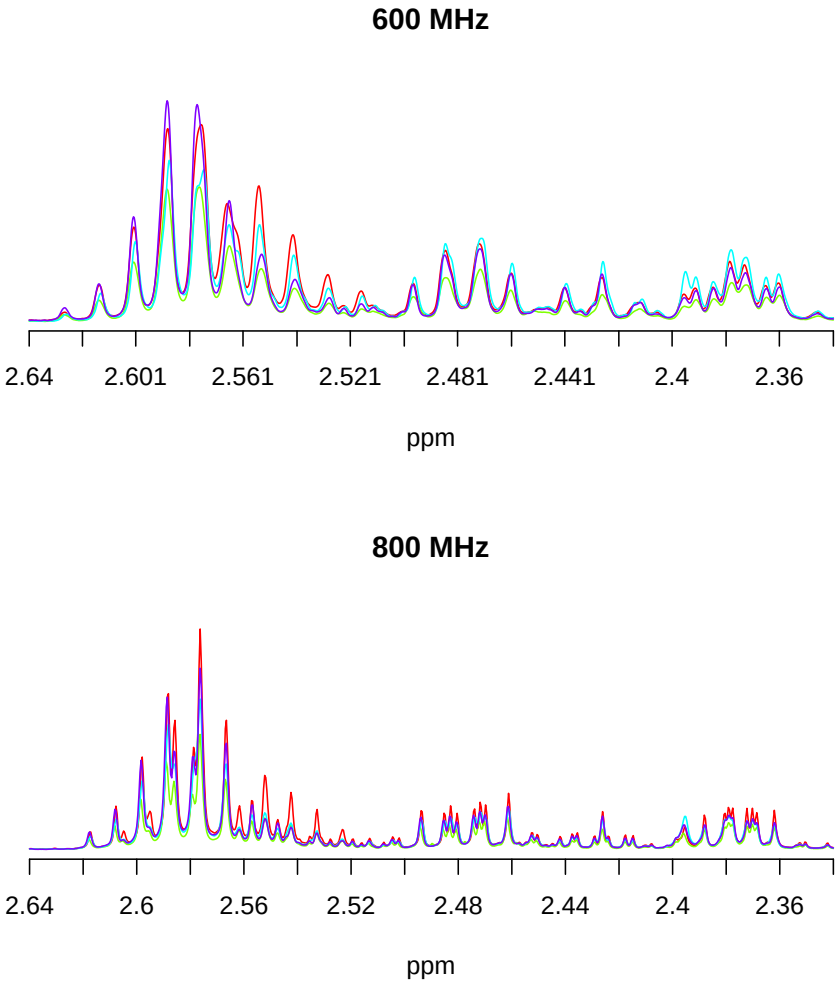

Figure 3.10: A comparison of 1D ^{1}H NMR spectra acquired from *P. falciparum* infected RBC metabolite extracts, using two different spectrometers: 600 MHz and 800 MHz. The resolution in the spectra acquired using the 800 MHz spectrometer is significantly higher allowing for more accurate binning.

Chapter 4

ProcNMR - Custom NMR Data Processing Software

4.1 Introduction

The ever-accelerating progress in computational techniques and the rise of the *-omics* family of sciences (including genomics, proteomics, transcriptomics and others) have brought bioinformatics into the forefront of biological sciences. As the experiments have grown in size and complexity the requirements for data processing and analysis tools have increased drastically. However, not all the branches of -omics have developed at a similar pace. While genomics was the fastest growing with the next generation sequencing technologies and the human genome project driving the progress and proteomics not far behind, metabolomics still seems to be rather immature as a science in terms of available tools and techniques. In particular NMR spectroscopy based metabolomics tools seem to be quite scarce and those available are quite limited.

In this chapter we introduce a custom piece of software developed for this PhD project - ProcNMR. It was built for NMR data import and processing in order to automate the procedure and reduce the required human input when handling data prior to analysis. The motivation for creating the software and available alternatives are discussed in Section 4.2. It is followed with the description of the implemented functionality and future plans (Section 4.3). In Section 4.4 we review some details of implementation and general design decisions that were taken. The software is being developed further and in Section 4.5 the potential development ideas are outlined.

4.2 Motivation and Alternatives

NMR data is collected in a shape of a free induction decay (FID) and stored on the computer controlling the spectrometer. It is then processed in order to convert it to a frequency domain and prepare for further analysis. The data is then inspected and subject to structural or statistical analysis algorithms. All these steps require specialised software solutions.

There are a wide array of NMR-related software currently available, ranging from large commercial products to free academic projects that implement some functionality required for particular applications. The commercial vendors that supply NMR spectrometers offer their proprietary software (e.g. Bruker Topspin and Amix, Varian Vnmr). This software is provided together with the spectrometers and is often seen as industry standard. There are companies that specialise in software such as Chenomx. inc and SpinWorks. While high quality, the commercial software is usually expensive and comes with predetermined features that in many cases can not be tailored to individual needs. New features only come in new versions of the software that has development cycles that can last years. On the other end of the spectrum are small software projects usually started in academic institutions in order to meet the needs of specific projects that are not be fulfilled by commercial solutions. Academic projects often tackle novel problems and required functionality that is often not present in well-established and standardised commercial software. Such projects however are usually developed in programming languages popular in academic circles such as Matlab (MetaboID [MacKinnon et al., 2013], Focus [Alonso et al., 2014]), or R (Batman [Hao et al., 2014] and BQuant [Zheng et al., 2011]) and are often abandoned past the stage of publishing the first working version. There is also an inbetween category of projects that started as academic open source initiatives and have grown into large scale projects e.g. CCPN [Chignola et al., 2011], NMRPipe [Delaglio et al., 1995].

ProcNMR at the moment of writing belongs to the second category. The software has been written to meet the specific needs of this project in the process trying to circumvent the shortcomings of software available to the project. First we chose Python as a programming language for this work. It is relatively fast (for a scripted language) and supports but does not rely on an object oriented paradigm. It is free and has a huge community of open source project contributors which often helps projects survive long term after being released as open source software.

ProcNMR was developed due to the lack of a software solution that would fulfil the requirements of the project. We required a tool for 1D NMR data import

and automated processing for analysis. It also had to be customizable, preferably free, completely automated and easily extendable. A high throughput pipeline intended for drug screening needed a robust method for processing the data acquired. One of the aims was to reduce the human input when it came to processing individual spectra due to possible human bias and time demands. This prompted the design and implementation of a command line tool that would allow high throughput data import and processing based on a set of predetermined parameters without any additional input from the user during the process. Such a solution would allow robust data treatment and save time once the method had been established and validated.

4.3 Functionality

ProcNMR is written as a command line tool and so far has been tested on Linux operating systems. While it is designed to be run in automatic mode it has a manual mode that allows the user to set up the parameters manually before the first run. The automatic mode requires the input, output and configuration files to be specified as command line parameters and runs without any interference from the user. The software prints feedback messages in the terminal describing the pipeline contents as well as the progress of the run (Fig. 4.1). The output can be conveniently piped into a text file and saved as a report of the run.

The manual mode invokes the configuration tool that facilitates the generation of the configuration files. It is a text based question and answer system that allows the choice of pipeline steps to be performed. The user is informed about the processing nodes available, chooses the processing steps required in turn and specifies the parameters required for each step (Fig. 4.2). It also includes a mechanism for assessing the pipeline in order to check for possible mistakes in the processing order e.g. any spectra processing steps would not be allowed before the data has been Fourier-transformed. Once the configuration parameters are set they can be saved in a file and reused later.

At the time of writing ProcNMR is capable of reading Bruker proprietary data files and import the raw FID data as well as metadata including the acquisition parameters. Once the data is imported it initiates a pipeline of processing steps that is assembled based on the processing parameters supplied either through the configuration file (automatic mode) or a text user interface (manual mode).

The functionality of the pipeline is presented in Table 4.1. Once the configuration is set the pipeline is assembled from functional modules the data is processed.

Data import	Reading of Bruker proprietary data files
Apodisation	Exponential, sine-bell or Gaussian transformations of FID
Zero-fill	Variable length zero fill
Fourier transform	Transforms the data from time domain to frequency domain
Phasing	Automatic or manual phasing of spectra
Referencing	Referencing the spectra to a standard peak e.g. TSP
Quality control	Control for spectra acquired with bad calibration
Slicing	Slicing of spectra for removal of unnecesary parts
Normalization	Normalization of spectra by total area, reference peak height or probabilistic quotient normalization
Binning and Integration	Uniform or custom binning and integration
Data export	saving the processed data to CSV format

Table 4.1: The functions performed by ProcNMR pipeline.

The spectra can be plotted and saved as *pdf* or *png* files for inspection. Once all the steps have been performed the data is saved as a comma separated value (CSV) file. Besides the configuration tool the software does not require any input from the user allowing performance of identical data processing procedures on any number of spectra or experiments.

```
        Welcome to ProcNMR!

The pipeline is running in automatic mode

Processing parameters not given, using default parameters.
Building processing node train

Reading bin file.

The pipeline consists of:
1 : Standard FID processing - em: lb - 0.3
2 : Spectrum phasing - auto
3 : Spectrum cleanup (rem. imag. part, reverse)
4 : Reference
5 : Quality control : 1.5 Hz
6 : Spectra trimming
7 : Bin integration: Custom bins


Creating Experiment from: /home/arturas/NMR_data/Arturas_140415_UER1

Reading: 4 - T12_C_CPMG
Reading: 3 - T6_C_CPMG
Reading: 5 - T24_C_CPMG


Performing auto-phasing: T12_C_CPMG
Optimization terminated successfully.
Performing auto-phasing: T6_C_CPMG
Optimization terminated successfully.
Performing auto-phasing: T24_C_CPMG
Optimization terminated successfully.

Writing data to file: /home/arturas/NMR_data/Arturas_140415_UER_1_out.csv
...T12_C_CPMG
...T6_C_CPMG
...T24_C_CPMG

Done.
```

Figure 4.1: Example output of a ProcNMR run.

```
                ProcNMR Pipeline Configuration Tool


The Pipeline consists of:
currently empty

Available nodes:

1. FID processing (apodisation, fourier transform)
2. Phase Correction
3. Cleanup (Required after phase correction)
4. Reference (to TSP peak)
5. Quality control
6. Slicing (remove unwanted regions of spectra)
7. Binning


To choose a node type the number and press <enter>.
To end the session type: 0
Node: 1
Phase Correction
Choose an apodisation method
(1) exponential, (2) sine-bell (3) Gaussian
Method: 1
Line broadening (Hz): 0.3

The Pipeline consists of:
1. FID processing (apodisation, fourier transform)


Available nodes:

1. FID processing (apodisation, fourier transform)
2. Phase Correction
3. Cleanup (Required after phase correction)
4. Reference (to TSP peak)
5. Quality control
6. Slicing (remove unwanted regions of spectra)
7. Binning


To choose a node type the number and press <enter>.
To end the session type: 0
Node: 0
Configuration complete

The Pipeline consists of:
1. FID processing (apodisation, fourier transform)
```

Figure 4.2: Example output of a ProcNMR configuration tool run.

4.4 Implementation Details

As previously mentioned ProcNMR is implemented in Python programming language and currently supports versions 2.6+. The implementation follows an object oriented design and is modular to facilitate extendibility. A series of packages are used in implementation including *SciPy* [Jones et al., 2001–], *NumPy* [van der Walt et al., 2011], *Matplotlib* [Hunter, 2007], *Pandas* [McKinney, 2010] and *Nmrglue* [Helmus and Jaroniec, 2013]. The last is a well designed library for NMR data import and manipulations that ProcNMR is heavily based on. NumPy arrays are utilized for storing spectra allow fast and efficient numerical calculations. Scipy is used for optimization procedures and Matplotlib for its high quality plotting capabilities. A schematic representation of the workflow is shown in Figure 4.3.

The **Spectrum** object holds the data as well as meta-data extracted from the Bruker data file. A collection of spectra are stored in an **Experiment** object and are treated as a single entity. The experiment is assumed to be composed of a collection of spectra that are to be processed in a uniform manner. However, this only applies to processing steps and parameters. Since each spectrum is stored in a separate object there are no limitations on uniformity of the spectral parameters in the experiment e.g. each spectrum could be acquired using varying pulse sequences or contain different number of points. Each spectrum carries its own meta-data and is processed accordingly.

The **Pipeline** is initiated from user supplied parameters. It consists of a series of processing nodes that each perform a processing step on the spectra. The **ProcessingNode** class is designed as an abstract class of objects that is used to implement various processing steps in a uniform manner. Each processing node is then built on this class and contains a *process()* method that the pipeline calls in order to apply the funtionality of the node to a spectrum. This design allows the processing nodes to be modified without any changes to the rest of the pipeline. Each node is a separate module of the pipeline and only interacts with the pipeline through the generic *process()* method. It allows easy addition of new nodes when a new piece of functionality is required. Many nodes have a series of methods they can apply. When the pipeline is initiated each node is dynamically assigned the function it will perform as well as processing parameters set by the user. Since all the nodes are composable in the order they are assembled, the pipeline does not have to know anything about the operations performed by each node. There are eight nodes currently included in ProcNMR.

FID processing node performs apodization using one of the following methods:

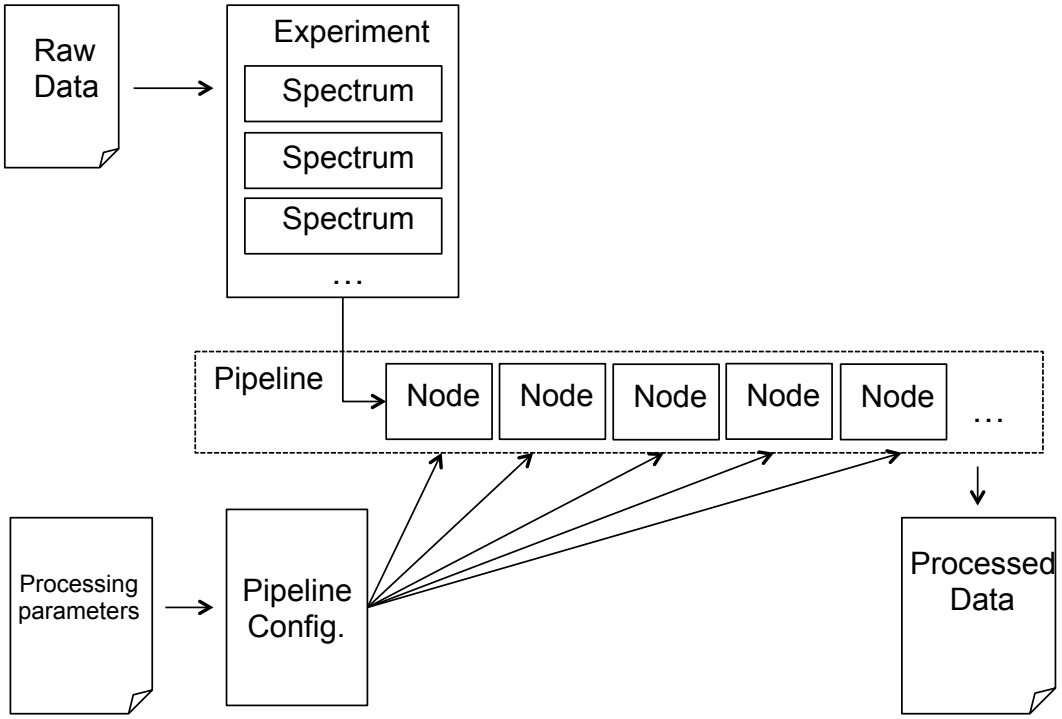

Figure 4.3: A schematic of the workflow in ProcNMR. The raw data is imported and stored as an Experiment object. The pipeline is assembled from processing nodes according to the user-supplied parameter file. The data is then processed in each node and outputted as a CSV file.

Exponential: multiplies the spectrum by the exponential function. The apodization window: $e(x_i) = exp(-\pi \times i \times lb)$, where lb stands for line broadening parameter in Hz.

Sine-bell: multiplies the spectrum by the exponential function. The apodization window: $sb(x_i) = sin(\frac{\pi \times off + \pi \times (end - off) \times i}{n-1})^p$, where off is the offset from the start of the spectrum, end - end of sine-bell, $size$ is the size of the spectrum and p is the power to raise sine-bell to (1 by default).

Gaussian: multiplies the spectrum by the Gaussian function. The apodization window: $f(x_i) = exp(-a \times i - b \times i^2)$, where a is an exponential term and b is the Gaussian term of apodization.

It then performs the zero fill at the end of the spectrum and Fourier transforms the data. The effect of apodisation (exponential) are demonstrated in Figure 4.4.

Spectrum phasing node performs manual (based on angles given) or automatic spectrum phase correction. The auto-phasing is performed by entropy minimisation,

implementing the method in Chen et al. [2002].

Clean-up node performs general house-keeping operations in preparation for further analysis. Currently it removes the imaginary part of the signal and reverses the spectrum.

Reference node finds the reference peak (TSP or TMS) and generates the *Hz* and *ppm* scales for the spectrum starting from this point ($\delta = 0$ ppm).

Quality control node performs quality control of the data (QC). Currently QC is performed by measuring the width of the reference peak in Hz at its mid-height point. In case this measurement is greater than 1.5 Hz the spectrum is flagged for bad quality.

Trim node performs the slicing of the spectra. It removes parts of the spectra that are not required for the further analysis. Currently mostly used to remove the noninformative ends of the spectra. However the node is being extended to include possibility of slicing the spectra into subsets e.g. when removing water signal or residual solvent peaks.

Normalisation node performs the spectra normalisation by the total area under the curve, the height of the reference peak, probabilistic quotient normalisation method [Dieterle et al., 2006a] or any chosen point in the spectrum. The last option is used in cases when an external standard of known concentration is present in the sample.

Binning node divides the spectrum into intervals (bins) and calculates the area under the curve. Currently uniform binning by specified ppm window or custom binning according to a custom bin table is possible. Custom binning uses a user supplied file where bins are given as ppm intervals. The integration is performed using the trapezoidal rule.

The Experiment object also has plotting functionality using *Matplotlib* library. Currently the spectra can be plotted in full or as a subset and is mainly used for checking the results of the processing. As the pipeline runs, the nodes give feedback about the results of processing that are streamed to the command line. This allows either real time following of the pipeline or redirecting the output to a log file for later review.

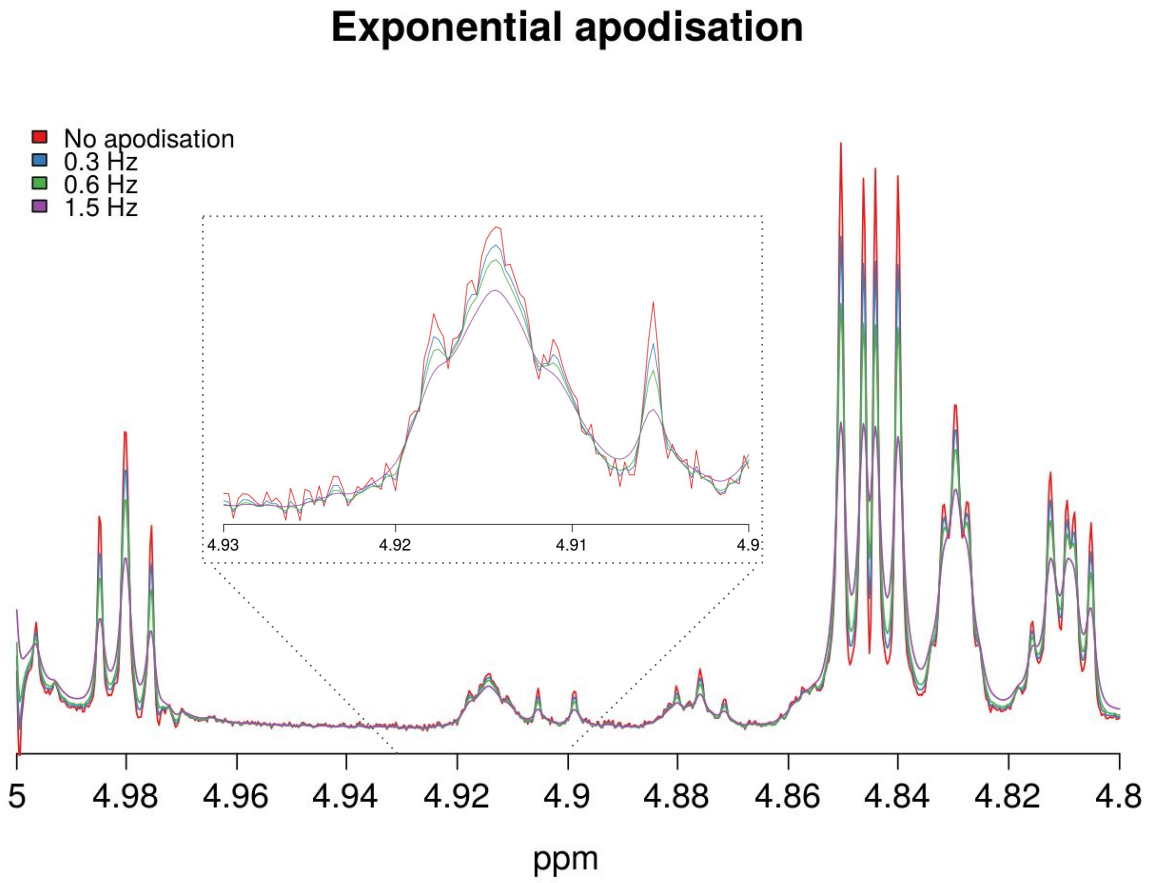

Figure 4.4: Example of effects of exponential apodisation applied with a range of values of the line broadening parameter (lb).

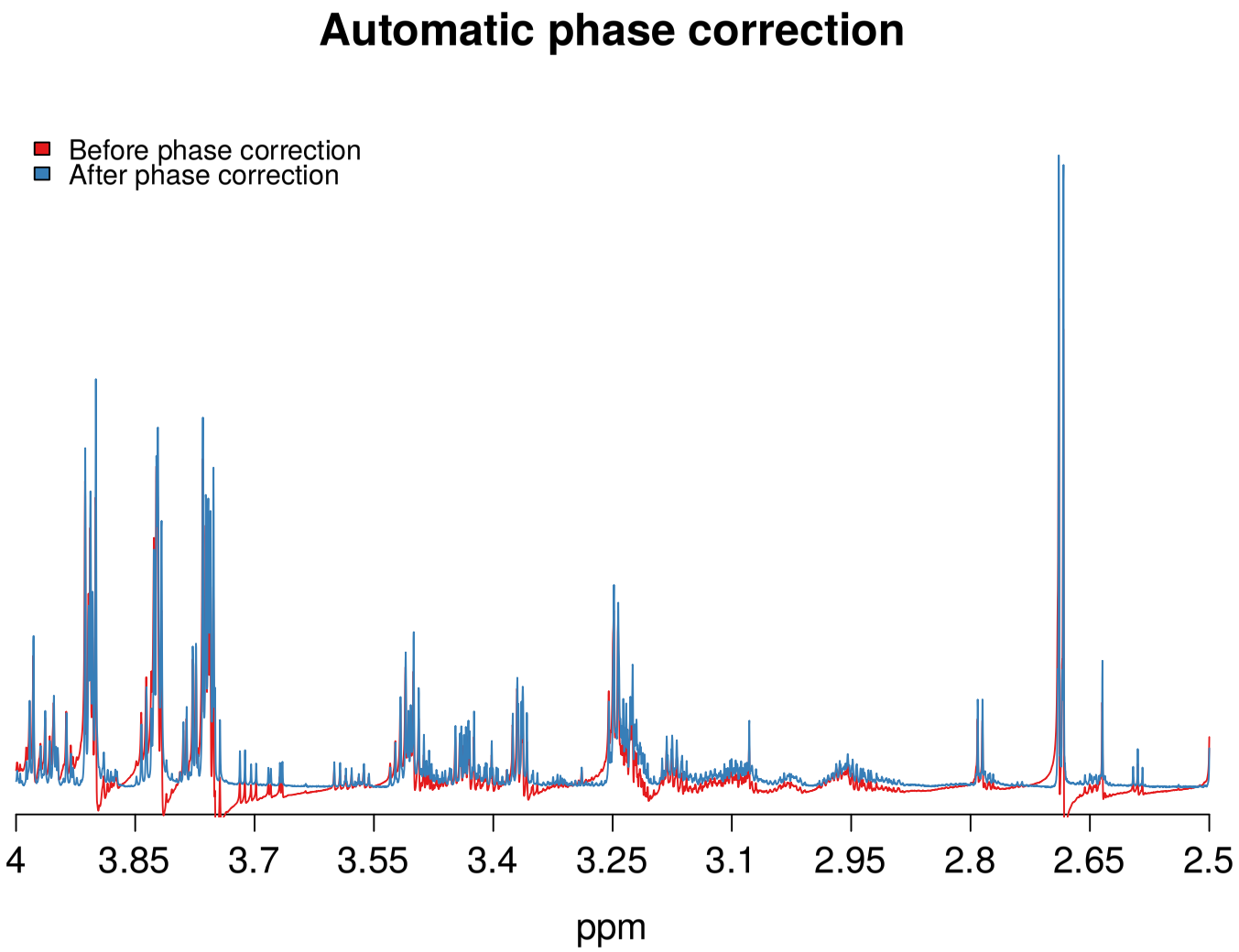

Figure 4.5: An overlay of a spectra before and after automatic phase correction in ProcNMR.

4.5 Further Develoment

At the time of writing the software is in fully working state and has been used for processing of most of the data described in the following chapters. However there still remain many improvements that can be made before the software is robust and ready for release.

Firstly the automatic phasing of spectra can take up to a few minutes per spectrum on slower machines. The routine can be optimized by adjusting the sequence of computations. It could be further improved by adding the possibility of processing spectra in parallel. This could potentially generate a significant improvement in processing time, especially since most desktop computers now have multi-core processors.

Currently the pipeline outputs the data in a CSV file format that is convenient for further analysis however the acquisition parameters and the processing parameters are not output at all. This information could be useful for further analysis as well as reporting the findings and depositing data in online repositories. For this purpose a different output format would be needed. While there is no established data standard for NMR data, *nmrML* is the most promising standard currently in development *www.nmrml.org)*. Once released this standard could become the default data type to be used by ProcNMR as it would not only help to preserve the experimental meta-data but also facilitate data sharing. The user interface for making processing parameter files is not very convenient and could be improved using a graphical dialogue window or web interface. Lastly there are processing steps that should be added such as spectral alignment and variable binning. At this time algorithms are being tested for alignment however a suitable solution had not been found yet. The potential misalignment is currently partly mitigated by custom binning of spectra.

ProcNMR is being developed further and hopefully can be released and used as a standalone tool or integrated into a larger pipeline.

Chapter 5

Metabolic Fingerprinting of *P. falciparum* Using FT-IR Spectroscopy

5.1 Introduction

FT-IR has been used in numerous metabolomic studies to date [Ellis and Goodacre, 2006]. It has proven to be a powerful technique for identification and research of a variety of species of bacteria, fungi and yeast [Naumann, 2000; Beekes et al., 2007]. However none of the studies have been carried out on *Plasmodium* species. *P. falciparum* is a complex target to study due to its intracellular life-cycle. Here we describe an FT-IR-based *P. falciparum* metabolomic fingerprinting study performed in order to assess the technique for use in antimalarial drug screening. As the drug modes of action potentially induce rather subtle changes in parasite metabolism the discriminatory power of the technique was first tested when applied to *P. falciparum* infected and uninfected RBCs followed by test of its discriminatory power of various stages of the parasite life-cycle. FT-IR was chosen due to its relatively rapid data acquisition and easy sample preparation (see Chapter 2). An experiment was also performed in order to test the DMSO effect on the RBC metabolic fingerprint as there was some evidence of such an effect from an earlier pilot study (not published).

5.2 Study of the Effects of DMSO on RBCs

In a previous study a difference between RBC samples incubated in standard RPMI medium and RPMI medium with 1% DMSO was observed. As some drugs are

dissolved in DMSO it was essential to account for potential solvent effects that might undermine future experiments. Therefore the initial experiment was designed with the aim of testing whether DMSO had any observable effects on the RBC metabolic fingerprint when cultured in standard culture media. The experiment was performed using *P. falciparum* infected and uninfected RBCs with and without DMSO treatment over 8 hours with sampling every 2 hours. Three replicates of each sample were collected resulting in a total of 42 collected spectra. PCA was performed in order to visualize the structure in the data and assess the similarity of samples in normal medium and DMSO-containing medium. The first two principal components of the PCA were plotted as a scatter plot (Fig. 5.1). The DMSO and control samples did not show any separation suggesting no difference between the sample groups. There was no clear time-related pattern either indicating that the cells did not exhibit any observable change over time. The analysis was repeated on infected and uninfected RBC data separately with the same results (data not shown).

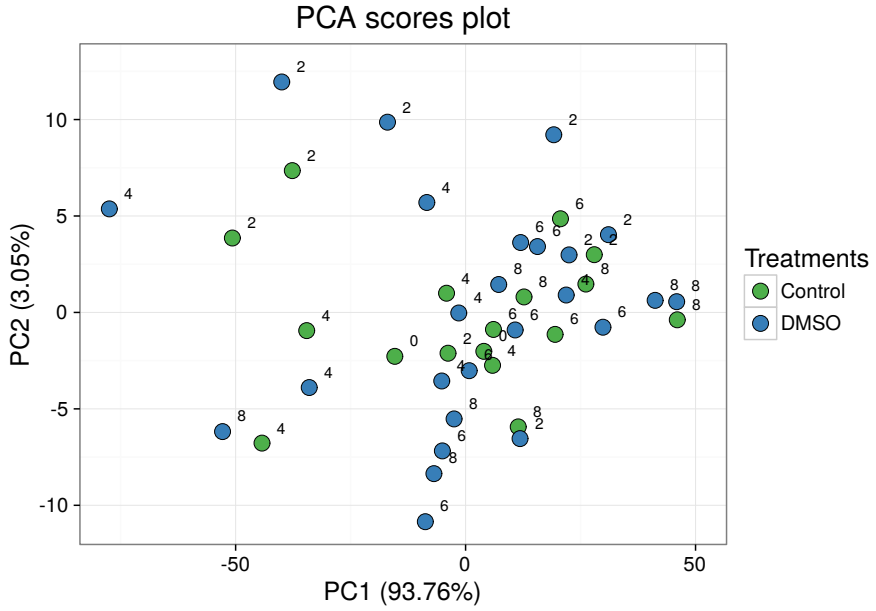

Figure 5.1: PCA scatterplot of an FTIR experiment testing DMSO effects on the RBCs. Control RBCs were incubated in standard RPMI-based medium, while the DMSO treated samples were incubated in the same medium with added 1% DMSO. The samples were taken for 8 hours every 2 hours. The numbers in the plot correspond to sampling time.

The data was further analysed using DA-PC. Since there were only two groups to be discriminated only one discriminant function was used and each group

of data-points was plotted as densities on one axis (Fig. 5.2). The groups of points overlapped significantly supporting the results of the PCA. The data suggested that the presence of 1% DMSO in culture medium did not have a significant impact on *P. falciparum* infected or uninfected RBC metabolic fingerprint or the impact was not observed in the FT-IR data due to sensitivity issues.

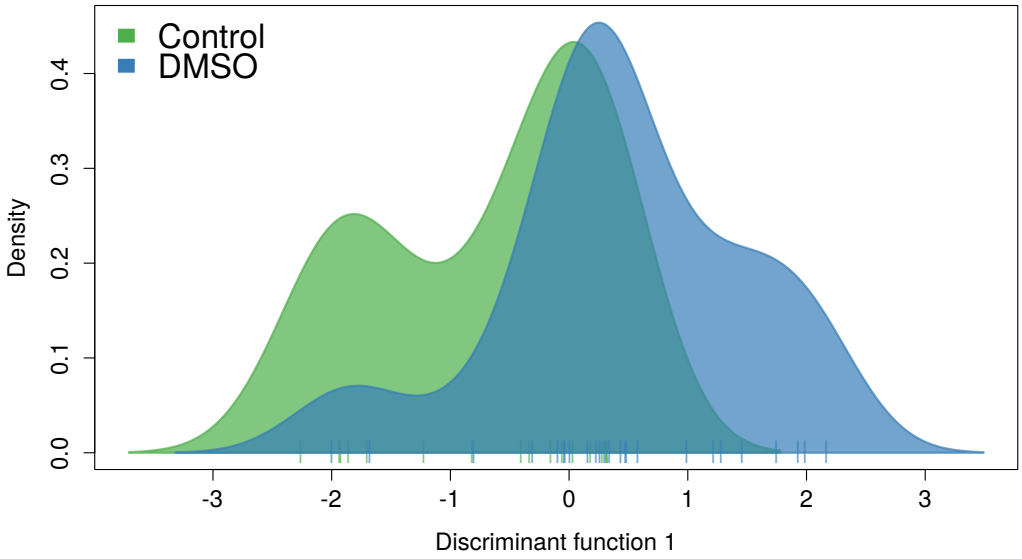

Figure 5.2: DA-PC density plot on the first discriminant function. The densities of each data set are significantly overlapping showing the similarity of the treated and untreated samples.

5.3 Discrimination Between *P. falciparum* Infected and Uninfected RBCs

As the first assessment of the suitability of FT-IR fingerprinting for *P. falciparum* studies the discriminatory power of the technique was tested on infected and uninfected RBCs. The ultimate aim was to show that FT-IR could be used in screening of antimalarial compounds based on their mode of action. Central to this aim is the ability of the analytical approach to be able to discriminate signal from the parasite from the background signal from the RBC. Samples of infected (parasitemia 90%, trophozoites) and uninfected RBCs we prepared and FT-IR spectra collected. PCA of the data was performed and the first two principal components plotted as a scat-

terplot (Fig. 5.3). The plot showed separation between data points collected from infected and uninfected RBCs. While there was a significant amount of variation in each group the between group separation suggested that the FT-IR data contained a significant amount of signal contributed by the parasites.

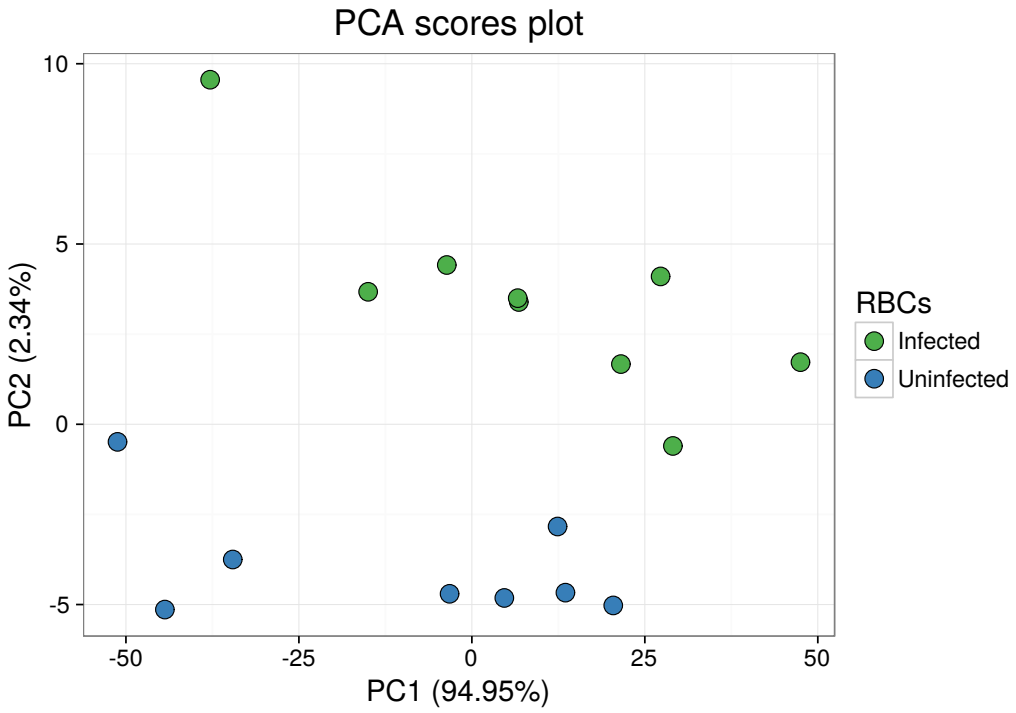

Figure 5.3: PCA scatterplot of the FTIR experiment comparing infected and uninfected RBCs. The plot shows that there is significant variation within each group however the between group variation still allows discrimination between the two conditions. It shows that FTIR data collected from *P. falciparum* infected and uninfected RBCs contains information contributed by the parasite that can be recognised.

The data was further analysed using DA-PC with the aim of separation of the two groups of spectra on one discriminant function. The results (Fig. 5.4) showed a clear separation between data points. This confirmed our findings in PCA. Infected and uninfected RBC samples produced significantly different FT-IR spectra. The loadings plot of the discriminant function in order to find the parts of the spectra that contributed the most to the discrimination of the groups is shown in Fig. 5.5. Most of the significant bands corresponded to carbon, nitrogen and hydrogen bond stretching. While the absorbance bands can usually be approximately assigned, in complex biological samples it is not practical and the data is better used as a metabolic "fingerprint" of the sample. Since the data showed clear separation

between *P. falciparum* infected and uninfected RBCs the discriminatory power of FT-IR was investigated further.

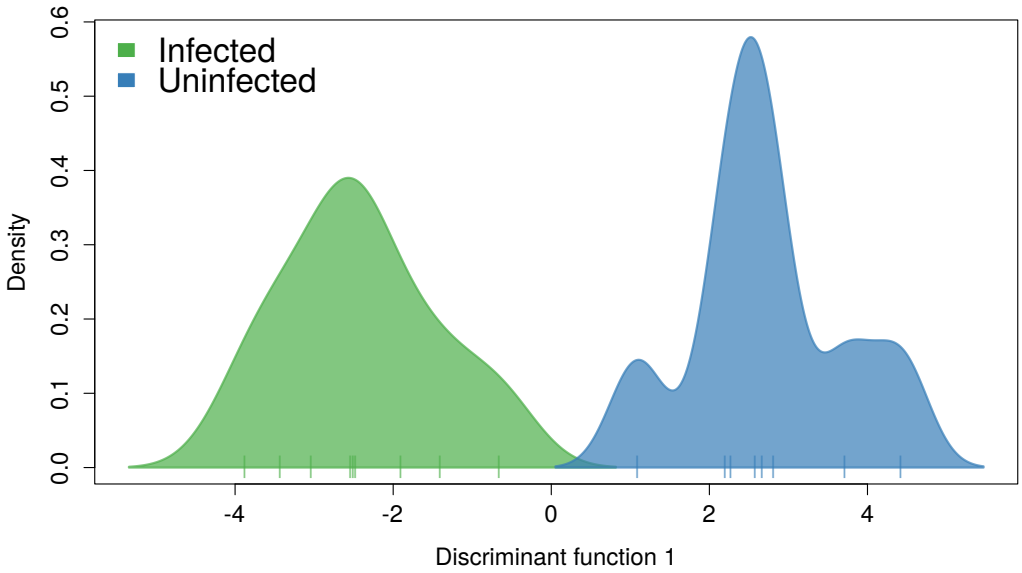

Figure 5.4: DA-PC density plot of the comparison between infected and uninfected RBC data from an FTIR experiment. The two densities are separated showing the clear difference between groups. This further confirms the PCA results in Fig. 5.3.

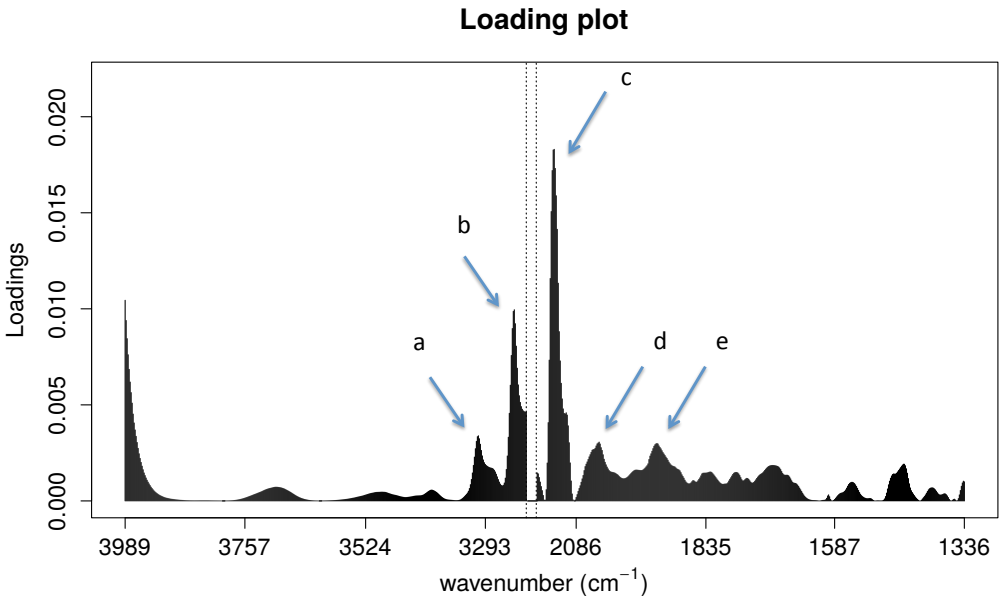

Figure 5.5: The loadings plot of the DA-PC shown in Fig. 5.4. The dotted lines show the region of spectra that has been removed due to lack of any biologically relevant information. Each peak corresponds to a region contributing to the separation of groups. The spectral bands can be approximately assigned to : a-b) =C-H or C=H stretching in aromatic compounds, secondary amine N-H stretching, c) C=C stretching or aromatic isonitrile -N≡C stretching, d-e) combination $N-H$ or $O-H$ stretching.

5.4 Discrimination Between Infected RBCs At Various Stages of the *P. falciparum* Life-cycle

Using FT-IR spectra we were able to show clear differences between *P. falciparum* infected and uninfected RBCs. In order to further investigate the information content of the data acquired in FT-IR fingerprints an experiment was performed to compare parasites at different stages of the intraerythrocytic life cycle. The samples were collected at the early (0-6 h post invasion) and late (6-12 h post invasion) ring, as well as trophozoite (24-38 h post invasion) and schizont (38 h post invasion) stages. The trophozoite stage parasites were collected using magnetic separation (Section 2.1.7) and samples were taken from the enriched culture. The rest of the

parasites were further incubated in standard medium. After incubation for 6 hours the parasites reached the schizont stage and were sampled again. The early and late ring stage samples were collected after further incubation of the culture for 6 and 12 hours respectively. The data was processed as usual and first analysed using PCA. The first two principal components of the PCA were plotted (Fig. 5.6) in order to assess the grouping structure in the data. It was clear from the plot that the four groups did not show any meaningful separation. None of the groups could be discriminated from the rest based on approximately 96.5% of the variance accounted for in the first two principal components.

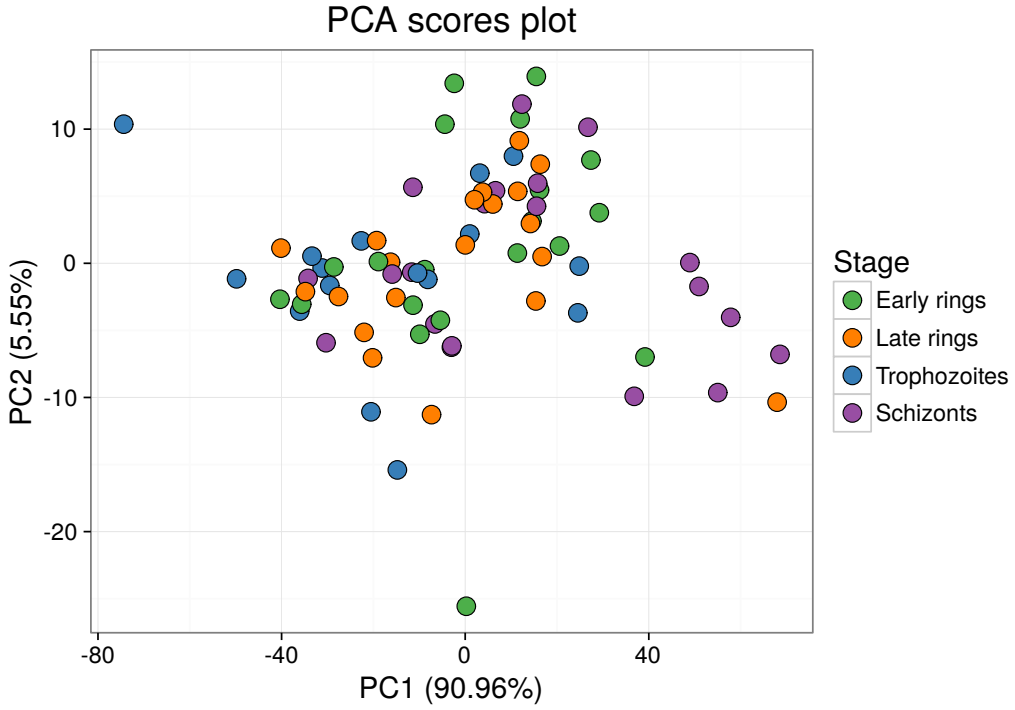

Figure 5.6: PCA scores plot of the FTIR experiment comparing the data collected from *P. falciparum* infected RBCs at different stages of the parasite life-cycle. There is no clear separation between groups of points showing similarity between the groups in the FT-IR data.

In order to investigate the data further DA-PC was performed using 3 discriminant functions. The DA-PC transformed data was plotted on the first two discriminant functions as a scatter plot. The trophozoite and schizont samples showed slight difference to ring samples in the DA-PC however the differences were minor and the majority of samples could not be discriminated. The data did not contain enough information of parasite composition and metabolism to discriminate

between the life-cycle stages.

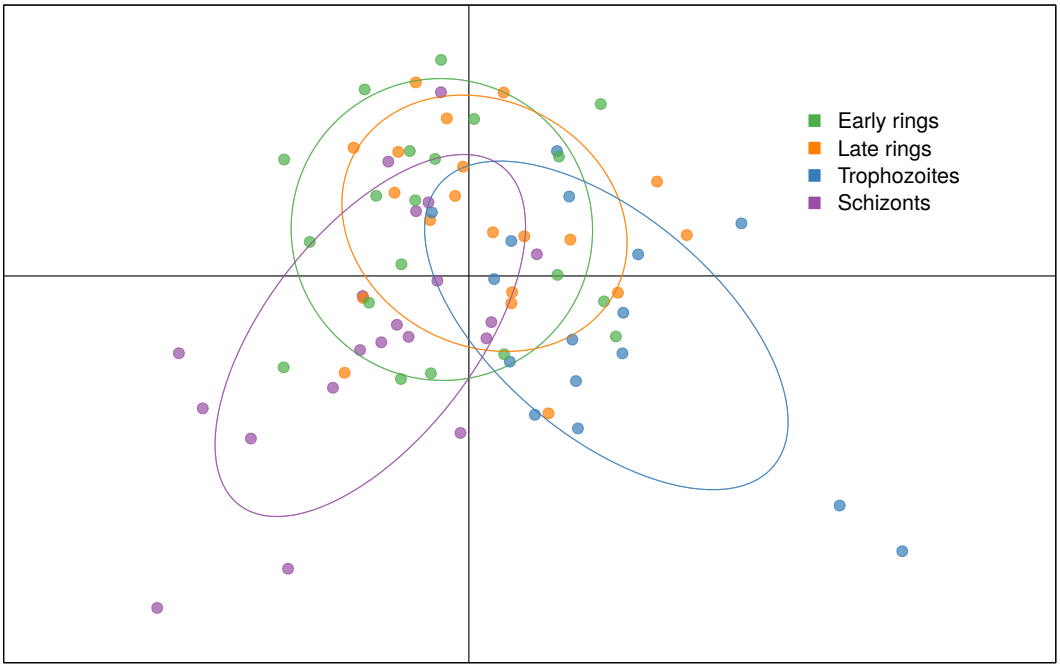

Figure 5.7: DA-PC plot of the first two discriminant functions of the FTIR experiment comparing RBCs infected with various stages of *P. falciparum*. The ellipses represent the 95% confidence region for each group. There is no clear separation between the groups of points indicating no differences between the different stages of the parasite in the FTIR data.

5.5 Discussion

FT-IR spectroscopy is a high throughput analytic tool that requires little sample preparation and allows data acquisition with minimal limitations to subject matter or state. It has also been shown to be effective at identification of bacterial species [Goodacre et al., 1998, 2004; Lin et al., 2004b,a, 2005; Al-Qadiri et al., 2006b,a; Al-Holy et al., 2006] often to subtypes. These results led to our trial application of FT-IR to antimalarial drug screening. However the problem at hand was of considerably higher complexity. The previous work done on bacteria was always performed on pure cultures. Purification of *P. falciparum* cultures while possible is not viable in high throughput studies especially when the whole life-cycle is to be studied. The background of the RBCs presented an obstacle in signal detection in a form of a substantial background signal in the collected spectra. Studies of mixed cultures by FT-IR were deemed non-viable by some authors [Naumann, 2000] without an

additional source of data (e.g. microscopy). While challenging the study attempted was motivated by the relative simplicity and potential high throughput capabilities of FT-IR spectroscopy.

The main aim of the study was to discriminate parasite metabolomes based on the modes of action of compounds they had been exposed to. It required a tool that could detect differences in the metabolic states of the parasites beyond large scale differences, e.g. in amount of membrane, used in previous drug sensitivity studies [Sockalingum et al., 1997; Bouhedja et al., 1997] and therefore the sensitivity of FT-IR spectroscopy had to be evaluated. The sensitivity of the technique was assessed in a step-wise manner by measurements of samples with differences of decreasing scale at every step requiring higher sensitivity to be detected.

We attempted to maximise the signal contributed by the *P. falciparum* parasites by magnetic separation of infected cells in order to enrich the samples. The *P. falciparum* infected RBCs were expected to be easily differentiable from the uninfected population due to the addition of the molecular structures present in the parasite that are not found in RBCs. The data collected from the two RBC populations showed a clear difference and the study was moved to the next stage of sensitivity estimation.

During its life-cycle the *P. falciparum* parasites go through considerable morphological changes. The differences in the parasites over the life-cycle were expected to be observable in FT-IR spectra as metabolic demands change. The data did not show any clear discrimination between the samples collected at different stages of the parasite life-cycle. This confirmed the limitation of the technique expressed by Naumann [2000]. The signal could potentially be improved by removing the parasites from the RBCs prior to measurement however this solution was not compatible with the aim of the study.

Chapter 6

The Effect of Drug Exposure to the Metabolome of *P. falciparum*: an NMR Spectroscopy Study

6.1 Introduction

As described earlier NMR spectroscopy is one of the most popular analytical tools used in metabolomics. It has some clear advantages over other techniques such as mass spectrometry in terms of reproducibility, relative simplicity of sample preparation and data collection as well as the possibility to identify metabolites if needed. These features of NMR experiments also make it a very useful tool for high throughput studies, especially since the introduction of automated sample changers and robotic sample preparation systems. We have performed a series of experiments with the aim of developing and optimizing an NMR spectroscopy-based *P. falciparum* screening method for the detection of novel modes of action of antimalarial compounds. The method described is based on metabolic fingerprinting of *P. falciparum* after exposure to antimalarial compounds. The protocol was developed to detect the metabolic perturbations induced in *P. falciparum* parasites following drug exposure *in vitro*. The resultant NMR data was used for compound clustering based on the shared modes of action. Our strategy was based on the comparison of the metabolic fingerprints of parasites exposed to well understood antimalarial drugs with the metabolic effects of novel compounds. A series of pilot experiments were designed and carried out in order to assess and implement an optimal strategy

for sample preparation and data collection. We first discuss the experiments carried out in order to assess the short term (5 hours) effects of established antimalarials with known or partially understood mechanisms of action. NMR was used to discriminate between known classes (Section 6.2). Initial experiments used a five-hour drug exposure window and subsequent studies, post optimisation, were carried out over a 6-hour time course (Section 6.3). The effect of life-cycle stage dependent drug effects is presented in Section 6.4.

6.2 5-Hour Drug Exposure Study

Initial studies used a reduced sample size as a proof of concept in order to test whether drug induced metabolic changes in *P. falciparum* could be observed at all using this NMR approach. The experiment was designed consisting of four drug treatments exposed at their predetermined IC_{90} concentrations over a 5-hour period of exposure. The drugs were selected in pairs based on their known modes of action. The four drugs used were the aminoquinolines chloroquine (CQ) and amodiaquine (AQ), an experimental drug CK-268, and 5-fluoroorotate (5-FOA). The first two compounds are heme binders and affect the parasites' ability to digest haemoglobin while the latter two target the respiratory chain in the parasites' single mitochondrion. Using this strategy of two example compounds targeting two very distinct mechanisms of action should be an adequate validation tests for the overall experimental approach. The prediction would be that the differences between groups in such case would be greater than the differences within groups. This idea of drug selection will be used in the later experiments as well. Data from untreated parasites in standard medium were used as negative controls. The experiments were performed following the optimised protocol described in Chapter 3. All samples were collected in triplicate.

The NMR spectra were collected using NOESY pulse sequence with presaturation and the data were investigated after uniform bucketing of 0.05 ppm and custom peak picking. PCA was performed in order to assess whether there was any clustering structure corresponding to treatments in the derived data. After inspection of the results (Fig. 6.1) it was clear that there was discrimination between some of the data points. Further analysis showed that all of the points on the left and top came from the same replicate (same culture). This suggested that the culture from which these samples were prepared was not viable and all the corresponding data points were removed from further analysis.

After removal of the data points it was possible to investigate the clustering

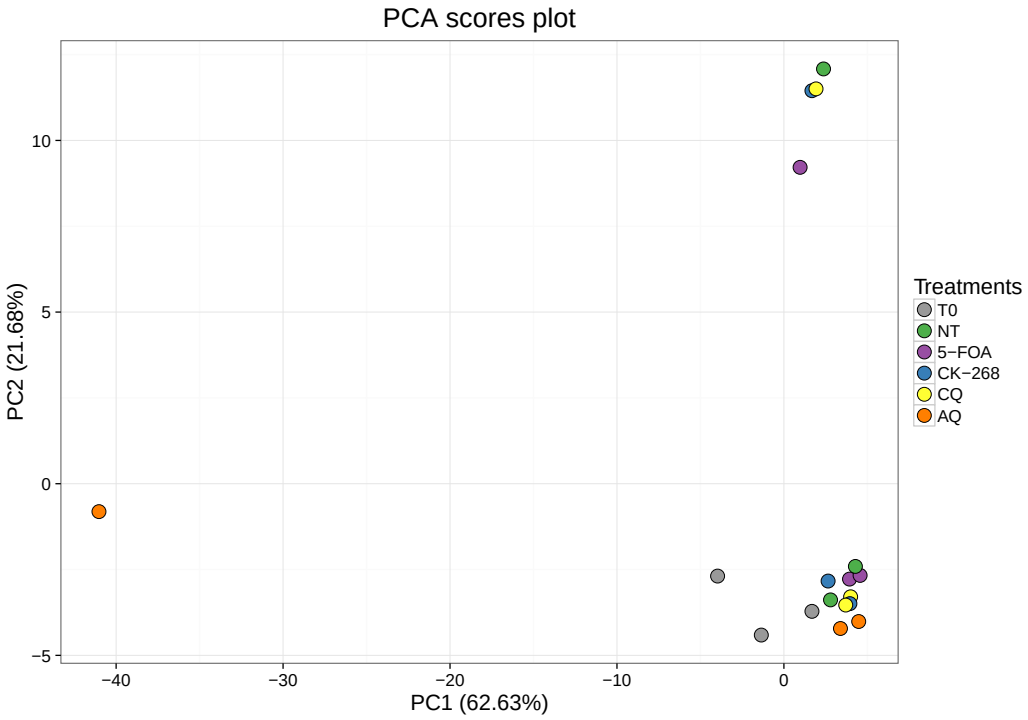

Figure 6.1: PCA of ^{1}H NMR spectra collected from *P. falciparum* infected RBC samples after 5-hour drug exposure; T0 - iRBC samples at the start of the experiment. Treatments : NT - untreated, 5-FOA - 5-fluoroorotate, CK-268 - an in-house compound, CQ - chloroquine, AQ - amodiaquine.

structure in the data (Fig. 6.2). The points corresponding to the two groups of drugs separated clearly from the untreated samples. While the differences between sample points especially in the respiratory chain targeting drug group were large, the separation between groups suggested that drug induced perturbations in the metabolism could be captured by the NMR measurements. Since only two remaining replicates were taken into consideration the results were inconclusive. A similar experiment was performed with the aim of providing more evidence for the findings.

6.2.1 A repeat of the 5-hour study

The 5-hour exposure experiment was repeated with five replicates and chloroquine was substituted by piperaquine (PPQ). Justification for this substitution was due to data from parallel LCMS studies that suggested that PPQ and AQ shared greater overlap in terms of metabolomic mechanism of action profile than chloroquine. (Mubaraki M, personal communication). The experiment was performed following the same protocol as previously described. Each replicate was derived from a

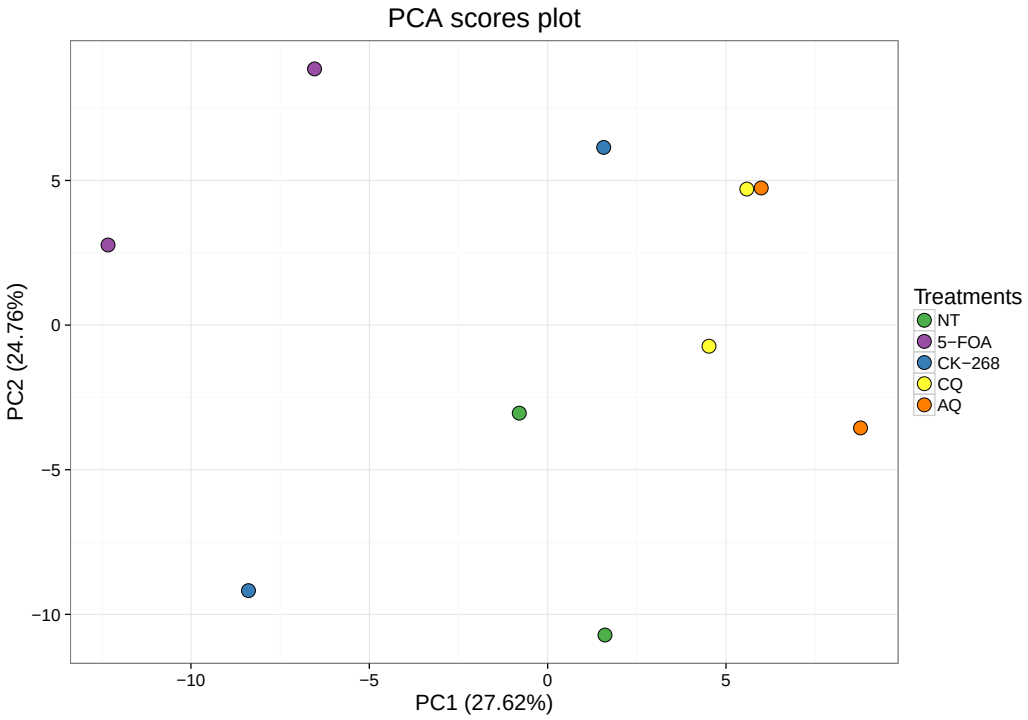

Figure 6.2: PCA of ^{1}H NMR spectra collected from *P. falciparum* infected RBC samples after 5 hour drug exposure; One replicate has been removed due to bad quality of the data. Treatments : NT - untreated, 5-FOA - 5-fluoroorotate, CK-268 - an in-house compound, CQ - chloroquine, AQ - amodiaquine.

separate parasite culture as before and was incubated in a separate 6-well plate (ref. to Section 2.3). Each culture was sampled before the incubation at time 0 hours. As previously PCA was performed on the processed data and the scores of the first two principal components plotted (Fig. 6.3).

After an inspection an outlier "untreated" sample was identified that did not cluster with the rest of the points. The other data points formed three clearly separable clusters. Points corresponding to the samples collected at the start of the experiment formed a cluster as did the untreated controls. All the treated samples formed the third cluster in between the first two. This suggested that based on the NMR data metabolic differences in the parasites at the start and at the end of the experiment as well as drug exposed parasites could be established. This result matched expectations as the drugged parasites were expected to be further developed in the life-cycle compared to the start of the experiment. However due to drug action limiting viability they would not have been expected to have developed as far as the untreated controls. In order to look more closely at the structure of

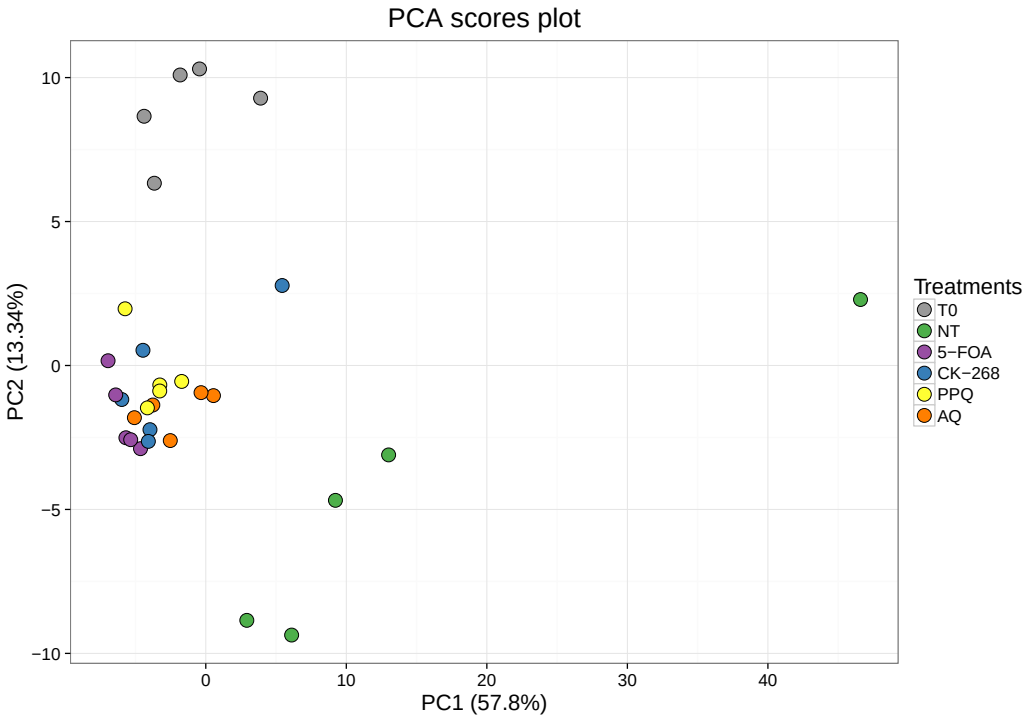

Figure 6.3: PCA of ^{1}H NMR spectra collected from *P. falciparum* infected RBC samples after 5 hour drug exposure; A repeat of the previous experiment including 5 replicates of each sample. Chloroquine has been substituted with piperaquine. Treatments : NT - untreated, 5-FOA - 5-fluoroorotate, CK-268 - an in-house compound, PPQ - piperaquine, AQ - amodiaquine.

the cluster of treated samples the analysis was repeated after removing the data for untreated and time 0h samples (Fig.6.4).

The results showed some structure in the data point location. Firstly, it was clear that two of the CK-268 samples had rather big differences compared to the rest of the data points, these were seen as potential outliers. It is also important to note that CK-268 treated samples had generated the most variable data in the previous experiment. We then inspected the cluster formed by the rest of the data points. The AQ/PPQ cluster seemed to be barely overlapping with 5-FOA cluster and slightly more with the CK-268 points. That could indicate greater similarity between AQ and PPQ than between AQ and 5-FOA. This result was promising as the clustering structure corresponded to the expected clustering by mode of action. In order to reinforce the findings and collect more data we repeated the experiment following the same procedure.

The data was processed and analysed in the same manner as previously. The first two principal components of the PCA were plotted in order to compare the

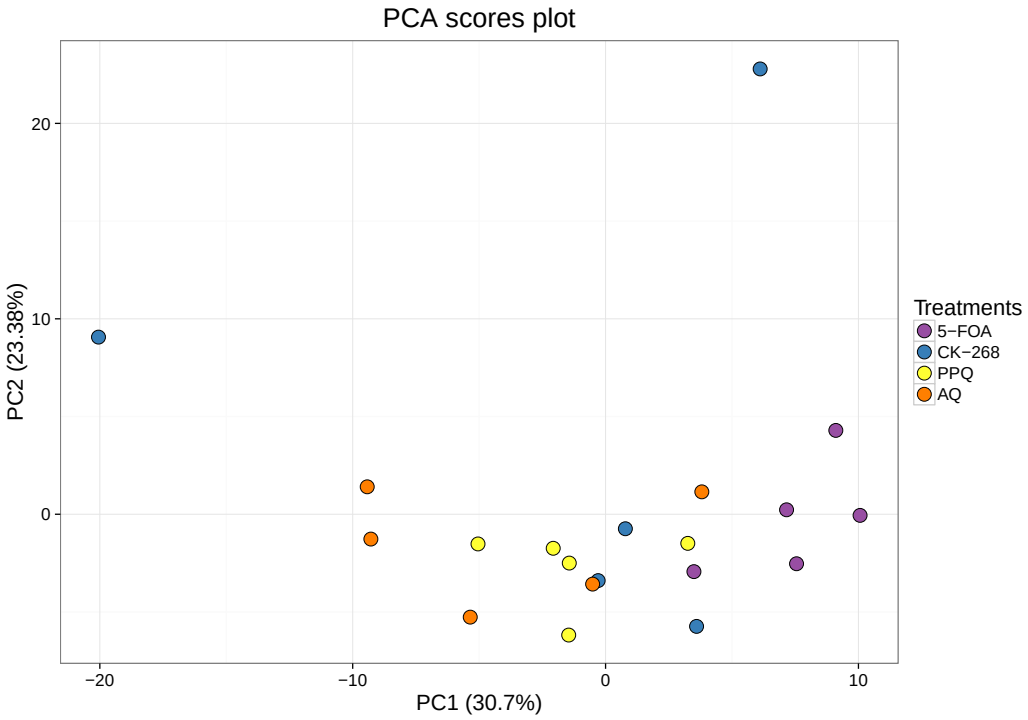

Figure 6.4: PCA of ^{1}H NMR spectra collected from *P. falciparum* infected RBC samples after 5 hour drug exposure; a repeat of the previous experiment including 5 replicates of each sample. The untreated and T=0 h samples have been removed. Treatments : NT - untreated, 5-FOA - 5-fluoroorotate, CK-268 - an in-house compound, PPQ - piperaquine, AQ - amodiaquine.

structure in the data to the previous experiment (Fig. 6.5). From the first inspection of the plot it was clear that the structure observed in the previous experiment, although not very significant, was totally absent. The samples from the start of the experiment (T=0 h) while more variable were still different to the rest of the samples. However, the samples from the negative controls, previously clearly different from the rest, were indistinguishable from treated samples. In turn the treated samples did not exhibit any visible discriminatory pattern at all. The results of this experiment indicated that the methodology needed further improvement. While some structure potentially corresponding to the drug treatments could be observed in the data, the variance either from biological sources or variability introduced in the experimental procedures was masking any real information pertaining to drug mode of action. The inability to generate any meaningful results forced a re-evaluation of the experimental procedures with the aim of finding further points of optimization or sources of unexpected variation that could be controlled for in the study design.

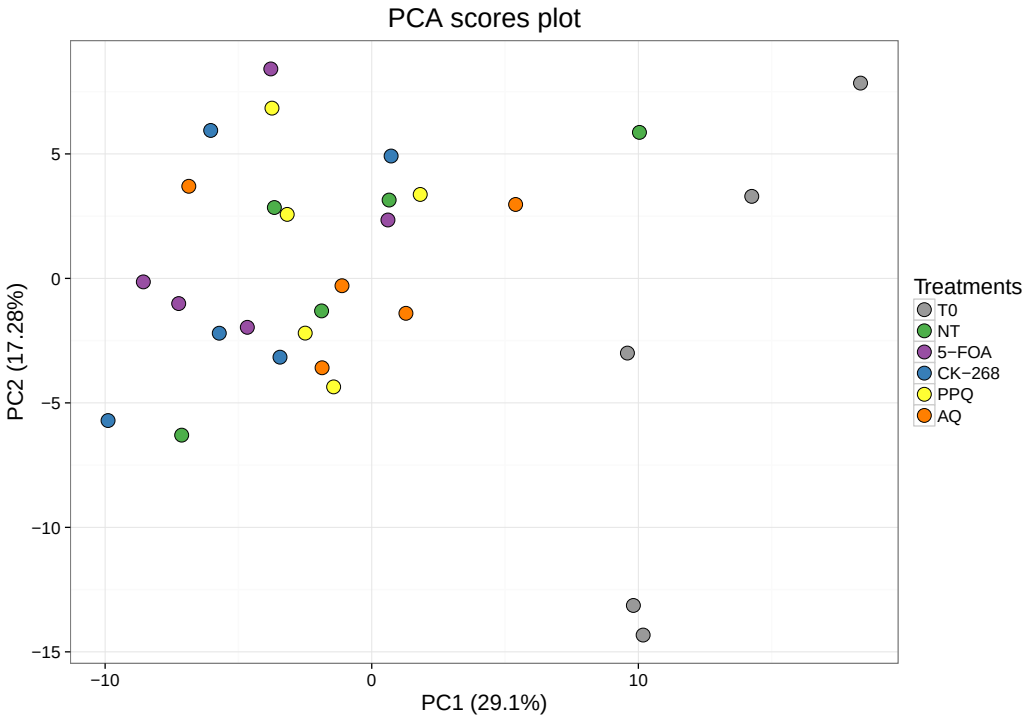

Figure 6.5: PCA of ^{1}H NMR spectra collected from *P. falciparum* infected RBC samples after 5 hour drug exposure; a repeat of the previous experiment. T0 - iRBC samples at the start of the experiment. Treatments : NT - untreated, 5-FOA - 5-fluoroorotate, CK-268 - an in-house compound, PPQ - piperaquine, AQ - amodiaquine.

6.2.2 Further Optimization of the Experimental Procedure

A serious limitation in expanding the number of replicates to five was the inability to co-locate the culture plates within a single gassing chamber without stacking. This introduced concerns about uneven gas distribution inside the plates which in turn could cause differences in growth conditions. This would undoubtedly introduce additional variation in the parasite metabolism. To address this problem a "shelf" was constructed to hold the incubation plates. It was assembled from parts of a similar incubation chamber and allowed the culture plates to be arranged at two levels inside the same chamber without stacking.

Secondly the replicate sampling procedure used so far was reconsidered. Until this point the production of biological replicate samples relied on separate parasite cultures. However it was recognized that such a strategy could potentially introduce additional variation to the experiments. The cultures used in the experiment were always split from the same "source culture" at least one life-cycle earlier. As

the parasites in each culture would replicate at least once before the experiment some additional variability could have been introduced between the samples during this single growth cycle. Other potential sources of variation that were considered included anything that could contribute to local differences in environmental conditions as parasite material was bulked up. This variability was initially considered an advantage as it allowed the natural variability to be taken into account, but it made data much harder to interpret. In response to these experimental problems the experimental design was re-evaluated.

The experimental strategy was modified and pooled parasite bulk cultures were used for all further experiments. The parasites were cultured as previously, but before the experiment was initiated individual culture flasks would be pooled, mixed and then re-split prior to starting experiments. This method also allowed some additional freedom in terms of experimental design. Firstly, if needed, larger sample volumes became possible as the size of the cultures was no longer a limitation. Also pooling the cells provided an effect of "averaging over" the variation in the parasite populations. This allowed avoidance of such events as reduced parasite viability in any one culture flasks, imperfect synchronization of cultures or slight alterations of parasite metabolism, resulting from different culturing parameters, such as nutrient availability due to differences in parasitemia.

6.2.3 A Test of Drug Viability

The failure of earlier experiments (Fig. 6.5) triggered a complete re-evaluation of all stages of decision making. An important factor to be considered was the antimalarial drug potency in the *in vitro* cultures. The drug potency was tested in a standard SYBR-Green-based IC_{50} assay. A fresh stock of artemisinin was used as a positive control. The calculated IC_{50} values are presented in Table 6.1. IC_{50} values vary between studies, strains and even isolates. The values reported in Table 6.1 are in line with expected values and supported the exposure levels selected for the subsequent metabolomics studies.

Table 6.1: The IC_{50} values for the antimalarials used in the study obtained from a standard SYBR green assay.

Compound	measured IC_{50} value (nM)	reported IC_{50} value (nM)
Piperaquine	3.18	36.9 [Fivelman et al., 2007]
Amodiaquine	4.67	18.4 [Fivelman et al., 2007]
CK-268	13.87	15.0 [Mubaraki M, personal comm.]
5-Fluoroorotate	5.22	6.0 [Rathod et al., 1989]

6.2.4 The Improved 5-hour Study Design

After the alterations to the experimental procedure outlined in Section 6.2.2 the 5-hour drug exposure experiment was repeated. Parasite cultures were pooled before the experiment and the 6-well plates containing the cultures during the incubation period were arranged in two levels in a well gassed culture chamber to avoid stacking and microenvironments. The data collected in the experiment were analysed using PCA and plotted as before. The results are shown in Figure 6.6. There was no improvement from previous experiment in terms of sample separation or differentiating patterns between treatments. Some of the samples were clustered separately from the rest of the points however they did not form any meaningful group suggesting some other artefact effect. As previously the time 0 group was clearly separable from the rest of the data, however the points corresponding to samples collected at the end of the exposure time were clustered together without any meaningful pattern.

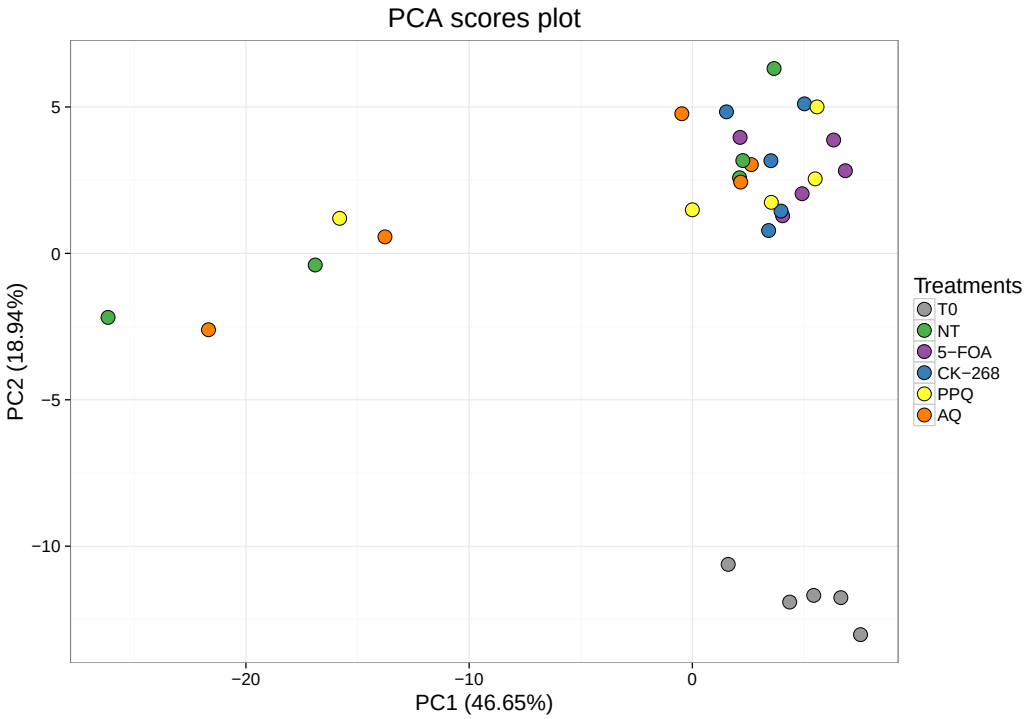

Figure 6.6: PCA of ^{1}H NMR spectra collected from *P. falciparum* infected RBC samples after 5 hour drug exposure at IC_{90} drug concentrations; T0 - iRBC samples at the start of the experiment. Treatments : NT - untreated, 5-FOA - 5-fluoroorotate, CK-268 - an in-house compound, PPQ - piperaquine, AQ - amodiaquine.

Drug exposure concentrations were pharmacologically relevant. An expla-

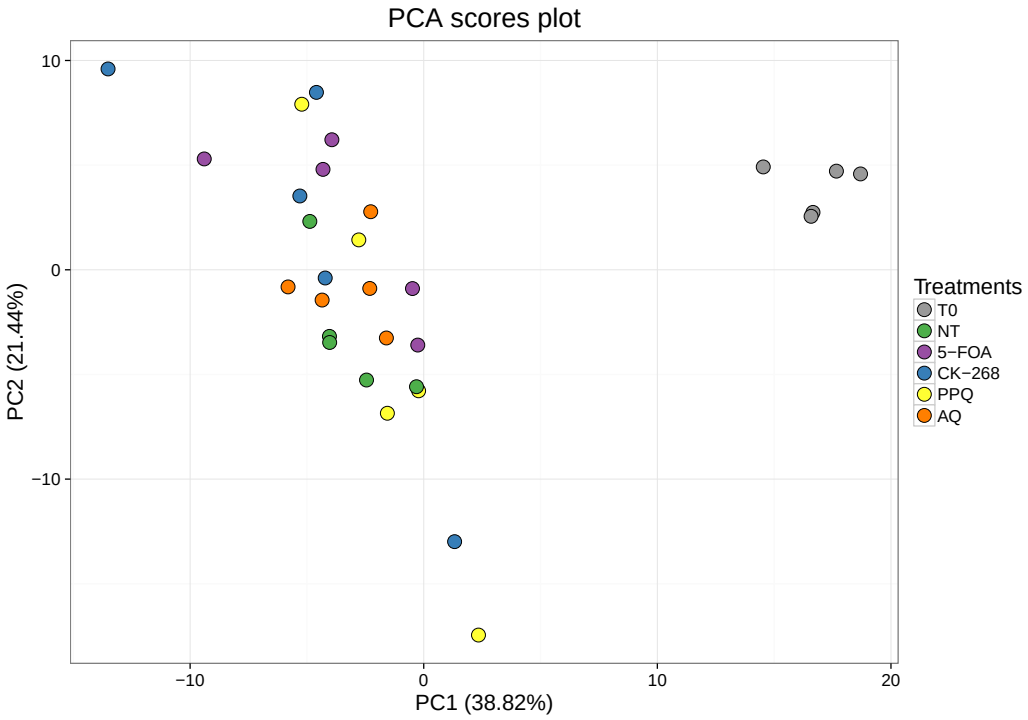

Figure 6.7: PCA of ^{1}H NMR spectra collected from *P. falciparum* infected RBC samples after 5 hour drug exposure at $10 \times IC_{90}$ drug concentrations; T0 - iRBC samples at the start of the experiment. Treatments : NT - untreated, 5-FOA - 5-fluoroorotate, CK-268 - an in-house compound, PPQ - piperaquine, AQ - amodiaquine.

nation for the lack of a drug effect could be due to the exposure timeframe of five hours. It is worth noting that IC_{50} concentrations are determined during a 48-hour assay and do not account for drug action variation over the different life-cycle stages of the parasite. As a next step the experiment was repeated using $10 \times IC_{90}$ drug concentrations.

The experiment was repeated following the same protocol with these 10-fold increased drug concentrations. The data processing and analysis were as in previous experiments. The results (Fig. 6.7) again did not show improvement in terms of information content. The samples collected at time 0 were clearly different from the rest of the data as before, however the data collected from the drug treated samples 5 hours after the start of the incubation did not show any separation. The untreated samples did not differ from the treated samples. We repeated the analysis after removal of the time 0 samples in order to investigate the structure within the cluster (Fig. 6.8) of points after 5-hour incubation. The cluster of data points did not show any meaningful structure. These experiments essentially ruled out

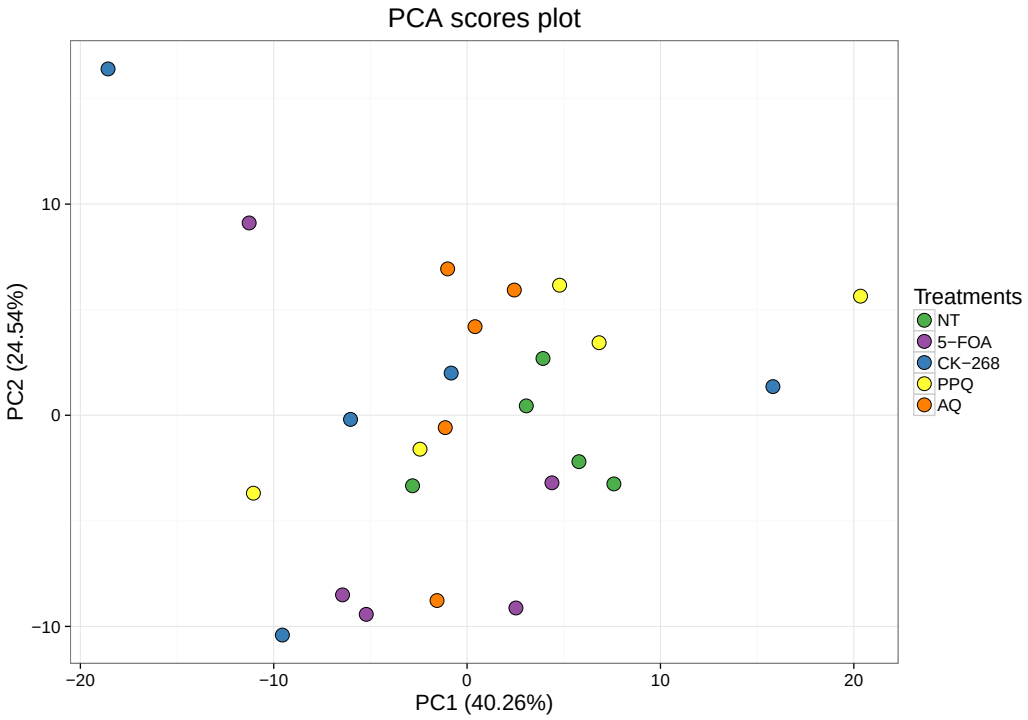

Figure 6.8: PCA of ^{1}H NMR spectra collected from *P. falciparum* infected RBC samples after 5 hour drug exposure at 10 × IC_{90} drug concentrations; T=0 samples have been removed from the analysis. Treatments : NT - untreated, 5-FOA - 5-fluoroorotate, CK-268 - an in-house compound, PPQ - piperaquine, AQ - amodiaquine.

the possibility of under-dosing which left the exposure time as the last variable to consider. In order to address this problem further experiments were conducted, one including a 20-hour exposure window and another including sampling every two hours.

6.2.5 20-Hour Drug Exposure

In addition to investigating potential changes in parasite metabolome in these studies the culture medium was also investigated as a potential source of information on nutrient utilisation and parasite waste elimination during the experimental procedures. The experimental set-up was altered to include sampling at two time points (5 and 20 hours post exposure). Together medium samples were collected at each time point. Because of the scope and complexity of the protocol and the demand for parasite biomass only two drugs could be investigated, namely amodiaquine and CK-268, with three replicates for all conditions under investigation. The samples

were collected at the beginning of the drug exposure as well as 5 and 20 hours after the start.

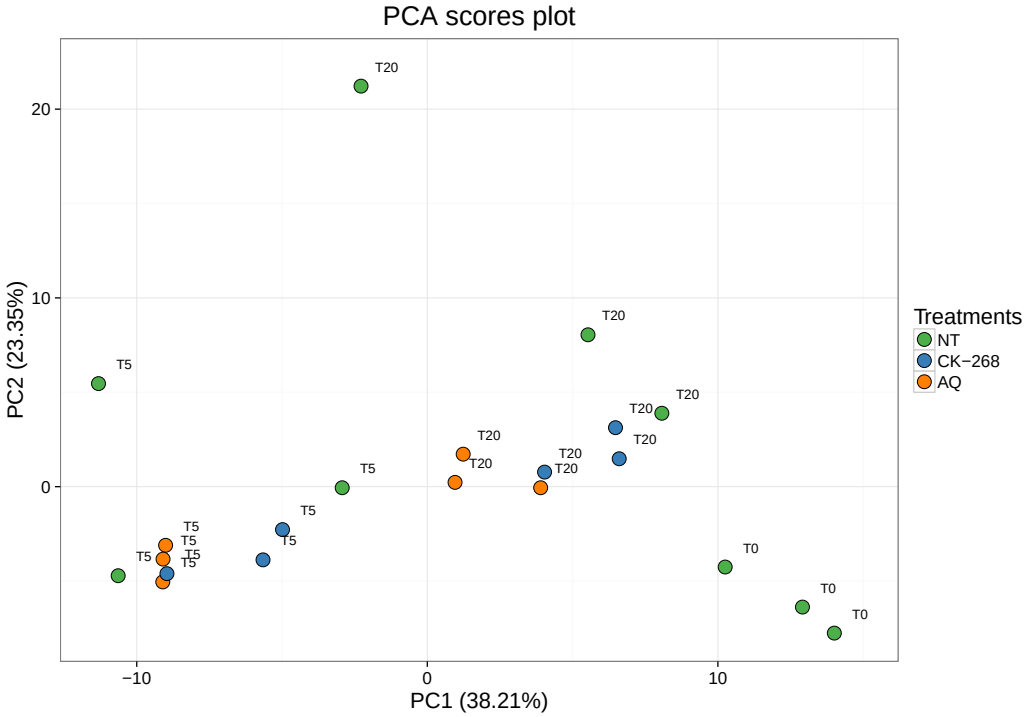

Figure 6.9: PCA of ^{1}H NMR spectra collected from *P. falciparum* infected RBC samples after 5 and 20 hour drug exposure at $10 \times IC_{90}$ drug concentrations; Treatments : NT - untreated, CK-268 - an in-house compound, AQ - amodiaquine, T0 - samples at the start of the experiment, T5 - samples after 5 hour exposure, T20 - samples after 20 hour exposure.

The same analysis was repeated as previously described and the results were plotted and are presented in Figures 6.9 and 6.10. Looking at the results of the parasite sample analysis (Fig. 6.9) there was a clear difference between time points. The clusters of points corresponding to each sampling time differed significantly. The data from samples collected at 5 hours were quite variable and did not cluster by treatment while the 20 hour samples seemed to have more structure. The medium analysis (Fig. 6.10) showed similar results. The samples collected at times 0, 5 and 20 hours were clearly separable. While the 5-hour samples did not seem to show any patterns in terms of treatment, the pattern in 20-hour samples was quite clear. Although the fact that there were only 3 replicates makes the result less significant the treatments seem to be separable showing differences in the composition of the medium after incubation of parasites with various antimalarials. Whether the differences were due to the varying length of parasite survival under drug exposure

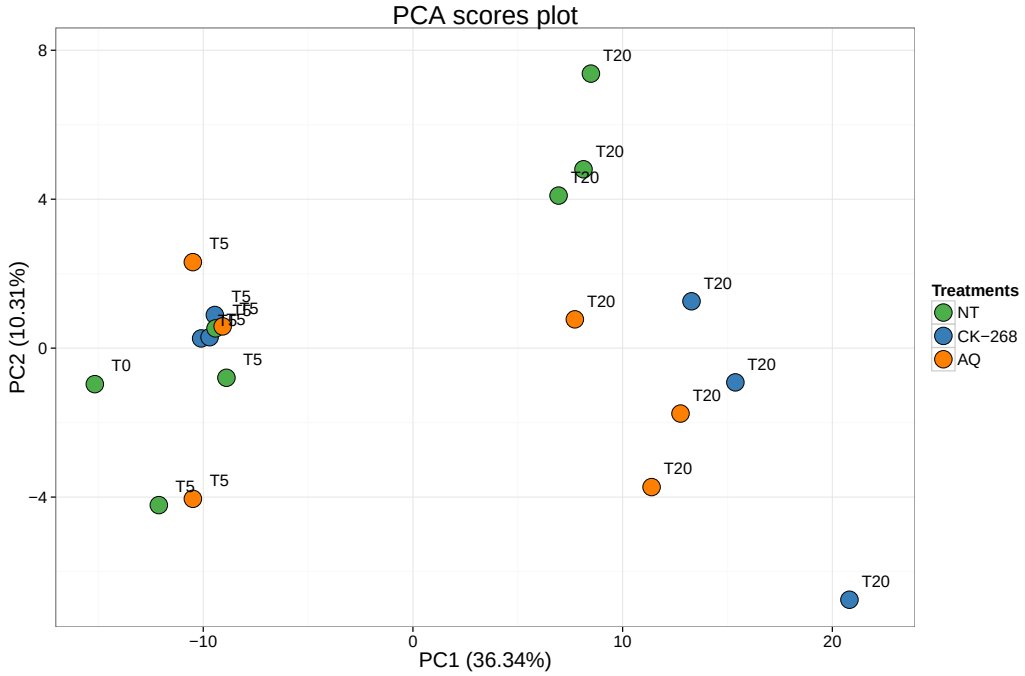

Figure 6.10: PCA of ^{1}H NMR spectra of medium samples collected from *P. falciparum* 20 hour drug exposure experiment using $10 \times IC_{90}$ drug concentrations; Treatments : NT - untreated, CK-268 - an in-house compound, AQ - amodiaquine, T0 - samples at the start of the experiment, T5 - samples after 5 hour exposure, T20 - samples after 20 hour exposure.

resulting in different rates of nutrient consumption or there were treatment-related changes in consumption and excretion of metabolites still had to be determined. This could also have been the result of presence or absence of the drug molecule signal in the medium samples. Even though the 5-hour time point samples did not show the same pattern the possibility of drug concentration being high enough to be detected in the NMR spectra was tested.

Three medium samples with the drugs used in the experiment as well as no treatment control were prepared. Samples contained 500 nM of CK-268, 500 nM of amodiaquine and a comparable amount of DMSO that would be used to dilute the drugs. The resulting spectra were inspected visually. No peak differences between spectra were observed suggesting that the drugs were not detectable at 500 nM concentration.

6.3 Re-interrogation of Short Time-course Drug Exposures

Drug exposures over 5 hours were inconclusive in terms of distinguishing NMR profiles. One explanation for this could have been that all the suble effects leading to parasite death occur even earlier after drug exposure. In order to address this the experimental protocol was modified to provide three sample times of 2, 4 and 6 hours post exposure. The working hypothesis was that for drugs with rapid onset of action (and especially at high concentrations) the observations made at 5h and beyond might represent dying parasites with distinct metabolic pathways leading to death only apparent at earlier periods of drug exposure.

6.3.1 The 6-Hour Time-Course

The experiment was carried out as described previously including collection of medium samples. The data analysis was performed and the results plotted following the same procedure as described in the previous section. Looking at the PCA scores plot of the cell samples (Fig. 6.11) the differences between the time points were clear. The amodiaquine treated samples were more similar to the control than CK-268 treated samples, especially at the 6-hour time-point. The loadings of the first two principal components were inspected as well as the raw spectra, however it was unclear which peaks would have made the CK-268 treated samples differ more. It suggested that rather than specific peaks the general pattern of peak intensity (areas under the peaks) was different. This could either have been the result of the treatment, e.g. large portion of parasites killed much earlier and contributing less to the signal, or some systematic effect in the data processing. One possibility could have been that normalization by the total area of the spectrum introduced a bias depending on highly variable residual solvent peaks. This possibility was investigated by normalizing raw data before and after removal of residual solvent peaks and reproducing the PCA on both data sets. The results did not vary significantly as a similar pattern of data points was obtained in each case. Investigation of raw data did not show any clear differences between spectra indicating that the drug induced perturbations were either not present or more likely not visible in the data.

The results of analysis of medium sample data (Fig. 6.12) showed a similar pattern. There were clear differences between time-points while the treatments at each time point were similar. It is important to note the similarity in medium composition during the whole experiments whether from treated or untreated samples. This suggested that the overall parasite use of media components and elimination

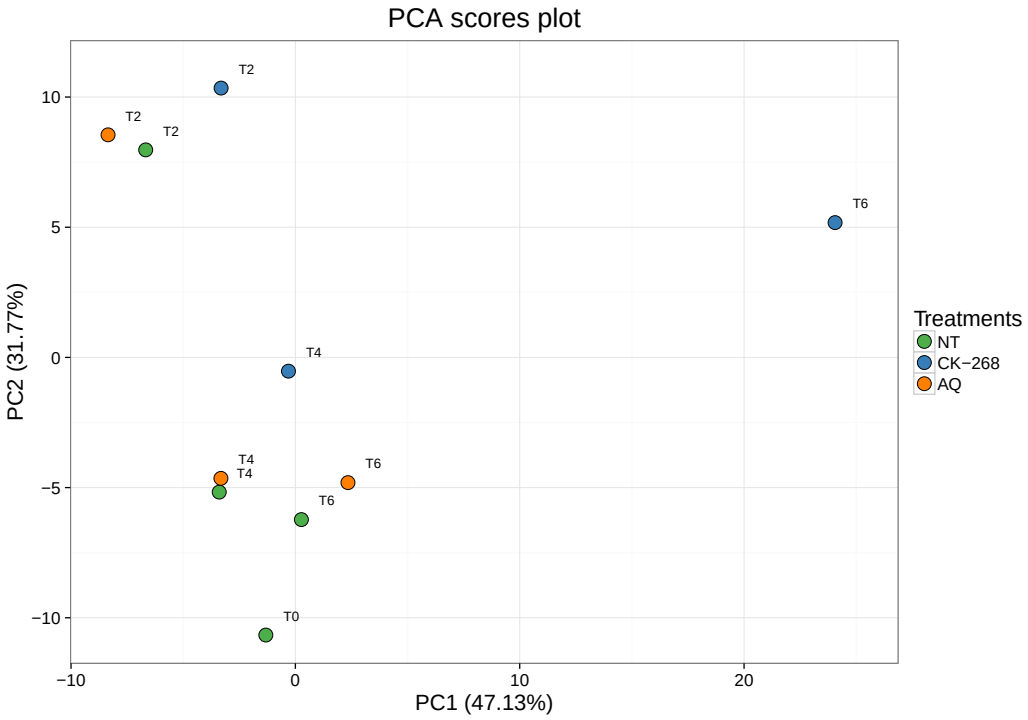

Figure 6.11: PCA of ^{1}H NMR spectra collected from *P. falciparum* infected RBC samples after 2, 4 and 6 hours of drug exposure at $10 \times IC_{90}$ concentrations; Treatments : NT - untreated, CK-268 - an in-house compound, AQ - amodiaquine, T0 - samples at the start of the experiment, T2-T6 - samples after 2-6 hour exposure.

of by-products was normal over those time periods.

Since the results to this point had proven inconclusive, in an attempt to improve the signal the number of parasite cells used per sample was increased. This optimisation step was left as one of the last measures since obtaining the parasite biomass was one of the major bottlenecks in terms of time. It is also important to note that the parasite biomass that is possible to obtain for one experiment is limited by the number of cultures that can be sustained simultaneously under similar conditions. To date 100 μL of cell pellet (centrifuged at 500 g for 5 min.) per sample was used in order to keep the experiment sample demands low with the scalability in mind. The starting incubation approach was changed from 6-well plates to 120 mL culture flasks in order to accommodate the higher number of cells. Each sample was additionally divided into three parts at extraction time. In order to be able to perform the extractions in 1.5 mL tubes thereafter the extracts were pooled (for the detailed protocol refer to Section 2.3). The rest of the protocol remained unchanged.

The experiment was performed and spectra collected using the standard pro-

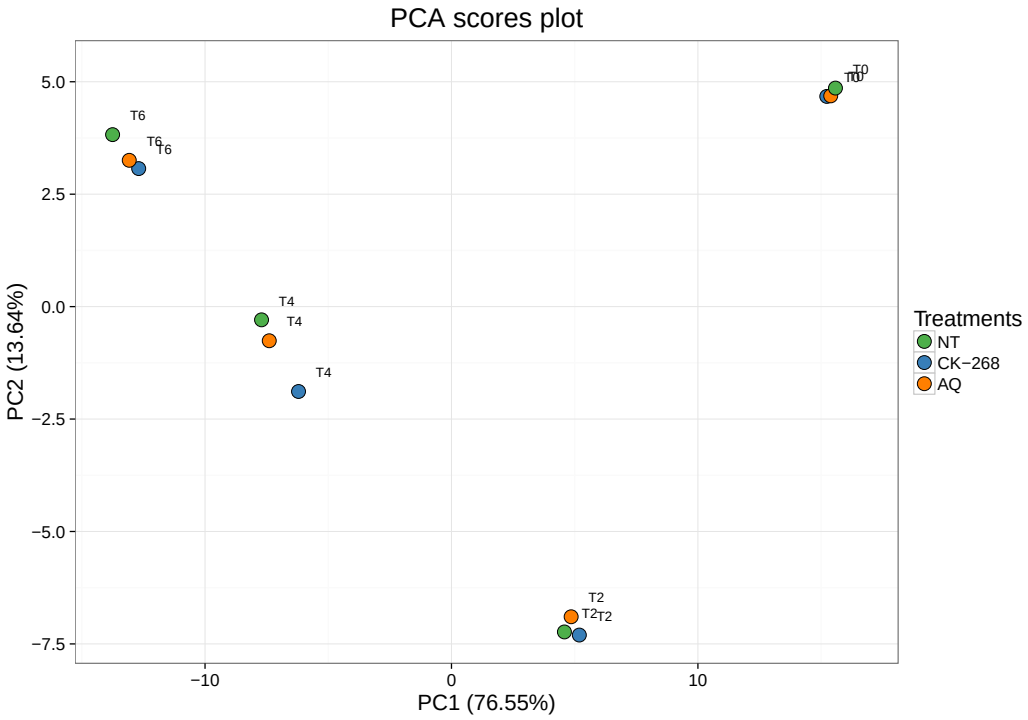

Figure 6.12: PCA of ^{1}H NMR spectra collected from medium samples of *P. falciparum* infected RBC drug exposure experiment 2, 4 and 6 hours after the start of the exposure. $10 \times IC_{90}$ drug concentrations were used; Treatments : NT - untreated, CK-268 - an in-house compound, AQ - amodiaquine, T0 - samples at the start of the experiment, T2-T6 - samples after 2-6 hour exposure.

tocol as previously described. Inspection of raw data showed baseline inconsistencies and broad peaks. This could be explained by the changes in the experiment design. As the samples in this experiment were extracted from higher volume of cell pellet the protein content could not be precipitated as efficiently resulting in more residual protein in the NMR samples. In order to address this problem the NMR data acquisition was repeated using an alternative pulse sequence - Carr-Purcell-Meiboom-Gill (CPMG). This pulse sequence was designed to "ignore" large molecules in the sample, potentially reducing residual protein signal in the spectra. For comparison of the data collected using both pulse sequences refer to Section 3.5. As the CPMG pulse sequence proved to produce better results all data collected in the further experiments has been collected using an NMR parameter set including the CPMG pulse sequence.

Data processing and analysis was carried out as described previously. The results are shown in Figure 6.13. After inspection of the PCA plot similar patterns were observed as in the previous experiment. The differences between time points

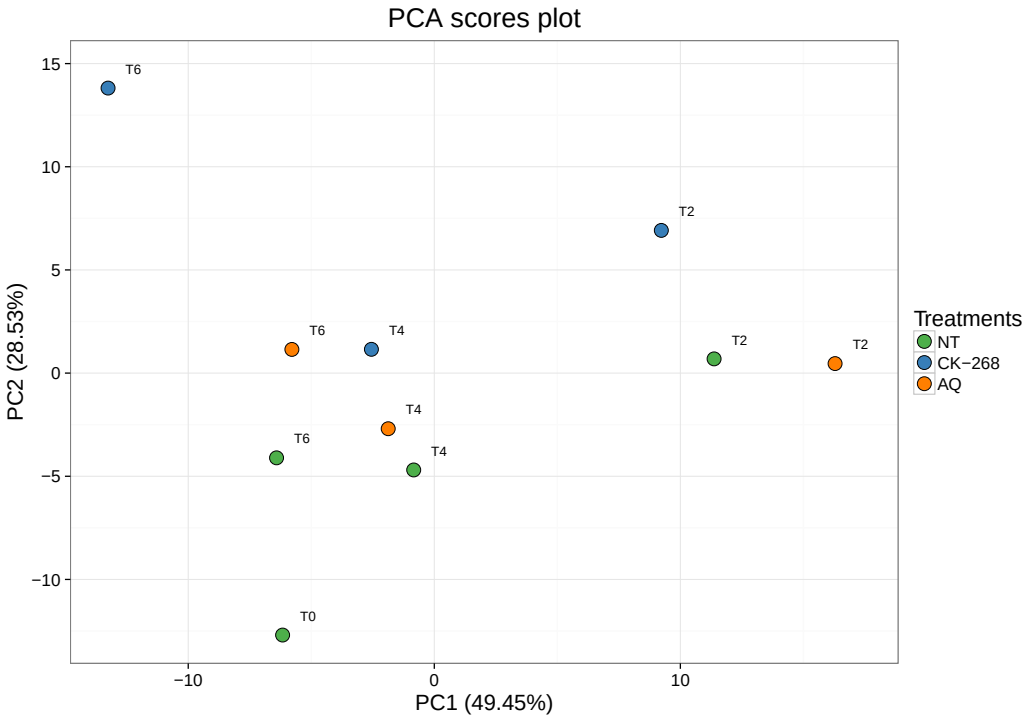

Figure 6.13: PCA of ^{1}H NMR spectra collected from *P. falciparum* infected RBC samples after 2, 4 and 6 hours of drug exposure at $10 \times IC_{90}$ concentrations; 1mL of cell pellet per sample was used. Treatments : NT - untreated, CK-268 - an in-house compound, AQ - amodiaquine, T0 - samples at the start of the experiment, T2-T6 - samples after 2-6 hour exposure.

were much more prominent than between treatments. One exception was the CK-268 treated samples at time 6 hours. The investigation of the loadings of the first two principal components and raw data again did not yield any clear conclusions as to what made the CK-268 treated sample different in terms of the NMR spectrum. It is important to note that in the last two data sets we did not have any replicates of samples due to constraints imposed by the high number of cells required for the experiments. While the PCA results could not be held in any way conclusive the data was also visually compared. Overlapped spectra at each time point were carefully inspected in an attempt to find peaks that differed significantly between the treatments indicating some potentially associated metabolite changes.

Due to the absence of any conclusive evidence for metabolic changes present in the data artemisinin was added as another drug treatment. Artemisinins are known to be the fastest acting antimalarial killing parasites within a few hours of exposure with death complete within 6 hours. The protocol was a repeat of the previous experiment but with addition of artemisinin as the third drug treatment.

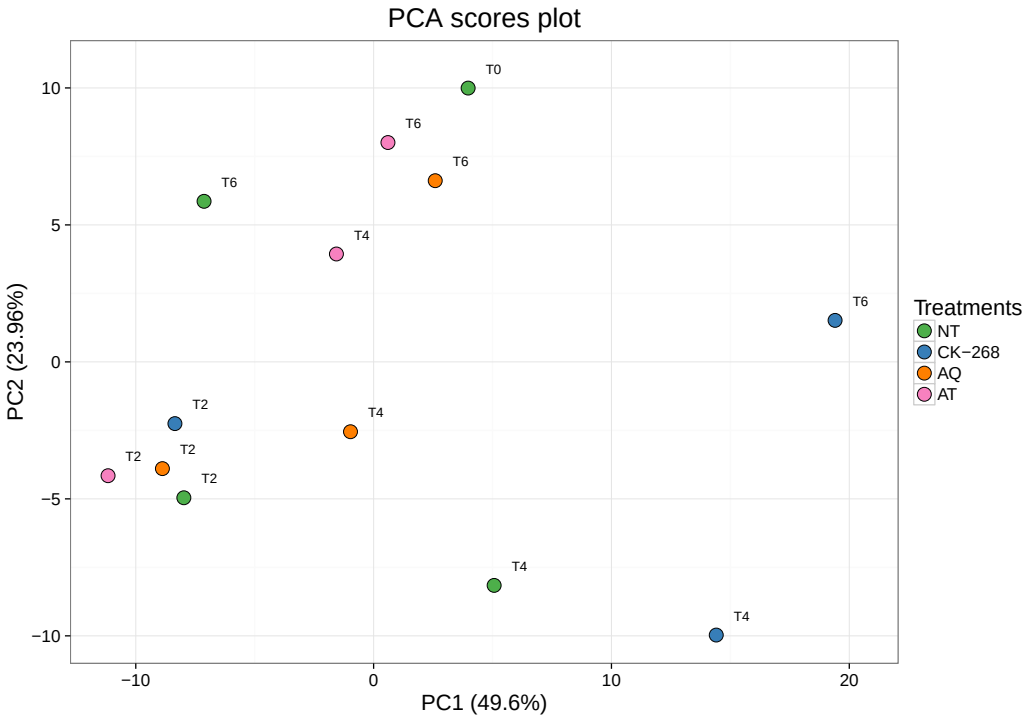

Figure 6.14: PCA of ^{1}H NMR spectra collected from *P. falciparum* infected RBC samples after 2, 4 and 6 hours of drug exposure at $10 \times IC_{90}$ concentrations; 1mL of cell pellet per sample was used. Treatments : NT - untreated, CK-268 - an in-house compound, AQ - amodiaquine, AT - artemisinin, T0 - samples at the start of the experiment, T2-T6 - samples after 2-6 hour exposure.

While the PCA was repeated as before (the results are presented in Figure 6.14) the main aim of the experiment was to inspect the raw data in order to determine if there were any significant differences between treatments at different times. While no clear metabolite differences could be identified there were some peaks that were variable between the treatments.

The conclusion from this series of very time consuming and resource demanding experiments suggested that NMR, under the conditions applied here, was unable to provide information that would allow to discriminate parasite metabolomes under suprapharmacological drug exposure for relatively short (0-6 h) periods. The project was continued by looking at longer exposure periods to see if the data would be more informative.

An experiment was designed adding 24 hour sampling time point. Due to technical problems the CK-268 treatment was removed from the design and only artemisinin and amodiaquine were used for comparison. These drugs have distinct mechanisms of action [Krishna et al., 2004; Marquez et al., 1972] and act at different

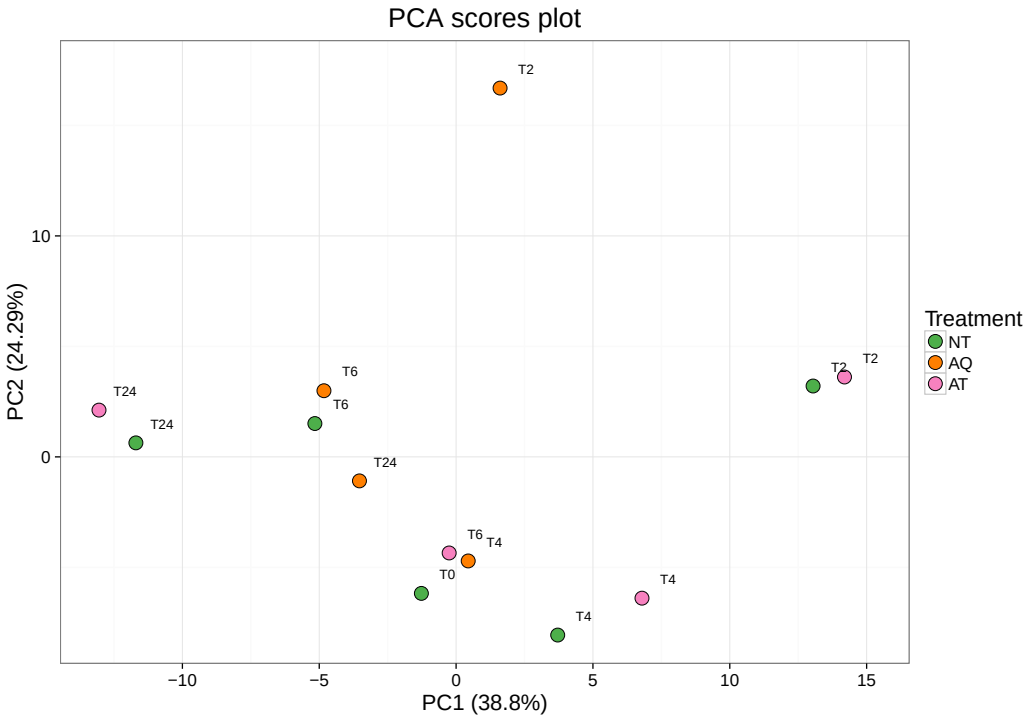

Figure 6.15: PCA of ^{1}H NMR spectra collected from *P. falciparum* infected RBC samples after 2, 4 and 6 hours of drug exposure at $10 \times IC_{90}$ concentrations; 1mL of cell pellet per sample was used. Treatments : NT - untreated, AQ - amodiaquine, AT - artemisinin, T0 - samples at the start of the experiment, T2-T6 - samples after 2-6 hour exposure.

stages of the life cycle [Delves et al., 2012]. These features were considered optimum for looking at discriminatory patterns between metabolomes in the NMR spectra, if indeed they were present. Spectra were collected as previously and data was processed and analysed (Fig. 6.15). The raw spectra were also inspected in search of peaks differing between treatments. Some differences were found in the spectra suggesting that potentially some perturbations in the metabolism were being captured. However as in the previous experiment the results were inconclusive.

In an attempt to get conclusive evidence and determine whether the method had any potential to be used for drug screening an experiment spanning the whole 48h parasite life cycle was designed including replicate samples.

6.4 Full Life-Cycle Drug Exposures

The results presented up to this point were mainly of relatively short time-course experiments designed to look for evidence of drug induced metabolic perturbations

in *P. falciparum* observed in the NMR spectra. The results obtained were both inconsistent and inconclusive and suggested that NMR spectroscopy, despite some strengths, is not a suitable analytical method for looking at drug action in *P. falciparum* at scale. In a last effort to test the potential of the approach a study was designed in the spirit of the envisioned procedure spanning the whole life-cycle of *P. falciparum* parasite.

The experiment was designed with four conditions including artemisinin, chloroquine, atovaquone and an untreated control and three replicates. Due to the scale of the experiment the data was collected over four separate experimental periods. The fourth repeat of the experiment was carried out using uninfected red blood cells as controls (values that could be subtracted from drug treated data sets as background in some analyses). Samples were collected at the beginning of the experiment and then at 3, 6, 12, 24 and 48 hours post drug exposure at $10 \times IC_{90}$ resulting in a total of 63 samples and 189 metabolite extractions. The sample preparation was carried out as in previous drug exposure experiments using 1 mL of cell pellet per sample. The NMR spectra were collected using the standard parameter set with CPMG pulse sequence in an 800 MHz spectrometer. The data were processed as explained previously (Section 3.4) and the three replicate data sets averaged. The data sets for uninfected RBC data as well as the mean infected RBC data with uninfected RBC measurements subtracted were also prepared for analysis.

First the spectra were inspected visually in order to assess the data quality in terms of peak shifts due to pH or salt content variation. We also looked for significant differences between treatments at each time point. The data were inspected by plotting overlapped spectra as well as using quantile plots. NMR quantile plots were produced by taking a group of spectra and plotting a "ribbon" between maximum and minimum peak height values at each point on the x-axis. The top of the "ribbon" then spanned all the maximum-height points in the group of spectra while bottom spanned the minimum-height points. The ribbon was then coloured based on quantile values of the group of spectra at each point on the x-axis resulting in a vertical colour gradient spanning quantiles from 0 to 100. A median spectrum is plotted on top for reference. Such a plot is a good visual cue of where the most variation is located in the group of spectra. Each time point was inspected separately in order to assess changes appearing over time (Fig. 6.16 - 6.18).

After 3 hours of drug incubation with drugs some differences started to appear between the samples (Fig. 6.16). It is worth noting that the quantile plots have a downside that if the peaks shift on the horizontal axis it is reflected in the

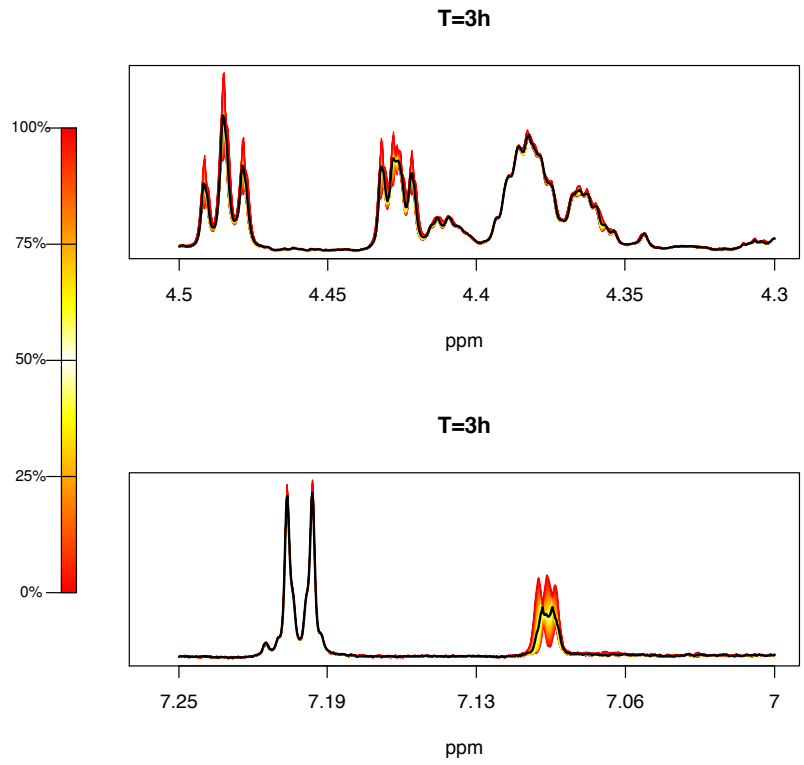

Figure 6.16: A quantile plot of ^{1}H NMR spectra collected from a *P. falciparum* drug exposure experiment after 3 hours of exposure. The fragments of the spectra presented contain the peaks that differ between spectra. The colour bar shows the gradient of colours representing percentiles of data calculated at each point of the spectrum. The black line represents the median (50^{th} percentile) spectrum.

plots as a difference between spectra. We inspected the overlapped spectra for such instances and ignored the differences in the quantile plots when they resulted from the misalignment of spectra. It was clear from the spectra that there were differences between the treatments already 3 hours after incubation. The peak at 7.1 ppm as well as peaks at 4.48 ppm and 4.43 ppm showed differences in height.

After 6 hours of incubation some new peak variation appeared in the aromatic region (Fig. 6.17a). The peaks at 8.54 and 8.59 ppm were showing some variation between treatments. At the 12 hour time point a new peak appeared at 6.69 ppm that was only present in the control sample (Fig. 6.17b).

After 24 hours of incubation new changes in peak height appeared in the 4.55-4.57 ppm region (Fig. 6.18). The previously identified differences around 6.68 ppm were more pronounced and contained multiple new peaks. However, no new changes were observed in the spectra at 48 hours after the start of the incubation

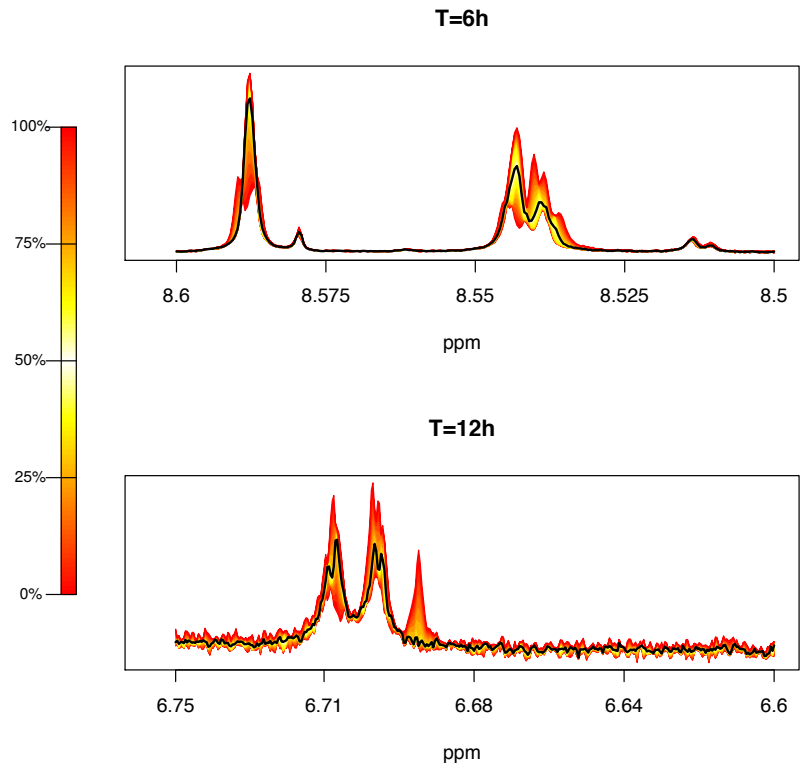

Figure 6.17: A quantile plot of ^{1}H NMR spectra collected from a *P. falciparum* drug exposure experiment after 6 and 12 hours of exposure. The fragments of the spectra presented contain the peaks that differ between spectra.The colour bar shows the gradient of colours representing percentiles of data calculated at each point of the spectrum. The black line represents the median (50^{th} percentile) spectrum.

compared to previous time point. This was unexpected as by the 48 hour time point the control parasites should have re-entered the next life cycle while most of the drug-exposed parasites were expected to be either arrested in development or dead (note the IC_{50} values were determined over 48 h). The data was further investigated through multivariate analysis. Notably while there were differences between some of the peaks in the spectra as illustrated in the quantile plots the majority of the spectra contained very little variation showing the reproducibility of NMR and the robustness of the sample preparation procedure, albeit with absence of any meaningful discriminatory information.

As mentioned above a total of three data sets were prepared for further analysis, namely an infected RBC extract dataset, an uninfected RBC dataset, and "parasite only" dataset, obtained after subtracting the RBC data from the mean

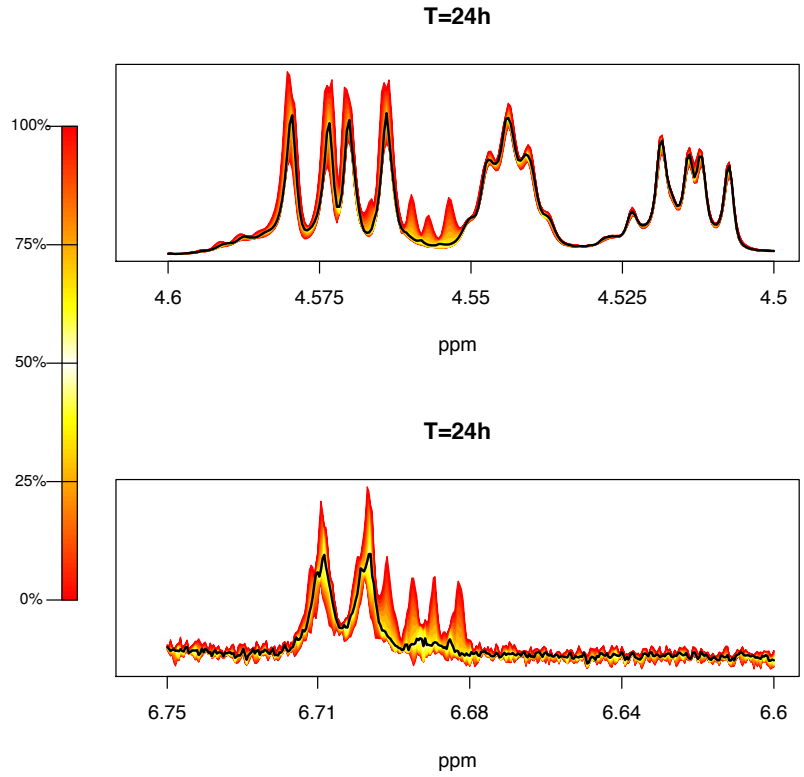

Figure 6.18: A quantile plot of ^{1}H NMR spectra collected from a *P. falciparum* drug exposure experiment after 24 hours of exposure. The fragments of the spectra presented contain the peaks that differ between spectra. The colour bar shows the gradient of colours representing percentiles of data calculated at each point of the spectrum. The black line represents the median (50^{th} percentile) spectrum.

data. First a PCA was performed in order to investigate the structure in the data as done previously. The first two principal components of the iRBC data were plotted (Fig. 6.19). Some patterns were clearly visible in the distribution of points. The data points clustered by the time they were sampled at. There seemed to be little difference between samples at 3 and 6 hours (in agreement with previous observations) - the data from those time points formed a cluster. The data points corresponding to samples collected at 12 and 24 hours had greater spread and could be clearly distinguished from earlier and later time points. It was interesting that the sample from the start of the experiment (T=0 h) was in this cluster as well. The last cluster we observed was the group of 48 hour time points. This cluster was the most distinct. The treated samples, however, did not separate from the untreated as anticipated. Drug treated parasites are arrested (or dead) compared

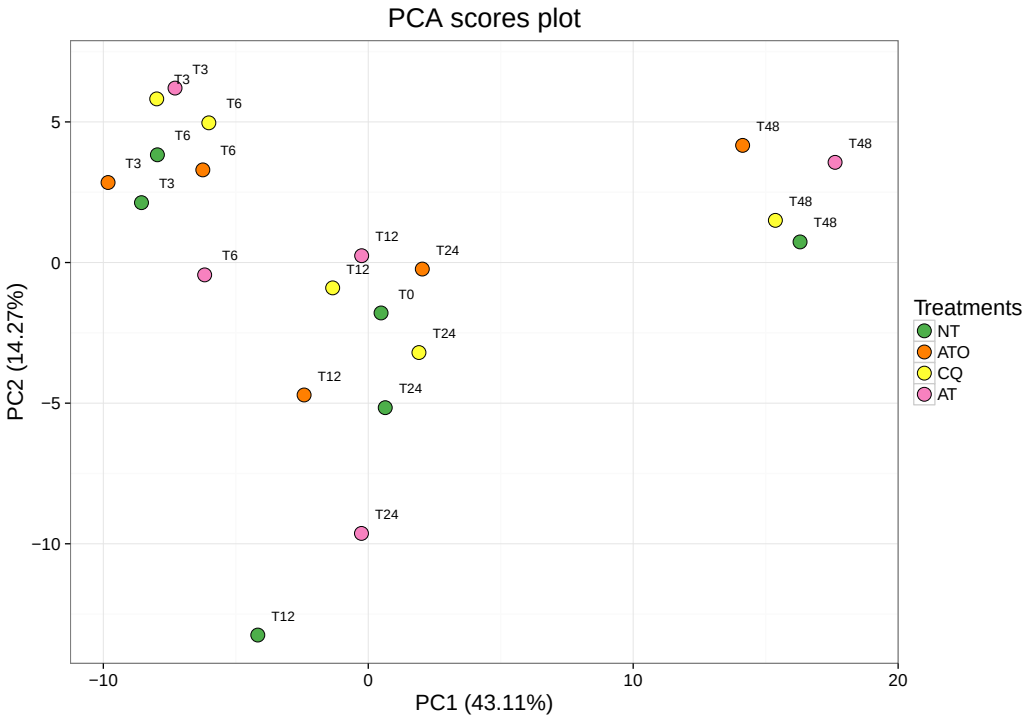

Figure 6.19: PCA of ^{1}H NMR spectra collected from *P. falciparum* infected RBC samples after 3, 6, 12, 24 and 48 hours of drug exposure at IC_{90} concentrations; 3 replicate spectra per sample were averaged. Treatments : NT - untreated, ATO - atovaquone,CQ - chloroquine, AT - artemisinin, T3-T48 - samples after 3-48 hour exposure.

to the untreated parasites that continue through the life cycle. It is inconceivable that these parasites have an equivalent metabolic state that should be discernable at the level of the metabolome.

PCA was also carried out on the uninfected RBC data. RBCs are relatively metabolically inactive while in culture yet as shown in Figure 6.20. PCA plot was very similar to that from iRBCs although although in this case the clusters were less distinct. Notably the time 0 sample here was clustered with early time points. We also noticed two outliers in the chloroquine group at 6 h and atovaquone at 12 h. After inspection of the spectra it was discovered that these samples were likely contaminated and were clearly different from the rest of the spectra. Consequently these data were discarded.

The iRBC data set was also investigated after subtraction of the RBC background. Since the RBC data set included two samples that were unusable they were excluded from this particular analysis. The plot of the first two principal components of the PCA (Fig. 6.21) showed similar patterns as before with some notable

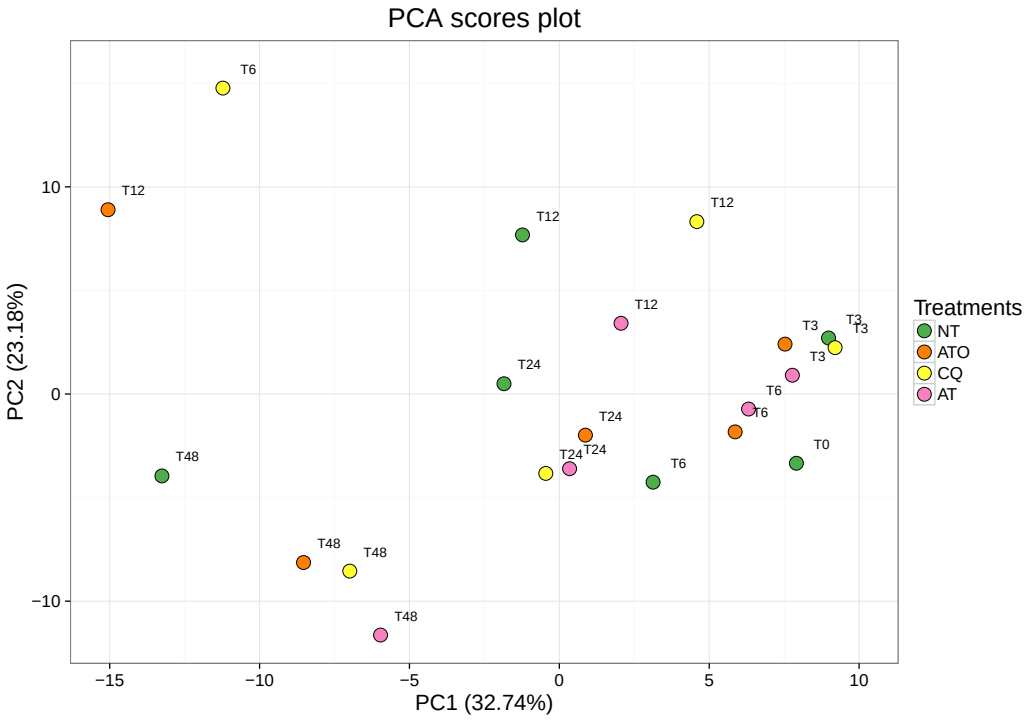

Figure 6.20: PCA of ^{1}H NMR spectra collected from RBC samples after 3, 6, 12, 24 and 48 hours of drug exposure at IC_{90} concentrations; Treatments : NT - untreated, ATO - atovaquone, CQ - chloroquine, AT - artemisinin, T3-T48 - samples after 3-48 hour exposure.

differences. Firstly without the RBC "background" a gradient distribution of points was observed, spreading from right to left according to the time they had been collected. The sample from the start of the experiment was now distinct from the rest of the data points and the groups of points from different time points form a trajectory following top to bottom and right to left. Some of the temporal effect in the data seemed to be removed through the subtraction of RBC data. However, it was not possible to draw any conclusions on whether the apparent temporal effect was introduced by the sampling procedure or RBC changes over time that might dominate the metabolic readouts.

Since only about half of the variance in the data was accounted for in the first two principal components of the PCA in each case, the data was further investigated using hierarchical clustering analysis (HCA). This clustering technique (ref. to Section 1.7.5) agglomerated points into groups in a stepwise manner allowing the clustering relationships to be represented in a tree-like structure - dendrogram. Hierarchical clustering was performed on all three datasets with the aim of elucidating

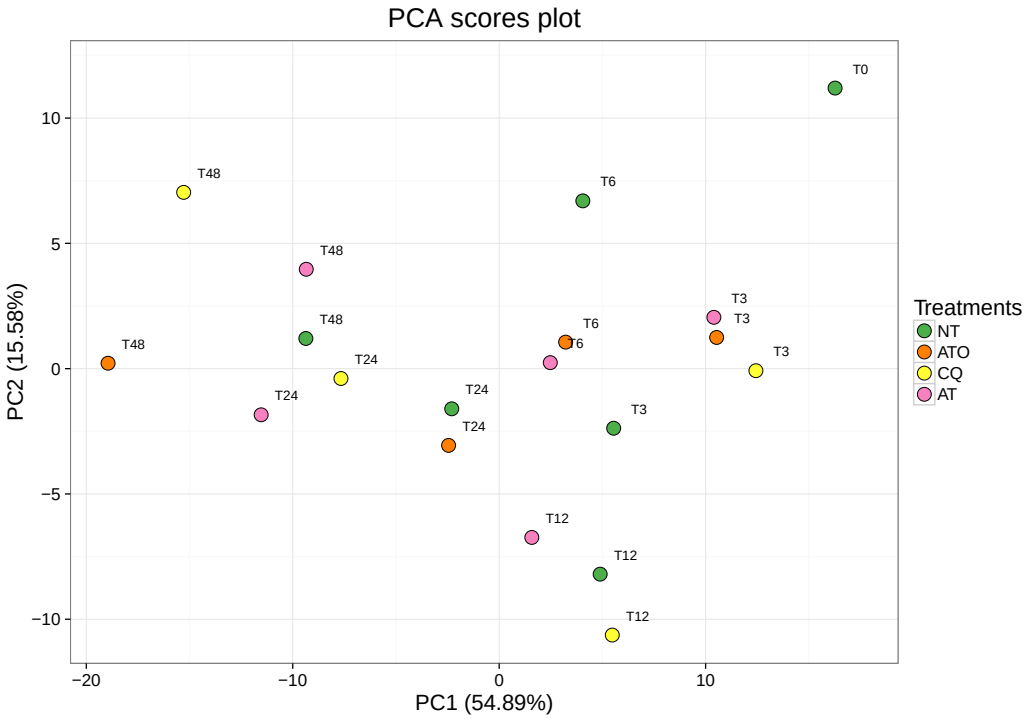

Figure 6.21: PCA of ^{1}H NMR spectra collected from *P. falciparum* infected RBC samples after 3, 6, 12, 24 and 48 hours of drug exposure at IC_{90} concentrations; 3 replicate spectra per sample were averaged and uninfected RBC data has been subtracted. Two samples (CQ-T6 and ATO-T12) have been removed due to bad quality data. Treatments : NT - untreated, ATO - atovaquone, CQ - chloroquine, AT - artemisinin, T3-T48 - samples after 3-48 hour exposure.

any further structure in the data that might have not been captured in the PCA plots. The dendrogram of the clustering structure of iRBC data (Fig. 6.22) showed similar clustering structure to the PCA. The data points grouped by time into three large clusters (here T=0 h is in the 48 h cluster) where two of the clusters further split into smaller clusters containing data from one time point each.

In addition the dendrogram of the RBC data (Fig. 6.23) confirmed the results of the PCA. The early data points formed a separate cluster while the later time points were more ambiguous. The outliers were clearly shown in a separate cluster. After subtraction of RBC data the clustering of the data remained essentially unchanged. Besides the outliers the rest of the points grouped by time and the time 0 sample here was in the cluster with the samples collected at 48 hours.

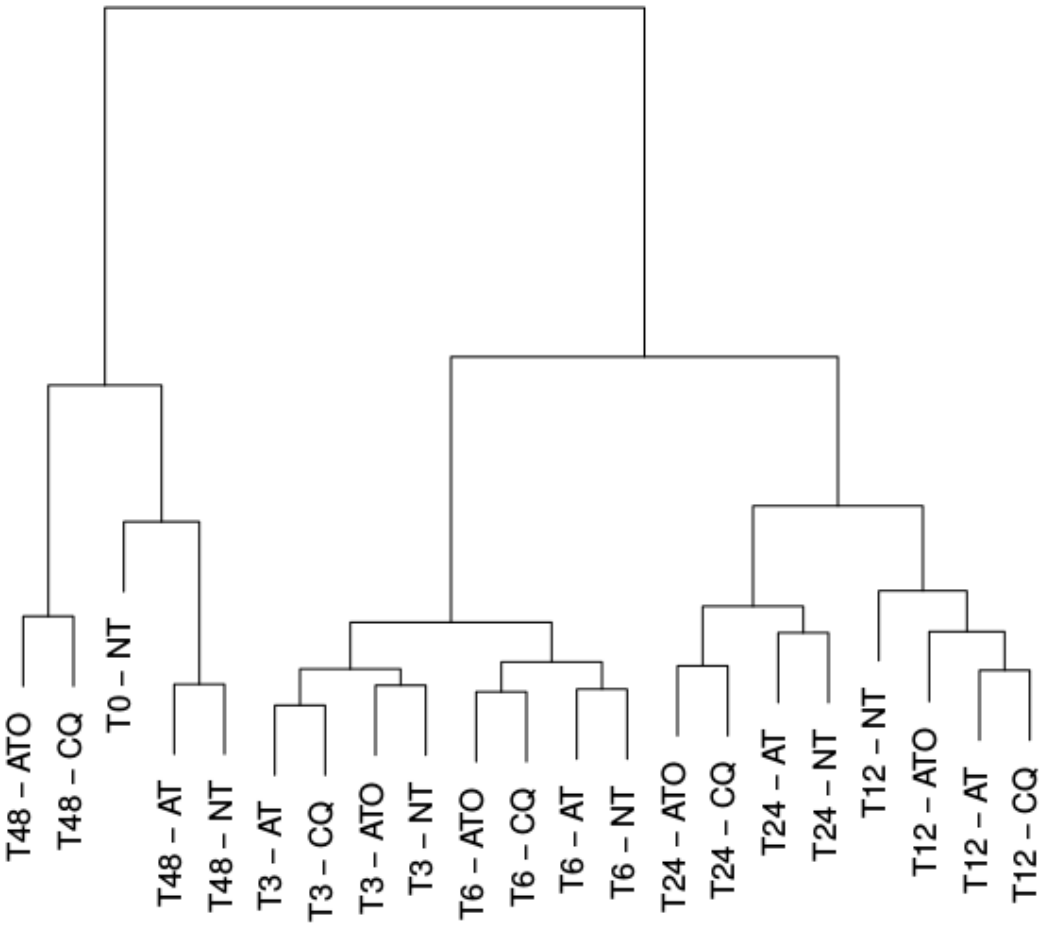

Figure 6.22: HCA dendrogram of ^{1}H NMR spectra collected from *P. falciparum* infected RBC samples after 3, 6, 12, 24 and 48 hours of drug exposure at IC_{90} concentrations; 3 replicate spectra per sample were averaged. Samples at t=0 h cluster with the samples at t=48h possibly due to the the parasites at 48 hours reaching the same stage in the next life cycle as they were at the start of the time-course. Treatments : NT - untreated, ATO - atovaquone, CQ - chloroquine, AT - artemisinin, T3-T48 - samples after 3-48 hour exposure.

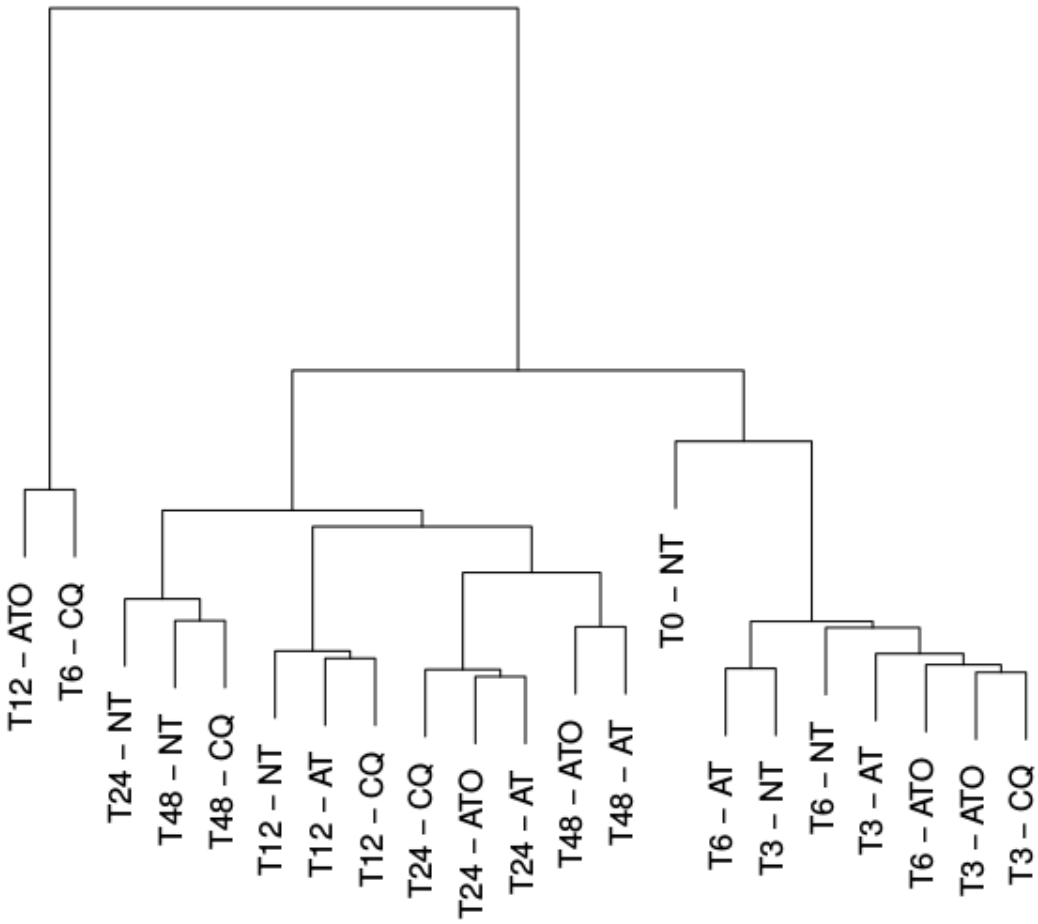

Figure 6.23: HCA dendrogram of ^{1}H NMR spectra collected from RBC samples after 3, 6, 12, 24 and 48 hours of drug exposure at IC_{90} concentrations; Treatments : NT - untreated, ATO - atovaquone,CQ - chloroquine, AT - artemisinin, T3-T48 - samples after 3-48 hour exposure.

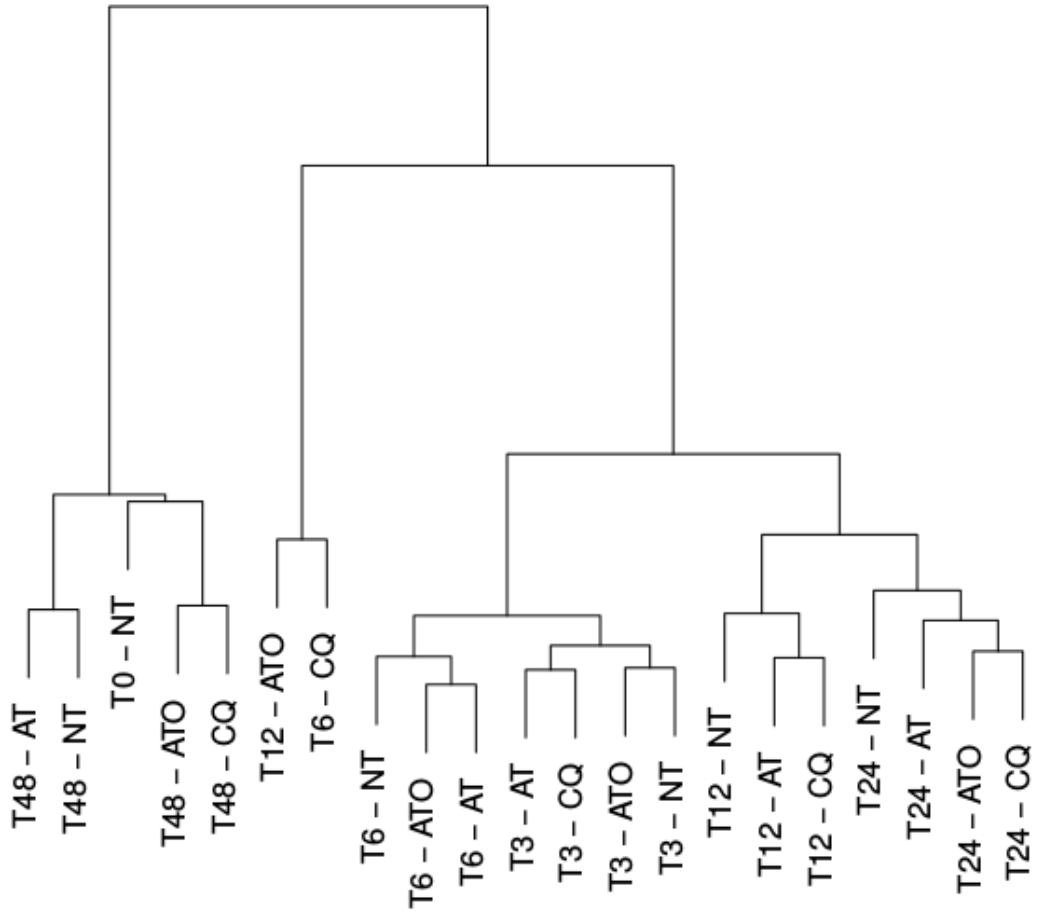

Figure 6.24: HCA dendrogram of ^{1}H NMR spectra collected from *P. falciparum* infected RBC samples after 3, 6, 12, 24 and 48 hours of drug exposure at IC_{90} concentrations; 3 replicate spectra per sample were averaged and uninfected RBC data was subtracted. Samples at t=0 h cluster with the samples at t=48h possibly due to the the parasites at 48 hours reaching the same stage in the next life cycle as they were at the start of the time-course. Treatments : NT - untreated, ATO - atovaquone, CQ - chloroquine, AT - artemisinin, T3-T48 - samples after 3-48 hour exposure.

6.5 Modeling Time-course data

In the analysis so far each sample has been treated as an independent data point only taking into account the time dependency in the interpretation of the results. This is a rather over simplification that could result in potential loss of information. While it was not necessarily incorrect, an important source of information in the data was being ignored. Due to the time-course nature of the experiment the data points were not independent samples and therefore were correlated. Each time point except for the time 0 was dependent and a direct consequence of the preceding time point. Taking into account this information could prove crucial for finding differences between the drug treatments as well as helping remove the time dependent pattern in the data. Such analysis required more advanced data modelling involving time series analysis. For this purpose we employed a method called multiple dataset integration (MDI) (ref. to Section 1.7.6). This method is capable of modelling time-series data and was used in order to investigate the similarity of behaviour of metabolites between conditions over time. MDI allows detection of clustering structure among the metabolites (NMR bins) and allows comparison of samples based on it. Similar clustering structure implies similar time-course behaviour of the metabolites between treatments.

MDI produces cluster assignment probabilities that are visualized by plotting heatmaps with intensities corresponding to the probabilities. A darker colour indicates a higher probability that these two items belong to the same cluster. The results of the analysis of iRBC data (Fig. 6.25) showed no differences between drug treatments. This indicated that the temporal behaviour of metabolites (NMR peaks) was similar between all conditions suggesting that none of them were affected by a treatment in any significant manner. Similar results were obtained after analysis of the data after subtraction of RBC data.

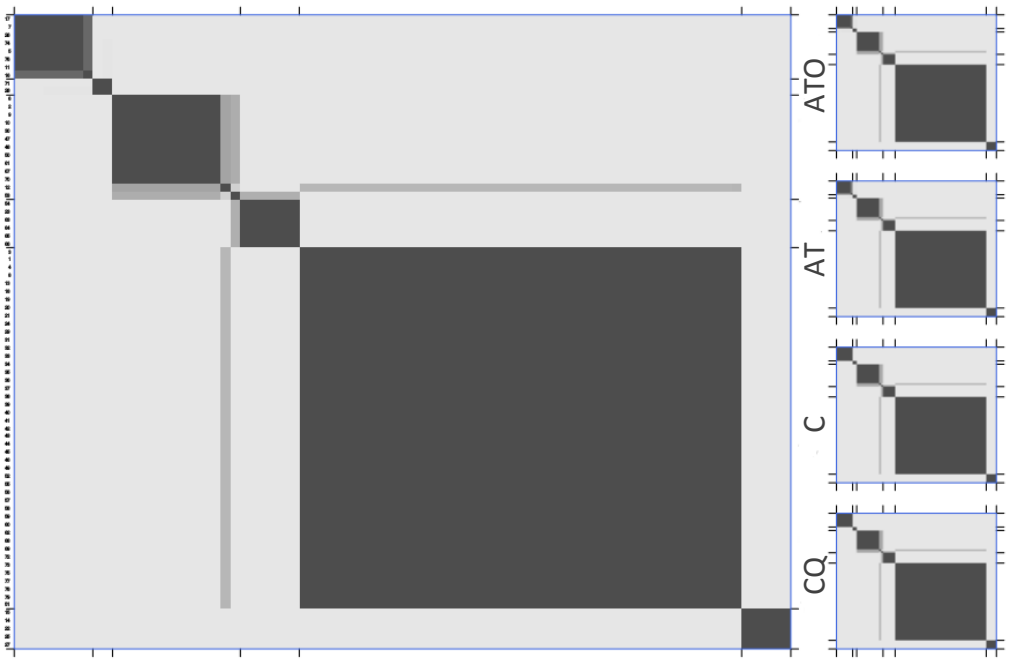

Figure 6.25: MDI cluster dependency heatmaps plotted for each treatment separately (on the right) and a consensus (on the left) calculated by averaging all the individual heatmaps. The darker fill indicates the probability of two points belonging to the same cluster. Each heatmap is represents a symmetric probability matrix where each row/column corresponds to one NMR bin. Gaussian process models have been fitted to the time-course of each metabolite. The spectra bins have been rearranged by cluster they have been assigned to. ATO - atovaquone, AT - artemisinin, C - control, CQ - chloroquine.

6.6 Discussion

Since its widespread adoption as a metabolomics technique NMR spectroscopy has been applied to a variety of biological problems [Kruger et al., 2008; Halouska et al., 2012b; Beckonert et al., 2007b; Frederich et al., 2011; Yuliana et al., 2011; Weljie et al., 2007]. Investigation of *P. falciparum* metabolism using NMR spectroscopy however has only been attempted on a handful of occasions [**?**Teng et al., 2014; Olszewski and Llinas, 2013; Lian et al., 2009]. **?**] investigated the effects of metabolite extraction solutions to the number of metabolites detected in the NMR experiments of *Plasmodium*. Over 50 metabolites were identified in the extracts using 1D and 2D NMR experiments and over 40 metabolite concentrations were estimated. In a similar study later Teng et al. [2014] established metabolics profiles of different *Plasmodium* strains using NMR spectroscopy. Both studies were performed using

parasites at the late trophozoite stage. This allowed parasite removal from the RBCs using saponin lysis, the limitations of which are discussed in earlier chapters. The study presented in Lian et al. [2009] followed a similar protocol. Alternatively Olszewski and Llinas [2013] have suggested a method for preparation of samples without saponin lysis. This method relied on performing extractions of the parasites together with the RBCs and was used as a basis for the method developed for this project. The publication did not present any results of an application of the method in NMR-based experiments. A similar method has been successfully applied by the same authors to MS-based metabolomics experiments of *Plasmodium* [Olszewski et al., 2009] where it helped to elucidate some peculiar features of the parasite metabolism. Numerous other metabolomics studies used LC-MS or GC-MS (or both) for investigation of *P. falciparum* metabolism [MacRae et al., 2013; Cobbold et al., 2013; Ke et al., 2015; Cobbold et al., 2016]. However, these techniques, while providing higher accuracy, are less reproducible, require complex sample preparation and longer data acquisition times due to the separation step before the analysis [Nagana Gowda and Raftery, 2015]. This makes application of MS difficult in high throughput *Plasmodium* studies.

The results presented in this chapter provide some insight into the advantages and limitations of the NMR-based metabolomics of malaria parasites and shed some light on the reasons for its rare adoption for such studies.

The intraerythrocytic nature of the parasite life cycle makes it inconvenient for metabolomics studies. The red blood cell background adds an enormous amount of undesired signal and removing the parasites from the RBCs before the experiments is not viable. The preferred parasitemia of *P. falciparum* in culture to ensure optimal viability is less than 10%. While a higher level of parasitemia is possible [Radfar et al., 2009a] due to limited availability of nutrients or frequent manipulations (with increases frequency of media changes) parasite growth can be compromised and metabolic states can be triggered through stress unrelated to the drug action. This constraint results in the low parasite to RBC biomass ratio in the culture and subsequently samples and metabolite extracts. Samples have to be prepared with the aim of maximising signal with the signal contributed by the parasite being readily detectable. In this work the parasite contributed signal was maximized by gradually increasing the sample size while keeping the parasitemia fixed at the optimal 8-10%. The largest amount of biomass used per sample was derived from a whole cell culture. The requirement of such a large amount of biomass is a serious limitation of NMR spectroscopy as a metabolomics technique in studies where the sample volume is a limiting factor, compared to other techniques such as LCMS

or GCMS where relatively low sample volumes can be effectively interrogated. For similar studies using MS the suggested volume of cell pellet used per sample was as low as 50 μL [Olszewski and Llinas, 2013], when the corresponding volume in our experiments was up to 1 mL.

A further challenge, especially in drug screening studies, is the selection of time points for sampling. During its 48-hour life cycle *P. falciparum* undergoes a series of morphologic as well as transcriptomic and metabolic changes [MacRae et al., 2013; Olszewski et al., 2009]. Currently used drugs have a range of modes of action and times of onset [Delves et al., 2012; Wilson et al., 2013]. In order to detect the mode of action in the metabolic fingerprint the time of sampling must coincide with the metabolic state that is uniquely attributable to the mode of action. As a drug screening would interrogate a range of compounds with a potentially diverse set of modes as well as times of action, in order to detect the drug effects the measurements of the metabolism would have to be made at appropriate times while keeping the experiments of manageable size. The assumption would be that dead parasites, no matter what the cause, would have a common metabolome reflecting death and not the subtle effects of drug that resulted in death. Frequent sampling would quickly increase the size of the experiment beyond manageable. Therefore a suitable set of sampling points has to be selected in order to maximize coverage of all potentially critical action-time points. In this work the question was addressed multiple times during the method development. The experimental design was changed from one fixed time sampling point to sampling at multiple time-points over durations ranging from 2 to 48 hours. In the metabolic profile analysis the time component always played the major role as the differences between the profiles at different time-points were more prominent than treatment effects. This could be explained in two ways. Firstly the differences could be arising as batch effects between separate sample preparations at each time point. While the conditions at each sampling time were kept as uniform as possible the possibility of a batch effect cannot be discounted. Another, and in our opinion more likely possibility, is that the death of parasites was not instant and not all parasites were affected by the compounds equally and synchronously. Even though the parasites were exposed to very high concentrations of antimalarial it is probable that there was a distribution of effects within the parasite population confounding the signal readouts. The challenge going forward is to be able to ensure that almost all of the population of parasites experience the effect of the drug and respond in synchrony, that the background RBC signal can be cleanly removed from the data and a method can be developed that removes the non-specific temporal changes seen in these experiments. Attempts to reduce

non-specific noise in the data was investigated by increasing drug concentrations to $10 \times IC_{90}$, using alternative drug probes with different mechanisms of action, increasing parasite biomass to the limit, increasing the number of replicates and looking at multiple exposure times. None of these manipulations generated any useful data linked to drug action. There is the possibility that the data just wasn't robust enough and there was the a need for greater signal or an alternative analytical approach such as LCMS. It is also possible that there is some useful information in the collected data that requires more advanced tools to be uncovered. A solution to this could be provided by a more advanced statistical analysis modelling the data as a time-course e.g. treating the data-points as sequential and correlated instead of independent. This was attempted using MDI [Kirk et al., 2012]. While the results suggested presence of different clustering patterns in NMR peaks between treatments, the variance between separate MDI runs was high indicating instability of cluster assignments. This could be explained by high variance in the data as well as low number of replicates per time-point and treatment (n=3).

The concentration of drugs used in the screening experiment is another key variable to be optimised. In most drug studies IC_{50} or IC_{90} concentrations are determined and used as indicators for drug efficacy. However, these concentrations are usually determined based on parasite survival after the 48-hour life cycle and do not provide information about possible dose dependent speed of action or targeted life cycle stages. As a forerunner to all future studies there need to be detailed evaluations of the time to kill, stage phasing and sensitivity to each test drug in order to design an exposure strategy that best fits with the pharmacology of the drug. In the current work range of drug concentrations used was from $1 \times IC_{90}$ to $10 \times IC_{90}$. This did not result in any improvement in the data.

The assumption that it would be possible to uniquely assign the modes of action of antimalarial compounds to their induced metabolic states relies on the ability of the analytical method, in this case NMR, to capture the information relevant to these states in a spectroscopic fingerprint. It is implied that at least a minimal number of affected metabolite concentrations have to be captured in the metabolic readouts. NMR spectroscopy was chosen for this work for its speed, robustness and relative simplicity in sample preparation and data collection. However, these advantages come at a heavy price in sensitivity. While signals from a wide range of metabolites can be captured (and identified) in complex biological mixtures [**?**], only the metabolites of highest abundance produce a measurable signal. Molecules at sub-micromolar concentrations are unlikely to be detectable in the resulting spectra. This is the major concern of this study. While similar attempts

have been successful in identifying metabolites altered by drug effects or toxicity, most of them were in experiments involving human or animal tissue or biofluids [Rozen et al., 2005; Lindon et al., 2004; Coen et al., 2004; Serkova and Boros, 2005] where the amount of starting material was not limiting. Due to the intraerythrocytic nature of *P. falciparum* many of the metabolites that could be detected in "pure" parasite samples are of relatively low concentration in infected RBC samples. Therefore an extensive analysis of metabolites detected in *P. falciparum* cultures (with and without RBCs) by NMR would be instrumental in any further considerations of using NMR spectroscopy as a metabolomics tool in studies of the malaria parasite. The latest study by Cobbold et al. [2016] demonstrated metabolic changes in the malaria parasite induced by a series of antimalarials. The study relied on both LC-MS and GC-MS in order to maximise the number of detected metabolites and used enriched parasites cultures as well as ^{13}C-labeled glucose for tracking of glycolytic intermediates. This huge effort illustrated the magnitude and the complexity of the task of investigating drug induced metabolic perturbations in malaria parasites.

Chapter 7

High Content Imaging Study of *P. falciparum* Phenotype After Exposure To Antimalarial Compounds.

High content imaging techniques have been growing in popularity in drug screening assays including in the targeting of a variety of tropical diseases [Sykes and Avery, 2015; Siqueira-Neto et al., 2012; Aulner et al., 2013; Clare et al., 2015]. However, although HCI platforms have been used to screen for drug activity [Plouffe et al., 2016; Lucantoni et al., 2015; Duffy and Avery, 2012] there have been no studies looking at the potential of HCI to identify common mechanisms of action based on drug treated phenotype. The intra-erythrocytic life-cycle of the malaria parasite makes metabolomic studies of *P. falciparum* particularly difficult due to contamination from signal originating from the host cell. However the spatial resolution of fluorescent imaging-based techniques avoids this problem. Here we present a proof of concept method of high throughput high content imaging to discriminate mechanisms of action of screening hits. The pilot study presented here was designed as a proof of concept that phenotypic changes that can be quantified in *P. falciparum* exposed to various antimalarial compounds are indicative of drug speed of kill and underlying mechanisms of action. Subsequently the method could be applied in high throughput screening of novel compounds in order to cluster drugs of unknown mechanisms of action with phenotypes characteristic of drugs with known mechanisms. We first used permutation testing coupled with PLS-DA models to show that the data generated by HCI contained information about the drug speed

of kill. A series of PLS-DA models were then built in order to learn the patterns from the known drug data and applied to the data collected from samples exposed to the original Malaria Box of 400 MMV compounds. The design of the study and discussion of the design decisions is presented first in Section 7.1, followed by the results of the data modelling and analysis in Section 7.2.

7.1 Study Design

The pilot study was designed with the aim of determining whether high content fluorescent imaging of *P. falcipatrum* nuclei could be used to discriminate between parasites exposed to drugs with different speeds of kill. We hypothesized that the exposure to various antimalarial compounds with specific modes of action would have a unique effect on *P. falciparum* phenotype as observed with HCI. With appropriate parameter measurements the fluorescent microscopy images could then be used to determine the speed of kill of the drug which could potentially contain additional information about the mode of action. A group of well established antimalarials with well characterised speeds of kill and modes of action were chosen for the study. The chosen drugs are summarized in Table 7.1.

The study observational period was 32 hours. The duration of the experiment was chosen based on the observation of the average time needed for parasites to reach late trophozoite-schizont stage from the early ring stage taking into account the window of synchronisation (about 8 hours). This duration was chosen to allow enough time for drugs to exert their pharmacological effect prior to cell division and merozoite formation. In these HCI experiments the focus was on the nucleus and the imaging software collected a series of parameters (nucleus size, average fluorescent

Table 7.1: The antimalarial drugs used in the imaging study. The speed of kill is assigned based on well established knowledge of drug action. DHODH - Dihydroorotate dehydrogenase.

Compound	Speed of kill	Group
Artemether (ATH)	fast	artemisinins
Artemisinin (AT)	fast	artemisinins
Dihydroartemisinin (DHA)	fast	artemisinins
Chloroquine (CQ)	fast	quinoline-like
Amodiaquine (AQ)	fast	quinoline-like
Quinine (Q)	slow	quinoline-like
DSM1	slow	DHODH inhibitor
Atovaquone (ATO)	slow	antifolate

intensity, roundness and texture features, see Table 2.2) from a series of imaging fields. The parasite nucleus undergoes significant and relatively rapid changes in the later stages of schizont development when merozoites are formed. Such changes significantly increased the noise in the data if the timing of the experiment was marginally off, e.g. if the measurements of nucleus size were taken at the late schizont stage when some of the parasites had already started nuclear division, progressed to merozoites or even reinfected and transitioned to the early ring stages while the rest of the culture were still in early schizogony (Fig. 7.1, right panel), then the average size measurement would be reduced. The size of the nucleus of a parasite arrested by drug action early in the life cycle would potentially be indistinguishable from a "second generation" parasite unaffected by the drug or a mixture of early schizonts and merozoites. The parasites at the late trophozoite - preschizont stage, the time when the measurements were taken, had the largest nucleus which allowed more accurate measurements of texture to provide the most discriminatory data for drug classification.

During the 32 hour observational period parasites were exposed to an IC_{90} concentration of the antimalarial drug or MMV probe compound cultured in a 96-well flat-bottomed plate. Each individual plate contained a set of the known antimalarials as positive controls and a non-drugged control medium (CM) wells used as the negative controls. After the exposure, the parasites were transferred to a 384-well imaging plate, fluorescent stain Hoechst [Latt et al., 1975] was added and the plates were incubated for 30 minutes. The parasites treated with different compounds were arranged on the plate in a staggered manner in order to diminish any systematic effects. Each plate contained five replicates of each known drug and ten replicates of the negative control. The rest of the plate contained MMV compounds - one replicate per plate. The replicate wells were arranged on the plate in columns while the readings were taken row-by-row to further diminish any machine drift or temporal biological effects. The reading of one plate took up to an hour and therefore potential temporal effects had to be taken into account. For added confidence in the predictions two plates of each set of MMV compounds were prepared. Each plate was prepared with an identical arrangement of samples. The HCI measurements were taken using an Operetta High Content Imaging platform and the data was extracted using Harmony software.

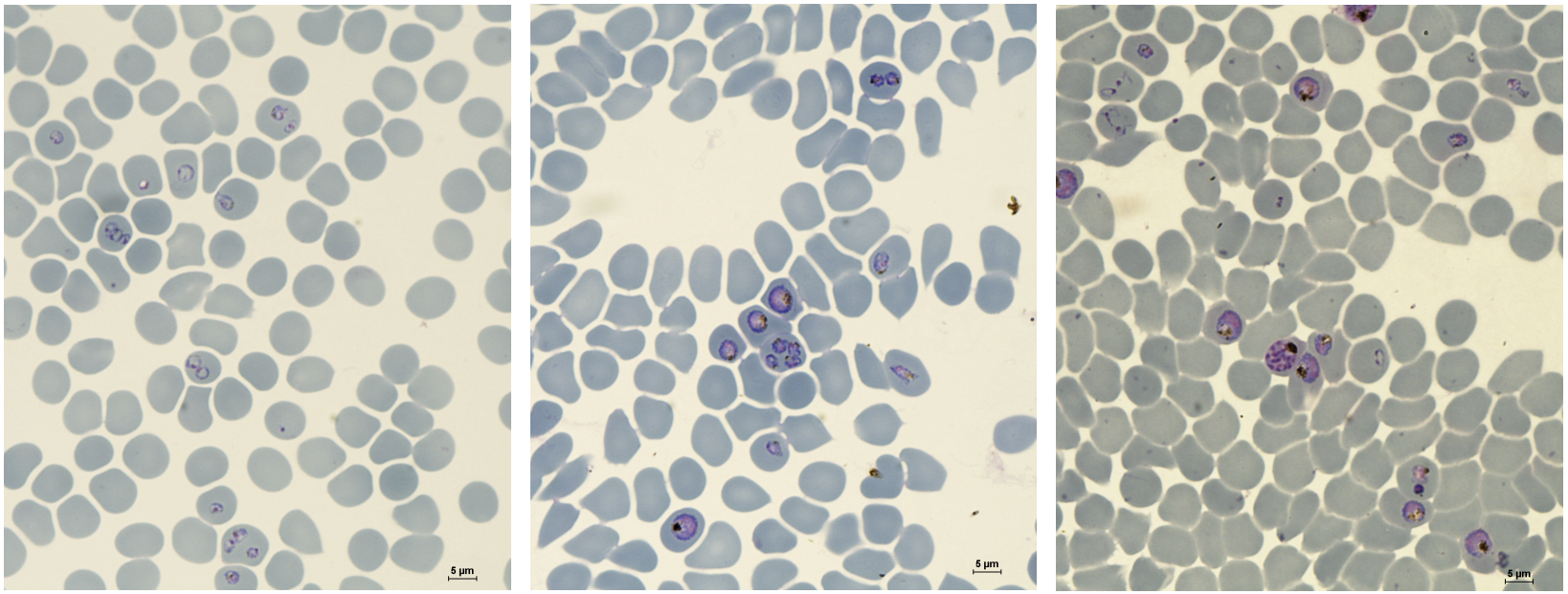

Figure 7.1: Images of infected red blood cells in Giemsa-stained smears. RBCs appear light blue-grey, and the parasites are stained dark purple. Left panel: rings (12 h), middle: trophozoites (32 h), right panel: schizonts and rings (42 h).

7.2 Data Processing and Analysis

The data collected in the experiment consisted of a set of measurements (See Table 2.2) of regions selected in the high resolution images. The region selections were made in an automated fashion by an algorithm set up to select high intensity fields in the images taken after the application of an emission filter. While the nuclei of the parasites were selected efficiently the images also included a range of artefacts (Fig. 7.2). Due to random clusters of dye molecules in the background, high intensity regions were occasionally formed that were detected and selected by the software as nuclei. In order to reduce the number of such artefacts a processing procedure was designed in Harmony software that was used to filter out the selections of the image regions that were unlikely to correspond to parasites by specification of area, intensity and roundness constraints. The regions that did not fit at least one of these constraints were removed from further analysis.

After filtering in Harmony the data was further cleaned and structured for analysis. First it was checked for outliers by visual inspection of scatterplots of signal size and intensity (Fig. 7.3). As mentioned previously the data contained some artefact signals and it was clear from the scatterplots that some artefacts remained even after filtering in Harmony. As each well contained a separate population of parasite cells, they were inspected separately. Each well contained a number of signals significantly larger or smaller in size or intensity (or both) than the average signal in the well.

Outliers were selected and removed using an anomaly detection algorithm on cell nucleus area and intensity values. First a two-dimensional Gaussian was fitted to logged cell 'Intensity' and 'Area' variables. Data from each well was fitted separately and probabilities of each data point were calculated from the resulting model. The signals that corresponded to values with probability less than 0.9 were then removed from further analysis. After cleaning, the majority of the outliers were removed as confirmed by visual inspection of the scatterplots of the data. Figure 7.4 shows the data from the same wells shown in Figure 7.3 after outlier removal.

The data was then formatted to only include size, intensity and texture parameters (see Table 2.2) and split into groups corresponding to 'knowns' - the positive control compounds - and 'MMVs'. The 'knowns' dataset consisted of 40 samples and was used for model building and validation. The trained models were used to predict the speed-of-kill of the 'MMV' group of probe compounds.

Modelling was performed using partial least squares discriminant analysis (PLS-DA) (see Section 1.7.3). A ten-fold cross-validation was performed for selection

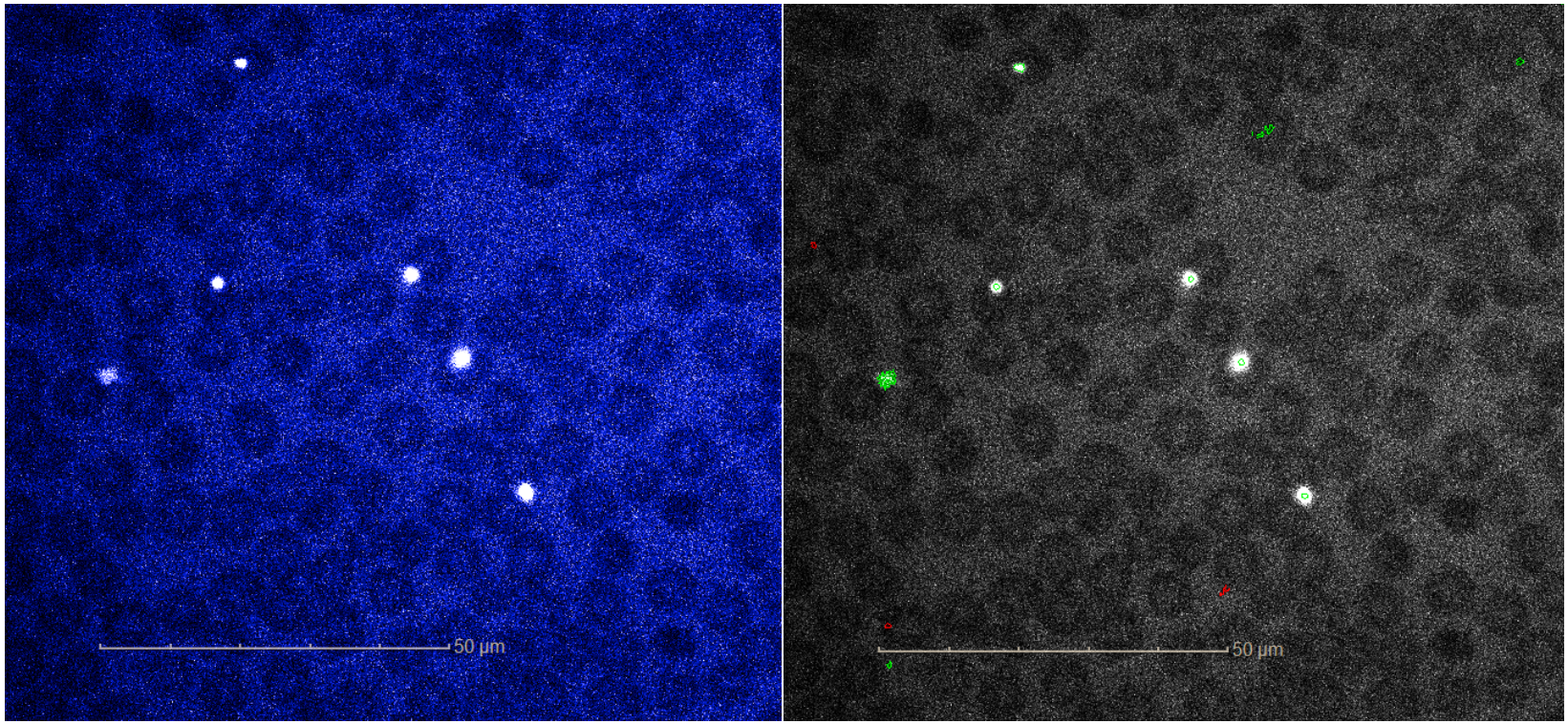

Figure 7.2: Fluorescent images of *P. falciparum* infected RBCs. Left panel: before automatic signal detection, right panel: after automatic signal detection. Red selections were automatically removed from the output data by the software while green selections were kept for further analysis. Some of the signal fields are selected due to random collection of bright pixels and do not correspond to parasites.

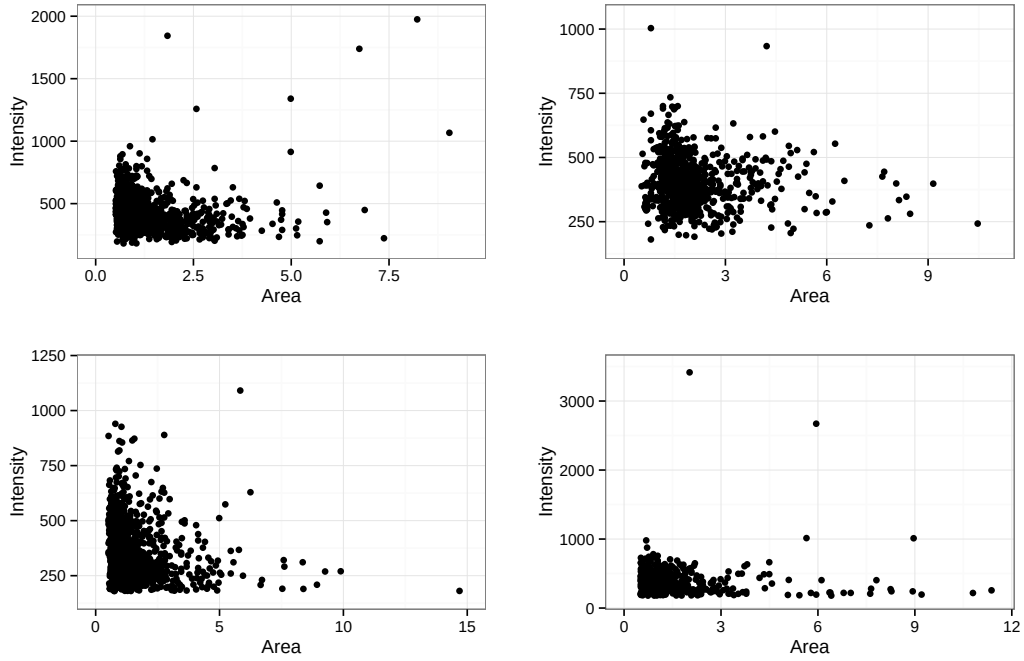

Figure 7.3: Example scatterplots of four wells from one of the imaging plates. The data includes a number of points that are quite different in area or intensity from the rest of the items; these were removed from further analysis.

of the number of PLS components in order to avoid overfitting and a 20-model ensemble was used for predicting the grouping of new unknown compound data.

In order to show that the images contained information about difference of effect in the two groups of compounds permutation tests (see Section 1.7.4) were performed. A series of PLS-DA models for each dataset with randomly permuted labels were used to simulate an empirical distribution of Q^2 "goodness-of-prediction" metric

$$Q^2 = 1 - \frac{\sum_{i=1}^{n}(y_i - \hat{y}_i)^2}{\sum_{i=1}^{n}(y_i - \bar{y})^2} \tag{7.1}$$

where y_i is the group (1,0) of i^{th} well, $\hat{y}_i$ is the predicted probability for i^{th} sample to be in group 1 and $\bar{y}$ is the mean response. This distribution was used to calculate a p-value for the Q^2 of the model fitted to correctly labelled data - $\hat{Q}^2$. The p-value in this case demonstrated how likely it was that the labels on the data were meaningful. If $\hat{Q}^2$ was close to the mean of the distribution, the model fit would be similar to those for randomly labelled data, suggesting that any random permutation of the labels could give similar predictions and the grouping of the

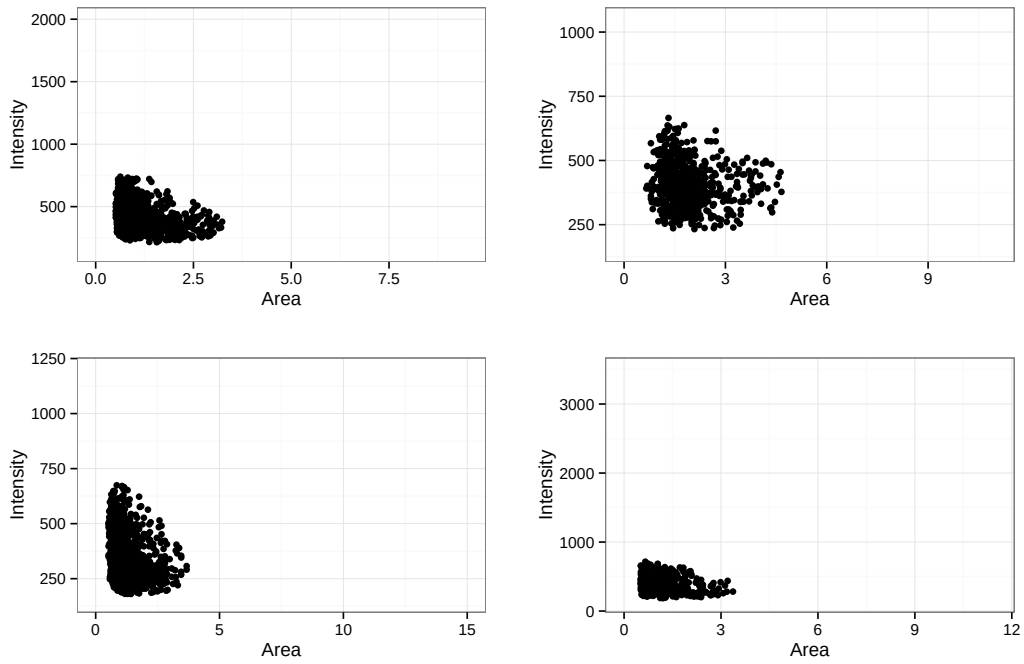

Figure 7.4: Example scatterplots of four wells from one of the imaging plates. The dataset has been cleaned in order to remove outliers.

drugs was not meaningful or their differential effects were not adequately captured in the data. On the other hand a low p-value would suggest that it was unlikely to obtain similar predictions from the models with any other permutation of labels. Therefore the labels must be meaningful and possibly correspond to drug effects captured in the data and detected by the model.

A permutation test was performed for each dataset (Fig. 7.5a). The results of all the runs are given in Table 7.2. It was clear that the differences between groups were significant and the method seemed to readily discriminate between the two groups of drugs. There was one case however where the p-value was high ($p_{val} = 0.194$). After further inspection of collected images and cell nucleus size data of the negative controls (Fig. 7.6) it was clear that the experiment did not work as expected. Due to unknown reasons the parasites did not grow in the majority of wells on the plate which is reflected by the lower mean area of the parasite nuclei compared to the other experiments. The results of the permutation test of that experiment are shown in Figure 7.5b.

This result suggested an additional application of the permutation test. After the models are shown to predict the drug effects, the results could be used as a quality control for future experiments. Since each experimental plate contains the same

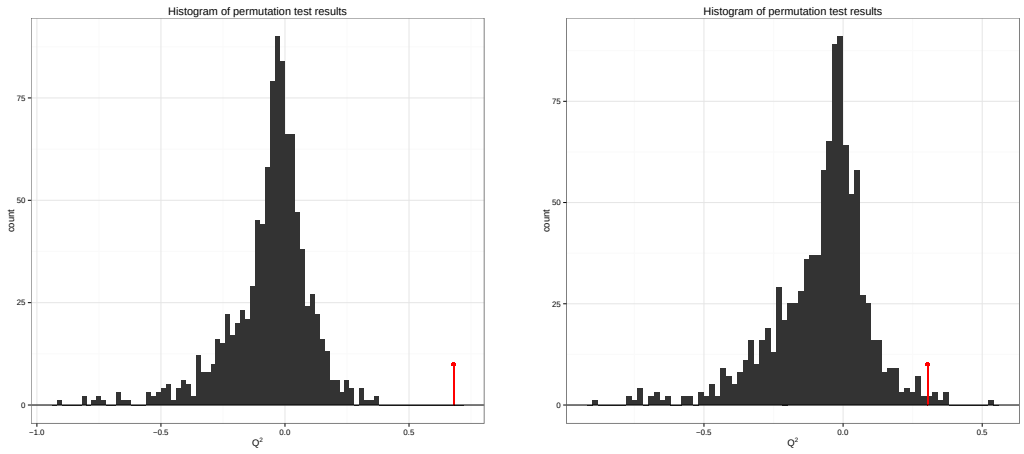

(a) (b)

Figure 7.5: A histogram representing the empirical distribution of Q^2 values calculated in a permutation test using PLS-DA models fitted to two groups ("fast" and "slow" acting compounds) of treatments. The red line denotes the Q^2 value of the model trained on the correctly labelled data. (a) The results using data from a successful experiment; (b) results from a technically unsuccessful experiment;

set of "known" drugs, each new experiment could be subjected to a permutation test and have the p-value calculated as described above. Since the differences between drug effects have been established an arbitrarily low (< 0.01) p-value would indicate a successful experiment. An ensemble of models could then be used to predict the unknown compound grouping.

PLS-DA models were fitted to data producing an ensemble of 20 models per dataset. The model fitting procedure included testing the model performance on a randomly selected partition of the data (see Section 2.5). The Q^2 value was calculated for each model and a mean Q^2 value for each model ensemble was reported (Fig. 7.7).

In order to fit a PLS-DA model the number of PLS components used for classification had to be optimized first. This procedure was performed by fitting a series of PLS-DA models with a varying number of components and the optimal number of components was selected based on the 'goodness-of-prediction' metric Q^2. The best performing parameter was then used to train 20 models using different splits of the data into training and test subsets in order to obtain robust models. The resulting model performances were assessed based on their respective Q^2 values. The 20 model "ensemble" was then used for the prediction of samples treated with "MMV" probe compounds. Each model predicted a probability of

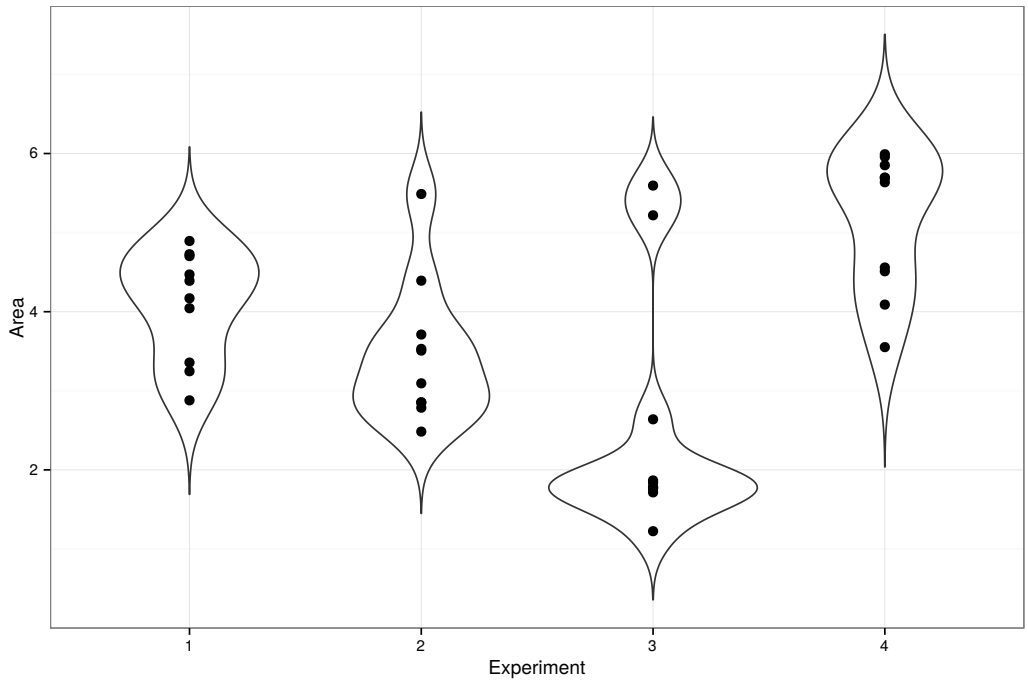

Figure 7.6: A violin plot of nucleus area measurements from control (untreated) parasites in four experiments. The violin plots show the density of the points along the y axis making the data distributions easier to compare. Experiments 1, 2 and 4 show a similar range of nucleus area while the majority of points in experiment 3 are lower, indicating insufficient growth of the parasites.

sample membership in the "fast" set. An average probability from the 20 models was used as the final prediction result. The samples with probabilities larger than 0.5 were classified as "fast". The prediction results were saved for validation of the assay. The set of compounds predicted as "fast" included 121 compound out of the 400 tested. This suggested that around a third of the compounds induced a parasite phenotype similar to the phenotype resulting from exposure to fast acting drugs. Since the method relied on fitting a model to latent variables the results were not easily interpretable. External validation is required in order better characterise the predictions. Further development of the method will involve parasite viability and time till death assays [Sanz et al., 2012; Linares et al., 2015]. These methods would provide additional information on the characteristics of the selected compounds and allow better understanding of the model properties such as the false discovery rate.

Table 7.2: The p-values from permutation tests in each experiment rounded to three significant digits. The p-values smaller than the significance level of 0.01 are marked with *.

Experiment	MMV set	p-value
1a	1-100	$< 0.001*$
1b	1-100	$< 0.001*$
2a	101-200	$< 0.001*$
2b	101-200	$< 0.001*$
3a	201-300	$0.009*$
3b	201-300	0.194
4a	301-400	$0.004*$
4b	301-400	$0.002*$

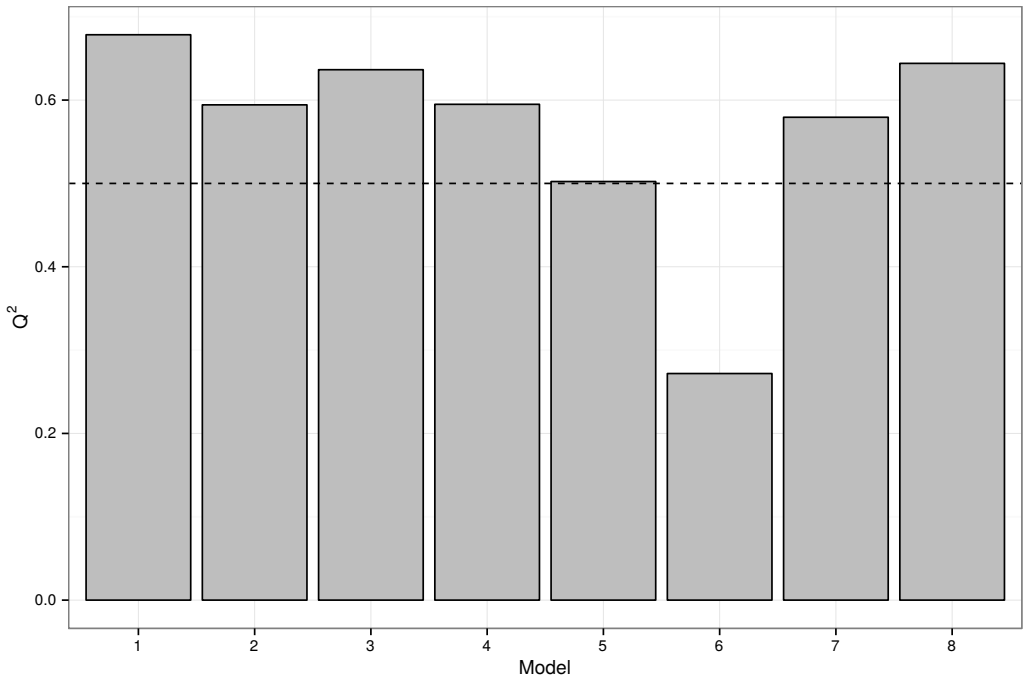

Figure 7.7: Mean Q^2 values for each ensemble of 20 models fitted to experiment data. The dashed line at 0.5 shows an arbitrary boundary for an acceptable model.

7.3 Discussion

Due to the high number of potent antimalarial hits reported in the literature from large chemical library screens there is a pressing need for new high throughput assays that can triage this data in order to select the most promising hits for lead development. Importantly since the emergence of artemisinin resistance the need for novel fast acting compounds has become particularly important [Diagana, 2015].

The current drug discovery pipelines start with whole cell assays and target-based screening and are capable of producing thousands of hits [Guiguemde et al., 2010; Gamo et al., 2010; Rottmann et al., 2010; Plouffe et al., 2008]. The next step usually is left to computational analysis and triage. The hit compounds are investigated based on their predicted chemical properties, cost, ease of synthesis as well as by scaffold comparison to already known compounds [Flannery et al., 2013]. However properties such as speed of kill, mode of action or the part of the parasite life cycle when the compound is active cannot be readily predicted. Therefore there is a need for novel hit selection methods that would allow the pre-selection of compounds based on their *in vitro* kill dynamic properties as opposed to general chemical properties or simple IC_{50}.

We have presented a prototype assay for antimalarial compound screening based on high content imaging. It has been designed to detect compounds acting quickly on the early stages of *P. falciparum* asexual growth and development. HCI was used to detect phenotypic features of the parasite nucleus by comparison to parasites exposed to well known fast acting drugs in the artemisinin family (artemether, artemisinin and dihydroartemisinin) and fast quinoline-like compounds (chloroquine and amodiaquine).

There is no unified definition of a fast-acting antimalarial besides clearance from patients or animal models, systems that cannot be used in triaging hits from library screens. Therefore we have used the phenotypic similarity of parasites affected by fast acting antimalarials as a measure of "speed of kill". Compounds that affect the parasite phenotype in a similar way to fast acting compounds are easily detected. Since the measurements of the phenotype are indirect measurements of the drug effects we first showed that the measured effects were associated with the treatment groups as expected. Antimalarials with well known action profiles were used as a proof of concept as well as the basis for subsequent comparison with novel compounds. While the assay has been validated by demonstration of the consistent predictive power within the scope of these well-established compounds it should be further validated against an alternative method such as the parasite reduction ratio

(PRR) based assay [Sanz et al., 2012] or a reinvasion based assay [Linares et al., 2015]. Nevertheless, the method has shown promise in the initial testing stages and has been used to make initial predictions on the compounds included in the "Malaria Box". Once the assay is validated the modelling procedure can be improved by receiver-operator characteristic (ROC) curve analysis in order to adjust the decision boundary and optimise the false discovery rate.

The prototype method presented here is a proof of concept that a high content imaging platform can be used for untargeted compound screening for hit preselection before lead optimisation in a manner that is related to *in vitro* effects rather than simple chemoinformatics analysis that lacks biological context.

Chapter 8

Conclusions

With the development of new technologies and improving quality and especially quantity of data collected in experiments, new challenges arise. In particular the development of high-throughput whole cell assays have allowed drug discovery to progress on an unprecedented scale. Antimalarial drug screening efforts have produced thousands of molecules able to kill malaria parasites at nanomolar concentrations. However with big numbers come new challenges. The time and capital required to investigate such a number of compounds is enormous and therefore further triage selection processes are needed. In this work we have investigated three ways to address the problem of hit pre-selection from antimalarial drug screening. Two of the methods investigated were based on metabolomic fingerprinting approaches aiming to classify antimalarials based on their biochemical modes of action. The third method was based on the measurement and classification of *P. falciparum* phenotypic changes under drug treatments using high-content imaging.

As one of the desired features of a hit screening method is high throughput, Fourier-transform infrared spectroscopy was investigated first. It allows for easy sample preparation and storage and as it also has been applied in similar work on bacteria the method was a natural choice for this study. The results however did not live up to expectations. While it could clearly capture information about the constituents of the parasite cells, with the infected RBCs readily differentiable from the uninfected RBCs, life cycle stages of *P. falciparum* were not discriminated. The sensitivity required to detect the differences in metabolite concentrations in drug mechanism studies needed to be much higher. Admittedly, the experiments were performed against a background of RBC signal potentially masking information specifically from the parasite. Therefore FT-IR was considered not sensitive enough as a metabolic fingerprinting technique for antimalarial compound screening.

In order to obtain improved quality information content without losing the high throughput potential NMR spectroscopy was selected as an alternative technique with the potential to discriminate the actions of different drugs/probes. NMR has been growing in popularity in the metabolomics world and as well as the collection of global information about the metabolites present in the sample it also allows metabolite identification in case this was required. While it proved to be more sensitive than FT-IR it still faced similar challenges posed by the complex nature of the *P. falciparum* life-cycle. Significant signal contamination originated from the red blood cells and in order to get any parasite signal a large parasite biomass was required prior to extraction and concentration of samples. Additionally there were further challenges to be addressed that emphasised the complexity of the problem. In order to investigate the drug impact on parasite metabolism it had to be measured at the right, tightly controlled, time. Without any prior knowledge of the drug action profile the assay would have to rely on a set of optimized time and dose choices that would suit a wide range of possible compounds. For an assay based on measurement of parasite metabolism, which is very dynamic, this was a crucial step to optimize. Despite significant effort and multiple strategies and attempts the metabolic perturbations resulting from the impact of an antimalarial drug could not be detected. The time dependent component of the metabolomic fingerprint constantly dominated the profiles from samples under different drug stresses. The assumption is that the subtle effects of drug on parasite metabolism important in the action of the drug was masked by the signals originating form the red blood cells and from the unperturbed aspects of the parasite metabolome. Depite significant effort to optimise all steps in the protocol, sample preparation, data acquisition and data analysis this approach failed to generate any data that could be used to cluster drugs with common mechanisms. The sensitivity issue could be addressed by a systematic study of all *P. falciparum* metabolites detected in the NMR, however this would steer the method into the realm of metabolic profiling and would arguably be better performed by using MS approaches. In order to eliminate the temporal effects on the the fingerprint that dominated the signal the data was analysed and modelled as a time series. Even with this more complex approach to the analysis it was still not possible to discriminate the effect of drug on the metabolome. It could be argued that the sample sizes used were small (3-5) which may have impacted on the resolving power of these studies. However the availability of parasite biomass is a constant issue that that is not easily overcome and would preclude this approach for high throughput demands.

The high-content imaging study was a completely different approach for com-

pound selection. It was based on the hypothesis that the phenotypic changes in *P. falciparum* nucleus under drug treatment would be indicative of the properties of the drug in terms of stage specific killing mechanism. In this study the method aimed to select and cluster compounds based on the speed of kill. The experiments were designed with reproducibility and robustness in mind. First, using statistical analysis, we were able to prove that the method captured differences in the nuclei of the parasite cells treated with two groups of antimalarial drugs that had different speed of kill profiles. We then developed a series of classification models for compound classification based on the high-content imaging data. As expected an important feature in the data was the size of the nucleus, as the parasites affected by the drugs earlier in the life cycle had shorter period to grow, however other features of the nuclei were able to improve the discriminatory quality of results. While the model predictions still have to be fully validated by an orthogonal approach the internal model validation showed clear differences between the groups of parasites treated with fast-acting compounds such as the artemisinins compared to slower killers such as atovaquone and quinine. The method could be further expanded to include selection of screening criteria and enable adjustments of false positive rate. This would allow further fine-tuning of the assay. The method is general enough so that a different stain could be used in order to collect a different set of features e.g. mitochondrial stain (MitoTracker, Thermo Fischer) could potentially allow detection of phenotypic changes after exposure to respiratory chain targetting compounds. A more systematic investigation of phenotypic changes under the effects of compounds with various modes of action could produce a library of specific profiles that could later be used for a more targeted screening approach. This study has demonstrated the potential of image-based assays for *P. falciparum* drug screening and suggested a simple framework for hypothesis testing, quality control and classification of compounds.

To conclude, *P. falciparum* is a complex parasite in terms of its life cycle and it provides a series of challenges for researchers. Metabolomics approaches attempted in this study highlighted the difficulties of studying the malaria parasite. However, a high-content imaging-based approach suggested a new angle on antimalarial compound screening. This approach showed potential in a pilot study and if pursued could become a new high-throughput platform for compound screening based on direct effects on the cells and so complement the currently popular chemoinformatic analyses.

Bibliography

M. Adams, V. J. Cookson, J. Higgins, H. L. Martin, D. C. Tomlinson, J. Bond, E. E. Morrison, and S. M. Bell. A high-throughput assay to identify modifiers of premature chromosome condensation. *J Biomol Screen*, 19(1):176–183, Jan 2014.

S. T. Agnandji, B. Lell, J. F. Fernandes, B. P. Abossolo, B. G. Methogo, A. L. Kabwende, A. A. Adegnika, B. Mordmuller, S. Issifou, P. G. Kremsner, J. Sacarlal, P. Aide, M. Lanaspa, J. J. Aponte, S. Machevo, S. Acacio, H. Bulo, B. Sigauque, E. Macete, P. Alonso, S. Abdulla, N. Salim, R. Minja, M. Mpina, S. Ahmed, A. M. Ali, A. T. Mtoro, A. S. Hamad, P. Mutani, M. Tanner, H. Tinto, U. D'Alessandro, H. Sorgho, I. Valea, B. Bihoun, I. Guiraud, B. Kabore, O. Sombie, R. T. Guiguemde, J. B. Ouedraogo, M. J. Hamel, S. Kariuki, M. Oneko, C. Odero, K. Otieno, N. Awino, M. McMorrow, V. Muturi-Kioi, K. F. Laserson, L. Slutsker, W. Otieno, L. Otieno, N. Otsyula, S. Gondi, A. Otieno, V. Owira, E. Oguk, G. Odongo, J. B. Woods, B. Ogutu, P. Njuguna, R. Chilengi, P. Akoo, C. Kerubo, C. Maingi, T. Lang, A. Olotu, P. Bejon, K. Marsh, G. Mwambingu, S. Owusu-Agyei, K. P. Asante, K. Osei-Kwakye, O. Boahen, D. Dosoo, I. Asante, G. Adjei, E. Kwara, D. Chandramohan, B. Greenwood, J. Lusingu, S. Gesase, A. Malabeja, O. Abdul, C. Mahende, E. Liheluka, L. Malle, M. Lemnge, T. G. Theander, C. Drakeley, D. Ansong, T. Agbenyega, S. Adjei, H. O. Boateng, T. Rettig, J. Bawa, J. Sylverken, D. Sambian, A. Sarfo, A. Agyekum, F. Martinson, I. Hoffman, T. Mvalo, P. Kamthunzi, R. Nkomo, T. Tembo, G. Tegha, M. Tsidya, J. Kilembe, C. Chawinga, W. R. Ballou, J. Cohen, Y. Guerra, E. Jongert, D. Lapierre, A. Leach, M. Lievens, O. Ofori-Anyinam, A. Olivier, J. Vekemans, T. Carter, D. Kaslow, D. Leboulleux, C. Loucq, A. Radford, B. Savarese, D. Schellenberg, M. Sillman, and P. Vansadia. A phase 3 trial of RTS,S/AS01 malaria vaccine in African infants. *N. Engl. J. Med.*, 367(24):2284–2295, Dec 2012.

S. T. Agnandji, B. Lell, J. F. Fernandes, B. P. Abossolo, A. L. Kabwende, A. A. Adegnika, B. Mordmuller, S. Issifou, P. G. Kremsner, M. M. Loembe, J. Sacarlal, P. Aide, L. Madrid, M. Lanaspa, S. Mandjate, J. J. Aponte, H. Bulo,

A. Nhama, E. Macete, P. Alonso, S. Abdulla, N. Salim, A. T. Mtoro, P. Mutani, M. Tanner, C. Mavere, G. Mwangoka, O. Lweno, O. A. Juma, S. Shekalaghe, H. Tinto, U. D'Alessandro, H. Sorgho, I. Valea, J. B. Ouedraogo, P. Lompo, S. Diallo, O. Traore, A. Bassole, E. Dao, M. J. Hamel, S. Kariuki, M. Oneko, C. Odero, K. Otieno, N. Awino, V. Muturi-Kioi, J. Omoto, K. F. Laserson, L. Slutsker, W. Otieno, L. Otieno, N. Otsyula, S. Gondi, A. Otieno, B. Ogutu, J. Ochola, I. Onyango, J. Oyieko, P. Njuguna, R. Chilengi, P. Akoo, C. Kerubo, C. Maingi, A. Olotu, P. Bejon, K. Marsh, G. Mwabingu, J. Gitaka, S. Owusu-Agyei, K. P. Asante, O. Boahen, D. Dosoo, G. Adjei, E. Adeniji, A. K. Yawson, K. Kayan, D. Chandramohan, B. Greenwood, J. Lusingu, S. Gesase, A. Malabeja, O. Abdul, C. Mahende, E. Liheluka, M. Lemnge, T. G. Theander, C. Drakeley, J. Mbwana, D. Ansong, T. Agbenyega, S. Adjei, H. O. Boateng, T. Rettig, J. Bawa, J. Sylverken, D. Sambian, A. Sarfo, A. Agyekum, F. Martinson, I. Hoffman, T. Mvalo, P. Kamthunzi, R. Nkomo, T. Tembo, G. T. Tsidya, J. Kilembe, C. Chawinga, W. Ballou, J. Cohen, Y. Guerra, E. Jongert, D. Lapierre, A. Leach, M. Lievens, O. Ofori-Anyinam, A. Olivier, J. Vekemans, D. Kaslow, D. Leboulleux, B. Savarese, and D. Schellenberg. Efficacy and safety of the RTS,S/AS01 malaria vaccine during 18 months after vaccination: a phase 3 randomized, controlled trial in children and young infants at 11 African sites. *PLoS Med.*, 11(7):e1001685, Jul 2014.

M. A. Al-Holy, M. Lin, A. G. Cavinato, and B. A. Rasco. The use of Fourier transform infrared spectroscopy to differentiate Escherichia coli O157:H7 from other bacteria inoculated into apple juice. *Food Microbiol.*, 23(2):162–168, Apr 2006.

H. M. Al-Qadiri, M. A. Al-Holy, M. Lin, N. I. Alami, A. G. Cavinato, and B. A. Rasco. Rapid detection and identification of Pseudomonas aeruginosa and Escherichia coli as pure and mixed cultures in bottled drinking water using fourier transform infrared spectroscopy and multivariate analysis. *J. Agric. Food Chem.*, 54(16):5749–5754, Aug 2006a.

H. M. Al-Qadiri, M. Lin, A. G. Cavinato, and B. A. Rasco. Fourier transform infrared spectroscopy, detection and identification of Escherichia coli O157:H7 and Alicyclobacillus strains in apple juice. *Int. J. Food Microbiol.*, 111(1):73–80, Aug 2006b.

A. Alonso, M. A. Rodriguez, M. Vinaixa, R. Tortosa, X. Correig, A. Julia, and

S. Marsal. Focus: a robust workflow for one-dimensional NMR spectral analysis. *Anal. Chem.*, 86(2):1160–1169, Jan 2014.

F. Ariey, B. Witkowski, C. Amaratunga, J. Beghain, A. C. Langlois, N. Khim, S. Kim, V. Duru, C. Bouchier, L. Ma, P. Lim, R. Leang, S. Duong, S. Sreng, S. Suon, C. M. Chuor, D. M. Bout, S. Menard, W. O. Rogers, B. Genton, T. Fandeur, O. Miotto, P. Ringwald, J. Le Bras, A. Berry, J. C. Barale, R. M. Fairhurst, F. Benoit-Vical, O. Mercereau-Puijalon, and D. Menard. A molecular marker of artemisinin-resistant Plasmodium falciparum malaria. *Nature*, 505(7481):50–55, Jan 2014.

N. Aulner, A. Danckaert, E. Rouault-Hardoin, J. Desrivot, O. Helynck, P. H. Commere, H. Munier-Lehmann, G. F. Spath, S. L. Shorte, G. Milon, and E. Prina. High content analysis of primary macrophages hosting proliferating Leishmania amastigotes: application to anti-leishmanial drug discovery. *PLoS Negl Trop Dis*, 7(4):e2154, 2013.

A. D. Bangham, R. W. Horne, A. M. Glauert, J. T. Dingle, and J. A. Lucy. Action of saponin on biological cell membranes. *Nature*, 196:952–955, Dec 1962.

Q. Bao, J. Feng, L. Chen, F. Chen, Z. Liu, B. Jiang, and C. Liu. A robust automatic phase correction method for signal dense spectra. *J. Magn. Reson.*, 234:82–89, Sep 2013.

Christian Bartels, Peter Güntert, and Kurt Wüthrich. IFLAT—A New Automatic Baseline-Correction Method for Multidimensional {NMR} Spectra with Strong Solvent Signals. *Journal of Magnetic Resonance, Series A*, 117(2):330–333, 1995.

S. Becker, L. Kortz, C. Helmschrodt, J. Thiery, and U. Ceglarek. LC-MS-based metabolomics in the clinical laboratory. *J. Chromatogr. B Analyt. Technol. Biomed. Life Sci.*, 883-884:68–75, Feb 2012.

O. Beckonert, H. C. Keun, T. M. Ebbels, J. Bundy, E. Holmes, J. C. Lindon, and J. K. Nicholson. Metabolic profiling, metabolomic and metabonomic procedures for NMR spectroscopy of urine, plasma, serum and tissue extracts. *Nat Protoc*, 2 (11):2692–2703, 2007a.

O Beckonert, H C Keun, TMD Ebbels, and J Bundy. Metabolic profiling, metabolomic and metabonomic procedures for NMR spectroscopy of urine, plasma, serum and tissue extracts. *Nature protocols*, 2007b.

Michael Beekes, Peter Lasch, and Dieter Naumann. Analytical applications of Fourier transform-infrared (FT-IR) spectroscopy in microbiology and prion research. *Veterinary microbiology*, 123(4):305–319, August 2007.

T. Berlage. Analyzing and mining image databases. *Drug Discov. Today*, 10(11): 795–802, Jun 2005.

C. Bhardwaj and L. Hanley. Ion sources for mass spectrometric identification and imaging of molecular species. *Nat Prod Rep*, 31(6):756–767, Jun 2014.

G. A. Biagini, N. Fisher, A. E. Shone, M. A. Mubaraki, A. Srivastava, A. Hill, T. Antoine, A. J. Warman, J. Davies, C. Pidathala, R. K. Amewu, S. C. Leung, R. Sharma, P. Gibbons, D. W. Hong, B. Pacorel, A. S. Lawrenson, S. Charoensutthivarakul, L. Taylor, O. Berger, A. Mbekeani, P. A. Stocks, G. L. Nixon, J. Chadwick, J. Hemingway, M. J. Delves, R. E. Sinden, A. M. Zeeman, C. H. Kocken, N. G. Berry, P. M. O'Neill, and S. A. Ward. Generation of quinolone antimalarials targeting the Plasmodium falciparum mitochondrial respiratory chain for the treatment and prophylaxis of malaria. *Proc. Natl. Acad. Sci. U.S.A.*, 109 (21):8298–8303, May 2012.

R. A. Blake, M. A. Broome, X. Liu, J. Wu, M. Gishizky, L. Sun, and S. A. Courtneidge. SU6656, a selective src family kinase inhibitor, used to probe growth factor signaling. *Mol. Cell. Biol.*, 20(23):9018–9027, Dec 2000.

C. J. Bolten, P. Kiefer, F. Letisse, J. C. Portais, and C. Wittmann. Sampling for metabolome analysis of microorganisms. *Anal. Chem.*, 79(10):3843–3849, May 2007.

W. Bouhedja, G. D. Sockalingum, P. Pina, P. Allouch, C. Bloy, R. Labia, J. M. Millot, and M. Manfait. ATR-FTIR spectroscopic investigation of E. coli transconjugants beta-lactams-resistance phenotype. *FEBS Lett.*, 412(1):39–42, Jul 1997.

L. Brennan. NMR-based metabolomics: from sample preparation to applications in nutrition research. *Prog Nucl Magn Reson Spectrosc*, 83:42–49, Nov 2014.

D.E. Brown. Fully Automated Baseline Correction of 1D and 2D {NMR} Spectra Using Bernstein Polynomials. *Journal of Magnetic Resonance, Series A*, 114(2): 268–270, 1995.

H. P. Buschman, E. T. Marple, M. L. Wach, B. Bennett, T. C. Schut, H. A. Bruining, A. V. Bruschke, A. van der Laarse, and G. J. Puppels. In vivo determination of

the molecular composition of artery wall by intravascular Raman spectroscopy. *Anal. Chem.*, 72(16):3771–3775, Aug 2000.

Li Chen, Zhiqiang Weng, LaiYoong Goh, and Marc Garland. An efficient algorithm for automatic phase correction of NMR spectra based on entropy minimization. *Journal of Magnetic Resonance*, 158(1–2):164–168, 2002.

F. Chignola, S. Mari, T. J. Stevens, R. H. Fogh, V. Mannella, W. Boucher, and G. Musco. The CCPN Metabolomics Project: a fast protocol for metabolite identification by 2D-NMR. *Bioinformatics*, 27(6):885–886, Mar 2011.

Christian Cieslar, G Marius Clore, and Angela M Gronenborn. Automatic phasing of pure phase absorption two-dimensional NMR spectra. *Journal of Magnetic Resonance (1969)*, 79(1):154–157, 1988.

R. H. Clare, D. A. Cook, K. L. Johnston, L. Ford, S. A. Ward, and M. J. Taylor. Development and validation of a high-throughput anti-Wolbachia whole-cell screen: a route to macrofilaricidal drugs against onchocerciasis and lymphatic filariasis. *J Biomol Screen*, 20(1):64–69, Jan 2015.

S. A. Cobbold, A. M. Vaughan, I. A. Lewis, H. J. Painter, N. Camargo, D. H. Perlman, M. Fishbaugher, J. Healer, A. F. Cowman, S. H. Kappe, and M. Llinas. Kinetic flux profiling elucidates two independent acetyl-CoA biosynthetic pathways in Plasmodium falciparum. *J. Biol. Chem.*, 288(51):36338–36350, Dec 2013.

S. A. Cobbold, H. H. Chua, B. Nijagal, D. J. Creek, S. A. Ralph, and M. J. McConville. Metabolic Dysregulation Induced in Plasmodium falciparum by Dihydroartemisinin and Other Front-Line Antimalarial Drugs. *J. Infect. Dis.*, 213(2): 276–286, Jan 2016.

M. Coen, S. U. Ruepp, J. C. Lindon, J. K. Nicholson, F. Pognan, E. M. Lenz, and I. D. Wilson. Integrated application of transcriptomics and metabonomics yields new insight into the toxicity due to paracetamol in the mouse. *J Pharm Biomed Anal*, 35(1):93–105, Apr 2004.

Norman B. Colthup, Lawrence H. Daly, and Stephen E. Wiberley. IR experimental considerations. In Norman B. Colthup, Lawrence H. Daly, and Stephen E. Wiberley, editors, *Introduction to Infrared and Raman Spectroscopy (Third Edition)*, chapter 2, pages 75–107. Academic Press, third edition edition, 1990. ISBN 978-0-12-182554-6.

James W. Cooley and John W. Tukey. An Algorithm for the Machine Calculation of Complex Fourier Series. *Mathematics of Computation*, 19(90):pp. 297–301, 1965.

J. M. Coteron, M. Marco, J. Esquivias, X. Deng, K. L. White, J. White, M. Koltun, F. El Mazouni, S. Kokkonda, K. Katneni, R. Bhamidipati, D. M. Shackleford, I. Angulo-Barturen, S. B. Ferrer, M. B. Jimenez-Diaz, F. J. Gamo, E. J. Goldsmith, W. N. Charman, I. Bathurst, D. Floyd, D. Matthews, J. N. Burrows, P. K. Rathod, S. A. Charman, and M. A. Phillips. Structure-guided lead optimization of triazolopyrimidine-ring substituents identifies potent Plasmodium falciparum dihydroorotate dehydrogenase inhibitors with clinical candidate potential. *J. Med. Chem.*, 54(15):5540–5561, Aug 2011.

F. E. Cox. History of the discovery of the malaria parasites and their vectors. *Parasit Vectors*, 3(1):5, 2010.

A. Craig, O. Cloarec, E. Holmes, J. K. Nicholson, and J. C. Lindon. Scaling and normalization effects in NMR spectroscopic metabonomic data sets. *Anal. Chem.*, 78(7):2262–2267, Apr 2006.

D. J. Creek and M. P. Barrett. Determination of antiprotozoal drug mechanisms by metabolomics approaches. *Parasitology*, 141(1):83–92, Jan 2014.

Richard A. Davis, Adrian J. Charlton, John Godward, Stephen A. Jones, Mark Harrison, and Julie C. Wilson. Adaptive binning: An improved binning method for metabolomics data using the undecimated wavelet transform. *Chemometrics and Intelligent Laboratory Systems*, 85(1):144–154, 2007.

C. A. Daykin, P. J. Foxall, S. C. Connor, J. C. Lindon, and J. K. Nicholson. The comparison of plasma deproteinization methods for the detection of low-molecular-weight metabolites by (1)H nuclear magnetic resonance spectroscopy. *Anal. Biochem.*, 304(2):220–230, May 2002.

F. Delaglio, S. Grzesiek, G. W. Vuister, G. Zhu, J. Pfeifer, and A. Bax. NMRPipe: a multidimensional spectral processing system based on UNIX pipes. *J. Biomol. NMR*, 6(3):277–293, Nov 1995.

M. Delves, D. Plouffe, C. Scheurer, S. Meister, S. Wittlin, E. A. Winzeler, R. E. Sinden, and D. Leroy. The activities of current antimalarial drugs on the life cycle stages of Plasmodium: a comparative study with human and rodent parasites. *PLoS Med.*, 9(2):e1001169, Feb 2012.

T. T. Diagana. Supporting malaria elimination with 21st century antimalarial agent drug discovery. *Drug Discov. Today*, 20(10):1265–1270, Oct 2015.

F. Dieterle, A. Ross, G. Schlotterbeck, and H. Senn. Probabilistic quotient normalization as robust method to account for dilution of complex biological mixtures. Application in 1H NMR metabonomics. *Anal. Chem.*, 78(13):4281–4290, Jul 2006a.

F. Dieterle, G. Schlotterbeck, A. Ross, U. Niederhauser, and H. Senn. Application of metabonomics in a compound ranking study in early drug development revealing drug-induced excretion of choline into urine. *Chem. Res. Toxicol.*, 19(9):1175–1181, Sep 2006b.

G. J. Ding, P. A. Fischer, R. C. Boltz, J. A. Schmidt, J. J. Colaianne, A. Gough, R. A. Rubin, and D. K. Miller. Characterization and quantitation of NF-kappaB nuclear translocation induced by interleukin-1 and tumor necrosis factor-alpha. Development and use of a high capacity fluorescence cytometric system. *J. Biol. Chem.*, 273(44):28897–28905, Oct 1998.

F. M. Drawnel, S. Boccardo, M. Prummer, F. Delobel, A. Graff, M. Weber, R. Gerard, L. Badi, T. Kam-Thong, L. Bu, X. Jiang, J. C. Hoflack, A. Kiialainen, E. Jeworutzki, N. Aoyama, C. Carlson, M. Burcin, G. Gromo, M. Boehringer, H. Stahlberg, B. J. Hall, M. C. Magnone, K. Kolaja, K. R. Chien, J. Bailly, and R. Iacone. Disease modeling and phenotypic drug screening for diabetic cardiomyopathy using human induced pluripotent stem cells. *Cell Rep*, 9(3):810–821, Nov 2014.

S. Duffy and V. M. Avery. Development and optimization of a novel 384-well antimalarial imaging assay validated for high-throughput screening. *Am. J. Trop. Med. Hyg.*, 86(1):84–92, Jan 2012.

M. T. Duraisingh and A. F. Cowman. Contribution of the pfmdr1 gene to antimalarial drug-resistance. *Acta Trop.*, 94(3):181–190, Jun 2005.

D. I. Ellis, D. Broadhurst, D. B. Kell, J. J. Rowland, and R. Goodacre. Rapid and quantitative detection of the microbial spoilage of meat by fourier transform infrared spectroscopy and machine learning. *Appl. Environ. Microbiol.*, 68(6): 2822–2828, Jun 2002.

David I Ellis and Royston Goodacre. Metabolic fingerprinting in disease diagnosis: biomedical applications of infrared and Raman spectroscopy. *The Analyst*, 131 (8):875–885, August 2006.

H. Failmezger, H. Frohlich, and A. Tresch. Unsupervised automated high throughput phenotyping of RNAi time-lapse movies. *BMC Bioinformatics*, 14:292, 2013.

V. Fernandez. Enrichment of late-stage infected erythrocytes in 60% Percoll. In *Methods in Malaria Research*, chapter American Type Culture Collection, page 25. Manassas, 2008.

D. A. Fidock, T. Nomura, A. K. Talley, R. A. Cooper, S. M. Dzekunov, M. T. Ferdig, L. M. Ursos, A. B. Sidhu, B. Naude, K. W. Deitsch, X. Z. Su, J. C. Wootton, P. D. Roepe, and T. E. Wellems. Mutations in the P. falciparum digestive vacuole transmembrane protein PfCRT and evidence for their role in chloroquine resistance. *Mol. Cell*, 6(4):861–871, Oct 2000.

C. D. Fitch. Ferriprotoporphyrin IX, phospholipids, and the antimalarial actions of quinoline drugs. *Life Sci.*, 74(16):1957–1972, Mar 2004.

Q. L. Fivelman, I. S. Adagu, and D. C. Warhurst. Effects of piperaquine, chloroquine, and amodiaquine on drug uptake and of these in combination with dihydroartemisinin against drug-sensitive and -resistant Plasmodium falciparum strains. *Antimicrob. Agents Chemother.*, 51(6):2265–2267, Jun 2007.

E. L. Flannery, A. K. Chatterjee, and E. A. Winzeler. Antimalarial drug discovery - approaches and progress towards new medicines. *Nat. Rev. Microbiol.*, 11(12): 849–862, Dec 2013.

S. Forcisi, F. Moritz, B. Kanawati, D. Tziotis, R. Lehmann, and P. Schmitt-Kopplin. Liquid chromatography-mass spectrometry in metabolomics research: mass analyzers in ultra high pressure liquid chromatography coupling. *J Chromatogr A*, 1292:51–65, May 2013.

P. Forgue, S. Halouska, M. Werth, K. Xu, S. Harris, and R. Powers. NMR metabolic profiling of Aspergillus nidulans to monitor drug and protein activity. *J. Proteome Res.*, 5(8):1916–1923, Aug 2006.

Jenny Forshed, Ina Schuppe-Koistinen, and Sven P. Jacobsson. Peak alignment of {NMR} signals by means of a genetic algorithm. *Analytica Chimica Acta*, 487(2): 189–199, 2003.

M. Frederich, J. N. Wauters, M. Tits, C. Jason, P. de Tullio, Y. Van der Heyden, G. Fan, and L. Angenot. Quality assessment of Polygonum cuspidatum and Polygonum multiflorum by 1H NMR metabolite fingerprinting and profiling analysis. *Planta Med.*, 77(1):81–86, Jan 2011.

F. J. Gamo, L. M. Sanz, J. Vidal, C. de Cozar, E. Alvarez, J. L. Lavandera, D. E. Vanderwall, D. V. Green, V. Kumar, S. Hasan, J. R. Brown, C. E. Peishoff, L. R. Cardon, and J. F. Garcia-Bustos. Thousands of chemical starting points for antimalarial lead identification. *Nature*, 465(7296):305–310, May 2010.

M. J. Gardner, N. Hall, E. Fung, O. White, M. Berriman, R. W. Hyman, J. M. Carlton, A. Pain, K. E. Nelson, S. Bowman, I. T. Paulsen, K. James, J. A. Eisen, K. Rutherford, S. L. Salzberg, A. Craig, S. Kyes, M. S. Chan, V. Nene, S. J. Shallom, B. Suh, J. Peterson, S. Angiuoli, M. Pertea, J. Allen, J. Selengut, D. Haft, M. W. Mather, A. B. Vaidya, D. M. Martin, A. H. Fairlamb, M. J. Fraunholz, D. S. Roos, S. A. Ralph, G. I. McFadden, L. M. Cummings, G. M. Subramanian, C. Mungall, J. C. Venter, D. J. Carucci, S. L. Hoffman, C. Newbold, R. W. Davis, C. M. Fraser, and B. Barrell. Genome sequence of the human malaria parasite Plasmodium falciparum. *Nature*, 419(6906):498–511, Oct 2002.

Paul Geladi and Bruce R. Kowalski. Partial least-squares regression: a tutorial. *Analytica Chimica Acta*, 185:1–17, 1986.

F. Giardina, S. Kasasa, A. Sie, J. Utzinger, M. Tanner, and P. Vounatsou. Effects of vector-control interventions on changes in risk of malaria parasitaemia in sub-Saharan Africa: a spatial and temporal analysis. *Lancet Glob Health*, 2(10): e601–615, Oct 2014.

D. F. Gilbert, G. Erdmann, X. Zhang, A. Fritzsche, K. Demir, A. Jaedicke, K. Muehlenberg, E. E. Wanker, and M. Boutros. A novel multiplex cell viability assay for high-throughput RNAi screening. *PLoS ONE*, 6(12):e28338, 2011.

S Golotvin and A Williams. Improved Baseline Recognition and Modeling of FT NMR Spectra. *Journal of Magnetic Resonance*, 146(1):122–125, 2000.

R Goodacre, E M Timmins, R Burton, N Kaderbhai, A M Woodward, D B Kell, and P J Rooney. Rapid identification of urinary tract infection bacteria using hyperspectral whole-organism fingerprinting and artificial neural networks. *Microbiology (Reading, England)*, 144 (Pt 5):1157–1170, May 1998.

Royston Goodacre, Seetharaman Vaidyanathan, Warwick B Dunn, George G Harrigan, and Douglas B Kell. Metabolomics by numbers: acquiring and understanding global metabolite data. *Trends in biotechnology*, 22(5):245–252, May 2004.

Albert H. Gough and Paul A. Johnston. Requirements, Features, and Performance of High Content Screening Platforms. In D. Lansing Taylor, Jeffrey R. Haskins,

and Kenneth A. Giuliano, editors, *High Content Screening*, volume 356 of *Methods in Molecular Biology*, pages 41–61. Humana Press, 2006.

A. Gregson and C. V. Plowe. Mechanisms of resistance of malaria parasites to antifolates. *Pharmacol. Rev.*, 57(1):117–145, Mar 2005.

J. H. Grimes and T. M. O'Connell. The application of micro-coil NMR probe technology to metabolomics of urine and serum. *J. Biomol. NMR*, 49(3-4):297–305, Apr 2011.

R. Gruetter, S. A. Weisdorf, V. Rajanayagan, M. Terpstra, H. Merkle, C. L. Truwit, M. Garwood, S. L. Nyberg, and K. U?urbil. Resolution improvements in in vivo 1H NMR spectra with increased magnetic field strength. *J. Magn. Reson.*, 135 (1):260–264, Nov 1998.

W. A. Guiguemde, A. A. Shelat, D. Bouck, S. Duffy, G. J. Crowther, P. H. Davis, D. C. Smithson, M. Connelly, J. Clark, F. Zhu, M. B. Jimenez-Diaz, M. S. Martinez, E. B. Wilson, A. K. Tripathi, J. Gut, E. R. Sharlow, I. Bathurst, F. El Mazouni, J. W. Fowble, I. Forquer, P. L. McGinley, S. Castro, I. Angulo-Barturen, S. Ferrer, P. J. Rosenthal, J. L. Derisi, D. J. Sullivan, J. S. Lazo, D. S. Roos, M. K. Riscoe, M. A. Phillips, P. K. Rathod, W. C. Van Voorhis, V. M. Avery, and R. K. Guy. Chemical genetics of Plasmodium falciparum. *Nature*, 465(7296): 311–315, May 2010.

S. Halouska, O. Chacon, R. J. Fenton, D. K. Zinniel, R. G. Barletta, and R. Powers. Use of NMR metabolomics to analyze the targets of D-cycloserine in mycobacteria: role of D-alanine racemase. *J. Proteome Res.*, 6(12):4608–4614, Dec 2007.

S. Halouska, R. J. Fenton, R. G. Barletta, and R. Powers. Predicting the in vivo mechanism of action for drug leads using NMR metabolomics. *ACS Chem. Biol.*, 7(1):166–171, Jan 2012a.

Steven Halouska, Robert J Fenton, Raúl G Barletta, and Robert Powers. Predicting the in vivo mechanism of action for drug leads using NMR metabolomics. *ACS chemical biology*, 7(1):166–171, January 2012b.

J. Hao, M. Liebeke, W. Astle, M. De Iorio, J. G. Bundy, and T. M. Ebbels. Bayesian deconvolution and quantification of metabolites in complex 1D NMR spectra using BATMAN. *Nat Protoc*, 9(6):1416–1427, 2014.

T. Harinasuta, P. Suntharasamai, and C. Viravan. Chloroquine-resistant falciparum malaria in Thailand. *Lancet*, 2(7414):657–660, Oct 1965.

George G Harrigan and Royston Goodacre. *Metabolic fingerprinting with Fourier transform infrared spectroscopy*, pages 111–124. Kluwer Academic, 2003.

T. R. Hata, T. A. Scholz, I. V. Ermakov, R. W. McClane, F. Khachik, W. Gellermann, and L. K. Pershing. Non-invasive raman spectroscopic detection of carotenoids in human skin. *J. Invest. Dermatol.*, 115(3):441–448, Sep 2000.

JonathanJ. Helmus and ChristopherP. Jaroniec. Nmrglue: an open source Python package for the analysis of multidimensional NMR data. *Journal of Biomolecular NMR*, 55(4):355–367, 2013. ISSN 0925-2738. doi: 10.1007/s10858-013-9718-x.

P. J. Hotez, M. Alvarado, M. G. Basanez, I. Bolliger, R. Bourne, M. Boussinesq, S. J. Brooker, A. S. Brown, G. Buckle, C. M. Budke, H. Carabin, L. E. Coffeng, E. M. Fevre, T. Furst, Y. A. Halasa, R. Jasrasaria, N. E. Johns, J. Keiser, C. H. King, R. Lozano, M. E. Murdoch, S. O'Hanlon, S. D. Pion, R. L. Pullan, K. D. Ramaiah, T. Roberts, D. S. Shepard, J. L. Smith, W. A. Stolk, E. A. Undurraga, J. Utzinger, M. Wang, C. J. Murray, and M. Naghavi. The global burden of disease study 2010: interpretation and implications for the neglected tropical diseases. *PLoS Negl Trop Dis*, 8(7):e2865, Jul 2014.

Y. Huang, S. Cai, Z. Zhang, and Z. Chen. High-resolution two-dimensional J-resolved NMR spectroscopy for biological systems. *Biophys. J.*, 106(9):2061–2070, May 2014.

J.D. Hunter. Matplotlib: A 2D Graphics Environment. *Computing in Science Engineering*, 9(3):90–95, May 2007. ISSN 1521-9615.

D. Jeannerat and J. Furrer. NMR experiments for the analysis of mixtures: beyond 1D 1H spectra. *Comb. Chem. High Throughput Screen.*, 15(1):15–35, Jan 2012.

M. P. Joachimiak, C. Chang, P. J. Rosenthal, and F. E. Cohen. The impact of whole genome sequence data on drug discovery–a malaria case study. *Mol. Med.*, 7(10): 698–710, Oct 2001.

T. Jombart and I. Ahmed. adegenet 1.3-1: new tools for the analysis of genome-wide SNP data. *Bioinformatics*, 27(21):3070–3071, Nov 2011.

Eric Jones, Travis Oliphant, Pearu Peterson, et al. SciPy: Open source scientific tools for Python, 2001–. URL `http://www.scipy.org/`. [Online; accessed 2015-09-16].

N. N. Kaderbhai, D. I. Broadhurst, D. I. Ellis, R. Goodacre, and D. B. Kell. Functional genomics via metabolic footprinting: monitoring metabolite secretion by Escherichia coli tryptophan metabolism mutants using FT-IR and direct injection electrospray mass spectrometry. *Comp. Funct. Genomics*, 4(4):376–391, 2003.

H. Ke, I. A. Lewis, J. M. Morrisey, K. J. McLean, S. M. Ganesan, H. J. Painter, M. W. Mather, M. Jacobs-Lorena, M. Llinas, and A. B. Vaidya. Genetic investigation of tricarboxylic acid metabolism during the Plasmodium falciparum life cycle. *Cell Rep*, 11(1):164–174, Apr 2015.

Douglas B Kell and Pedro Mendes. Snapshots of Systems. pages 3–25. Springer Netherlands, Dordrecht, 2000.

H. C. Keun, T. M. Ebbels, H. Antti, M. E. Bollard, O. Beckonert, G. Schlotterbeck, H. Senn, U. Niederhauser, E. Holmes, J. C. Lindon, and J. K. Nicholson. Analytical reproducibility in (1)H NMR-based metabonomic urinalysis. *Chem. Res. Toxicol.*, 15(11):1380–1386, Nov 2002.

Hector C. Keun, Timothy M.D. Ebbels, Henrik Antti, Mary E. Bollard, Olaf Beckonert, Elaine Holmes, John C. Lindon, and Jeremy K. Nicholson. Improved analysis of multivariate data by variable stability scaling: application to NMR-based metabolic profiling. *Analytica Chimica Acta*, 490(1–2):265–276, 2003. Papers presented at the 8th International Conference on Chemometrics and Analytical Chemistry.

Charles C Kim, Emily B Wilson, and Joseph L Derisi. Improved methods for magnetic purification of malaria parasites and haemozoin. *Malaria Journal*, 9 (17), 2010.

T. H. Kim, D. H. Choi, V. Vauthier, J. Dam, X. Li, Y. J. Nam, Y. Ko, H. J. Kwon, S. H. Shin, J. Cechetto, V. Soloveva, and R. Jockers. Anti-obesity phenotypic screening looking to increase OBR cell surface expression. *J Biomol Screen*, 19 (1):88–99, Jan 2014.

P. Kirk, J. E. Griffin, R. S. Savage, Z. Ghahramani, and D. L. Wild. Bayesian correlated clustering to integrate multiple datasets. *Bioinformatics*, 28(24):3290–3297, Dec 2012.

E. Y. Klein. Antimalarial drug resistance: a review of the biology and strategies to delay emergence and spread. *Int. J. Antimicrob. Agents*, 41(4):311–317, Apr 2013.

K. Konig, S. F. Goethel, V. M. Rusu, and M. Vogeser. Deproteination of serum samples for LC-MS/MS analyses by applying magnetic micro-particles. *Clin. Biochem.*, 46(7-8):652–655, May 2013.

A. K. Kosmides, K. Kamisoglu, S. E. Calvano, S. A. Corbett, and I. P. Androulakis. Metabolomic fingerprinting: challenges and opportunities. *Crit Rev Biomed Eng*, 41(3):205–221, 2013.

S Krishna, A C Uhlemann, and R K Haynes. Artemisinins: mechanisms of action and potential for resistance. *Drug Resistance Updates*, 2004.

Nicholas J Kruger, M Adrian Troncoso-Ponce, and R George Ratcliffe. 1H NMR metabolite fingerprinting and metabolomic analysis of perchloric acid extracts from plant tissues. *Nature protocols*, 3(6):1001–1012, 2008.

N. Kubben, K. R. Brimacombe, M. Donegan, Z. Li, and T. Misteli. A high-content imaging-based screening pipeline for the systematic identification of anti-progeroid compounds. *Methods*, Sep 2015.

C Lambros and J P Vanderberg. Synchronization of Plasmodium falciparum erythrocytic stages in culture. *The Journal of parasitology*, 1979.

S. A. Latt, G. Stetten, L. A. Juergens, H. F. Willard, and C. D. Scher. Recent developments in the detection of deoxyribonucleic acid synthesis by 33258 Hoechst fluorescence. *J. Histochem. Cytochem.*, 23(7):493–505, Jul 1975.

K I Laws. Rapid texture identification. In *Society of Photo-Optical Instrumentation Engineers (SPIE) Conference Series*, pages 376–380, 1980.

Geun-Cheol Lee and David L Woodruff. Beam search for peak alignment of {NMR} signals. *Analytica Chimica Acta*, 513(2):413–416, 2004.

S. Lee and B. J. Howell. High-content screening: emerging hardware and software technologies. *Meth. Enzymol.*, 414:468–483, 2006.

L. Y. Lian, M. Al-Helal, A. M. Roslaini, N. Fisher, P. G. Bray, S. A. Ward, and G. A. Biagini. Glycerol: an unexpected major metabolite of energy metabolism by the human malaria parasite. *Malar. J.*, 8:38, 2009.

M. Lin, M. Al-Holy, H. Al-Qadiri, D. H. Kang, A. G. Cavinato, Y. Huang, and B. A. Rasco. Discrimination of intact and injured Listeria monocytogenes by Fourier transform infrared spectroscopy and principal component analysis. *J. Agric. Food Chem.*, 52(19):5769–5772, Sep 2004a.

M. Lin, M. Al-Holy, M. Mousavi-Hesary, H. Al-Qadiri, A. G. Cavinato, and B. A. Rasco. Rapid and quantitative detection of the microbial spoilage in chicken meat by diffuse reflectance spectroscopy (600-1100 nm). *Lett. Appl. Microbiol.*, 39(2): 148–155, 2004b.

M. Lin, M. Al-Holy, S. S. Chang, Y. Huang, A. G. Cavinato, D. H. Kang, and B. A. Rasco. Rapid discrimination of Alicyclobacillus strains in apple juice by Fourier transform infrared spectroscopy. *Int. J. Food Microbiol.*, 105(3):369–376, Dec 2005.

M. Linares, S. Viera, B. Crespo, V. Franco, M. G. Gomez-Lorenzo, M. B. Jimenez-Diaz, I. Angulo-Barturen, L. M. Sanz, and F. J. Gamo. Identifying rapidly parasiticidal anti-malarial drugs using a simple and reliable in vitro parasite viability fast assay. *Malar. J.*, 14:441, 2015.

J. C. Lindon, E. Holmes, M. E. Bollard, E. G. Stanley, and J. K. Nicholson. Metabonomics technologies and their applications in physiological monitoring, drug safety assessment and disease diagnosis. *Biomarkers*, 9(1):1–31, 2004.

L. Lucantoni, F. Silvestrini, M. Signore, G. Siciliano, M. Eldering, K. J. Dechering, V. M. Avery, and P. Alano. A simple and predictive phenotypic High Content Imaging assay for Plasmodium falciparum mature gametocytes to identify malaria transmission blocking compounds. *Sci Rep*, 5:16414, 2015.

N. MacKinnon, B. S. Somashekar, P. Tripathi, W. Ge, T. M. Rajendiran, A. M. Chinnaiyan, and A. Ramamoorthy. MetaboID: a graphical user interface package for assignment of 1H NMR spectra of bodyfluids and tissues. *J. Magn. Reson.*, 226:93–99, Jan 2013.

J. I. MacRae, M. W. Dixon, M. K. Dearnley, H. H. Chua, J. M. Chambers, S. Kenny, I. Bottova, L. Tilley, and M. J. McConville. Mitochondrial metabolism of sexual and asexual blood stages of the malaria parasite Plasmodium falciparum. *BMC Biol.*, 11:67, 2013.

V. E. Marquez, J. W. Cranston, R. W. Ruddon, L. B. Kier, and J. H. Burckhalter. Mechanism of action of amodiaquine. Synthesis of its indoloquinoline analog. *J. Med. Chem.*, 15(1):36–39, Jan 1972.

R. E. Martin, R. V. Marchetti, A. I. Cowan, S. M. Howitt, S. Broer, and K. Kirk. Chloroquine transport via the malaria parasite's chloroquine resistance transporter. *Science*, 325(5948):1680–1682, Sep 2009.

E. A. Mathe, A. D. Patterson, M. Haznadar, S. K. Manna, K. W. Krausz, E. D. Bowman, P. G. Shields, J. R. Idle, P. B. Smith, K. Anami, D. G. Kazandjian, E. Hatzakis, F. J. Gonzalez, and C. C. Harris. Noninvasive urinary metabolomic profiling identifies diagnostic and prognostic markers in lung cancer. *Cancer Res.*, 74(12):3259–3270, Jun 2014.

T. U. Mayer, T. M. Kapoor, S. J. Haggarty, R. W. King, S. L. Schreiber, and T. J. Mitchison. Small molecule inhibitor of mitotic spindle bipolarity identified in a phenotype-based screen. *Science*, 286(5441):971–974, Oct 1999.

Wes McKinney. Data Structures for Statistical Computing in Python. In Stéfan van der Walt and Jarrod Millman, editors, *Proceedings of the 9th Python in Science Conference*, pages 51–56, 2010.

C. W. McNamara, M. C. Lee, C. S. Lim, S. H. Lim, J. Roland, A. Nagle, O. Simon, B. K. Yeung, A. K. Chatterjee, S. L. McCormack, M. J. Manary, A. M. Zeeman, K. J. Dechering, T. R. Kumar, P. P. Henrich, K. Gagaring, M. Ibanez, N. Kato, K. L. Kuhen, C. Fischli, M. Rottmann, D. M. Plouffe, B. Bursulaya, S. Meister, L. Rameh, J. Trappe, D. Haasen, M. Timmerman, R. W. Sauerwein, R. Suwanarusk, B. Russell, L. Renia, F. Nosten, D. C. Tully, C. H. Kocken, R. J. Glynne, C. Bodenreider, D. A. Fidock, T. T. Diagana, and E. A. Winzeler. Targeting Plasmodium PI(4)K to eliminate malaria. *Nature*, 504(7479):248–253, Dec 2013.

S. Meiboom and D. Gill. Modified SpinEcho Method for Measuring Nuclear Relaxation Times. *Review of Scientific Instruments*, 29(8):688–691, 1958.

S. Meier and S. R. Beeren. Simultaneous determination of binding constants for multiple carbohydrate hosts in complex mixtures. *J. Am. Chem. Soc.*, 136(32): 11284–11287, Aug 2014.

S. Moon, S. Lee, H. Kim, L. H. Freitas-Junior, M. Kang, L. Ayong, and M. A. Hansen. An image analysis algorithm for malaria parasite stage classification and viability quantification. *PLoS ONE*, 8(4):e61812, 2013.

I. B. Muller and J. E. Hyde. Antimalarial drugs: modes of action and mechanisms of parasite resistance. *Future Microbiol*, 5(12):1857–1873, Dec 2010.

O. Muller, C. Traore, B. Kouyate, Y. Ye, C. Frey, B. Coulibaly, and H. Becher. Effects of insecticide-treated bednets during early infancy in an African area of intense malaria transmission: a randomized controlled trial. *Bull. World Health Organ.*, 84(2):120–126, Feb 2006.

M. Y. Mushtaq, Y. H. Choi, R. Verpoorte, and E. G. Wilson. Extraction for metabolomics: access to the metabolome. *Phytochem Anal*, 25(4):291–306, 2014.

G. A. Nagana Gowda and D. Raftery. Can NMR solve some significant challenges in metabolomics? *J. Magn. Reson.*, 260:144–160, Nov 2015.

D. Naumann. Infrared Spectroscopy in Microbiology. In R. A. Meyers, editor, *Encyclopedia of Analytical Chemistry*, pages 102–131. John Wiley & Sons, Ltd, 2000.

B. Neumann, T. Walter, J. K. Heriche, J. Bulkescher, H. Erfle, C. Conrad, P. Rogers, I. Poser, M. Held, U. Liebel, C. Cetin, F. Sieckmann, G. Pau, R. Kabbe, A. Wunsche, V. Satagopam, M. H. Schmitz, C. Chapuis, D. W. Gerlich, R. Schneider, R. Eils, W. Huber, J. M. Peters, A. A. Hyman, R. Durbin, R. Pepperkok, and J. Ellenberg. Phenotypic profiling of the human genome by time-lapse microscopy reveals cell division genes. *Nature*, 464(7289):721–727, Apr 2010.

J. K. Nicholson, J. C. Lindon, and E. Holmes. 'Metabonomics': understanding the metabolic responses of living systems to pathophysiological stimuli via multivariate statistical analysis of biological NMR spectroscopic data. *Xenobiotica*, 29(11): 1181–1189, Nov 1999.

L. J. Nkrumah, P. M. Riegelhaupt, P. Moura, D. J. Johnson, J. Patel, K. Hayton, M. T. Ferdig, T. E. Wellems, M. H. Akabas, and D. A. Fidock. Probing the multifactorial basis of Plasmodium falciparum quinine resistance: evidence for a strain-specific contribution of the sodium-proton exchanger PfNHE. *Mol. Biochem. Parasitol.*, 165(2):122–131, Jun 2009.

E. Nkuipou-Kenfack, F. Duranton, N. Gayrard, A. Argiles, U. Lundin, K. M. Weinberger, M. Dakna, C. Delles, W. Mullen, H. Husi, J. Klein, T. Koeck, P. Zurbig, and H. Mischak. Assessment of metabolomic and proteomic biomarkers in detection and prognosis of progression of renal function in chronic kidney disease. *PLoS ONE*, 9(5):e96955, 2014.

S G Oliver, M K Winson, D B Kell, and F Baganz. Systematic functional analysis of the yeast genome. *Trends in biotechnology*, 16(9):373–378, September 1998.

P. L. Olliaro, R. K. Haynes, B. Meunier, and Y. Yuthavong. Possible modes of action of the artemisinin-type compounds. *Trends Parasitol.*, 17(3):122–126, Mar 2001.

K. L. Olszewski and M. Llinas. Extraction of hydrophilic metabolites from Plasmodium falciparum-infected erythrocytes for metabolomic analysis. *Methods Mol. Biol.*, 923:259–266, 2013.

K. L. Olszewski, J. M. Morrisey, D. Wilinski, J. M. Burns, A. B. Vaidya, J. D. Rabinowitz, and M. Llinas. Host-parasite interactions revealed by Plasmodium falciparum metabolomics. *Cell Host Microbe*, 5(2):191–199, Feb 2009.

S. Patel and S. Ahmed. Emerging field of metabolomics: big promise for cancer biomarker identification and drug discovery. *J Pharm Biomed Anal*, 107:63–74, Mar 2015.

L. Pauling, A. B. Robinson, R. Teranishi, and P. Cary. Quantitative analysis of urine vapor and breath by gas-liquid partition chromatography. *Proc. Natl. Acad. Sci. U.S.A.*, 68(10):2374–2376, Oct 1971.

R. Pepperkok and J. Ellenberg. High-throughput fluorescence microscopy for systems biology. *Nat. Rev. Mol. Cell Biol.*, 7(9):690–696, Sep 2006.

M. Persson, A. F. L?ye, T. Mow, and J. J. Hornberg. A high content screening assay to predict human drug-induced liver injury during drug discovery. *J Pharmacol Toxicol Methods*, 68(3):302–313, 2013.

L. Peyre, G. de Sousa, S. Barcellini-Couget, A. P. Luzy, N. Zucchini-Pascal, and R. Rahmani. High-content screening imaging and real-time cellular impedance monitoring for the assessment of chemical's bio-activation with regards hepatotoxicity. *Toxicol In Vitro*, 29(7):1916–1931, Oct 2015.

D. Plouffe, A. Brinker, C. McNamara, K. Henson, N. Kato, K. Kuhen, A. Nagle, F. Adrian, J. T. Matzen, P. Anderson, T. G. Nam, N. S. Gray, A. Chatterjee, J. Janes, S. F. Yan, R. Trager, J. S. Caldwell, P. G. Schultz, Y. Zhou, and E. A. Winzeler. In silico activity profiling reveals the mechanism of action of antimalarials discovered in a high-throughput screen. *Proc. Natl. Acad. Sci. U.S.A.*, 105 (26):9059–9064, Jul 2008.

D. M. Plouffe, M. Wree, A. Y. Du, S. Meister, F. Li, K. Patra, A. Lubar, S. L. Okitsu, E. L. Flannery, N. Kato, O. Tanaseichuk, E. Comer, B. Zhou, K. Kuhen, Y. Zhou, D. Leroy, S. L. Schreiber, C. A. Scherer, J. Vinetz, and E. A. Winzeler. High-Throughput Assay and Discovery of Small Molecules that Interrupt Malaria Transmission. *Cell Host Microbe*, 19(1):114–126, Jan 2016.

R. N. Price, A. C. Uhlemann, A. Brockman, R. McGready, E. Ashley, L. Phaipun, R. Patel, K. Laing, S. Looareesuwan, N. J. White, F. Nosten, and S. Krishna. Mefloquine resistance in Plasmodium falciparum and increased pfmdr1 gene copy number. *Lancet*, 364(9432):438–447, 2004.

R Core Team. *R: A Language and Environment for Statistical Computing*. R Foundation for Statistical Computing, Vienna, Austria, 2013. URL `http://www.R-project.org/`.

A. Radfar, D. Mendez, C. Moneriz, M. Linares, P. Marin-Garcia, A. Puyet, A. Diez, and J. M. Bautista. Synchronous culture of Plasmodium falciparum at high parasitemia levels. *Nat Protoc*, 4(12):1899–1915, 2009a.

Azar Radfar, Darío Méndez, Carlos Moneriz, María Linares, Patricia Marín-García, Antonio Puyet, Amalia Diez, and José M Bautista. Synchronous culture of Plasmodium falciparum at high parasitemia levels. *Nature protocols*, 4(12):1899–1915, 2009b.

P. K. Rathod, A. Khatri, T. Hubbert, and W. K. Milhous. Selective activity of 5-fluoroorotic acid against Plasmodium falciparum in vitro. *Antimicrob. Agents Chemother.*, 33(7):1090–1094, Jul 1989.

O. Rausch. High content cellular screening. *Curr Opin Chem Biol*, 10(4):316–320, Aug 2006.

D. G. Robertson, M. D. Reily, R. E. Sigler, D. F. Wells, D. A. Paterson, and T. K. Braden. Metabonomics: evaluation of nuclear magnetic resonance (NMR) and pattern recognition technology for rapid in vivo screening of liver and kidney toxicants. *Toxicol. Sci.*, 57(2):326–337, Oct 2000.

P. J. Rosenthal. Falcipains and other cysteine proteases of malaria parasites. *Adv. Exp. Med. Biol.*, 712:30–48, 2011.

M. Rottmann, C. McNamara, B. K. Yeung, M. C. Lee, B. Zou, B. Russell, P. Seitz, D. M. Plouffe, N. V. Dharia, J. Tan, S. B. Cohen, K. R. Spencer, G. E. Gonzalez-Paez, S. B. Lakshminarayana, A. Goh, R. Suwanarusk, T. Jegla, E. K. Schmitt, H. P. Beck, R. Brun, F. Nosten, L. Renia, V. Dartois, T. H. Keller, D. A. Fidock, E. A. Winzeler, and T. T. Diagana. Spiroindolones, a potent compound class for the treatment of malaria. *Science*, 329(5996):1175–1180, Sep 2010.

A W Rowe, E Eyster, and A Kellner. Liquid nitrogen preservation of red blood cells for transfusion; a low glycerol-rapid freeze procedure. *Cryobiology*, 5(2):119–128, September 1968.

J. A. Rowe, A. Claessens, R. A. Corrigan, and M. Arman. Adhesion of Plasmodium falciparum-infected erythrocytes to human cells: molecular mechanisms and therapeutic implications. *Expert Rev Mol Med*, 11:e16, 2009.

S. Rozen, M. E. Cudkowicz, M. Bogdanov, W. R. Matson, B. S. Kristal, C. Beecher, S. Harrison, P. Vouros, J. Flarakos, K. Vigneau-Callahan, T. D. Matson, K. M. Newhall, M. F. Beal, R. H. Brown, and R. Kaddurah-Daouk. Metabolomic analysis and signatures in motor neuron disease. *Metabolomics*, 1(2):101–108, 2005.

P. Sandusky and D. Raftery. Use of selective TOCSY NMR experiments for quantifying minor components in complex mixtures: application to the metabonomics of amino acids in honey. *Anal. Chem.*, 77(8):2455–2463, Apr 2005.

L. M. Sanz, B. Crespo, C. De-Cozar, X. C. Ding, J. L. Llergo, J. N. Burrows, J. F. Garcia-Bustos, and F. J. Gamo. P. falciparum in vitro killing rates allow to discriminate between different antimalarial mode-of-action. *PLoS ONE*, 7(2): e30949, 2012.

L W Scheibel, S H Ashton, and W Trager. Plasmodium falciparum: microaerophilic requirements in human red blood cells. *Experimental parasitology*, 47(3):410–418, June 1979.

J. Schripsema. Application of NMR in plant metabolomics: techniques, problems and prospects. *Phytochem Anal*, 21(1):14–21, 2010.

N. Serkova and L. G. Boros. Detection of resistance to imatinib by metabolic profiling: clinical and drug development implications. *Am J Pharmacogenomics*, 5 (5):293–302, 2005.

J. R. Sheedy, P. R. Ebeling, P. R. Gooley, and M. J. McConville. A sample preparation protocol for 1H nuclear magnetic resonance studies of water-soluble metabolites in blood and urine. *Anal. Biochem.*, 398(2):263–265, Mar 2010.

J. L. Siqueira-Neto, S. Moon, J. Jang, G. Yang, C. Lee, H. K. Moon, E. Chatelain, A. Genovesio, J. Cechetto, and L. H. Freitas-Junior. An image-based high-content screening assay for compounds targeting intracellular Leishmania donovani amastigotes in human macrophages. *PLoS Negl Trop Dis*, 6(6):e1671, 2012.

G. D. Sockalingum, W. Bouhedja, P. Pina, P. Allouch, C. Mandray, R. Labia, J. M. Millot, and M. Manfait. ATR-FTIR spectroscopic investigation of imipenem-susceptible and -resistant Pseudomonas aeruginosa isogenic strains. *Biochem. Biophys. Res. Commun.*, 232(1):240–246, Mar 1997.

T. Spangenberg, J. N. Burrows, P. Kowalczyk, S. McDonald, T. N. Wells, and P. Willis. The open access malaria box: a drug discovery catalyst for neglected diseases. *PLoS ONE*, 8(6):e62906, 2013.

I. K. Srivastava, H. Rottenberg, and A. B. Vaidya. Atovaquone, a broad spectrum antiparasitic drug, collapses mitochondrial membrane potential in a malarial parasite. *J. Biol. Chem.*, 272(7):3961–3966, Feb 1997.

I. K. Srivastava, J. M. Morrisey, E. Darrouzet, F. Daldal, and A. B. Vaidya. Resistance mutations reveal the atovaquone-binding domain of cytochrome b in malaria parasites. *Mol. Microbiol.*, 33(4):704–711, Aug 1999.

B.H. Stuart. *Infrared Spectroscopy of Biological Applications.* John Wiley & Sons, Ltd, 2006.

Melissa L. Sykes and Vicky M. Avery. Development and application of a sensitive, phenotypic, high-throughput image-based assay to identify compound activity against Trypanosma cruzi amastigotes. *International Journal for Parasitology: Drugs and Drug Resistance*, pages –, 2015.

S. Takala-Harrison, C. G. Jacob, C. Arze, M. P. Cummings, J. C. Silva, A. M. Dondorp, M. M. Fukuda, T. T. Hien, M. Mayxay, H. Noedl, F. Nosten, M. P. Kyaw, N. T. Nhien, M. Imwong, D. Bethell, Y. Se, C. Lon, S. D. Tyner, D. L. Saunders, F. Ariey, O. Mercereau-Puijalon, D. Menard, P. N. Newton, M. Khanthavong, B. Hongvanthong, P. Starzengruber, H. P. Fuehrer, P. Swoboda, W. A. Khan, A. P. Phyo, M. M. Nyunt, M. H. Nyunt, T. S. Brown, M. Adams, C. S. Pepin, J. Bailey, J. C. Tan, M. T. Ferdig, T. G. Clark, O. Miotto, B. MacInnis, D. P. Kwiatkowski, N. J. White, P. Ringwald, and C. V. Plowe. Independent emergence of artemisinin resistance mutations among Plasmodium falciparum in Southeast Asia. *J. Infect. Dis.*, 211(5):670–679, Mar 2015.

A. M. Talman, A. M. Blagborough, and R. E. Sinden. A Plasmodium falciparum strain expressing GFP throughout the parasite's life-cycle. *PLoS ONE*, 5(2):e9156, 2010.

R. Teng, A. M. Lehane, M. Winterberg, S. H. Shafik, R. L. Summers, R. E. Martin, D. A. van Schalkwyk, P. R. Junankar, and K. Kirk. 1H-NMR metabolite profiles of different strains of Plasmodium falciparum. *Biosci. Rep.*, 34(6):682–699, 2014.

Rongwei Teng, Pauline R Junankar, William A Bubb, Caroline Rae, Pascal Mercier, and Kiaran Kirk. Metabolite profiling of the intraerythrocytic malaria parasite Plasmodium falciparum by (1)H NMR spectroscopy. *NMR in biomedicine*, 22(3): 292–302, April 2009.

S. Tiziani, A. Lodi, F. L. Khanim, M. R. Viant, C. M. Bunce, and U. L. Gunther. Metabolomic profiling of drug responses in acute myeloid leukaemia cell lines. *PLoS ONE*, 4(1):e4251, 2009.

W Trager and J B Jensen. Human malaria parasites in continuous culture. *Science (New York, N.Y.)*, 193(4254):673–675, August 1976.

H. Tsugawa, T. Bamba, M. Shinohara, S. Nishiumi, M. Yoshida, and E. Fukusaki. Practical non-targeted gas chromatography/mass spectrometry-based metabolomics platform for metabolic phenotype analysis. *J. Biosci. Bioeng.*, 112(3):292–298, Sep 2011.

R. A. van den Berg, H. C. Hoefsloot, J. A. Westerhuis, A. K. Smilde, and M. J. van der Werf. Centering, scaling, and transformations: improving the biological information content of metabolomics data. *BMC Genomics*, 7:142, 2006.

F. van der Kooy, F. Maltese, Y. H. Choi, H. K. Kim, and R. Verpoorte. Quality control of herbal material and phytopharmaceuticals with MS and NMR based metabolic fingerprinting. *Planta Med.*, 75(7):763–775, Jun 2009.

S. van der Walt, S.C. Colbert, and G. Varoquaux. The NumPy Array: A Structure for Efficient Numerical Computation. *Computing in Science Engineering*, 13(2): 22–30, March 2011. ISSN 1521-9615.

S. Vangala and A. Tonelli. Biomarkers, metabonomics, and drug development: can inborn errors of metabolism help in understanding drug toxicity? *AAPS J*, 9(3): E284–297, 2007.

Kirill A. Veselkov, John C. Lindon, Timothy M. D. Ebbels, Derek Crockford, Vladimir V. Volynkin, Elaine Holmes, David B. Davies, and Jeremy K. Nicholson. Recursive Segment-Wise Peak Alignment of Biological 1H NMR Spectra for Improved Metabolic Biomarker Recovery. *Analytical Chemistry*, 81(1):56–66, 2009. PMID: 19049366.

Nicola Volpi and Francesca Maccari. *Capillary Electrophoresis of Biomolecules*. Number 984 in Methods in Molecular Biology. Humana Press, 2013.

Dajana Vuckovic. Sample Preparation in Global Metabolomics of Biological Fluids and Tissues. In Haleem J. IssaqTimothy D. Veenstra, editor, *Proteomic and Metabolomic Approaches to Biomarker Discovery*, chapter 4, pages 51–75. Academic Press, Boston, 2013. ISBN 978-0-12-394446-7.

A. M. Weljie, R. Dowlatabadi, B. J. Miller, H. J. Vogel, and F. R. Jirik. An inflammatory arthritis-associated metabolite biomarker pattern revealed by 1H NMR spectroscopy. *J. Proteome Res.*, 6(9):3456–3464, Sep 2007.

WHO. World Malaria Report 2014. Technical report, World Health Organisation, 2014.

WHO. Global Technical Strategy For Malaria 2016-2030. Technical report, World Health Organisation, 2015.

D. W. Wilson, C. Langer, C. D. Goodman, G. I. McFadden, and J. G. Beeson. Defining the timing of action of antimalarial drugs against Plasmodium falciparum. *Antimicrob. Agents Chemother.*, 57(3):1455–1467, Mar 2013.

R J Wilson, G Pasvol, and D J Weatherall. Invasion and growth of Plasmodium falciparum in different types of human erythrocyte. *Bulletin of the World Health Organization*, 55(2-3):179–186, 1977.

S. E. Winograd-Katz, S. Itzkovitz, Z. Kam, and B. Geiger. Multiparametric analysis of focal adhesion formation by RNAi-mediated gene knockdown. *J. Cell Biol.*, 186 (3):423–436, Aug 2009.

Bradley Worley and Robert Powers. Generalized adaptive intelligent binning of multiway data. *Chemometrics and Intelligent Laboratory Systems*, 146:42–46, 2015.

M. Wu, M. Zheng, W. Zhang, S. Suresh, U. Schlecht, W. L. Fitch, S. Aronova, S. Baumann, R. Davis, R. St Onge, D. L. Dill, and G. Peltz. Identification of drug targets by chemogenomic and metabolomic profiling in yeast. *Pharmacogenet. Genomics*, 22(12):877–886, Dec 2012.

Y. Xi and D. M. Rocke. Baseline correction for NMR spectroscopic metabolomics data analysis. *BMC Bioinformatics*, 9:324, 2008.

Yuanxin Xi, JeffreyS. de Ropp, MarkR. Viant, DavidL. Woodruff, and Ping Yu. Automated screening for metabolites in complex mixtures using 2D COSY NMR spectroscopy. *Metabolomics*, 2(4):221–233, 2006.

C. Yu, E. Gestl, K. Eckert, D. Allara, and J. Irudayaraj. Characterization of human breast epithelial cells by confocal Raman microspectroscopy. *Cancer Detect. Prev.*, 30(6):515–522, 2006.

N. D. Yuliana, A. Khatib, Y. H. Choi, and R. Verpoorte. Metabolomics for bioactivity assessment of natural products. *Phytother Res*, 25(2):157–169, Feb 2011.

A. Zhang, H. Sun, H. Xu, S. Qiu, and X. Wang. Cell metabolomics. *OMICS*, 17 (10):495–501, Oct 2013.

X. Zhang and M. Boutros. A novel phenotypic dissimilarity method for image-based high-throughput screens. *BMC Bioinformatics*, 14:336, 2013.

C. Zheng, S. Zhang, S. Ragg, D. Raftery, and O. Vitek. Identification and quantification of metabolites in (1)H NMR spectra by Bayesian model selection. *Bioinformatics*, 27(12):1637–1644, Jun 2011.

H. Zipper, H. Brunner, J. Bernhagen, and F. Vitzthum. Investigations on DNA intercalation and surface binding by SYBR Green I, its structure determination and methodological implications. *Nucleic Acids Res.*, 32(12):e103, 2004.

Appendix A

NMR spectra of ring and trophozoite life cycle stages of *P. falciparum*

The spectra have been collected on a 600MHz Bruker Avance III spectrometer equipped with TCI gradient cryoprobe using CPMG pulse sequence, 4 dummy scans and 128 scans per sample with spectral width of 20 ppm at 298K. Spectra are divided into four regions: 0.7 - 2.7 ppm, 2.7 - 4.7 ppm, 5.5 - 7.0 ppm and 7.0 - 9.5 ppm for better visualisation. The region containing water signal (4.7 - 5.5 ppm) has been removed. Figures A.1-4 contain raw spectra while Figures A.5-8 contain quantile plots.

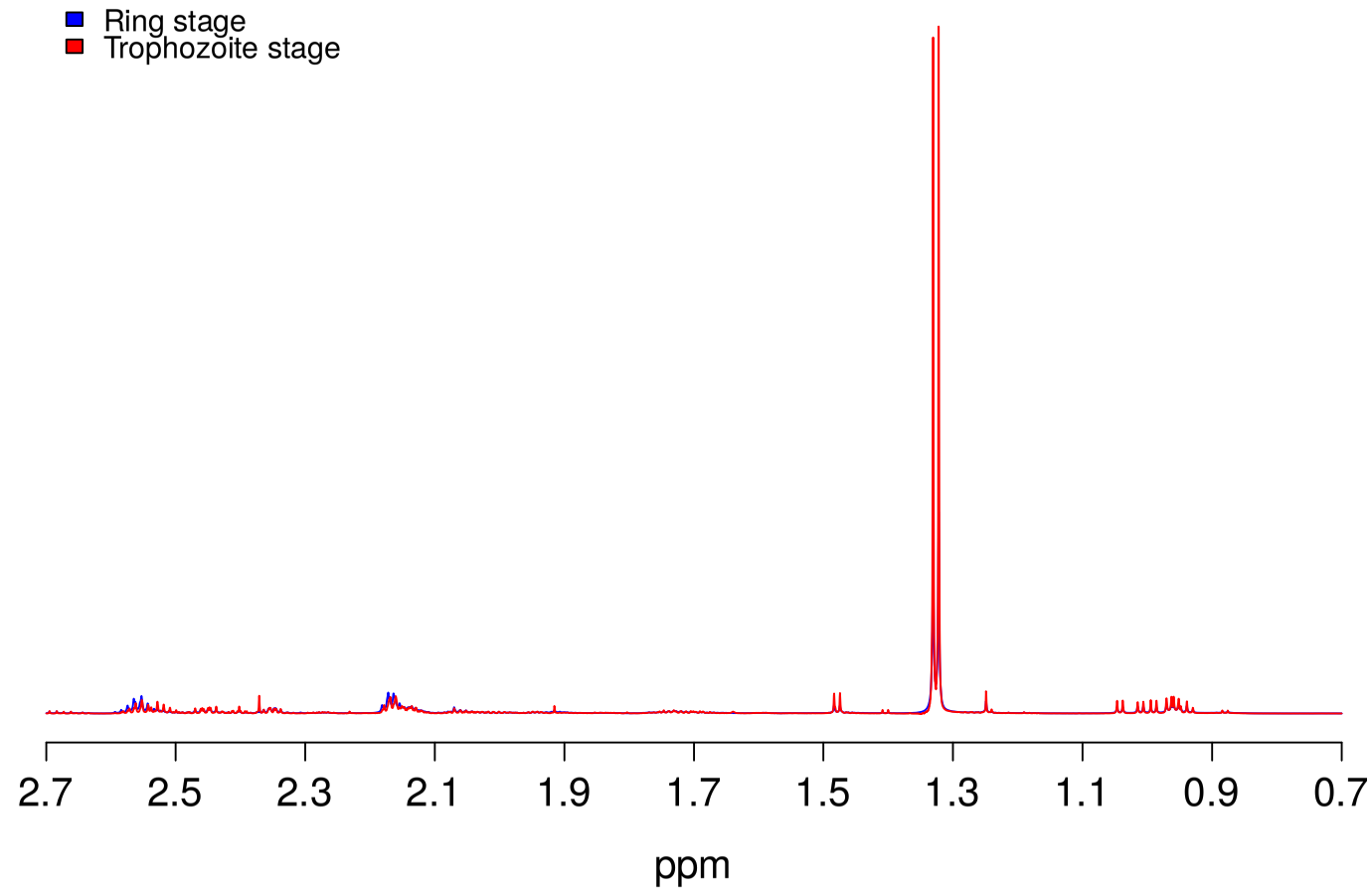

Figure A.1: 1D ^{1}H NMR spectra of RBC samples infected with *P. falciparum* at ring and trophozoite stage, extracted using ice-cold 1:1 methanol and water and 2:2:1 acetonitrile, methanol and water. The spectra were referenced to tsp signal at 0 ppm.

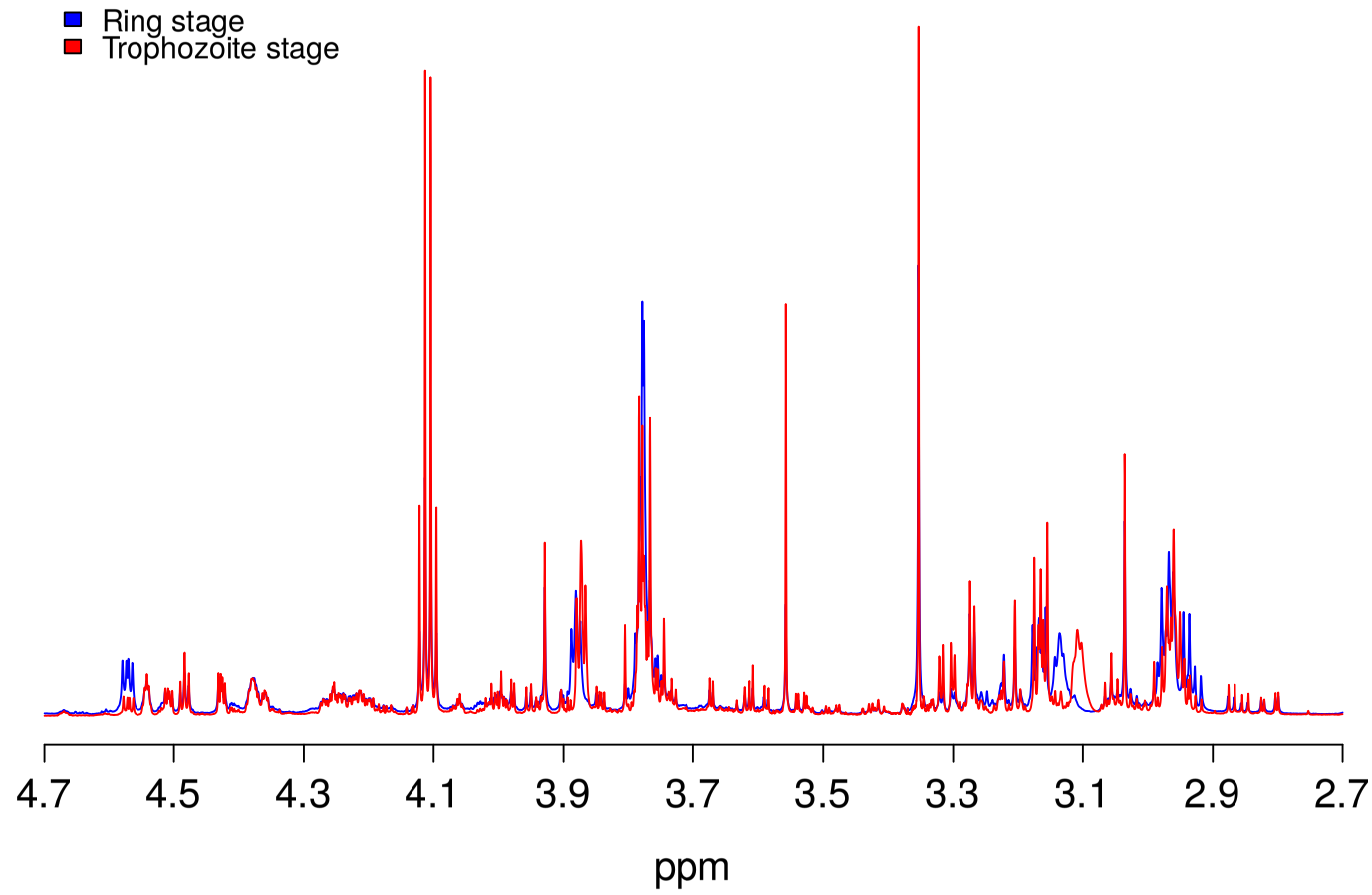

Figure A.2: 1D ^{1}H NMR spectra of RBC samples infected with *P. falciparum* at ring and trophozoite stage, extracted using ice-cold 1:1 methanol and water and 2:2:1 acetonitrile, methanol and water. The spectra were referenced to tsp signal at 0 ppm.

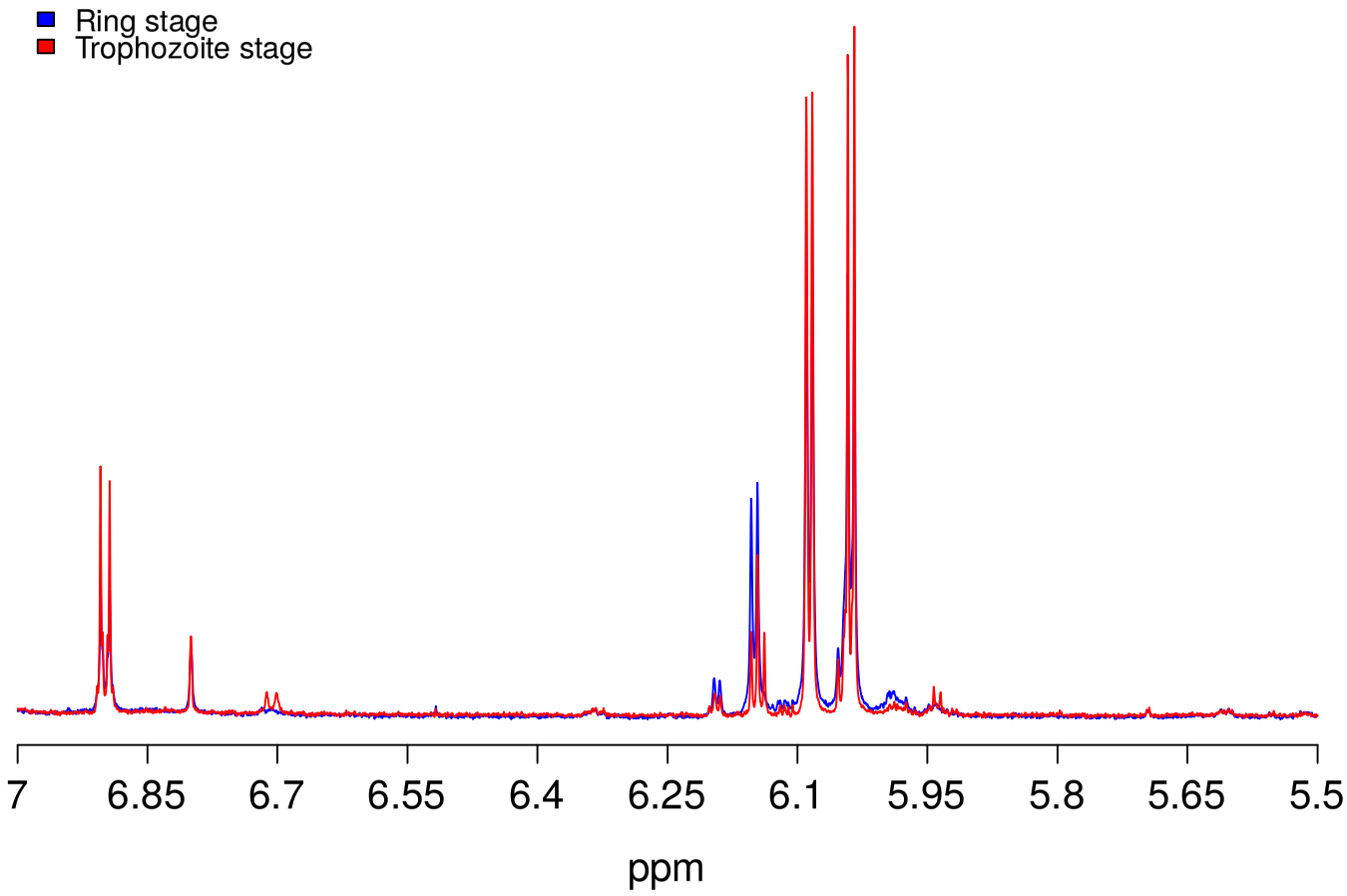

Figure A.3: 1D ^{1}H NMR spectra of RBC samples infected with *P. falciparum* at ring and trophozoite stage, extracted using ice-cold 1:1 methanol and water and 2:2:1 acetonitrile, methanol and water. The spectra were referenced to tsp signal at 0 ppm.

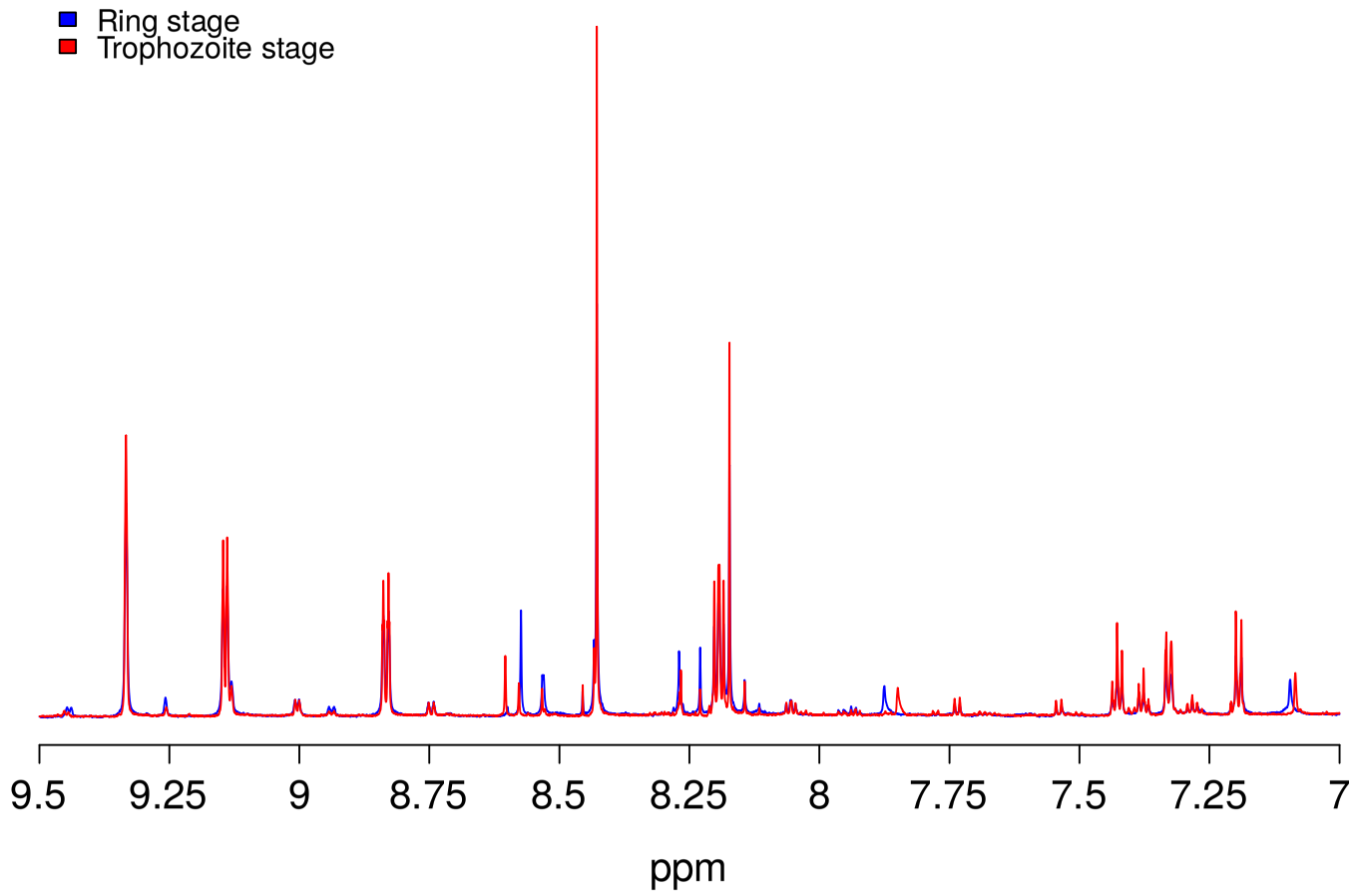

Figure A.4: 1D ^{1}H NMR spectra of RBC samples infected with *P. falciparum* at trophozoite stage, extracted using ice-cold 1:1 methanol and water and 2:2:1 acetonitrile, methanol and water. The spectra were referenced to tsp signal at 0 ppm.

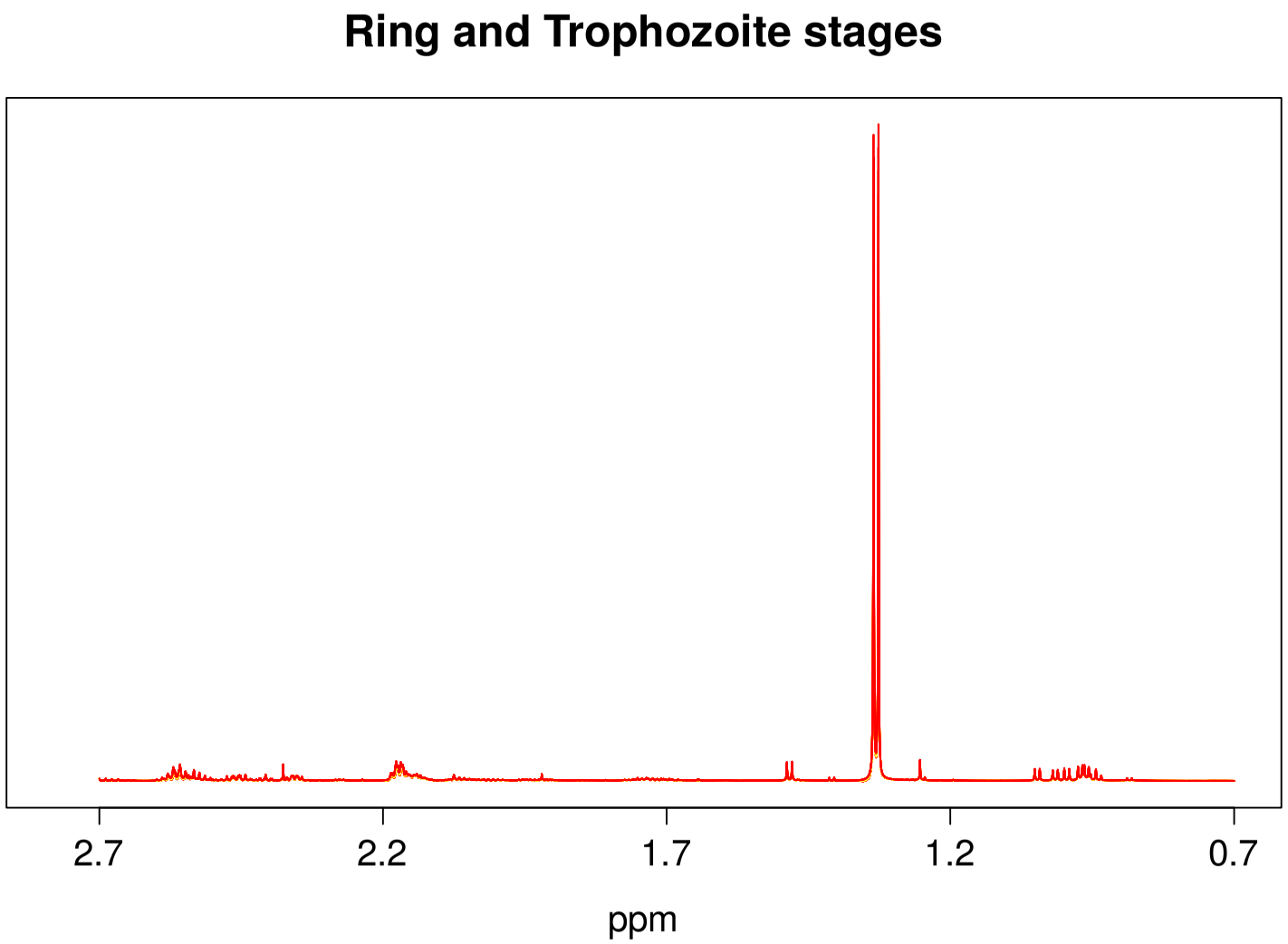

Figure A.5: Quantile plot of 1D ^{1}H NMR spectra of RBC samples infected with *P. falciparum* at trophozoite stage, extracted using ice-cold 1:1 methanol and water and 2:2:1 acetonitrile, methanol and water. The spectra were referenced to tsp signal at 0 ppm.

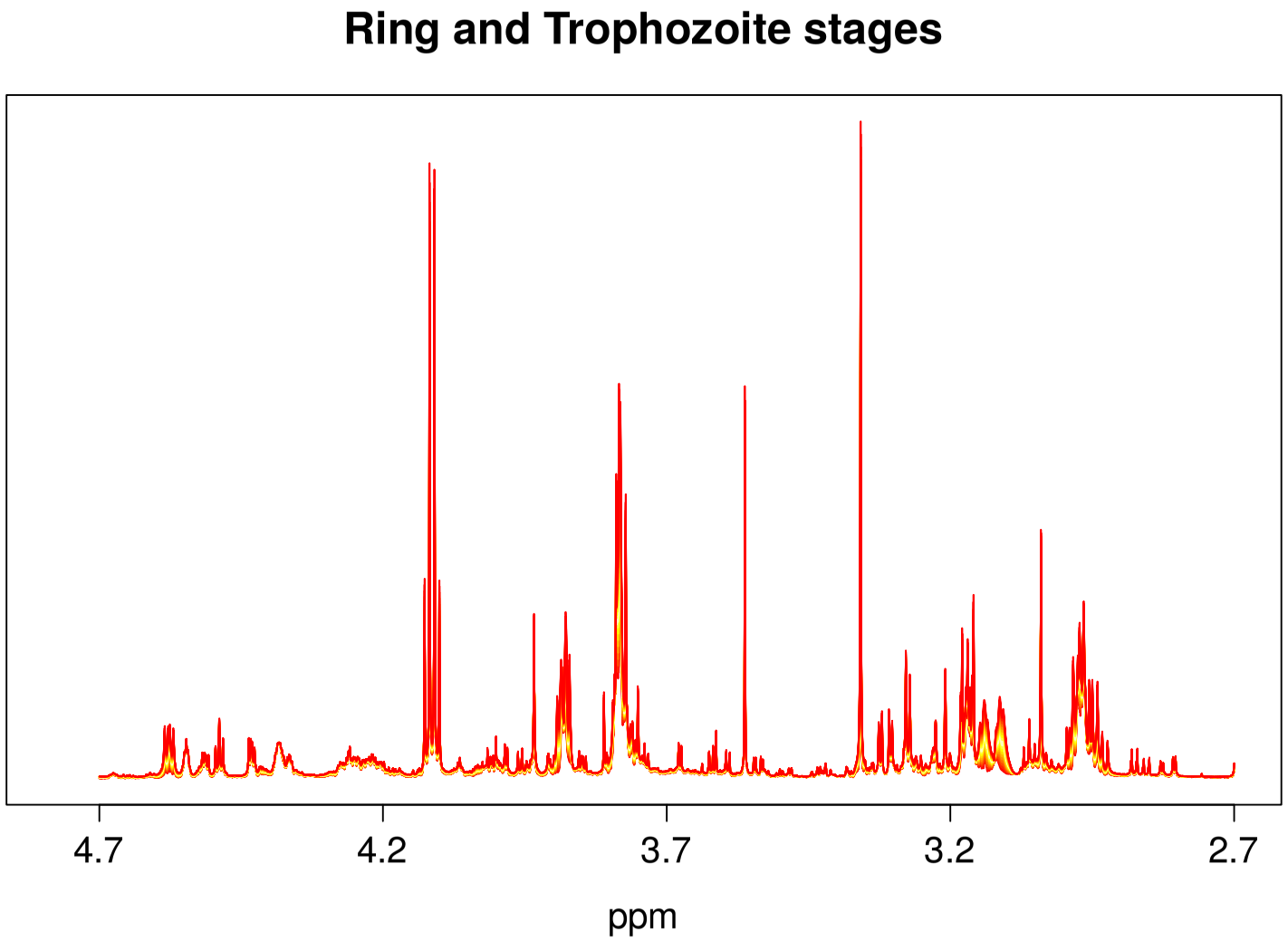

Figure A.6: Quantile plot of 1D ^{1}H NMR spectra of RBC samples infected with *P. falciparum* at trophozoite stage, extracted using ice-cold 1:1 methanol and water and 2:2:1 acetonitrile, methanol and water. The spectra were referenced to tsp signal at 0 ppm.

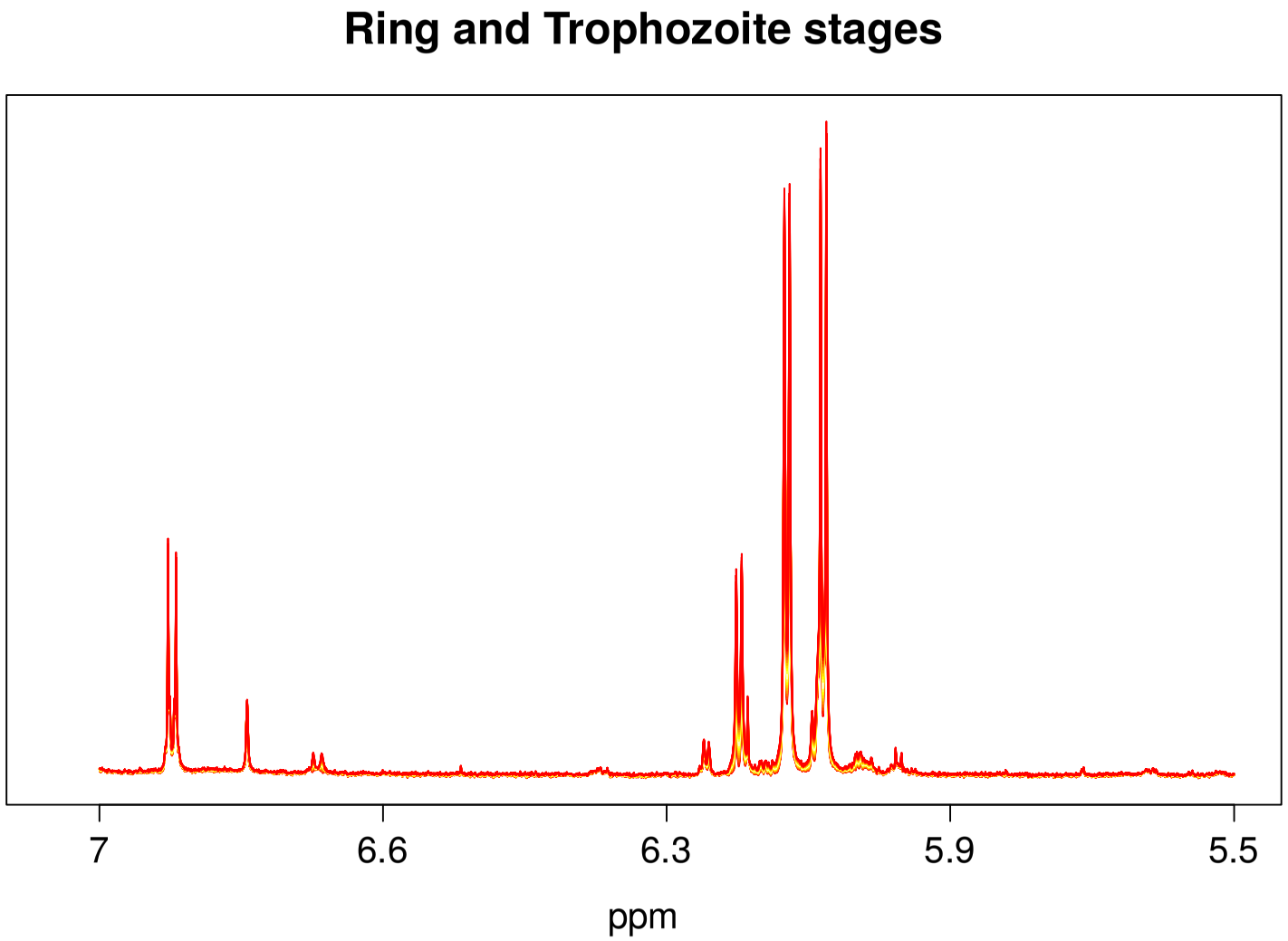

Figure A.7: Quantile plot of 1D ^{1}H NMR spectra of RBC samples infected with *P. falciparum* at trophozoite stage, extracted using ice-cold 1:1 methanol and water and 2:2:1 acetonitrile, methanol and water. The spectra were referenced to tsp signal at 0 ppm.

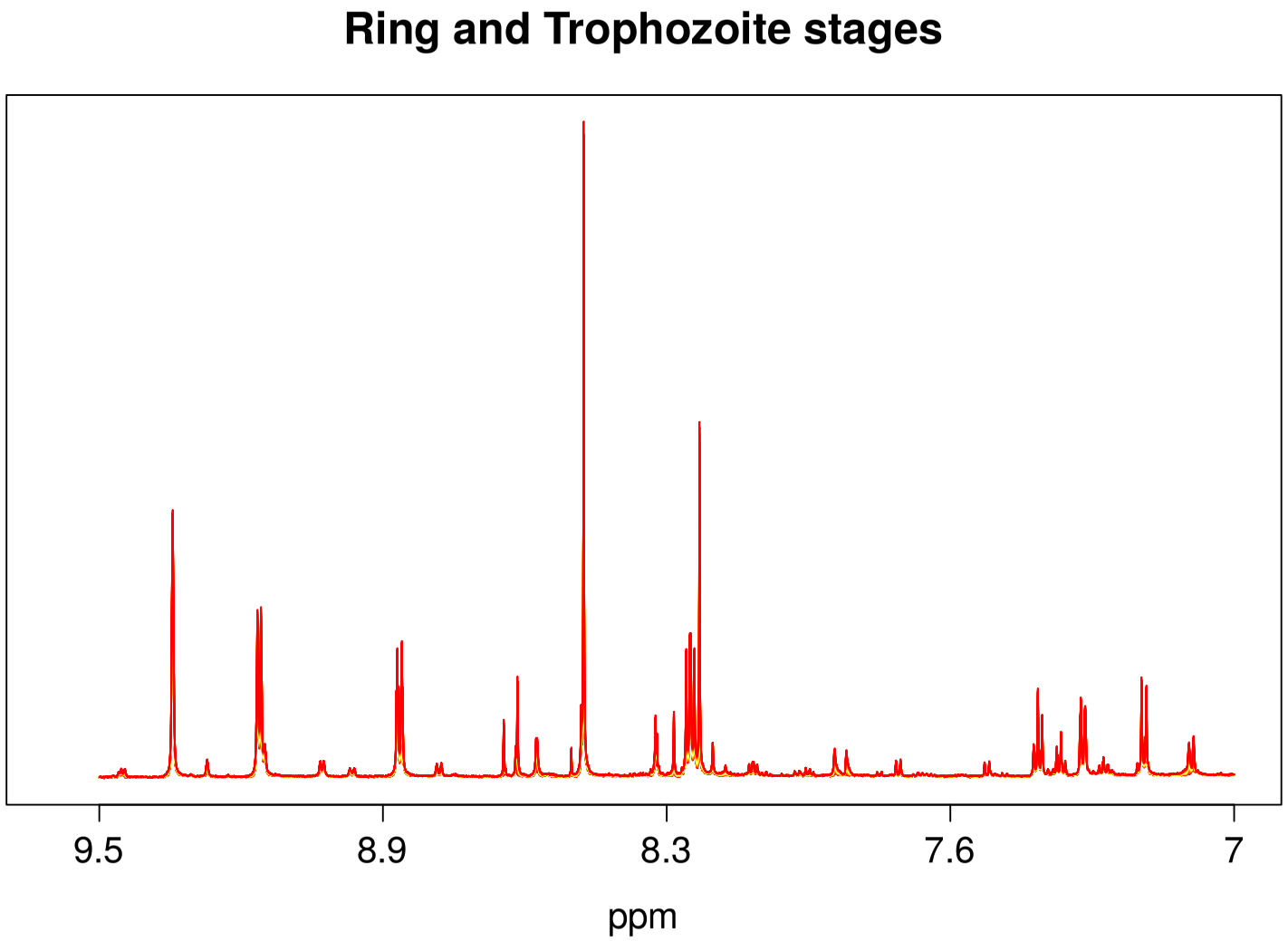

Figure A.8: Quantile plot of 1D ^{1}H NMR spectra of RBC samples infected with *P. falciparum* at trophozoite stage, extracted using ice-cold 1:1 methanol and water and 2:2:1 acetonitrile, methanol and water. The spectra were referenced to tsp signal at 0 ppm.